Chemical Engineering and Reactor Design of a Fluidised Bed Gasifier.

Thesis submitted to Cardiff University in Fulfilment of the Requirements for the degree of Doctor of Philosophy in Chemical Engineering-Reactor Design

By

Abbas Abdulkareem Mahmood AL-Farraji

B.Sc. Chemical Eng. & M.Sc. Chemical Eng.

School of Engineering-Cardiff University

Cardiff, United Kingdom

June 2017

Declaration

This work has not previously been accepted in substance for any degree and is not concurrently submitted in candidature for any degree.

Signed ……. (Candidate) Date ….....

STATEMENT 1

This thesis is being submitted in partial fulfilment of the requirements for the degree of PhD

Signed ……. (Candidate) Date ….....

STATEMENT 2

This thesis is the result of my own work/investigation, except where otherwise stated. Other sources are acknowledged by explicit references.

Signed ……. (Candidate) Date ….....

STATEMENT 3

I hereby give consent for my thesis, if accepted, to be available for photocopying and for inter-library loan, and for the title and summary to be made available to outside Organisations.

Signed ……. (Candidate) Date ….....

STATEMENT 4

I hereby give consent for my thesis, if accepted, to be available for photocopying and for inter-library loans after expiry of a bar on access previously approved by the Graduate Development Committee.

Signed ……. (Candidate) Date ….....

Acknowledgments

Thanks to the Ministry of Higher Education, Iraq Government (Al-Nahrain University) for providing me with a scholarship which has made my PhD possible. Thanks for the staff of the Iraqi cultural attaché in London for their help and support.

I would like to express my sincerest gratitude to Dr. Richard Marsh for giving me the opportunity to study a PhD at Cardiff University. He has been incredibly supportive of my work and ideas that I have had about my research. He has been very patient with my demanding nature, and I really appreciate having been able to knock on his door whenever I have needed help.

I extend my deepest thanks to Dr. Julian Steer for his expertise and willingness to help and make time for me in spite of inconvenience caused to his busy schedule. In addition, I would like to thank Dr. Agustin Valera-Medina for his supervisory support and finance.

Without the help of the Engineering Workshop I would not have been able to design and produce a gasifier. In particular, Malcolm Seabourne has always been there to translate my ideas into a workable solution. His technical support has been invaluable to meeting my practical needs.

I would like to thank Julian Herbert for supporting me during the difficult days of writing up of this thesis.

Thank you to Dr. Qinglong Meng (a visiting academic at Cardiff University), School of Civil Engineering, Chang'an University, Xi'an, China, for being so kind enough as to support me in my study.

I would like to say thank you to my father and mother for encouraging me to finish my PhD. Special thanks to my lovely wife Wissam for being patient with me during the whole period of study and always pushing me forward to achieve my best. I could have not done this without you. Lastly, I would like to give a special thanks to my children for their love and support over the last 4 years.

Abstract

The design, modelling and optimisation of biofuel thermochemical processes are mainly based on the knowledge of reliable chemical kinetics. The determination of reaction kinetics of biomass at high heating rate still highly depends on the extrapolation of results from kinetic data determined at a comparatively low heating rate. To provide more comprehensive kinetic data for gas-solid reactions under isothermal conditions, a thermogravimetric fluidized bed reactor (TGFBR) was designed. Using this novel fluidised bed, gravimetric measurements and high heating rate, the thermal conversion of biomass was investigated.

Using a thermogravimetric analyser (TGA) as a fixed bed and the TGFBR as a fluidized bed, the pyrolysis kinetics of olive kernels was studied. The pyrolysis in the TGFBR was analysed using the isothermal kinetic approach and it was theorised that the pyrolysis decomposition reaction occurred by two mechansims. Dependent on the temperature, the resultant activation energy was 67.4 kJ/mole at <500 °C and 60.8 kJ/mole at >500 °C. For comparsion, the TGA gave a higher activation energy of 74.4 kJ/mole due to external particle diffusion.

To study the impact of torrefaction on gasification performance, gasification experiments were performed on “as received olive kernels” (AROK) and “as received torrefied olive kernels” (ARTOK) in the TGFBR. The effect of equivalence ratio (ER) (0.15-0.35) and bed temperature (550-750°C) on gasification performance was investigated. Based on thermogravimetric measurements using a mass balance model, the activation energy of AROK was found to be 84 kJ/mole, whereas ARTOK was found to be 106 kJ/mole. The results suggest that diffusion controls the reaction of AROK, while oxidation controls the reaction of torrefied biomass.

The pyrolysis of date palm stones was also studied in the TGFBR, and the kinetic expression was determined using a model fitting method. The most probable reaction mechanism for the thermal decomposition of palm stones was three-dimensional diffusion. The activation energy for experiments between 350°C and 600°C for date palm stones was 27.67 kJ/mole. Furthermore, the gasification of date palm stones was investigated at ER (0.15-0.35) and a temperature range of 600-750°C in 50°C increments. Based on the energy yield (7 MJ/kg), the results suggest that the optimum conditions were at T=750°C and ER=0.2.

Overall, the result reveals that the TGFBR, in comparison with TGA, would be a viable reactor that enables kinetic analysis of gas-solid reactions under isothermal conditions, benefiting from its features. The parameters obtained from the kinetic study of TGFBR are essential in the scale-up design of useful conversion technologies such as gasification. Also, the pre-treatment of biomass via torrefaction is a promising route to improve gas production in a bubbling fluidised bed gasifier.

Publications

- A comparison of the Pyrolysis of Olive Kernel Biomass in Fluidised and Fixed Bed Conditions. Waste and Biomass Valorization, June 2017 (Journal).
- Fluidised Bed Pyrolysis of Olive Kernel Biomass in a Thermogravimetric Reactor. (Poster, 21st International Symposium on Analytical and Applied Pyrolysis). France, 2016.

Table of Contents

List of Figures

List of Tables

Nomenclature

x	=	Conversion	dimensionless
k	=	Rate constant	s^{-1}
E	=	Activation Energy	kJ/mole
AROK	=	as received olive kernels	
ARTOK	=	as received torrefied olive kernels	
R	=	Universal gas constant	J/mole.K
A	=	Pre-exponential factor	dimensionless
m_o	=	Initial sample mass	gram
m	=	mass of sample at any time, t	gram
m_f	=	Final sample mass	gram
f(x)	=	Reaction function	dimensionless
β	=	Heating rate	°C/min
H_s	=	Static bed Height	mm, cm
D	=	Fluidized bed reactor diameter	mm, cm
d_p^*	=	Dimensionless particle size	dimensionless
u^*	=	Dimensionless gas velocity	dimensionless
d_p	=	Mean particle size of sand	μm
g	=	Acceleration of gravity	m/s^2
μ	=	Viscosity of air	g/cm.s
ρ_g	=	Density of air	g/cm^3
ρ_s	=	Density of sand	g/cm^3
u_{mf}	=	Minimum fluidization velocity	m/sec
u	=	Superficial velocity	m/sec
ε_{mf}	=	Bed voidage at U_{mf}	
ε_m		Bed voidage of the expanded bed	
TDH	=	Transport Disengaging Height	m
ND	=	Density of orifice	No. holes/cm^2
ER	=	Equivalence ratio	
$[AFR]_a$	=	Actual air fuel ratio	
$[AFR]_s$	=	Stoichiometry air fuel ratio	
$\dot{m}_f$	=	Mass rate of fuel	g/min, kg/hr
$\dot{m}_{air}$	=	Mass rate of air	g/min
HHV	=	Higher heating value of dry gas	MJ/Nm^3
Qa	=	Volume flow rate of air	Nm^3/hr
Y	=	Gas yield	Nm^3/kg
μ_c	=	Carbon conversion efficiency	
η	=	Cold gas efficiency	
HHV_f	=	The gross caloric value of the fuel	MJ/kg
F	=	Char feed rate	g/sec
Y_{ch}	=	Char yield (gram of char/gram of biomass)	
m	=	Mass of char in the reactor	g
R_r	=	Chemical reaction rate	g/s
m(t)	=	Mass of char at any time, t	g
m_{ss}		Amount of char in the reactor at steady state	gram

Chapter 1

Background

Global warming, due in part to the increase in CO_2 emissions from fossil fuels, remains a major threat to our planet. The problem is set to become worse due to population growth, civilization and modernization causing an increase in the demand for energy for electricity generation, heating and transportation.

Among the different human activities that produce greenhouse gases, the use of energy represents by far the largest source of emissions, accounting for an estimated 70% of global emissions [1]. According to new and stronger evidence, most of the warming observed over the last 50 years can be attributed to human activities [2]. Billions of tonnes of CO_2 gas are discharged annually to the ecosystem from the consumption of fossil fuels. Therefore, it is necessary to reduce CO_2 concentration in the atmosphere to a lower level to mitigate against the effects of human interference with the climate.

Additional challenges arise in estimating fossil fuel resources; fossil fuels play a crucial role in the world energy market. However, this resource for world energy supply will soon decline [3]. According to Shafiee [4], the depletion times for oil, coal and gas are approximately 35, 107 and 37 years respectively. There is a lot of research into other reliable energy resources to replace the dwindling supply of fossil fuels, and uncertainty in fossil fuel production will drive this.

As world population and emissions continue to grow and the limited amount of fossil fuels begins to decline, it may not be possible to keep pace with demand by chiefly relying on fossil fuels to generate energy. Human civilization has started realizing how much harm they have already caused to the environment, and regarding solutions to these environment problems, the focus is shifting to alternative energy sources. Alternative energy does not come from fossil fuels, and thus produces little to no greenhouse gases such as CO_2. Additionally, it has potential to supplement the deficiency in fossil resources. These resources including biomass, wind, geothermal, hydropower, and solar. They can all provide sustainable energy and a net reduction of pollutants over conventional energy sources. Figure 1-1 illustrates projected global direct fuel use. In these scenarios, renewable biomass energy is expected to account

for about 25% of global direct energy use in 2025 and 40% by 2050; it includes fuels such as methanol, ethanol, hydrogen, and biogas [5].

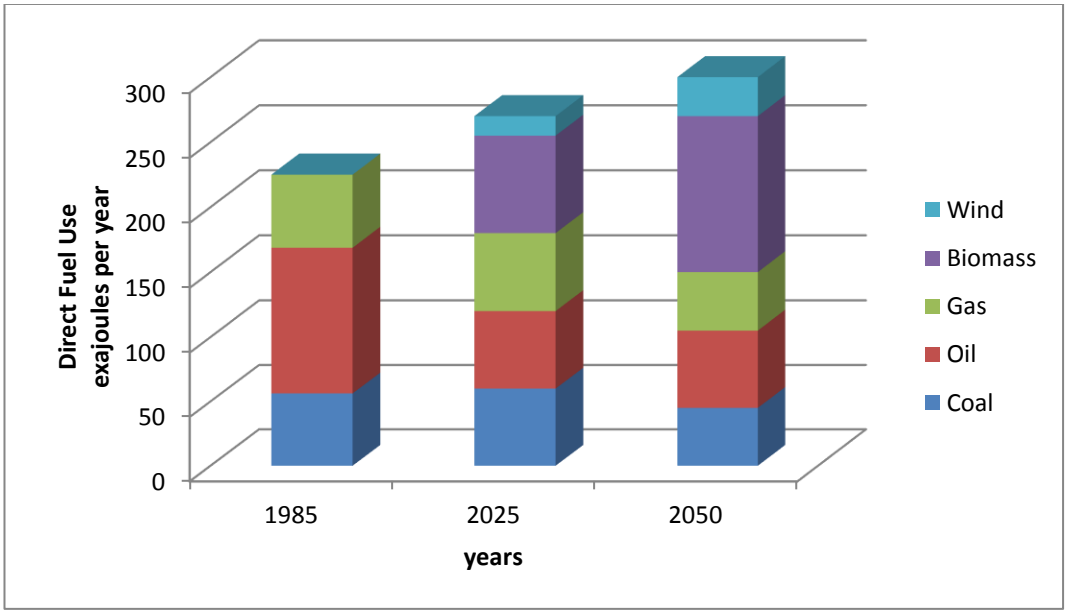

Figure 1-1 Direct fuel-use for renewable-intensive global energy scenario [10].

Confronting the challenge of climate change requires two approaches, namely mitigation and adaptation [6]. Mitigation involves the replacement of high carbon fossil fuels with low carbon alternatives, hence an overall reduction in greenhouse emissions, lessening climate change. Adaptation seeks to change production and consumption, so it relies on people actively changing their lifestyles to achieve the desired effect. Sims et al. [7] reported, several broad methods for mitigation of carbon dioxide emissions exist; one of these is increasing the use of renewable sources of energy. The scope of this study falls under the mitigation approach, as we are seeking low carbon alternatives for providing energy.

The World Energy Council provides a broad term for energy sustainability that includes three key factors [8]. These are "energy security, energy equity, and environmental sustainability", and together they constitute the 'energy trilemma'. Each point of the trilemma shall now be defined. *Energy security* relates to the ability to provide reliable energy to all users both currently and in the future. As part of this, energy production, energy supply and infrastructure need to be carefully planned and

managed. *Energy equity* is to ensure that energy is available to all members of a population and at an affordable price. *Environmental sustainability* must be addressed for energy production to be low carbon. Also, it needs to encompass energy efficient practices in both energy generation and consumer usage. The energy trilemma relates to gasifier design because there must be a consistent energy source (biomass) and reliable industrial gasification equipment. The cost of the feed biomass and running of a gasifier need to be carefully considered if the energy is to be affordable. Biomass is inherently low carbon, so gasification of biomass is beneficial to achieving environmental sustainability.

1.1 Biomass as an alternative to fossil fuel

Currently, climate change mitigation and energy security are driving the worldwide efforts to utilise biomass for renewable, sustainable fuel and energy development. Biomass is a fuel derived from organic matter on a renewable basis, and is among the biggest sources of energy on the earth, third only to coal and oil [9].

Prior to the industrial revolution, wood was considered the main source of the world's energy supply. With the uptake of coal, this situation changed and energy consumption began to rely on coal. Further diminishment in biomass' contribution to total energy came with the utilisation of other fossil fuels i.e. crude oil and natural gas. However, increased attention has focussed on biomass due to the modern energy resource pressures.

Today, biomass is a vital contributor to the world economy, as different types of biomass energy are expended all over the world. Biomass delivers a potentially renewable energy source that could improve the environment, economy and energy security. The EU strategy for the next 40 years is to maintain the global temperature rise below 2°C by reducing greenhouse emissions by an uptake of renewable energy such as biomass [10]. The physical properties, organic, inorganic and energy content of biomass differs from coals. Relative to coal, biomass has higher moisture content, lower heating value, less carbon, more silica and potassium, and lower density [11].

The advantages of using biomass as an alternative fuel are listed as follows:

1. Mitigation of climate change, because biomass absorbs CO_2 from the atmosphere during photosynthesis, and the CO_2 is returned to the environment after combustion.
2. For both the developing world and the richer countries, biomass has great potential as a renewable energy source. Biomass production in the world is estimated at 146 billon metric tons a year, mostly wild plant growth [12].
3. Emissions of SOX and NOX are reduced when energy production is based on biomass because it contains less sulphur and nitrogen than fossil fuels [13].
4. The production of biomass can enhance the local economy, especially if it is possible to use poor quality land which is unsuitable for growing food.
5. There are many sources of biomass which makes it different from other alternative energy sources, and many conversion processes can be used to convert biomass into energy [12].

Biomass is renewable in the sense that only a short period is required to substitute what is used as an energy resource. The only renewable energy source that emits carbon dioxide in use is biomass. But biomass utilises the carbon dioxide from the environment to store energy as it grown during photosynthesis. With the exception of transport and production, there are no net carbon emissions over the life of biomass production if it is being grown sustainably. Therefore, cultivation of plants is one of the most significant factors which lead to the closure of the carbon cycle. Figure 1.2 illustrates a biomass energy cycle and the manner in which biomass is used for energy production [14].

Although biomass is seen as an environmentally friendly fuel, there are many factors in its production and transportation that need to be considered. These include land use; usage of fertilizers (and whether these are produced using fossil fuels); use of agricultural machinery when growing and harvesting biomass; and delivery from the field to the gasifier. These all have a carbon emission attached to them, which needs to be taken into account when working with biomass.

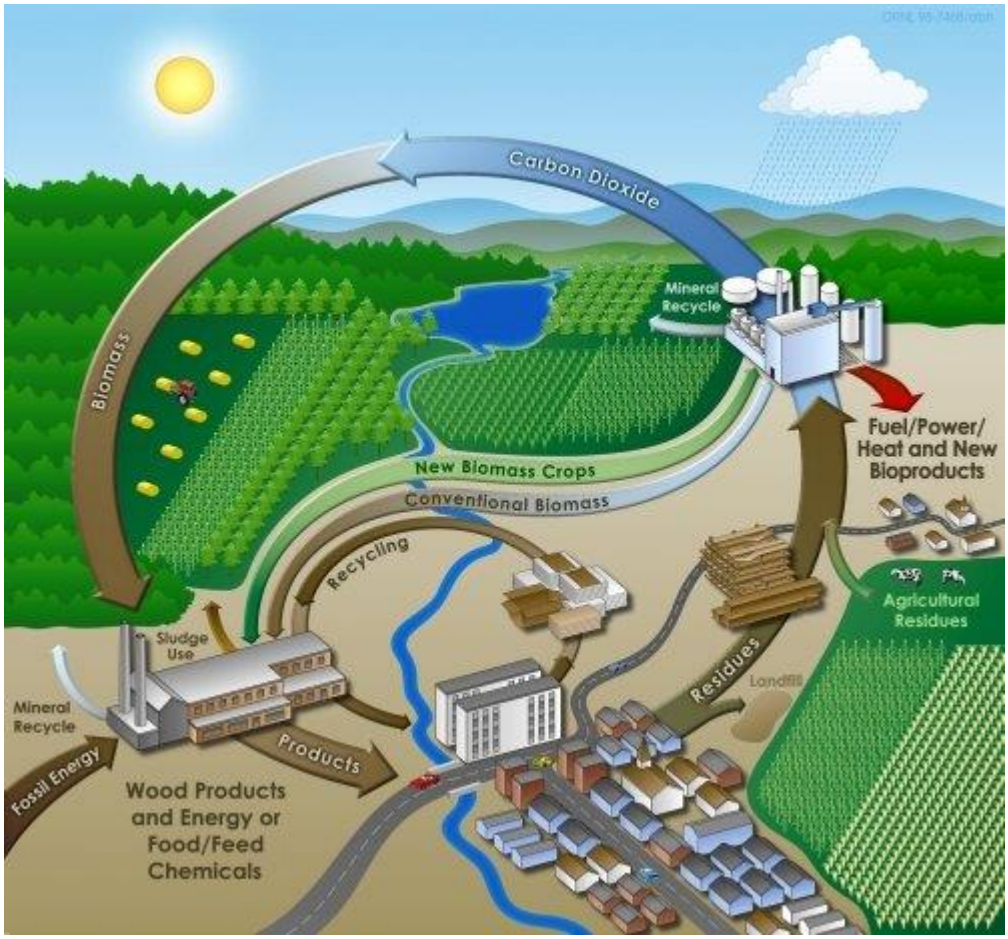

Figure 1-2 Biomass Energy Cycle [15]

Biomass is organic material derived from plants such as trees, algae and crops; it is essentially storage and collection of the suns energy obtained by photosynthesis. Biomass can be utilised in a sustainable way through a cyclical process of fixation and release of CO_2 [16]. Biomass has been recognized as a major world energy source to compensate declining fossil fuel resources [17].

Cellulose, lignin and hemi-cellulose are found in biomass fuels. The molecular weights of cellulose vary depending on the molecular structure. Hemi-cellulose has an undefined molecular structure and a lower molecular weight than that of cellulose. This causes to it have higher reactivity and less thermal stability. The molecular structure of lignin is similar to low-rank coal, and it is a complex process to extract it from biomass without using a sophisticated process [18]. Biomass for bioenergy can

be obtained directly from the farm, as crops or residues resulting from the processing of crops for food or waste from the forestry industry.

Biomass energy has the potential to be implemented worldwide, and it is possible to convert it into other useful forms such as gases, liquids, or electricity. Some of these technologies are commercially available while others are still in the development stage.

1.1.1 Olive kernel and palm stones as a renewable energy source

This research focuses on biomass in with a form of agricultural waste biomass, which is widely available but not largely exploited in the energy recovery field. The use of biomass as an alternative energy source in developing countries has been of high interest, since the economies of these countries are based on agriculture and forestry. In Europe, currently less than 50% of potentially available biomass is used [19].

Olive kernels (see Fig. 1-3) are a waste product of agricultural activity in the Mediterranean basin. Olive cultivation is a typical activity in Spain, Greece, Portugal and Italy. Olive production is significant in these countries because the economy is based mainly on agriculture and food export activities. The annual olive oil production reaches 1,600,000 tons according to a global scale [20]. . The major solid by-products obtained from olive oil production are the kernels, as well as, olive tree pruning and harvest residues.

Figure 1-3 Olive kernels biomass.

Greece is the 3rd largest olive oil producer and accounts for nearly 15% of world production. As a result, a massive amount of solid residues such as olive kernels are produced seasonally from agricultural and industrial activities; the estimated amount of olive kernels is approximately 400,000 tons [21]. Olive kernels have already been used as a low cost solid biofuel (0.046 €/kg), utilised mainly for conventional combustion If not used, this resource could accumulate and contribute negatively to environmental pollution due to its phytotoxic (toxic to plants) nature. The olive kernel in Greece is predominately used as an energy source in conventional combustion, but this constitutes a serious environmental issue due to emissions that are harmful to health. It was noted that olive kernels showed high calorific value and high bulk density. This makes them an attractive proposition for an alternative fuel in energy production.

Iraq, like other developing countries, needs to exploit all of its available resources in the field of national sustainable development. Iraq mainly depends on oil and gas for power demand. However, year on year there is an increase in fossil fuel

related emissions, with a rising growth rate observed during recent years [22]. According to the same author, the CO_2 emissions in 2011 were found to be higher than 2010 because of increasing reliance on fossil fuels. Also, emissions of heavy pollution are being created from major industrial zones, manufacturing facilities, office buildings, and the increasing number of vehicles.

Significant reserves of alternative energy sources are not yet used in this country. Iraq and other Arabic countries are the home land of the date palm. Recent studies showed that Arabic countries possess 70% of the world's 120 million date palms and are responsible for 67% of global date production [23]. The total production for Iraqi dates is estimated at 400,000 ton per year [24]. Annually a huge amount of date palm stone waste is generated while processing date palm fruit. These unwanted date stones can cause environmental hazards such as fire, bait for insects and diseases. It is interesting to note that date stones represent about a third of a date's mass. This untapped resource (see Fig. 1-4) is not being exploited and hence could potentially serve as a source of energy. Therefore, it is necessary to find technologies with the ability to exploit this biofuel as energy as well as to reduce emissions. It is worth noting that, due to its higher density (560 kg/m^3), the date stone could be used without densification, thus reducing major pre-processing costs [25]. Iraq is a major oil exporter in the world, therefore, the potential of biomass resources, such as date stones as a renewable source of energy, has not been fully exploited.

Figure 1-4 Date stones biomass.

1.2 Thermal conversion technologies

Thermal conversion is the use of heat to convert biomass feedstocks into other forms of energy. Thermal conversion is undertaken with or with-out the presence of oxygen. These technologies including combustion, gasification, pyrolysis and torrefaction will be briefly introduced.

1.2.1 Torrefaction process

There are many obstacles to biomass thermal conversion for example high moisture content, low calorific value and low bulk density. This makes biomass expensive to implement, which hinders its use as an alternative fuel. Therefore, a lot of researchers are trying to find solutions to overcome these problems and improve the properties of biomass. One of the most well known solutions is torrefaction.

Torrefaction is a promising route to convert a range of biomass into energy dense fuels, readily appropriate for subsequent thermochemical conversion [26]. It is a mild thermal pre-treatment of biomass carried out in inert environments in a temperature

between 200°C-300°C. Under these circumstances, biomass properties are upgraded through limited devolatilization [27]. In most laboratory tests, nitrogen is frequently used as a carrier gas to create inert conditions. Torrefaction and pyrolysis are conducted under similar conditions (in the absence of oxygen) but the latter takes between 350°C and 650°C, thus torrefaction is termed mild pyrolysis as it occurs in the lower temperature range of the pyrolysis process [28]. The biomass is changed mainly into a high quality of solid biofuel, whose characteristics are intermediate between biomass and coal, and can be used for combustion and gasification [29]. Lower moisture, higher energy density, improved ignitability, enhanced reactivity, and better grind-ability are the characteristics of torrefied biomass when compared to its parent biomass. Typically the moisture content of torrefied biomass ranges from 1-6 wt%, depending on the conditions of torrefaction [28]. The gas produced from torrefaction consists of at least 60 wt% of incombustible components such as water and CO_2, while the rest is acetic acid, lactic acid, furfural, and a trace of phenol. Torrefied biomass is considered more valuable than raw biomass [30]. The product gas from gasification of torrefied biomass has higher hydrogen and carbon monoxide content, in addition to higher cold gas efficiency and exergy efficiency, compared to raw biomass [31].

Approximately 60 to 75% of the total cost of biofuel goes towards the cost of biomass feedstock processing [32]. In addition, the unfavourable properties of raw biomass such as its high bulk volume, high moisture content and relatively low calorific value, lead to the transport price of raw biomass being more expensive. Raw biomass can be defined as having a relatively high moisture content and being hydroscopic, that is, it has the ability to absorb water due to the presence of OH groups. However, during biomass torrefaction, most of the moisture as well as components of low-moleculer weight volatiles are released. Therefore, this pre-treatment process gives a more homogeneous feedstock of consistent quality [33]. Furthermore, in comparison to raw biomass, torrefied biomass is more easily fluidizable and less likely to agglomerate[34].

Additionally, torrefaction lowers the O/C ratio of biomass [35]. It has been reported that fuels of lower O/C ratio, such as coal, can attain higher gasification efficiencies than fuels with high O/C ratios [36]. Classification is important when choosing biomass for thermochemical conversion because it enables us to infer the conversion

potential. The ratio of ligno-cellulose constituents and atomic ratios are the methods of classifying and ranking fuels. Atomic ratios are used to classify all hydrocarbon fuels. Figure 1-5 illustrates the variation in atomic ratios of H/C and O/C from biomass through peat, lignite, coal and anthracite, according to Van Krevelen who developed a diagram demonstrating the change in composition. From this figure, as the oxygen to carbon ratio decreases, the property of biomass tends towards that of coal. The ratio of O/C decreases with increasing geological age [37]. The energy content of fuel increases as a result of increasing carbon content.

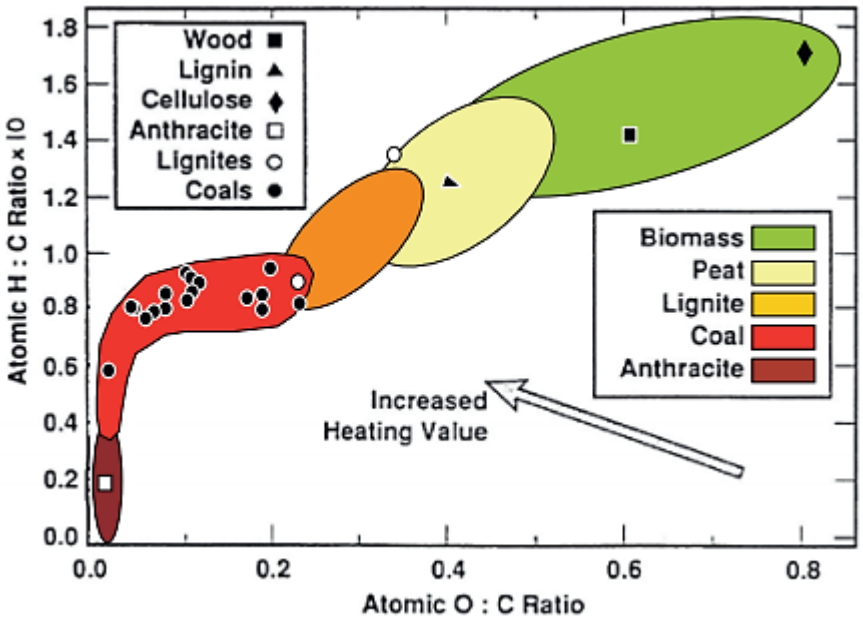

Figure 1-5 Van Krevelen diagram for different solid fuels[38]

Biomass consists of hemicellulose, cellulose, and lignin as the three major components, together with small amounts of other constituents such as minerals. Hemicellulose comprises 20-40 wt% of biomass while cellulose and lignin are composed of 40-60 wt% and 10-25 wt% on a dry basis, respectively [39]. According to Yang et al [40] who investigated the pyrolysis characteristics of the three main components of biomass (hemicellulose, cellulose and lignin) using a thermogravimetric analyser (TGA) with differential scanning calorimetry (DSC) capability, and it was concluded that hemicellulose was readily decomposed at

temperatures between 220-315℃; cellulose was pyrolysed at 315-400℃; while lignin decomposition covered a wide range of temperature 150-900℃ and was more difficult to decompose. More tar in the syngas is produced when the feedstock contains high concentrations of hemi-cellulose and lignin in the presence of moisture [41]. According to the same authors, they concluded that torrefaction of Miscanthus x giganteus reduces the moisture, hemi-cellulose and O/C ratio. In addition, it improves the porous structures and give larger specific surface area as well as a higher content of alkali metals.

The pre-treatment of biomass using torrefaction can be classified into light, mild and severe torrefaction conditions; the temperatures according to these conditions are approximately 200-235, 235-275 and 275-300℃, respectively [42]. The moisture and low molecular weight volatiles are released from biomass during light torrefaction, while cellulose and lignin are only partly or hardly affected [43]. For this reason, a small weight loss occurs accompanied by a slight increase in calorific value. In mild torrefaction, the volatile release is intensified, and hemicellulose is basically consumed while cellulose is also decomposed to a certain extent. Hemicellulose is completely consumed during severe torrefaction, and cellulose is oxidized to a large extent. Lignin is less affected by thermal decomposition under these conditions. In addition to temperature, the duration of torrefaction is also another important factor in calculating the performance of torrefaction. Residence time for torrefaction is claimed to be anywhere between a few minutes and 3 h [44, 45]. Residence times reported have generally been relatively long (30 min to 3 h), and this may not be feasible in a commercial scale reactor because investment costs increase with longer residence time due to the increase in plant size requirements [46]. Therefore, in this study 30 min was used only.

For thermochemical conversion of biomass, torrefaction is considered an effective pre-processing method because it relies on heat-related treatment of the biomass at temperature range (200-300℃) in an inert atmosphere to increase the volumetric energy density, which can enhance the biomass conversion efficiency during gasification. Torrefied biomass is expected to have a better combustion stability than raw biomass, similar to that of coal [47]. Also, the torrefaction of biomass improves the fluidisation characteristics according to Bergman et al. [48]. The main goal of the gasification process is to produce a combustible gas rich in H_2, CO and CH_4 with a

medium to high LHV, making the product suitable for exploitation in internal combustion engines and turbines and this could be achieved by using biomass with higher heating values [49].

1.2.2 Pyrolysis process

Pyrolysis is one of a thermochemical conversion methods has been used to convert the feedstock such as biomass into bio-oil and bio-char [50]. When biomass is used as a feedstock, gas, bio-oil, and bio-char are the common products, as shown in Figure 1-6. Aside from being a significant process in itself, it is considered the essential first step in carbonization, gasification and combustion of biofuel [51]. The gas composition comprises mainly CO and CO_2, with lower amounts of H_2 and low hydrocarbons.

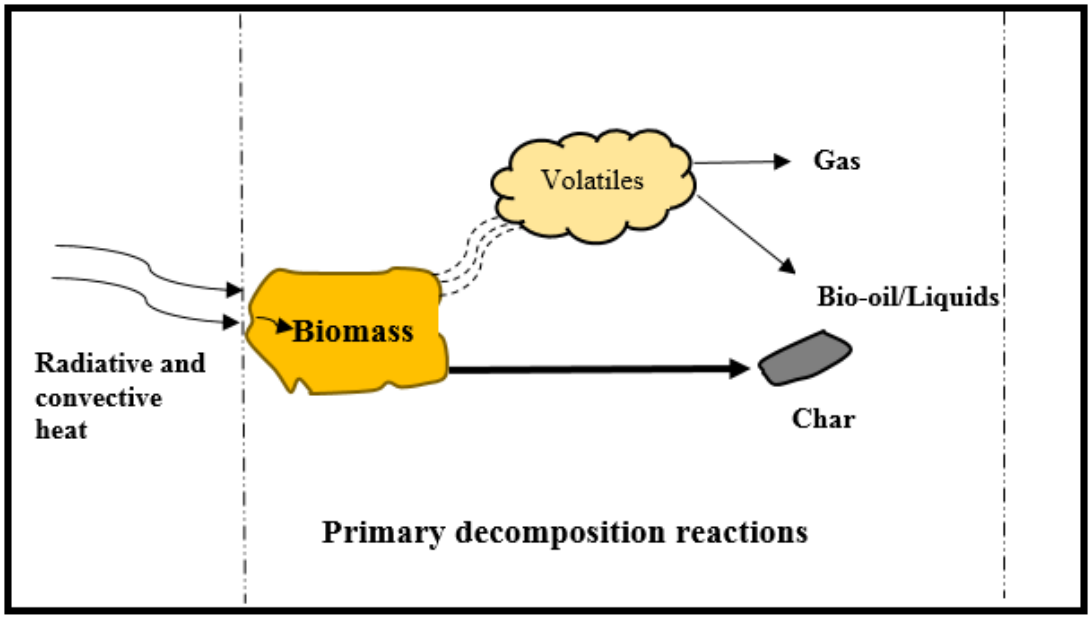

Figure 1-6 Pyrolysis in Biomass Particle

Pyrolysis takes place in the absence of oxygen and typically at temperatures exceeding 300°C. Pyrolysis products mainly depend on operating conditions such as temperature, heating rate and residence time, which are adjusted based on the desired product. High heating rates, moderate temperature and short residence time are the characteristics of fast pyrolysis, which leads to the production of liquids and volatiles more than char

[52]. Fast pyrolysis provides a liquid fuel which can substitute fuel oil in any static heating or electricity generation application. Furthermore, a range of speciality and commodity chemicals can be produced from this liquid [53] . The sector of producing liquid fuels from biomass started to develop since the oil crisis in the mid-1970s. The liquid fuels produced possess many advantages over the original biomass in terms of transportability, ease of storage and conveyance into reactors [54], which is favourable when the energy required is remote from biomass resources [55]. The pyrolysis liquid is homogeneous, but has around 50% of the heating value of conventional fuel oil.

Slow pyrolysis or conventional pyrolysis is a process that takes place at a low heating rate. It has been used for thousands of years, mainly for charcoal production. However, the slow heating rate and long residence time lead to high char yields with moderate liquid production [56].

The reactor is considered the heart of the fast pyrolysis process. The cost of the reactor is about 10-15% of the overall capital cost of an integrated system. Based on a variety of feedstocks, different reactor configurations have been developed and tested such as ablative pyrolysis, bubbling fluidised beds, circulating fluidised beds, vacuum pyrolysis, screw and augur kilns, fixed bed, microwave, and hydro-pyrolysis [57]. However, fluidised beds and circulating fluidised beds are the most popular configurations due to their ease of operation and ability to be scaled-up.

1.2.3 Combustion

Combustion is an exothermic chemical reaction which occurs between fuel and oxidant accompanied by large heat generation, which leads to the spontaneous reaction, driven by energy from the heat generated [58]. The main products of biomass combustion are CO_2 and H_2O with heat and a visible flame [59]. These gases are produced at temperatures of around 800-1000°C. Any type of biomass can be burned in this temperature range, but realistically only biomass less than 50% in moisture content is feasible otherwise pre-drying is necessary [60]. Oxygen deficiency leads to incomplete combustion, along with the formation of products related to these conditions. On the other hand, excess air chills combustion reactions. The amount of air required for combustion depends on the chemical and physical characteristics of

the biomass. Biomass combustion relates to the fuel burn rate, firing temperature, combustion products, and required excess air for complete combustion [11].

In principle, the utilisation of biomass and waste is divided into two routes in the power industry: the first is using biomass as a single fuel in combined heat and power plants of limited capacity as shown in Figure 1-7 [61] and the second is co-utilisation in existing coal fired power stations [62] which reduces cost and emissions (SO_X and NO_X), and improves efficiency. However, greater formation of deposits in the boiler due to undesirable changes of ash composition occurring from biomass means that attention must be paid to the amount of biomass used in combustion. Biomass fuel input occupies approximately 10% of total fuel input [63]. The coal/biomass blends of the co-combustion process will help to reduce the consumption of fossil fuels. Occasionally the coal is mixed with biofuel products to achieve good control of the burning process. A volatile matter content higher than 35% is sought to supply a stable flame during co-combustion, and this can be attained by using biomass [64].

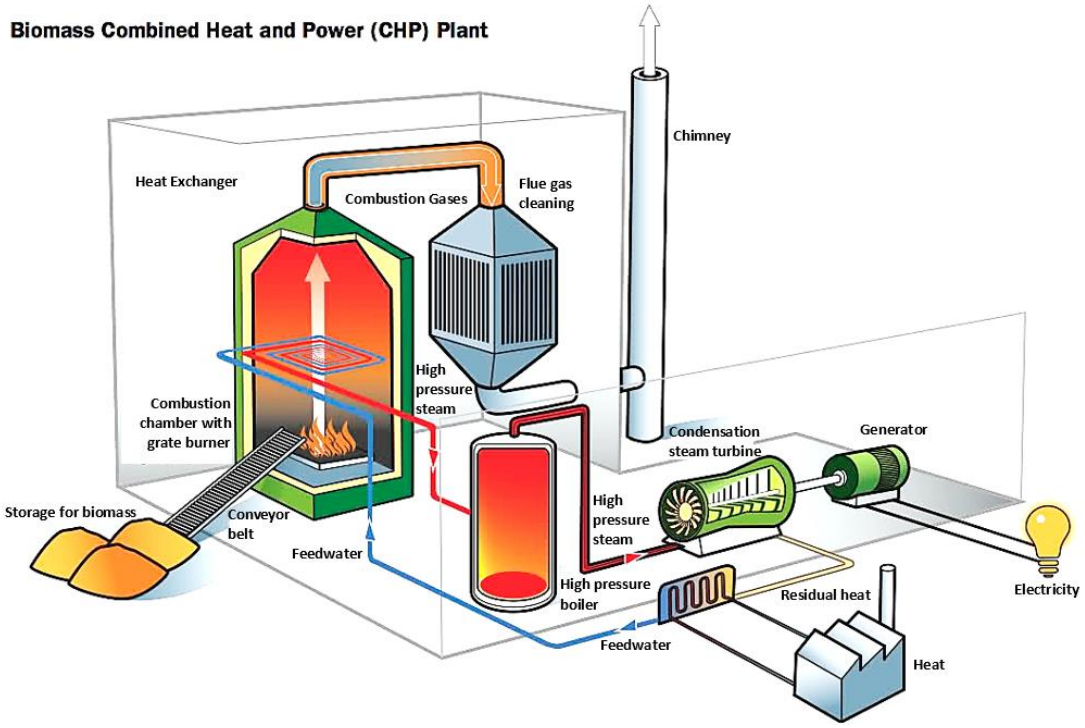

Figure 1-7 Biomass for power generation and combined heat and power (CHP) [61]

1.2.4 Gasification

Gasification is a thermochemical process in which biomass or any feedstock undergoes partial oxidation reaction with an oxidizing agent such as (air, steam, oxygen or carbon dioxide) to obtain gases that can be used for different applications. Therefore, gasification is defined as a process that comprises the conversion of any carbonaceous material to product gases. Combustion is not included in this definition because the flue gas produced does not possess any residual heating value. Gasification, under certain practices (integrated gasification in combined cycles with engines, turbines, etc.), leads to higher overall efficiencies (45-50%) compared to that usually achieved via combustion (25-35%) [21]. It is possible use low value biomass as a feedstock and convert it, not only into electricity but also, into fuels for use in transportation. Gasification is predicted to become a major technology for global energy supply [65].

Gasification is considered one of the most efficient routes by which solid biofuel is converted totally or partially into gases. Historically, the first commercial gasifier for continuous air-blown gasification of solid fuels was installed in 1839, yielding what is currently known as product gas. Gasifiers were then modified for different sectors such as heating applications and industrial power up to the 1920s, after which oil-fueled systems gradually took over the systems that were once fueled by product gas [66].

In response to increasing prices of fossil fuels and increasing awareness about climate change, gasification technology has returned to become more important and reliable, along with access to widely available feed-stocks and low operating costs when compared with fossil fuels. Gasification is carried out at different temperatures, (500-1400°C), and pressures (from atmospheric reach up to 3.3 MPa). Carbon monoxide, carbon dioxide, nitrogen and hydrogen are the main constituents of the product gas from gasification. Poor-quality gas by air gasification with heating values between 4-7 MJ/m^3 is suitable for boiler, engine and turbine operation, however, it is not suitable for pipeline transportation because of its low energy density. High quality gas is

obtained by using oxygen as gasification agent with heating values between 10-18 MJ/m^3 which makes it suitable for use as synthesis gas for conversion to, for example, methanol and gasoline. Gasification based on air is widespread because this avoids the risk and costs associated with oxygen production and usage [67].

1.3 Hypothesis and Objectives of this study

The use of biomass is seen one of the solutions to tackle climate change. In order to use it effectively at commercial scale, the kinetic and thermal properties need to be understood. Currently, it is possible to use a bench top TGA for this purpose, but this has its limitations. Hence, this study is concerned with the design of a novel thermogravimetric fluidised bed reactor (TGFBR) and subsequent testing of biomass within. It is proposed that the TGFBR overcomes some of the limitations of a traditional TGA by testing larger quantities of sample in an environment that is representative of industrial gasifiers. [***The goal of this research*** *is to understand reaction kinetics of biomass conversion in a bubbling fluidised bed. To achieve this goal a TGFBR was developed and applied to several pyrolysis and gasification experiments which use olive kernels and palm stones as the feed material*]. The following paragraphs elaborate upon this introduction.

The thermogravimetric method is considered to be the most accurate way to determine the kinetic parameters, and suitable for reactions in which there is no solid product such as gasification reactions, and can be used for several gas-solid reactions without recalibration [68].

Bench top TGA analysis of kinetics is a rapid and valuable method for comparing the behaviour of biomass reactivity, but the small sample sizes tested and low heating rates place limits on the relevance of results. Other authors have noted the effect of the heating rate on the reaction kinetics in a TGA, which limits how comparable these results are with high heating rate systems such as fluidised bed or circulating bed gasifiers [69].

Therefore, the potential of using biomass in an industrial application is still challenging and needs more investigation. This highlights the need to develop efficient energy conversion systems that have the ability to provide reliable kinetic data for

industrial applications through: reducing the diffusion rate limitation; quick heating for isothermal conditions; and testing using gravimetric analysis. Pilot plant bubbling fluidised bed reactors fitted with load cells allow detailed measurements at conditions likely to be more representative of those encountered on large scale systems where heat distribution, heat transfer and mass diffusion effects play a major role in the reactivity of biomass.

This experimental investigation focuses on biomass pyrolysis and gasification. The major **objectives** have been to:

- Build a thermogravimetric fluidised bed reactor (TGFBR) equipped with built-in load cells for the dynamic measurement of biomass conversion characterised by rapid heating rates at high flow rates and uniform temperature distribution inside the bed.
- Study and compare the kinetics of olive kernels pyrolysis in isothermal conditions at high heating rate by using TGFBR, and non-isothermal conditions at low heating rate using fixed bed thermogravimetric analysis (TGA).
- Study the effect of operating conditions such as temperature, equivalence ratio, bed height and particle size of biomass in a bubble fluidised bed on the product gases. Upgrade the olive kernel properties via torrefaction and compare the gasification performance with the raw olive kernel.
- Evaluate the kinetic parameters of gasification of raw and torrefied olive kernels in TGFBR and identify the reaction mechanisms that explain the best experimental results. The significance of this study is to implement a gasification test for biomass with air in the TGFBR under minimised limitations from mass and heat transfer.
- Study the kinetics of palm stone pyrolysis in TGFBR and investigate the potential of using Iraqi palm stones in a gasification process to evaluate their usefulness for energy production.

1.4 Thesis Overview

This work is presented in the following chapters.

Chapter 1: In this chapter, the general overview of climate change and alternative resources are highlighted. The thermal conversion processes are described briefly. The hypotheses, objectives and thesis structure are also described.

Chapter 2: The concept of the gasification process and its reactions are described. The influence of gasifier operating conditions on the product gas is presented. The technologies used in the gasification process are explained; these include fixed bed and fluidised bed.

Chapter 3: A brief description of homogeneous and heterogeneous reaction rate; thermal degradation kinetics under isothermal and non-isothermal conditions; and the factors that affect inadequacy of kinetic data obtained from TGA. Also, a literature review of previous work in kinetics.

Chapter 4: The materials and methods to characterise the biomass and silica sand are explained. The method of determining the minimum fluidised bed velocity and terminal velocity are presented. In addition, the methods of pyrolysis, torrefaction, and char yield of pyrolytic biomass are described in detail.

Chapter 5: In this chapter, the details of the experimental rig are described. The procedures that were used during the gasification test are explained. The mass balance model and equations used in gasification performance are presented.

Chapter 6: The results and discussion of the pyrolysis of olive kernels including the kinetic study in a fixed bed TGA, and fluidised bed reactor under isothermal and non-isothermal conditions, are presented in this chapter.

Chapter 7: This chapter shows the results and discussion of the isothermal kinetic study of raw and torrefied olive kernels in a fluidised bed reactor. In addition, the effect of operating conditions on gasification performance is discussed.

Chapter 8: This chapter shows and discusses the thermal decomposition and kinetic study of palm stones in a fluidised bed reactor under isothermal conditions. The effect of operating conditions on gasification performance, and the overall mass balance and carbon mass balance, are presented.

Chapter 9: Concludes the findings from this study and recommends further work to be done in the field of pyrolysis and gasification to improve the gas yield and heating value.

Chapter 2

LITERATURE REVIEW

The first section of this chapter highlights gasification concepts and its reactions. The difference between product gas and syngas from the gasification process are presented in Section 2.2. The impact of operating conditions such as ER (equivalence ratio), temperature, bed height, gasification agent, and particle size on gasification performance are detailed in Section 2.3.1. Finally, in Section 2.3.2, the types of gasifier used in a gasification processes are reviewed, including fixed bed and fluidised bed.

2.1 The gasification concept and reactions.

Gasification is a way to convert biomass into more easily utilised compounds for renewable fuels or chemicals. Gasification occurs at a high temperature in an oxygen lean combustion atmosphere. The heat required to sustain the gasification reactions can be supplied from outside the gasifier but is normally generated by burning a part of the biofuel.

Gasification of biomass consists mainly of two steps as shown in Figure 2-1. Pyrolysis (an endothermic reaction) plays an important role as the first chemical step in gasification and combustion. Pyrolysis product yield and compositions are dependent on several important factors, which include the biomass species, chemical and structural composition of biomass, particle size, temperature and heating rate [70]. Both temperature and heating rate are highly affected by pyrolysis conditions, for example, when pyrolysis occurs under high heating rate a more reactive char is produced for both combustion and gasification [71].

Pyrolysis occurs at temperatures higher than 300 °C where the moisture and most of the volatile components are released as H_2, CO, CO_2, CH_4, and tar; this is known as devolatilization. Typically, biomass produces 70-86% of volatile materials in the form of gases and liquids. The remaining non-volatile material is called char; it mainly contains carbon and ash [72]. The liquids consists mainly of large condensable

molecules (phenol and acids) called primary tars, which are saturated by oxygenated compounds that give its high reactivity.

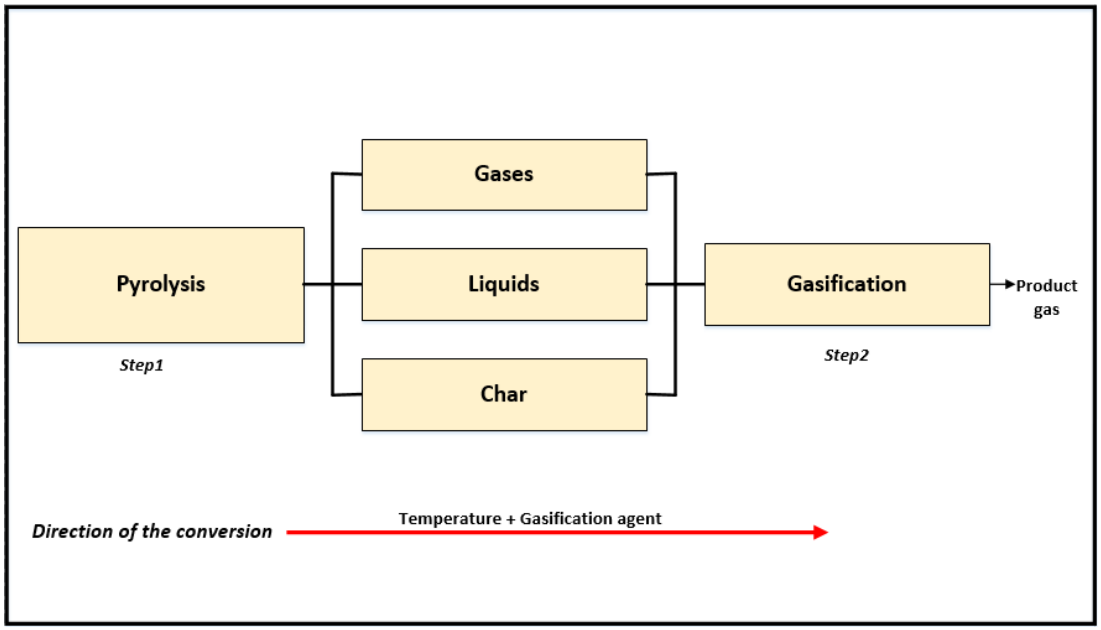

Figure 2-1 Gasification Process

In the presence of a gasifying agent and relatively high temperature, the volatile components and char obtained from the first step are continuously converted into a product gas or bio-syngas depending on the temperature of the second step. For example, the proportion of H_2 and CO increases with temperature while CO_2 and CH_4 decreases [73]. Gasification includes a series of exothermic and endothermic reactions. The thermal energy required for the endothermic reactions is obtained from combustion of part of the fuel, char or gases, depending on the reactor design. The selection between air or oxygen as a gasification agent affects whether the product gas or bio-syngas contains nitrogen. Generally, the aim of the gasification process is to obtain the maximum yield of hydrogen and carbon monoxide in the product gas by using air, oxygen and steam as a gasification agent [74].

The gas, liquid and solid products of pyrolysis react among themselves as well as with the gasifying agent to produce the final gasification product [75]. The majority of these reactions take place inside the reactor, but some may occur in the downstream gas depending on the residence time and temperature. The main gasification reaction is that of carbon. Instead of burning it completely, the carbon can be gasified by

restricting the amount of oxygen supply. The carbon then produces 72% less heat than in combustion (heat of combustion of carbon is -393.7MJ/kmol). The product of incomplete combustion is CO gas, which when subsequently combusted in sufficient oxygen, produces the remaining 72% (-283 MJ/kmol) of heat. Therefore, the CO holds only 72% of the energy of the carbon, but in adequate gasification, the energy recovery can reach 75 to 88% owing to the 'lost' 28% of energy from the incomplete carbon combustion giving energy to the endothermic production of hydrogen gas and other hydrocarbons [75]. From the above it can be concluded that typical gasification of biomass might involve the following:

- Drying.
- Pyrolysis or thermal decomposition of biomass (fast step).
- Combustion of some volatile material and char to sustain the reaction.
- Gasification of decomposition products.

The gasification step that occurs after pyrolysis involves heterogeneous reactions (gas-solid) and homogeneous reactions (gas-gas) among the hydrocarbons in the biomass as well as the evolved gases. The produced gas from the gasification process is the result of a series of endothermic and exothermic chemical reactions taking place between carbon in the char and carbon dioxide and steam and hydrogen in the reactor. These reactions are strongly dependent upon operating parameters such as temperature and pressure. In addition to pyrolysis, fundamental chemical reactions occurring in the gasifier are described in the following section.

2.1.1 Water-gas reaction

The water-gas reaction is a heterogeneous reaction that occurs between carbon and superheated steam at high temperatures ($C+H_2O \rightarrow H_2+CO$), the gaseous products are a mixture of carbon monoxide and hydrogen, known as synthesis gas. The water-gas reaction is endothermic so the biomass fuel must be continuously heated to maintain the reaction.

2.1.2 Water-gas shift reaction

The water-gas shift reaction is a homogeneous reaction occurring between water vapour and carbon monoxide ($CO+H_2O \leftrightarrow CO_2+H_2$). It can be used to reduce the

carbon monoxide and increase the hydrogen content in the product gas. The water-gas shift reaction is an exothermic reversible reaction sensitive to temperature.

2.1.3 Boudouard reaction

The Boudouard reaction, is a highly endothermic reaction between carbon and carbon dioxide ($C+CO_2 \rightarrow 2CO$). At high temperatures (>700 °C), the free energy change becomes negative, making the formation of carbon monoxide gradually more favored [76].

2.1.4 Methanation reaction

Methanation reaction is classified as the exothermic reaction between carbon and hydrogen or carbon monoxide and hydrogen to produce methane gas, which is favoured gas due to its higher heating value. In order to promote methane production as based on Le Chatelier's principle, low temperature and high pressure should be used [77].

2.1.5 Char Combustion reactions

In order to provide the required heat for endothermic reactions, drying and pyrolysis, a certain amount of exothermic combustion is required in the gasifier. The combustion of biochar particles occurs after devolatilization in the gasifier. During gasification, oxygen is transported from the main stream of gas to the char particle surface. If sites of active carbon are not available on the char particle surface, the oxygen will diffuse inside through the pores until facing an active site of carbon. According to Lee et al, the formation of CO and CO_2 during char combustion depends on particle size. For small char particle sizes, the CO formed during combustion diffuses out quickly, while for large char particles, the CO gas burns within the boundary layer of the particle and CO_2 is transported out as a result of slow diffusion [78].

The above describes the common reactions involved during gasification. However, the heterogeneous reactions in gasification are slower, which govern the overall conversion rate [79]. According to Basu et al. [75], the char reactivity and the reaction potential of the gasifying agent are the main two factors that affect the rate of char gasification. For example, oxygen is more active than steam and CO_2. Therefore, the rate of the char-oxygen reaction ($C+0.5O_2 \rightarrow CO$) is the fastest of the heterogeneous

reactions. The relative rates, R, may be explained as $R_{C+O2} >> R_{C+H2O} > R_{C+CO2} >> R_{C+H2}$. As the char gasification rate is much slower than the pyrolysis rate, the operation and design of gasifiers are basically dependent on the gasification of char [80].

2.2 Product gas and biosyngas from biomass gasification

The gases produced from gasification differ from those produced by combustion where the product gas has a low heating value due to the complete oxidation, Whereas gasification converts the intrinsic chemical energy of the carbon in biomass into a combustible gas with high heating values. Combustible gases can be standardised in terms of quality making them easier and more universal to use than the parent biomass. Applications include energy for gas engines and gas turbines, or use as a chemical feedstock to produce liquid fuels [81].

Regarding the utilisation of gases from gasification, it is worth mentioning that gas specifications are different for the diverse gas applications. Gasification gas composition mainly depends on the type of process, gasification agent and temperature [82]. Based on the general composition and typical applications, there are two major types of gasification gas, namely product gas and biosyngas, as illustrated in Figure 2-2 [83].

- **Product gas**: this is sometimes called (raw) biosyngas [84]. It consists mainly of CO, H_2, CH_4, C_XH_Y aliphatic hydrocarbons, benzene, toluene and tars as well as H_2O and CO_2. About 50% of the energy in the syngas is found in H_2 and CO. Product gas is produced when the reactor temperature during gasification is less than 1000 °C. The product gas is mainly used directly for power generation and heat. This can either be in stand-alone combined heat and power (CHP) plants or product gas co-firing in large-scale power plants. The focus in the study is on product gas because a gasifier works at a temperature below 1000°C.

- Bio syngas: can be obtained from non-catalytic gasification of biomass at a high temperature (approximately more than 1200°C), or catalytic gasification which requires much lower temperatures. Under both circumstances biomass is completely converted into bio-syngas, which is rich in H_2 and CO with small amounts of CO_2 and CH_4 [17]. The non-catalytic route requiring high temperature generally involves an entrained flow gasifier. The catalytic route involves a fluidised bed gasifier with a

downstream catalytic reformer, typically operating at 900 °C. The purpose of the catalytic reformer is to convert hydrocarbons into hydrogen and carbon monoxide [85]. Thermal cracking or catalytic reforming of product gas can also create bio syngas. This syngas can be used to produce organics molecules such as synthetic natural gas (CH_4) or liquid biofuels such as synthetic diesel (via Fischer-Tropsch synthesis) after it has been cleaned of impurities and tar.

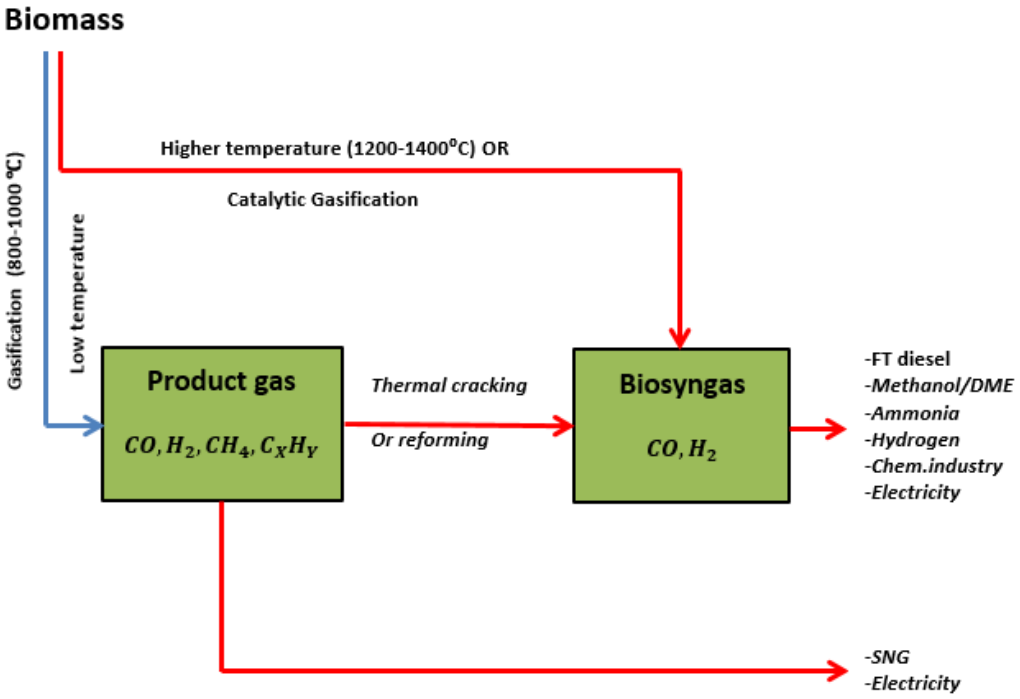

Figure 2-2 Difference between biosyngas and product gas and their typical applications

2.3 The parameters effect on product gas

Product gas quality encompasses composition, energy content and gasification performance, which relies upon feedstock origin, gasifier configuration, and operating conditions [86]. It is important to understand which parameters influence the quality of the product gas. A number of gasification parameters will be explained, and some will be verified with experimental work.

2.3.1 Operating conditions

The operating conditions play a significant role during biomass gasification in all aspects, for example, carbon conversion, tar formation, tar reduction, and product gas composition [82]. The operating conditions of: temperature, ER, gasification agent, feeder location, static bed height, and particle size are described briefly in the following section.

2.3.1.1 Bed Temperature

The composition of product gas depends on the operating temperature of the reactor because all of the chemical reactions are temperature dependent. As explained previously, a series of endothermic and exothermic reactions take place in gasification. Increasing the gasifier temperature significantly increases the combustible gas content, heating value, gas yield, and hydrogen content, meanwhile the tar content is dramatically reduced. In addition, the higher bed temperatures improve secondary cracking and reforming of heavy hydrocarbons [87]. Narvaez et al. [88] showed that as temperature was increased from 700°C to 800°C the H_2 content doubled; CO rose from 12 to 18 vol %; there was a slight decrease in CO_2; and a drastic reduction (about 74%) in tar content. Another author found that the hydrogen initially increased with temperature, reached a maximum, and then gradually decreased at the highest temperature [89]. Increasing the temperature inside the reaction zone increases the gas yield and decreases its heating value, even when various feedstocks are used, because the high temperature eliminates some of the hydrocarbons [90]. Wilson et al. [91] studied coffee husk gasification using air/steam agent at high temperatures; the study revealed that high temperature improved the gasification process. It was also reported that increasing the reaction temperature led to a linear increase in the CO concentration in the produced gas for all gasification conditions. Gas composition from eucalyptus wood chip gasification was studied at different bed temperatures. The results revealed that CO and H_2 increased with temperature as a result of the promoted endothermic water-gas and Boudouard reactions, while CO_2 decreases, meanwhile CH_4 concentration did not change significantly [92]. However, from an overall process perspective, the risk of ash agglomeration is likely to increase with temperature, which practically, may limit gasification up to 750°C [93].

2.3.1.2 Equivalent Ratio ER.

The equivalence ratio (ER) is defined as the chosen ratio of the air or oxygen to fuel mass flow rate divided by that required stoichiometrically for complete combustion. It is a dimensionless factor used in the thermal conversion process.

ER is a significant factor in air-blown biomass gasification performance. When the equivalence ratio is plotted versus temperature as in Figure 2.3, the different thermochemical zones that can be visualised are pyrolysis, gasification, and combustion. The ER value is a significant factor dictating the quality of biomass gasification product gas. Lv et al. [94] reported that with the variation of ER in the gasifier, temperature level is controlled by the interaction between endothermic and exothermic reactions. Hence, when the ER is too low, the temperature in the gasification zone is low, which is unfavourable for further gas producing reactions so the H_2 yield drops. When the ER value is too large, oxidation reactions are strong, which produces more CO_2 gas, but less H_2 gas. Therefore, the ER can improve the product quality to a certain extent.

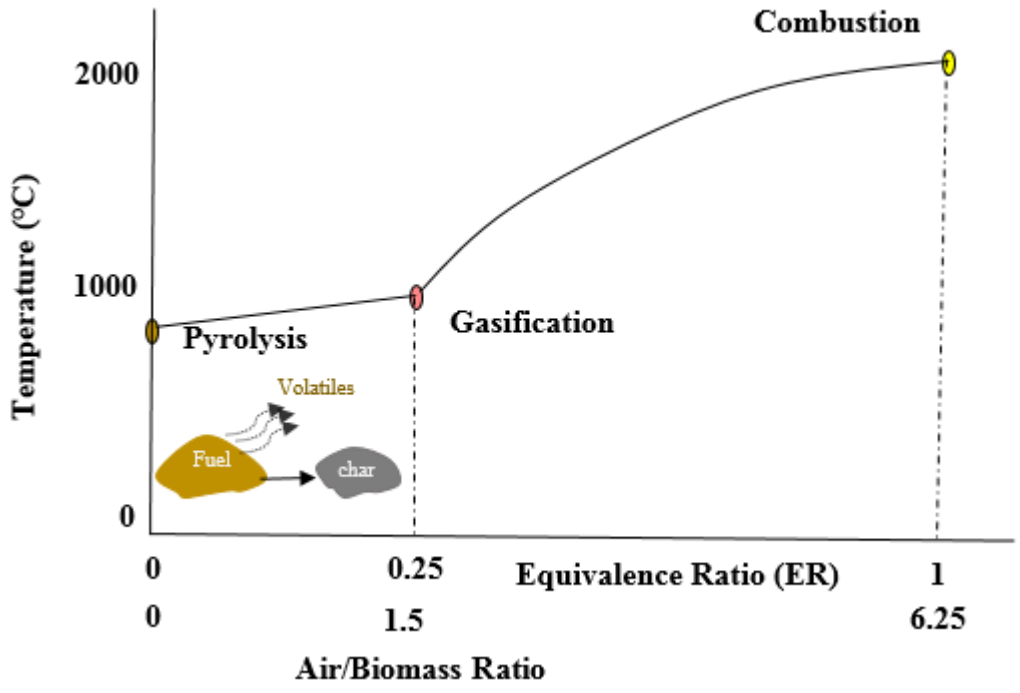

Figure 2-3 Equivalence Ratio and Air/ fuel diagram

Increasing the ER causes the heating value of the product gas to decrease due to the high percentage of CO_2 gas present as a proportion of the yield [88]. The concentration of CO and H_2 decrease with increase ER, while CH_4, C_2H_2 and C_2H_4 are not significantly impacted. CO_2 increases with ER due to increasing partial oxidation as well as char oxidation [95]. CO_2 increase coupled with H_2 and CO decrease, as ER is increased, was observed during the gasification of pine wood in a bubbling fluidised bed [96]. Skoulou et al. [97] studied the effect of ER on the quality of product gas from olive kernels, and as mentioned, H_2 and CO decreased due to an increase in oxidation (combustion) inside the gasifier, as ER was raised. At high ER, a lower heating value for product gas was obtained due to dilution with N_2 gas, in addition to enhanced oxidation reactions. Further increasing the ER (exceeding 0.4) results in excessive formation of the products of complete combustion. For example, the formation of CO_2 and H_2O at the expense of desirable products such as H_2 and CO [98]. Per the same author, the carbon conversion efficiency increases for ER up to 0.26, and then it starts to drop.

In gasification, the energy required to sustain the endothermic reactions is obtained by limited combustion of the biomass. Equivalence ratio determines the fraction of biomass that is gasified and the fraction that is combusted. For biomass gasification, the ER range is typically between 0.2 to 0.4, according to the literature. The optimum ER should supply sufficient air for partial oxidation of biomass and self-sustain the process without significantly affecting the product gas yield (H_2 and CO) [89].

2.3.1.3 Gasification Agent

The oxidizing agent has a significant effect on the heating value of gas produced. The heating value and hydrogen gas content of syngas are higher when gasification of biomass or coal occurs with steam than when it occurs with air [96]. However, steam is the most commonly used *indirect* gasification agent and it needs an external energy source to maintain the reaction temperature, while oxygen and air are used in *direct* gasification because the oxidation reactions provide the energy required to sustain the temperature of the reaction [99].

As illustrated in Table 2-1 [99], the product gas heating value is influenced by the gasification agent. Indirect gasification (using steam) yields the highest heating value in the product gas resulting from the absence of nitrogen from the gasification agent. Gasification with pure oxygen has similar advantages to steam gasification. However, the cost of oxygen production is estimated to be more than 20% of the overall electricity production [99]. Oxygen is known to be the best gasifying agent; however, using oxygen is more costly. Moreover, with high amounts of oxygen, the gasification process shifts to combustion and the resulting product instead of being "fuel gas" becomes "flue gas" [100]. Direct gasification with air results in a product gas of lower heating value to the presence of nitrogen in the air which acts as a diluent.

Table 2-1 Gasification processes with various gasification agents [99]

Process	Gasification agent	Product gas heating value (MJ/Nm^3)
Direct gasification	Air	4-7
Pure oxygen gasification	Oxygen	10-12
Indirect gasification	Steam	15-20

Gil et al. [96] carried out gasification experiments using pine wood in a bubble fluidised bed gasifier. They set out to study the effect of the gasification agent on product distribution (gas, char, and tar yield). A relationship between ER, steam to biomass ratio (SB), and steam plus O_2 to biomass ratio termed as gasifying ratio GR are mentioned for comparison by the authors of the paper. Under selected conditions, more tar is formed with steam, than with a steam–O_2 mixture and the least with air as a gasifying agent. However, gasification with air gave the lowest heating value.

2.3.1.4 Location of Feeding

The distribution of product gas is affected by the location of biomass feeding. According to Corella et al. [101], there is a big difference between feeding at the top or the bottom of the gasifier. Pyrolysis products pass through whole bed when the biomass is fed to the bottom of the bed and this provides good mixing of the product gases. Furthermore, the yield of the stable gases is increased due to the increased occurence of tar cracking throughout the bed, which also means that the product gases have lower tar contents. However, the heating value of product gas may reduce due to

combustion of the gases and this is because the region near to a bottom feed point is still rich in oxygen gas. In the case of feeding of biomass from the top of the bed, the gas phase, including tar does not flow through the hot bed, therefore, there are higher tar contents with top feeding [102].

Not only is the product distribution different for top and bottom feeding, but also, the emission levels of nitrogen oxides. Bottom feeding has been found to generate higher NH_3 and NOx than top feeding, when gasifying biomass [103]. In addition, top feeding is less mechanically complex than bottom feeding which also suffers from issues where the erosion of sand at the screw feeder leads to more carryover of fines from the bed [88]. To avoid the above, feeding from the top was selected.

2.3.1.5 Bed height

Regarding bed height selection, it is necessary to ensure a sufficiently high residence time of the biomass to provide good carbon conversion in the bed. However, the bed height has limitations due to the economic aspect (high beds lead to higher pressure losses and higher reactors) and fluidization dynamics such as a slugging flow which causes not only inadequate mass transfer but also might lead to mechanical failure of common support structures [104]. When the ratio of static bed height to diameter is increased beyond 2, channelling is observed due to the mesh forming tendencies of particles [105]. On the other hand, when bed height is increased, H_2, CO, CO_2, CH_4 and C_2H_4 concentrations increase. A long residence time means more heat transfer and, hence an increase in the amount of char and tar conversion to product gas. For a given fluidizing velocity, increasing the static bed would extend the product's residence time in the high temperature reaction zone. This will promote secondary cracking of heavy hydrocarbons such as tar and char, which will lead to an increase in gas yield [106]. According to Sadaka et al. [107], conversion efficiency is greater with a higher bed height. However, lower bed temperature was noticed due to the fly-wheel effect of the bed material. When the amount of bed material is reduced, the fly-wheel effect is significantly decreased and higher bed temperatures are obtained.

The carbon and cold gas efficiencies increase with increasing residence time [108]. Hernandez et al. [109] reported that when the residence time increases inside the gasifier, the CO and H_2 contents, cold gas efficiency, gas low heating value, and fuel conversion are improved. Font et al. [110] reported increases in CO, H_2, CO_2, and CH_4

when the residence time was increased by increasing the bed height. In this study, the target bed height is 0.5D.

2.3.1.6 Biomass particle size

In addition to the gasifier operating conditions as described above, biomass properties such as particle size, moisture content, and ash content can influence the product gas quality. In this study, we focus only on the effect of particle size. In a gasification process, it has been known that the overall energy efficiency increases significantly with smaller particle sizes, but it also increases the gasification process cost. According to some studies, about 10% of the output energy is required to reduce the particle size for a 5-10 MWe gasification plant [111]. On the other hand, pre-treatment cost of biomass is reduced as the particle size increases, however, devolatilization time increases, and thus for a defined throughput, the gasifier size increases [49]. Therefore, all these factors should be considered in the gasification process.

Product yield and product composition from pyrolysis are dependent on the heating rate of sample particles. Higher heating rate leads to an increase in the amount of light gases and a reduction in char and condensate substances. Smaller particles contribute to a larger surface area and a faster heating rate [112]. At the same bed temperature, Luo et al. [113] studied the effect of particle size on pyrolysis. They report that the smaller particle size produced more gas compared to the larger particle size because of high heat transfer resistance in the large particle, hence the actual temperature inside the particle is lower. The heat transfer in biomass particles is improved with smaller particle sizes. Maa and Bailie [114] found that there was chemical reaction control for sizes less than 0.2 cm, and for sizes 0.2-6 cm both chemical reaction and heat transfer controlled. Exceeding 6 cm, heat transfer controlled the pyrolysis of cellulose material. As the particle size increases, not only does heat transfer control but also diffusion controls, since the resultant product gas inside the particle has more difficulty in diffusing out.

The H_2 and CO contents increase with a decrease in particle size, according to as investigated by Yin et al. [115] into the effect of biomass particle size on the gasification performance in a downdraft fixed bed gasifier. Also, the low heating value of the gas decreases slightly with increasing particle size. Three types of biomass (grape marc, sawdust wastes and grapevine prunings) were tested by Hernandez et al.

[109] to investigate the effect of particle size in an entrained flow gasifier and it was concluded that reduction in the biomass particle size leads to improvement in gasification performance. Lv et al. [116] studied the effect on product gas quality of biomass particle size in four ranges of 0.6-0.9 mm, 0.45-0.6 mm, 0.3-0.45 mm and 0.2-0.3 mm. It was concluded that small particle sizes produced more CO, CH_4 and C_2H_4 and less CO_2 in comparison to large particles. For biomass gasification, smaller particles were more favourable for gas quality and yield. Jand et al. [117] observed during a study of the effect of wood particle size in fluidised bed gasification that increasing particle size reduced the CO and carbon content of the product gas, while CO_2 content and the amount of char increased. The increase in CO_2 was justified by the tendency of the large particles to undergo char combustion, which accelerates the release of CO_2.

2.3.2 Gasifier Design

Gasification technologies have recently been used successfully on a large scale for biomass. However, real operational experience is restricted, and more trust in the technology is required. In addition, flexible gasifier designs are required so that different varieties of fuels can be used in gasification process efficiently. Typically, the gasification process consists of three basic elements: (1) the gasifier is used to produce combustible gases; (2) a clean-up process is used to remove contaminant material such as tar and sulphur from the combustible gases; (3) energy recovery systems. In this study, only the gasifier design will be considered due to time constraints.

The gasifier is the reactor in which the feedstock (e.g. biomass) is converted into gases such as H_2, CO, CO_2, CH_4 and tar in the presence of a gasification medium. Gasifiers can be classified depending on the relative movement and type of contact between biomass, gasifying agent and product gas [107].

Gasifier design influences the level of tar produced in the product gas. For instance, a counter current moving bed gasifier with internal recycling and a separate combustion zone can drastically reduce the tar amount to less than 0.1 g/Nm^3, while the tar content can exceed 100 g/Nm^3 when an updraft gasifier is used [75]. Table 2-2 shows the product gas composition of dry wood that was tested experimentally in four types of gasifier; the gasification agent was air [90]. This table gives us an indication that

gasifier type is important to improve product gas quality and the amount of tar; tar reduction reduces the cost of gas clean-up.

Table 2-2 Characteristics of the produced gas for atmospheric gasifiers (dry wood) [90].

Property	Downdraft	Updraft	BFB	CFB
$Tar\ (mg/Nm^3)$	10-6000	10000-150000	Not defined	2000-30000
$LHV\ (MJ/Nm^3)$	4.0-5.6	3.7-5.1	3.7-8.4	3.6-5.9
$H_2\ (vol\%)$	15-21	10-14	5-16.3	15-22
$\mathrm{CO}\ (vol\ \%)$	10-22	15-20	9.9-22.4	13-15
$CO_2\ (vol\ \%)$	11-13	8-10	9-19.4	13-15
$CH_4(vol\ \%)$	1-5	2-3	2.2-6.2	2-4
$C_nH_m\ (vol\ \%)$	0.5-2	Not defined	0.2-3.3	0.1-1.2

Different types of gasifier can be applied to gasify biomass, for example fluidised bed and fixed bed, and each one has specific characteristics and variations which restrict the amount of feedstock required and extent of pre-treatment [118].

2.3.2.1 Fixed Bed Gasifiers

The fixed bed is the simplest type of gasifier consisting of: the reactor where gasification of fuel occurs; a grate to support the solid fuel; a reactive material unit such as air or oxygen; and an ash removal device. The fixed bed gasifier is constructed simply and operates with low gas velocity, long residence time and high carbon conversion [119]. In the case of this reactor technology, fixed beds have a wide temperature distribution. This includes possibilities for low specific capacity, hot spots with ash fusion, long periods for heat up, and limited scale-up potential [111]. It is difficult to maintain uniform operating temperatures and ensure adequate gas mixing in the bed. The gas yield can be unpredictable due to the above reasons. Depending on how the gasifying agent enters the reaction zone, fixed bed gasifiers are classified into updraft, down draft and cross-draft [120].

In an ***updraft gasifier*** as illustrated in Figure 2-4 a [98], the feed of biomass from the top moves downwards while the gasifying agent such as air is fed into the bottom of the distributor. Therefore the combustion occurs at the bottom of the reactor near to the distributor, which is the hottest area in the reactor. The drying and pyrolysis steps mainly occur in the top of gasifier because the hot product gases exit the gasifier from the top and help to remove immediately the moisture content in the biomass feed [121]. The combustion of char (the residual material remaining after the release of volatiles) occurs immediately above the grate where high temperatures of around 1000°C are generated. The hot gases travel upwards through the bed and ash falls through the grate at the bottom [81].

In a ***downdraft*** fixed bed gasifier, the fuel and product gas flows downwards through the reaction zone which allows these tar-containing gases to pass through a throated hot bed of char enabling thermal cracking of most of the tars into light hydrocarbons and water. The gasification agent, such as air, is usually admitted to the fuel bed through intake nozzles at the throat causing pyrolysis of biomass to charcoal and volatiles which partially burn as they are produced, see Figure 2-4 b [122]. The updraft process is more thermally efficient than the downdraft process, but the tar content of the gas is very high [123] because the products from devolatilization do not pass the high temperature zone of the reactor. However, downdraft gasification is a comparatively inexpensive method [124].

Cross-draft gasifiers approximately exhibit several operating characteristics of the downdraft gasifier. The gasification agent is introduced into the side of the gasifier near to the bottom while the gases produced are drawn off on the opposite side [107]. The advantage of using this design over updraft and downdraft gasifiers is a short start up time, but due to their minimal tar converting capabilities, it was found suitable only for high fuel quality (low volatile content) such as charcoal [125]. Figure 2-4c shows the cross draft gasifier [126].

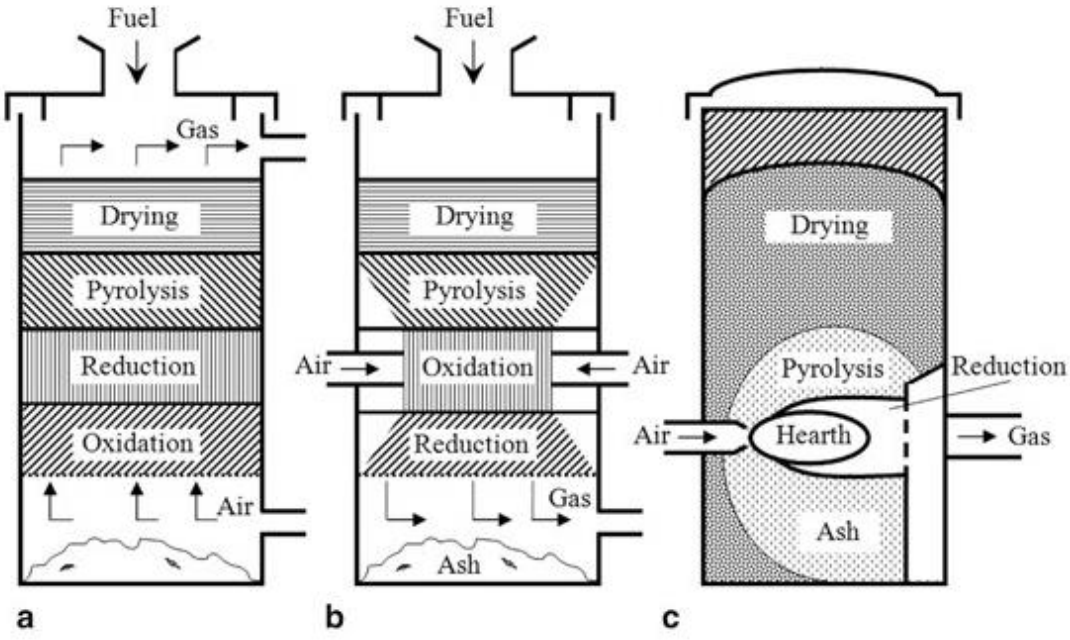

Figure 2-4 Fixed bed gasifier: a) Updraft, b) Downdraft, c) Cross draft [126]

2.3.2.2 Fluidised Bed Gasifiers

In a fluidised bed gasifier, the hydrodynamic phenomena cause turbulent mixing in which there is a consistent mixture of new particles blended with the older, partially and fully gasified particles. The turbulent mixing also enhances uniform temperatures throughout the bed [127].

Due to their ability to accomplish high heat and mass transfer rates, fluidised bed gasifiers are considered promising for biomass thermochemical conversion in large scale applications. Such processes are leading to a high conversion rate and more tolerance towards the feedstock feeding when compared with the fixed bed [20]. Fluidization is a process similar to liquefaction through which solid particles in a bed are transformed into a fluid-like state through suspension in a gas or liquid. Fluidization is used in a wide range of applications including pyrolysis, gasification and combustion of a wide range of feedstocks including biomass [128].

In gasification, the efficiency of fluidised bed gasifiers is approximately five times that of fixed bed gasifiers [99]. As a result of high mixing rates, in contrast to fixed bed gasifiers, there are no different reaction zones in a fluidised bed gasifier. Also,

fluidised beds have been confirmed to be among the most appropriate approaches for thermal conversion of different kinds of biomass fuel because it provide a sufficient heat and mass transfer for the reactants [129]. There are three types of fluidised bed gasifier which are classified as follows.

- **Spout fluidised bed gasifier**

The spout fluidised bed, as shown in Figure 2-5, has mainly been used in the chemical and petrochemical industry. Recently the application of this process has been extended to combustion and gasification processes [130].

The conventional spout bed consists of a conical cylindrical vessel with an orifice in the middle of the conical base. There are two regions in the bed, the spout and the annulus. The spout is a central core where the particles in a low-density phase are sent upwards due to high fluid velocity injected from the orifice. After reaching some level above the bed, the solid particles rain back down as a fountain onto the annulus which is of high particle density, where they spread and slowly move downward. A systematic cyclic pattern of particles is thus established, with excellent contact between fluid and particles, and with unique hydrodynamics [131]. A spout fluidised bed is similar to a fluidised bed, but the difference is in the solid particles' dynamic behaviour. A regular cyclic pattern of solid movement is established with effective contact between the gas and the solids in a spouted bed [132]. The spouted bed system is an alternative technique to fluidization of particulate solids that are uniform in size and too coarse for good fluidization [131]. Morever, spouted bed gasifiers can handle high ash content making them suitable to gasify fuels with high ash content such as coal [133]. The spouted fluidised bed can be deal with a wide range of fluidisation velocities without surrendering to slugging, which normally reduces the efficiency of the gasification system. In addition, increasing the fluidization rate accelerates the fluid-solid contact in the annular regions and minimises the probability of particles agglomerating and sticking to the vessel wall [134]. Like fluidised bed reactors, spouted beds have a certain minimum velocity called the minimum spouting velocity. However, unlike fluidised bed, spouted bed capacity is restricted because there is a maximum spouted bed height beyond which the spout ceases to exist [135]. In spouted fluidised bed, no maximum spoutable bed height can be established because it depends on gas inlet diameters and particle diameters. Nevertheless, as general effects, the

maximum spoutable bed height increases as the particle size decreases and with contactor angle increase [136].

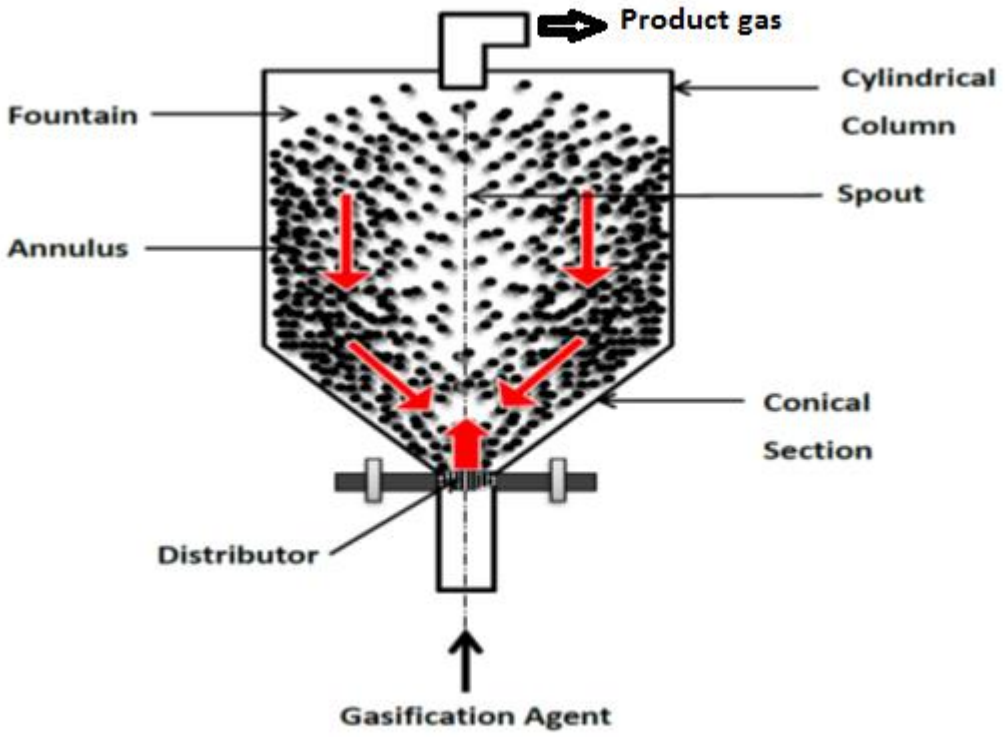

Figure 2-5 Spout Fluidised Bed Reactor

- **Bubbling fluidised bed gasifier.**

Bubbling fluidised bed reactors (BFB) are a type of multiphase reactor, through which the gas is blowing in the form of bubbles inside the packed bed solid phase. It is used in a vast number of industrial applications such as cracking, reforming of hydrocarbons, drying, adsorption, granulation, biological waste water treatment, the polymerization of olefins, and biomass gasification.

Historically, the BFB gasifier was developed by Fritz Winkler in 1921, and for many years the BFB gasifier has been used commercially for coal gasification. BFB is considered to be one of the most popular technologies for biomass gasification [75]. Figure 2-6 illustrates a BFB gasifier where the gasification agent is admitted at sufficient velocity through a bed of particles to keep them in a state of suspension. The

biomass particles are fed into the hot bed material and are very quickly mixed and heated up to the bed temperature. BFBs consist of a fluidised bed with freeboard column unit, biomass feeder, air blower, gas plenum, the diffuser plate, and cyclone.

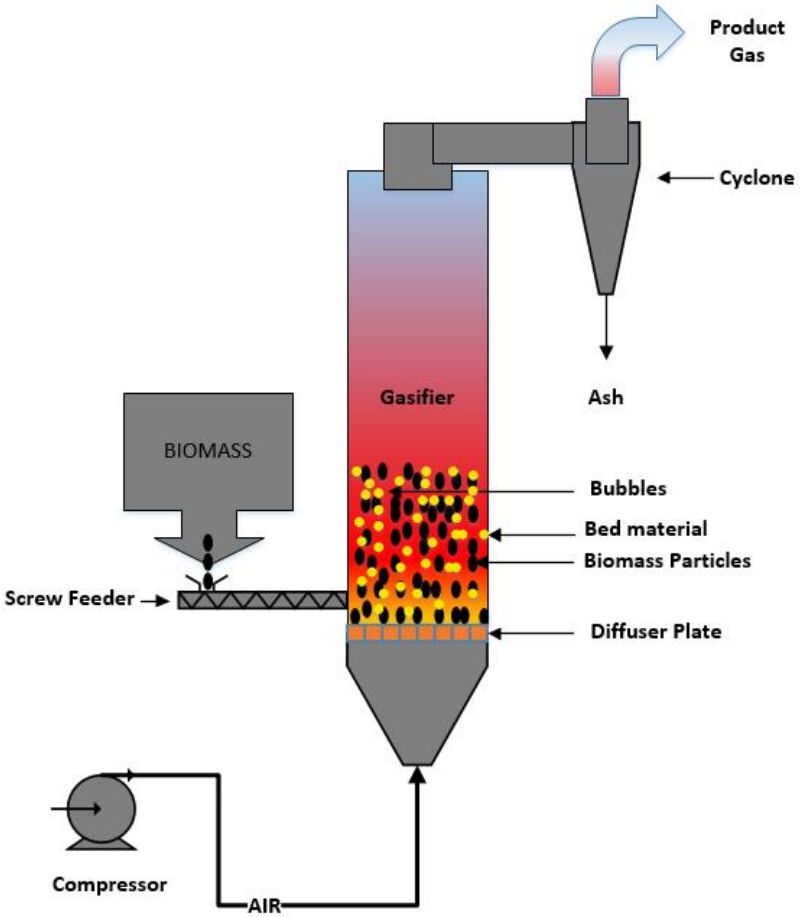

Figure 2-6 Bubble Fluidised Bed Gasifier

Fluidised bed gasifiers are used to convert biomass, particularly agricultural residues, into energy because they possess many advantages. These include: high gas-solid interaction; a high degree of random movement; good mass and heat transfer characteristics; effective temperature distribution; increased volumetric capacity and heat storage [9]. It is possible to add a catalytic bed and in addition they can be operated at partial load.

Bubbling fluidised beds are convenient and cost-effective for continuous biomass gasification. A wide variety of biomass and different particle sizes, including

pulverized, can be gasified. Gas produced from a bubbling fluidised bed gasifier has low tar content and low amounts of unconverted carbon [137] [138].

Unlike the spout-fluid bed, the bubble fluidised bed BFB is sensitive to ash content. When the biomass fuel has a high ash content, and the gasification temperature is higher than 950°C, the potential for agglomeration increases, which causes bed de-fluidization and reduces gasifier efficiency. Therefore the maximum temperature of operation is restricted by the melting point of the bed material [139]. In addition, due to the low operating temperatures and short gas residence times, the gasification reactions do not reach their chemical equilibrium unless a catalyst is used. BFB operating range is between the minimum fluidisation velocity and the entrainment velocity on which the bed particle would be dragged by the passing gas, being usually 1.2 m/sec [140].

Gasification of biomass in a BFB, using air as the gasifying agent, is a promising technique because yields of gaseous fuel have relatively high heating values, requiring minimum to no heat addition to the gasifier [141]. However, due to uncertain understanding, in particular of the hydrodynamics and reaction kinetics, of the heterogeneous (gas-solid) phenomena occurring in a fluidised bed, scaling-up of BFBs to commercial size is still a complex and troublesome endeavour [142].

- **Circulating fluidised bed**

Fluidised beds are increasing in popularity in the field of biomass gasification. However, due to the high level of solid material mixing, as well as particle entrainment, high solid conversion cannot be achieved by a BFB alone [143]. The circulating fluidised bed CFB, as illustrated in Figure 2-7, overcomes these problems by incorporating recirculation. The addition of a recirculating loop enables unreacted particles captured by a cyclone to be returned to the reaction zone thus leading to increased solid residence time, which subsequently improves the conversion [144].

CFB is widely used in the industry, especially for biomass and coal gasification [145]. Ten residual biomass fuels were tested successfully in a 500 KW_{th} CFB gasification facility by Drift et al. [146]. They concluded that the CFB is very flexible concerning the conversion of different kinds of biomass. However, these systems require fine particles of relatively uniform size distribution, necessitating added preparation.

The high stream velocity and recirculation provide appropriate contact time and mixing which boosts the mass and heat transfer within the gasifier. Therefore, the quality of the product gas is improved as a result of the suitable environment created for gasification [49]. The fluidization velocity of a CFB (4.5-6.7 m/s) is higher than in a BFB [140]. The overall conversion of carbon is greater than in a BFB due to the high speed of recirculation and excellent mixing of material [147]. However, CFBs require a high gas velocity to provide good gas-solid mixing, which can lead to higher erosion rates than in a BFB [111, 148]. Other disadvantages of a CFB involve: higher capital cost; increased overall reactor height; and added complexity in design, construction and operation [149]. Furthermore, a temperature gradient occurs in the direction of solid flow in a CFB. Indeed, CFB has lower transfer efficiency than BFB [150].

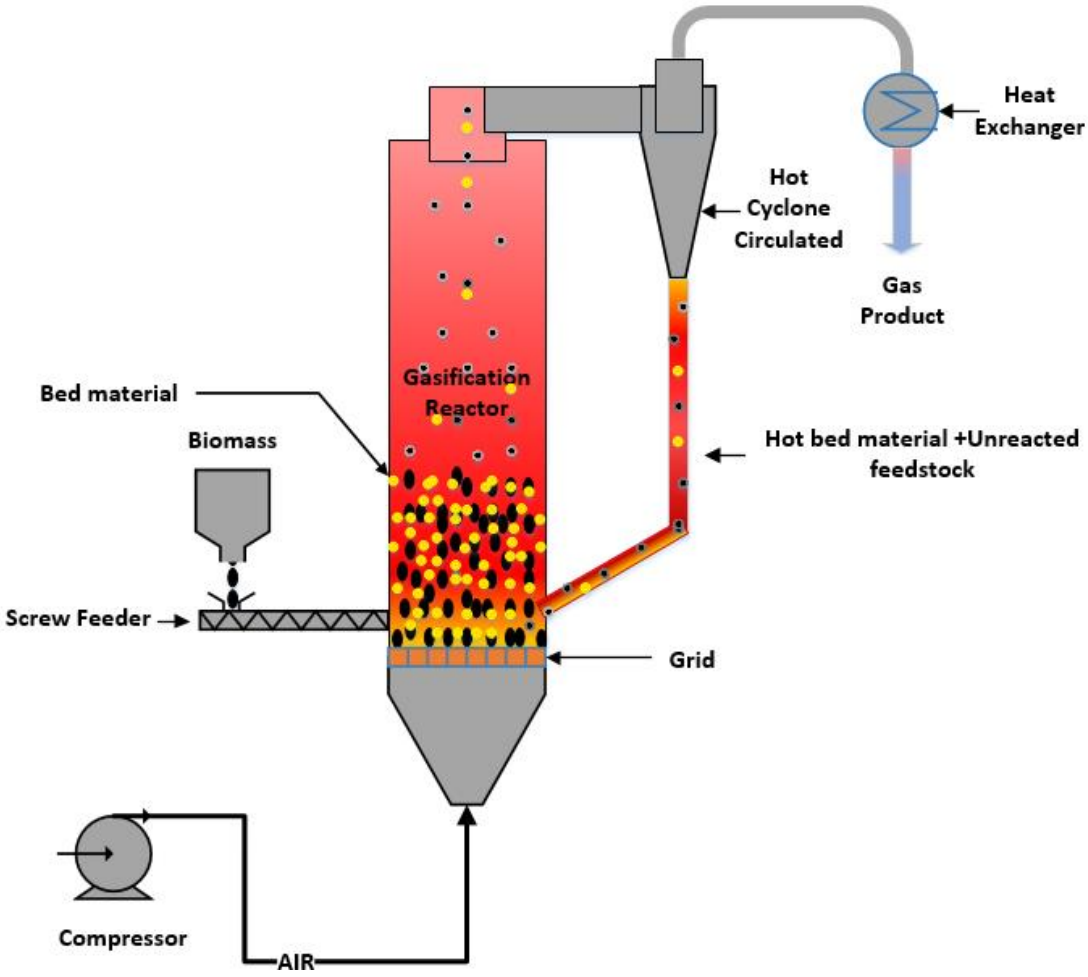

Figure 2-7 Circulating Fluidised Bed Reactor

2.4 Summary

Gasification reactions are affected by operating conditions, and this chapter highlighted their effect on the product gas. It was identified in the literature that in high temperature gasification, endothermic reactions as well as the secondary cracking and reforming of heavy hydrocarbons is favoured. Reduction of biomass particle size was seen to improve the product gas. Changing the ER produces different effects. At low ER, the biomass reactions approach pyrolysis conditions and the temperature of the reactor decreases, while at high ER combustion can occur leading to a low heating value of obtained product gas. The ER from literature was 0.2-0.4, so this study will take place in the range of 0.15-0.35. Top feeding of biomass improved the gas heating value, but the amount of tar increased.

Two different types of the gasifier, namely, fixed bed and fluidised bed are described. According to this literature, a bubble fluidised bed reactor is one of the most suitable technologies to gasify the biomass. The range of LHV was between 3.7 and 8.4 MJ/Nm^3, which is suitable internal combustion engines. So fluidised bed gasifier will be used in this study.

Chapter 3:

Theoretical Background

This chapter aims to put the research on pyrolysis kinetics into context. Reaction rate expressions for homogeneous and heterogeneous processes are discussed, beginning with the background theory, and proceeding to review the experimental and modelling work that has been carried out previously. The main purpose is to illustrate the equations used in kinetic calculations.

3.1 Chemical reaction engineering and kinetics

Chemical reaction engineering can be simply defined as engineering activity that is concerned with the application of chemical reactions in the commercial sector. Thermodynamics, chemical kinetics, fluid mechanics, mass transfer and heat transfer, are the main chemical engineering disciplines that provide information, knowledge and experience for reactor design [151].

Chemical kinetics and thermodynamics are the two main principles involved in establishing conditions for performing a reaction. Chemical kinetics is the study of rate and mechanism by which chemical species are converted. The rate gives us an indication of how fast the chemical reaction occurs, while chemical thermodynamics is only related to the initial state of the reactant material before a reaction takes place and the latter state of the reaction when an equilibrium is reached i.e. there is no further change [152]. Reversible and irreversible chemical reactions commonly occur in the thermochemical process. If adequate time is allowed until reversible reactions reach equilibrium, no matter how fast the reaction takes place, the chemical equilibrium constant k, determines how far the reaction can proceed. However, the equilibrium approach does not give a true representation of the process during relatively low operating temperatures (750-1000 °C), especially in a fluidised bed gasifier, therefore this approach is more suitable to describe the gasification process occurring in a downdraft gasifier [153]. In addition, the tar is not considered in equilibrium models, which is found in the product gas of fluidised bed gasifiers [154]. Alternatively, for the irreversible reaction when the chemical equilibrium constant is very large,

chemical kinetics is used to determine the rate at which the controlling chemistry will proceed [155].

The kinetic study involves following a reaction as a function of time. This can be performed by using an appropriate analytical technique to estimate the concentrations of reactants, or the products of the reaction or both, at different times during the progress of the reaction. The kinetic parameters and the yield and nature of the reaction products strongly rely on the properties of biomass and the reaction conditions [156]. The measurements are nominally taken under isothermal conditions to avoid any changes in temperature that lead to a change in the rate of reaction [157].

According to Higman et al. [79], the kinetics of gasification are not as developed as the thermodynamic theory. Homogeneous reactions such as gas phase reaction chemistry can frequently be described by a simple equation, but heterogeneous reactions are more complicated, as is the case with gasification of particles such as biomass. Therefore, more investigation is required in this area where appropriate kinetic studies could help in the design of future gasification reactors. According to Galwey et al. [158], the vast majority of kinetic studies of chemical reactions have two principal objectives. One of these principles is finding the rate equation that can satisfactorily describe the extent of the conversion of reactants with time. The second is to study the effect of temperature on the rate of reaction. By comparing the data obtained from experimental work with values predicted from a range of theoretical kinetic expressions, the rate equation that describes the experimental measurements can be determined.

3.2 Reaction rate expression

The rate of reaction gives us an indication of the number of moles of chemical species being consumed in reactants to form a new product, or the change in concentration of some species with time. The unit of rate of reaction is the reactant consumption per unit time per unit volume, based on the unit volume of reacting fluid or based on the mass of solid [159]. The reactions inside the reactor are mainly classified into categories [160]:

1. Homogeneous reactions occur when the reactant materials are found in one phase only inside the reactor, i.e. liquids only or gases only.

2. Heterogeneous reactions take place when the reaction mixtures are present in more than one phase inside the reactor, i.e. gas-solid, liquid-solid, gas-liquid or solid-gas-liquid.

3.2.1 The rate of reaction in liquid or gas phase.

The rate of a reaction in both liquid and gas phase depends on the change in concentration of some reactant or product with time. The power law modal is the most common form of functional dependence on concentration. The order of the reaction or power law can be defined as a number that relates to a chemical reaction with the concentration of the reacting substances: the sum of all the exponents of the terms expressing concentrations of the molecules or atoms determining the rate of the reaction.

Consider the reaction with only one reactant and irreversible [161];

$$A \rightarrow B \tag{3.1}$$

The rate is simply the slope of a plot of reactant or product concentration against time as illustrated in Figure 3-1, the concentration of A decreases and the concentration of B increases during reaction progress, after that the rate of chemical reaction is determined;

$$\text{rate} = -\frac{d[A]}{dt} = +\frac{d[B]}{dt} \tag{3.2}$$

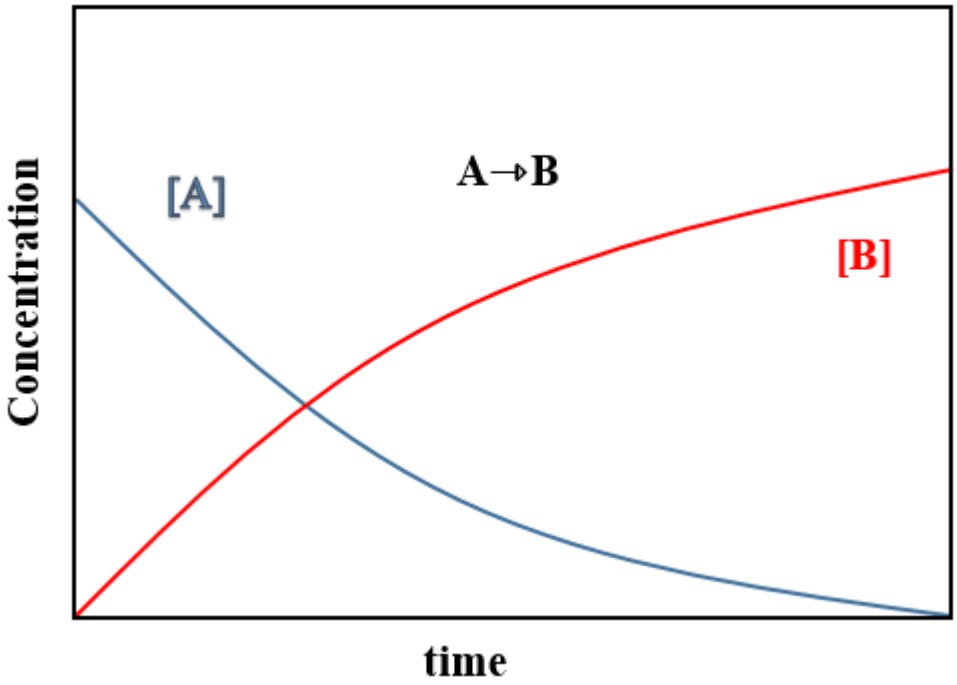

Figure 3-1 Concentration of reactants and products vs. time.

The negative sign means the concentration of A reduces with time, while the positive sign expresses the appearance of product B with time.

The terms of concentration per unit time are always the units of $-r_A$ while the units of constant rate k_A depend on reaction order as explained below;

Zero order reaction $-r_A = k_A$ n=0

(k_A unit) =Concentration/ time.

This implies that changing of the concentration of A has no effect on the rate of reaction.

First order reaction $-r_A = k_A C_A$ n=1

(k_A unit) =1/time

This implies that rate and concentration of A are directly proportional.

Second order reaction $-r_A = k_A C_A^2$ n=2

(k_A unit) =1/ (Concentration. Time)

This implies that the rate is directly proportional to the square of the concentration of A.

Also, the reaction at some time consists of two reactants, therefore, the overall order of the reaction, n is

$$n=\alpha+\beta$$

$$-r_A = k_A C_A^{\alpha} C_B^{\beta} \tag{3.3}$$

If the reaction orders are identical with the stoichiometric coefficients of the reactant material, this reaction follows an elementary rate law [162]. The experimental observations are important to determine the rate law depending on the measuring the concentration of either reactant or product with time.

3.2.2 The rate of reaction in heterogeneous phase.

Non-catalytic heterogeneous reactions involve liquid-gas, solid-liquid, and gas-solid regimes. In this study, only the gas-solid reactions system is considered. Many fields of technology, such as chemical engineering, chemistry, energy, environment and materials use gas-solid reactions in the fundamental research and development. Non-catalytic gas-solid reactions are an important class of heterogeneous reactions. In specialised literature, they have received considerable attention and lots of models and techniques for their solutions are available [163].

Noncatalytic, fluid-solid reactions (pyrolysis and gasification) may be represented by one of the following [164]:

$$Solid\ reactants \rightarrow fluid\ and\ solid\ products \tag{3.4}$$

$$Fluid\ and\ solid\ reactions \rightarrow fluid \tag{3.5}$$

The heterogeneous chemical reaction is used to described the pyrolysis and gasification of solid state materials, such as biomass, since during pyrolysis and gasification, phase changes occur due to release of volatile materials and gas. In such cases, three key elements can affect the reaction dynamics and chemical kinetics of the heterogeneous process [158], i.e., changing reaction geometry, redistribution of chemical bonds, and the interfacial diffusion of reactants and products. Unlike homogeneous reactions, concentration cannot be used to monitor the progress of the

kinetics of the heterogeneous reaction, because the concentration parameter can vary spatially [165]. According to House [166], the reacting molecules do not move freely and collide at a rate controlled by the thermal energy of the system as happens in gases and liquids. Therefore, the rate of reaction in the solid state relies on properties other than concentration.

In the previous section, we described that the rate of reaction in solution and gas is $-\frac{d[A]}{dt}$ where [A] is the concentration of unreacted material that remains after a certain time of reaction, t. In a homogeneous reaction where the reactants and products are in the same phase, it is possible to determine the kinetics through the concentration of products or reactants. For heterogeneous reactions, the concept of concentration of reactants or products does not play the significant role that it does in homogeneous reactions. Thus, the progress of reaction may be measured as the fractional reaction or degree of conversion x, where x is defined in terms of the change in mass of the solid sample [167]**,** or equivalent definitions in terms of gas evolved. In a similar way, rate laws for solid reactions are written in terms of (1- x), which is the fraction of unreacted material after some period of reaction time; t. The rate of reaction can be written in this form $\frac{dx}{dt}$, and the reaction has gone to completion when the fraction x is equal to one.

3.3 Kinetics study techniques

Accurate monitoring of conversion over time is required to perform kinetic analysis of reaction progress. This goal may be accomplished by using a technique that reflects the real reaction inside the reactor. The rate of heterogeneous reaction (gas-solid) has commonly been measured using one of the following techniques;

I. Measurement of some change in the properties of the solid material.

II. Measurement of some change in properties of the gas product from this reaction.

Both techniques are used for following the progress of the reaction. Group I involves the continuous measurement of thickness of layers such as in the oxidation of the surface of metal. The rate of reaction can be described in terms of thickness of layer with time, as explained in the parabolic rate law; or geometrically such as changing

surface area with time [166], and continuous measurement of the weight of reacted solid material such as pyrolysis of biomass using thermogravimetric analysis (TGA).

The commonest methods in group II include the analysis of gas evolved from reaction, such as using gas analysis to track continuously the measurement of the composition of the gas exiting the reaction zone. This procedure depends ultimately on the attainable yield of volatiles and gases. However, this kind of measurement does not reflect the real reaction inside the reactor because the volatile material consists of a wide range of hydrocarbons gases, which are difficult to detect with a gas analyser. Instead of continuous measurement, gas chromatography as an intermittent analytical procedure can be used to measure the rate of reaction depending on the wide range of gases, but there is a limitation to using this instrument because tars cannot be detected [168].

Among these methods, a gravimetric method is the most accurate method, and once the equipment has been set up, it can be used for many types of gas-solid reactions without recalibration. Also, this method is considered the most suitable for gasification reactions [68].

Generally, the kinetic data source can be obtained from the measured change in physical property of a material as a function of time. In the field of thermal analysis, kinetic data is usually collected by measuring changes in mass (thermogravimetry). These mass changes are converted to a dimensionless value called the degree of conversion, x. From the above it can be concluded that kinetic data has a dependence of x on time. TGA is commonly used as a standard method for determining kinetic parameters. According to Vyazovkin [169], two aspects of kinetic measurement: sample and instrument, impinge upon the adequacy of the kinetic data to the process kinetics, as shown in Figure 3-2.

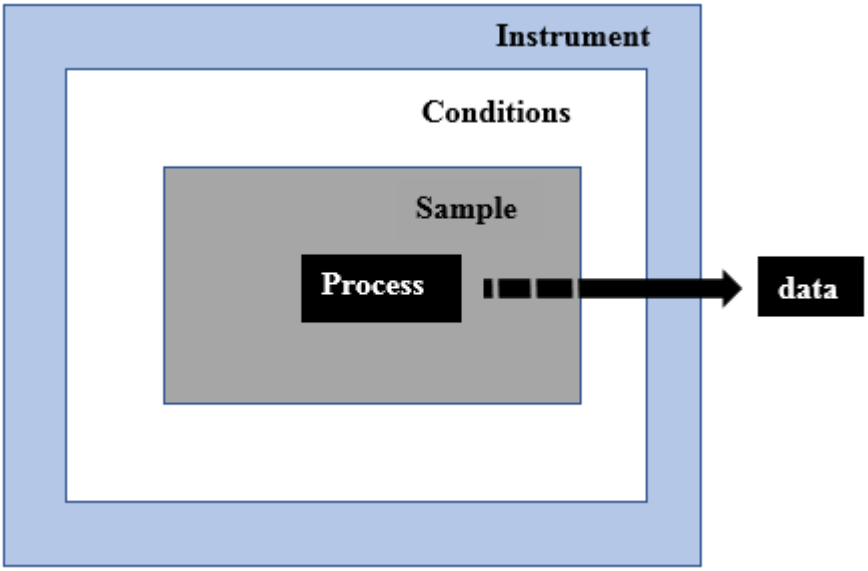

Figure 3-2 The data is inevitably affected by the sample and the instrument.

Due to the fact that the process is confined to the sample, it is influenced by the sample parameters, such as sample form and size, as well as the sample holder (crucible or pan). The sample is exposed to many conditions controlled by the instrument such as temperature, heating rate, flow rate, and gas atmosphere. The kinetic data may become inadequate in cases when the conditions defined by means of the sample or the instrument are poorly controlled.

Traditional TGA (see Figure 3-3) is essentially a fixed bed technique with a relatively low heating rate when compared to larger scale systems where biomass is added directly to the reactor at the reaction temperature; where the particle heating rate is significantly greater. Meanwhile, the chemical processes in TGA are affected by the interfacial gas diffusion between the reactor space and the solid sample inside the TGA cell [170]. Other authors have noted the effect of the heating rate on the reaction kinetics in a TGA, which limits how comparable these results are with high heating rate systems such as fluidised bed or circulating bed gasifiers [69]. In addition, it has been reported that conventional TGA suffers from the following limitations [171, 172];

1. The temperature distribution throughout the sample is non-uniform.
2. Poor solid-solid and gas-solid distribution and mixing within the sample.

3. A homogeneous sample is difficult to achieve given the small amount of solid sample tested.
4. Error in temperature measurement of the sample, because the thermocouple is not generally in contact with the sample. According to Agrawal [173], the difference in the temperature reading may be as much as 45K between the sample's real temperature and the thermocouple measurement.

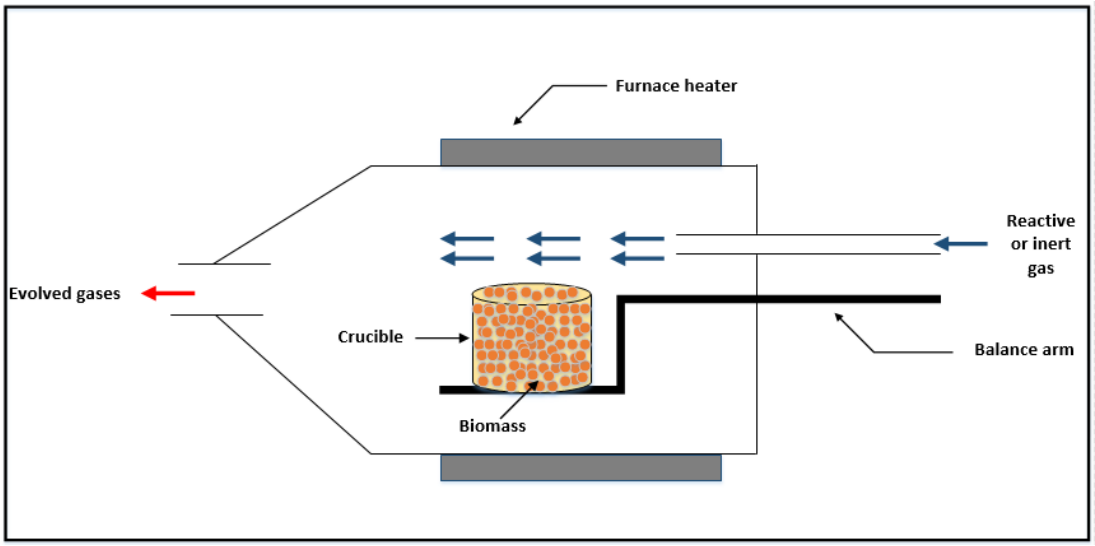

Figure 3-3. Schematic diagram for thermogravimetric analysis technique.

The effective design of a reactor is based mainly on a knowledge of reliable rate data. The rate of reactions in the heterogeneous system varies considerably depending on conditions under which the experiment is achieved. The physical effects such as diffusion and heat transfer can lead to an erroneous rate expression if they are not correctly determined. If the determination of the reaction order and the activation energy is misleading, the result may be a disastrous plant operation, when it is scaled up. Therefore, it is necessary to eliminate, as much as possible, the physical effects from purely chemical processes [164] to overcome these issues and offer accurate and more comprehensive data. In this study, the gravimetric method was adopted through a novel design to track the gas-solid reaction in batch and continuous mode using a fluidised bed reactor under isothermal conditions, details of which can be found in Chapter 5.

3.4 Arrhenius rate expression and the significance of the kinetic parameters

Activation energy also known as transition state, as illustrated in Figure 3-4, is the height of the energy barrier over which the reactants must pass on the way to becoming products. Activation energy as an energy barrier is important because it may supply the required information about the critical energy needed to start the reaction [174]. If the molecules in the reactants have kinetic energy and this energy is higher than transition state energy, then the reaction will take place, and products will form. On the other hand, the higher the activation energy, the harder it is for a reaction to occur. Activation energy represents the difficulty of forming the gas component [170]. Knowing the activation energy and the rate of thermal decomposition of biomass are important for an adequate design of gasification equipment, which both depend on kinetic studies of the biomass during the gasification process [175].

In order to avoid any changes in the reaction rate with temperature, most of the kinetic studies are performed under isothermal conditions. In the 1800s, the scientist Arrhenius suggested the rate of most reactions varies with temperature, as illustrated in Equation (3.6); this is often called the Arrhenius rate expression. Every kinetic model proposed employs a rate law that obeys the fundamentals of this expression. The relationship between rising temperature and reaction rate can be explained by using Arrhenius equation as follows:

$$k = A \exp[\frac{-E_a}{RT}] \tag{3.6}$$

Where E_a is the activation energy (KJ/mole), A is the pre-exponential factor, R is the universal gas constant, and k is the rate constant (s^{-1}).

The Arrhenius equation allows the drawing of a so-called Arrhenius plot. In this diagram, the natural logarithm of rate constant is on the y-axis, and the reciprocal temperature is on the x-axis. When we graph lnk versus 1/T, a straight line is obtained; the slope of this line x is equal to - $\frac{E_a}{R}$ and a y-intercept of this line is equal to lnA.

The rate constant k is not truly a constant; it is merely independent of the concentrations of reacted material. The quantity k is referred to as either the specific

reaction rate or the rate constant and it strongly depends on temperature [176]. However, the frequency factor A does exhibit a slight temperature dependency [177].

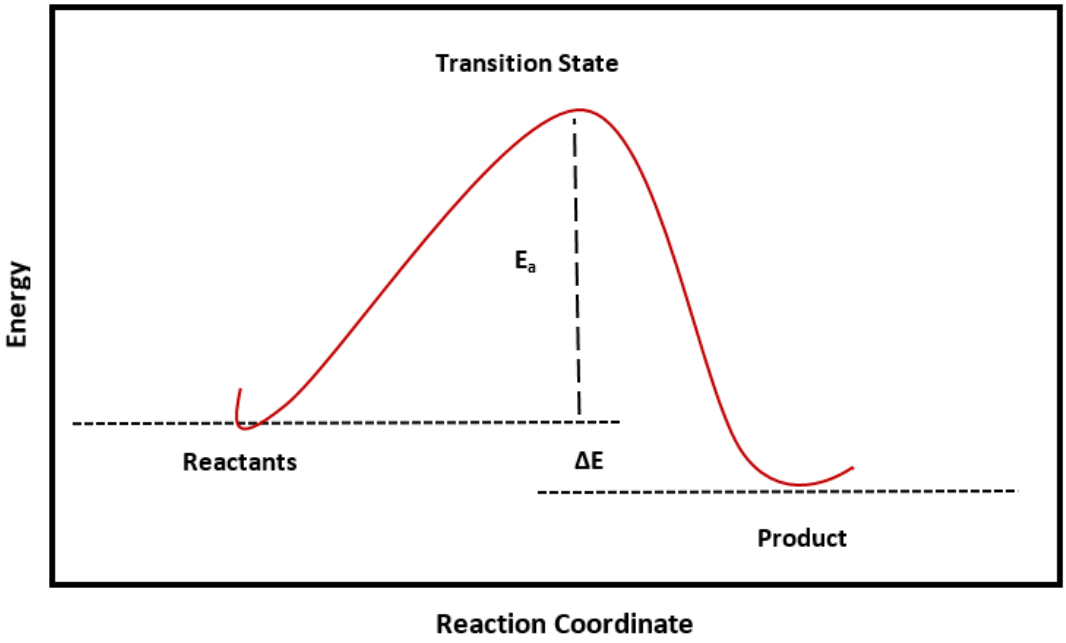

Figure 3-4 The energy profile of a chemical reaction

The Arrhenius rate expression plays a key role in heterogeneous reactions systems. According to Agrawal [173], the Arrhenius expression is the most satisfactory equation used to explain the temperature dependence of the rate constant in solid state decomposition kinetics.

3.5 Thermal degradation kinetics

Besides for the production of biochar and bio-oil, pyrolysis is also known as the first step in the gasification process. Understanding the kinetics of pyrolysis is therefore important. During pyrolysis, many chemical reactions occur, producing a wide range of chemical compounds. However, for engineering applications, the pyrolysis products are often simplified into only char and volatiles [178]. It has been reported that the single reaction global schemes have provided reasonable agreement with experimentally observed kinetic behavior [179, 180]. Therefore, a single decomposition reaction scheme is used to describe the degradation of solid fuel by

means of experimentally measured rates of weight loss, where the initial solid biomass fuel is converted to the product, which includes tar and gases as shown in the following formula:

$$\text{Biomass} \xrightarrow{k} \text{product}$$

Besides selecting a physical model, the mathematical model processing of the experimental data to formulate the selected reaction mechanisms and to estimate the kinetic parameters is also a significant part of the kinetic study. The kinetic study attempts to determine how the thermal decomposition occurs, by finding the best kinetic model that fits and describes the mechanism of the reaction to determine the kinetic parameters. This is crucial to the design, build and operation of a large –scale industrial reactor for the olive kernel biomass and palm stones, the subject of the present study.

In order to predict the thermal decomposition behaviour of biomass during pyrolysis, a variety of mathematical models have been proposed. However, mathematical models with high complexity are difficult to apply and are not usually utilised for practical purposes. Therefore, simpler models are favoured for approximate computations in design calculations [181].

In solid state kinetic analysis, it is appropriate to describe the reaction in terms of the conversion, x, defined as [25]:

$$X = \frac{m_O - m}{m_O - m_f} \tag{3.7}$$

Where m_o is the initial mass of the sample, m is the instantaneous mass of the pyrolysis sample, and m_f is the final residual mass.

The calculation of activation energy is considered one of the most important parameters of kinetics. It used to evaluate the reactivity, which is mainly calculated based on the model- free/iso-conversional method or model–fitting method [182]. The first approach can be used to calculate the activation energy regardless of the assumption of reaction model; it is assumed that the reaction function f(x) in the rate equation does not depend on either temperature or heating rate, and the reaction rate constant, k, depends on the reaction temperature. In these methods, activation energy

can be determined without any knowledge of the reaction model such as Flynn-Wall-Ozawa (FWO) method, Kissinger-Akahira-Sunose (KAS) method, and Friedman method [183]. The disadvantage of the iso-conversional method is that a series of measurements need to be taken at different heating rates for the same sample mass and the same gas flow rate. Fluctuation in the mass and gas flow rate can cause errors when the kinetic parameters are evaluated [184]. However, the latter approach is based on different model fitting, which is the process of evaluating kinetic parameters by assuming a reaction mechanism that represents the decomposition rate. There are 19 rate law models that have been used to provide a kinetic description of reactions in the solid state. Table 3-1 shows the rate laws of different mathematical forms used in gas solid reactions [185].

Table 3-1 Typical Reaction Mechanism for Heterogeneous Solid-State Reaction [185].

Symbol	*Reaction mechanism*	*f(x)*	G(x)
G1	One- dimensional diffusion, 1D	$1/2x$	x^2
G2	*Two- dimensional diffusion, (Valensi)*	$[-\ln(1-x)]^{-1}$	$x+(1-x)\ln(1-x)$
G3	*Three-dimensional diffusion, (Jander)*	$1.5(1-x)^{2/3}[1-(1-x)^{1/3}]^{-1}$	$[1-(1-x)^{1/3}]^2$
G4	*Three-dimensional diffusion, (G-B)*	$1.5[1-(1-x)^{1/3}]^{-1}$	$1-2x/3-(1-x)^{2/3}$
G5	*Three-dimensional diffusion(A-J)*	$1.5(1+x)^{2/3}[(1+x)^{1/3}-1]^{-1}$	$[(1+x)^{1/3}-1]^2$
G6	*Nucleation and growth(n=2/3)*	$1.5(1-x)[-\ln(1-x)]^{1/3}$	$[-\ln(1-x)]^{2/3}$
G7	*Nucleation and growth (n=1/2)*	$2(1-x)[-\ln(1-x)]^{1/2}$	$[-\ln(1-x)]^{1/2}$
G8	*Nucleation and growth (n=1/3)*	$3(1-x)[-\ln(1-x)]^{2/3}$	$[-\ln(1-x)]^{1/3}$
G9	*Nucleation and growth(n=1/4)*	$4(1-x)[-\ln(1-x)]^{1/3}$	$[-\ln(1-x)]^{1/4}$
G10	Autocatalytic reaction	$x(1-x)$	$\ln[x/(1-x)]$
G11	*Mampel power law(n=1/2)*	$2x^{1/2}$	$x^{1/2}$
G12	*Mampel power law(n=1/3)*	$3x^{2/3}$	$x^{1/3}$
G13	*Mampel power law(n=1/4)*	$4x^{3/4}$	$x^{1/4}$
G14	*Chemical reaction(n=3)*	$(1-x)^3$	$*[(1-x)^{-2}-1]/2*$
G15	*Chemical reaction(n=2)*	$(1-x)^2$	$*(1-x)^{-1}-1*$
G16	*Chemical reaction(n=1)*	$1-x$	$*-\ln(1-x)*$
G17	*Chemical reaction(n=0)*	1	x
G18	*Contraction sphere*	$3(1-x)^{2/3}$	$1-(1-x)^{1/3}$
G19	Contraction cylinder	$2(1-x)^{1/2}$	$1-(1-x)^{1/2}$
Note: A-J: Anti- Jander; G-B: Ginstling-Brounshtein			

Since the pyrolysis of the olive kernel or palm stones in BFB is a heterogeneous solid state reaction, the universal kinetics of the thermal decomposition of biomass can be expressed as [186]:

$$\frac{dX}{dt} = k(C_g, T)f(X) \tag{3.8}$$

Where T is the reaction temperature; t is the reaction time; f(x) is the differential reaction model; k(T) is the temperature dependant reaction rate that can be expressed by the Arrhenius equation (see Equation (3.6)). Assuming that the concentration of the gasification agent (Cg) remains constant during the process, the gasification reaction rate depends on temperature only.

The two experimental methods that can be used to study the kinetics are the non-isothermal method and the isothermal method. Taking measurements under isothermal conditions is advantageous when compared to non-isothermal measurements because there is a homogeneous sample temperature. However, in order to obtain kinetic data, several experiments need to be carried out at different temperatures which require more samples and takes more time. Under non-isothermal conditions, it is more difficult to take temperature measurements that are representative of the whole sample, owing to the existence of a temperature gradient within the sample, which are caused by the non-stationary heating conditions. Therefore, the thermal decomposition will be based on temperature and time parameters. Over an entire temperature range, only a single measurement can provide sufficient data for the formal kinetic evaluation, and this is one of the advantages of using non-isothermal analysis. In practice, the non-isothermal analysis is used only by TGA because it has the ability to measure the mass variation with temperature.

For **isothermal** methods, the integral model fitting method has been used in BFB to calculate the kinetic parameters, if Equation (3.8) above is transposed and integrated we obtain the following:

$$\int \frac{dx}{f(x)} = \int k(T)dt \tag{3.9}$$

$$G(x) = \int \frac{dx}{f(x)} \tag{3.10}$$

and

$$G(x) = k(T)t \tag{3.11}$$

Where the term G(X) symbolises the various integral model equations that can be obtained from Table 3-1 and applied to Eq.(3.11) [185]. The expression of the reaction by a reaction equation model is tested according to linearity and linear range of G(X) against t at various temperatures. The rate constant at different temperatures are calculated using the best fitting model.

Taking logarithm of the both sides of Equation (3.6), we obtain

$$\ln k(T) = \ln(A) - E/RT \tag{3.12}$$

The experiments are completed at several constant temperatures. The Arrhenius equation is used to plot $\mathbf{\ln k \ vs. \ 1/T}$ (where T is absolute temperature) and from the slope of this plot the value of activation energy is calculated.

For the **non-isothermal** process in TGA, different experimental techniques have been utilised that allow for the study of the changes in a sample as the temperature increases. As the temperature increases, the value of rate constant **k** also increases. This allows derivation of activation energy and A from one single experiment instead of many experimental tests at several temperatures [187]. Similar to the isothermal method, non-isothermal thermogravimetric analysis can be split into fitting models and free models. The first approach is necessary to assume the reaction mechanism, which can be obtained also Table 3-1.

By substituting the Arrhenius equation in equation (3.9) giving:

$$\int \frac{dx}{f(x)} = \int A \exp^{-E/RT} dt \tag{3.13}$$

At constant heating rate the variation of temperature with time given by;

$$T = T_o + \beta t \tag{3.14}$$

Where β heating is rate, and T_o is the initial temperature of the reaction. By differentiating both sides of the equation above gives:

$$dT = \beta dt \quad \text{or} \quad dt = dT/\beta \tag{3.15}$$

Then Equation (3.13) becomes:

$$\int \frac{dx}{f(x)} = \int_0^T \frac{A}{\beta} \exp^{-E/RT} dT \quad (3.16)$$

The right-hand side is a non- integrable function, however the left side of equation is again G(x).

$$G(X) = \int_0^T \frac{A}{\beta} \exp^{-E/RT} dT \quad (3.17)$$

The equation (3.18) shown below describes the Frank-Kameneskii approximation equation that can be used to select the reaction mechanism model.

$$\int_0^T \exp(-\frac{E}{RT}) dT = \frac{RT^2}{E} \exp(-\frac{E}{RT}) \quad (3.18)$$

By combining Eqs. (3.16) and (3.17), equation (3.18) is obtained and represented by the Coats-Redfern equation [188].The Coats-Redfern integral method is a single heating rate method and is used widely in analysing the kinetic parameters of non-isothermal operation conditions [183]. According to this method:

$$\ln(\frac{G(x)}{T^2}) = \ln(\frac{AR}{\beta E}) - \frac{E}{RT} \quad (3.19)$$

Thus, a plot of $\ln(\frac{G(x)}{T^2})$ Versus 1/T gives a straight line with a slope –E/R since ln (AR/βE) is almost constant. The mechanism function G(x) involves the reaction mechanism, by substituting a model from Table 3-1 into Eq. (3.19), one can determine if the mechanism function model describes approximately the reaction depending on the linearity using the Pearson correlation coefficient (R^2). The model has been selected to describe the reaction mechanism, based on the highest regression value for the tested model, and that allows extraction of the activation energy value. The aim of the present study was to quantify the biomass pyrolysis kinetics of olive kernels and palm stone in a batch reactor.

3.6 Previous work in kinetics

Various systems such as a drop tube furnace, a tube reactor, an entrained flow reactor and thermogravimetric analyser are used to study the thermal behavior of biomass. The standarded method of measuring the kinetic parameters of pyrolysis and gasification processes is via thermogravimetric analysis (TGA), where by a small

sample of the feedstock (5-15 mg typically) is heated at a certain rate while simultaneously recording weight, time and temperature. The volume of publications in the field of biomass combustion and pyrolysis kinetics is enormous. Therefore, a brief description of some of these publications has been mentioned in this thesis.

Pyrolysis and combustion kinetics of date palm biomass (leaf, steam and seed) were investigated using TGA. The result revealed various activation energies for various date palm biomasses. Kinetics parameters of date palm biomass exhibited on activation energy in the range 9.7-42.6 kJ/mole under pyrolysis condition, while in air is in the range of 9.04-30.95 kJ/mole [25].

Munir et al. [189] investigated the thermal degradation, reactivity and kinetics of biomass materials sugarcane bagasse, cotton stalk, and shea meal under pyrolysis and oxidising (dry air) conditions, using a non-isothermal TGA. The result revealed that the average rate of weight loss associated with combustion was twice that for weight loss under pyrolysis conditions. Also, it was found that the activation energy value increased in the presence of oxygen.

White et al. [165] used iso-conversional and model-fitting methods for estimating kinetic parameters of pyrolysis of two agricultural residues using TGA. Many factors can influence the kinetic parameters, including heat and mass transfer limitations and process conditions. Kinetic parameters for combustion of four varieties of rice husks with oxygen were investigated by using TGA. The result showed two distinct reactions zones for all varieties of rice husk [190]. The first reaction zone was found higher than the second zone; the activation energies were 142.7-188.5 $kJmol^{-1}$ and 11.0-16.6 $kJmol^{-1}$ for first and second reaction zones respectively. They explained that the lower activation energy in the second stage might be due to the presence of lignin, which has lower decomposition rate compared to cellulose and hemicelluloses components of biomass.

The kinetic parameters for the thermal behaviour of different date palm residues (leaflets, rachis, trunk, stones and fruitstalk prunings) were investigated under inert and oxidative atmospheres [191]. Non-isothermal TGA data was used for evaluation of the kinetic parameters. The activation energy found under inert condition was less than the activation energy under the oxidative conditions for all the biomass tested.

Different configurations of TGA devices were used by Gronli et al. [192], to study the kinetic parameters of cellulose pyrolysis. A first order reaction model was used to determine the activation energy and pre-exponential factors. However, at the high heating rate, the kinetic parameters found were very sensitive to the device used. It was explained that these differences in the kinetic parameters values resulted from the differences in thermal lag among the various devices that were used in thermal decomposition.

By using TGA and gas analysis, the mass losses of sawdust and the mole fraction of evolved gases during pyrolysis of sawdust in a nitrogen atmosphere were measured. A single and parallel model was used to describe the experimental data from mass losses and evolved species, respectively. Using a first order reaction in the non-isothermal method, the activation energy of a single model was evaluated and found as 145 kJ/mole. Based on TGA and gas analyser data, the activation energy of evolved gases was determined [193].

Other facilities were modified and used by the researcher to predict the kinetic parameters of combustion and pyrolysis of biomass instead of using (TGA). Kinetic parameters of Beer lees (deposits of dead yeast from fermentation) as biomass was investigated by Yu et al. [194] using micro-fluidised bed reactor. The biomass sample was injected into the inside of the hot fluidised bed at a preset temperature in less than 0.1 sec. The pyrolysis kinetics were determined based on the analysis of gas release for both single gas components and the pyrolysis gas mixture. They found the activation energy of individual product gases were different and indicate different mechanisms in forming the individual gas species. A Shrinking core model was used to calculate the overall pyrolysis activation energy and found as 11.7 kJ/mole and compared with TGA measurements 120 kJ/mole which is more accurate. However, a small amount of solid sample (10-50 mg) was used, which is not enough to represent its homogeneity. In addition, the kinetic data measurements of the given reaction are based only on evolved gas analysis such as CO, CO_2, H_2, and CH_4 and all the other hydrocarbons such as tar were neglected.

Kinetic analysis of Beech and pine woods has been investigated by using the gravimetrical method, where the biomass samples were placed in a stainless steel capsule, suspended on an electronic balance and placed inside an oven [195]. The

activation energy of primary pyrolysis was 87.5 kJ/mole. However, two limitations of this procedure are the heat transfer between the oven atmosphere and the capsule biomass sample, which is normally not as good as the heat transfer in a fluidised bed, and the large particle size being 11-13 mm diam. and 6 cm in length (for one pellet).

Employing a combination of the gravimetric and optical method (two different UV-LEDs with different wavelength), the rate constant of thermal decomposition of pellets to gas was determined by Reschmeier et al. [196]. The total mass loss of biomass was measured by locating the fluidised bath on a balance, while the mass of tar was measured using UV-LEDs for real time tar analysis. The mass loss of gas was determined based on the difference between total mass and mass of tar. It was found that the first order reaction approach with the conversional mass was suitable for the mass-loss curves. The activation energy of wood was 60 kJ/mole. However, the fluidised bath was also designed to provide heat for immersed objects. The heat was achieved with immersion heaters inside the bed, but this led to hindered fluidisation and poor mixing. Therefore, temperature stability and uniformity could not be achieved in the fluidised medium itself or the gas distribution, if the diameter used was more than 228 mm. Furthermore, the height of the reactor was 350 mm, hence, it was difficult to keep the sand inside the reaction zone as a result of elutriation.

A laboratory captive sample reactor identified as a wire mesh microreactor was used to investigate the effect of temperature on yields and composition of pyrolysis products of olive wood (cutting) and olive kernel. A first order kinetics model was used to calculate the kinetic parameters of olive kernel pyrolysis in a captive sample reactor. The calculation of kinetics based on the ultimate attainable yield of decomposition (ultimate yield of volatile and gases) [19]. The activation energies of olive wood and olive kernel were 2.62 and 11.14 kcal $gmol^{-1}$ respectively.

Gai et al. [185] used iso-conversional and model-fitting approaches to study the thermal cracking of phenol as the model compound of biomass tar in a micro fluidised bed reactor. Pyrolysis kinetics of individual gaseous compound evolved from reaction, including H_2, CH_4, CO and CO_2 were investigated. They reported that the most probable reaction mechanism for the formation of hydrogen and methane was three-dimension diffusion while chemical reaction and contracting sphere could describe the

generation of carbon monoxide and carbon dioxide, respectively. The results also show that CO was the major composition of pyrolysis gas mixture from phenol.

Micro fluidised bed reactor and TGA were used to study gas-solid reaction mechanism under isothermal and non-isothermal condition by Yu et al. [188]. They used model-fitting approaches to determine the kinetic parameters of combustion of graphite in a micro-fluidised bed depending on the gas evolved from the reaction and TGA. The reaction under isothermal and non-isothermal conditions was found to be subject to the nucleation and growth model. However, it was found the delay between the actual reactant sample temperature and the measured TG temperature is increased with heating rate. The activation energy of graphite was found equal to 172.2 kJ/mole by using TGA and 164.9 kJ/mole using micro-fluidised bed reactor.

The isothermal reactions kinetics of char gasification with CO_2 were investigated in micro fluidised bed and TGA [197]. The shrinking core model was used to describe the heterogeneous reaction in both the micro fluidised bed and TGA. The carbon conversion was estimated from the concentration of CO formed during the reaction. However, the shrinking core model found allowed for good correlation only at lower conversions.

3.7 Summary

In this chapter, homogeneous and heterogeneous reactions are described briefly. The concept of concentration measurement of reactants or products in a homogeneous reaction does not play a significant role in the heterogeneous reaction. Instead, mass variation was found as the best way to measure the conversion between gas-solid phases.

Two experimental methods, isothermal and non-isothermal methods, were used in the literature to evaluate the thermal degradation kinetics. The model-fitting method was used to determine the kinetic parameters and mechanism of reaction under isothermal and non-isothermal conditions.

From the previous work in kinetics, it can be concluded that TGA can be considered to be a fixed bed technique with a relatively low heating rate compared to larger scale systems, where biomass is added directly to the reactor at the reaction temperature, so the particle heating rate is significantly greater. Meanwhile, the chemical processes in TGA are affected by the interfacial gas diffusion between the reactor space and the solid sample inside the TGA cell. During thermal decomposition of biomass, the heat and mass transfer as transport phenomena have a great influence on kinetic analysis. For example, using a fixed bed in thermal decomposition increases the probability of mass transfer control.

Due to the complication and difficulties in extracting data from dynamic thermogravimetric analysis, reliable data on the kinetic parameters such as activation energy E are not easily available for thermal decomposition of biomass at a high heating rate and a preset temperature.

Chapter 4:

Materials and methods of characterisation

4.1 Introduction

This chapter describes the preparation and characterization methods for the biomass fuel material and sand bed material. The procedure for the measurement of the minimum fluidised bed velocity as the most important hydrodynamic parameter in bubbling fluidised bed gasifiers is described. The minimum fluidised bed velocity is used to provide essential data used in the calculation of gasification performance. The methods of pyrolysis, torrefaction, char yield of pyrolytic biomass, and TGA are highlighted in this chapter.

4.2 Characterisation of biomass

The descriptions of the as received olive kernels, as received torrefied olive kernels, and date palm stones, and characterisation methods used in the investigation of the gasification performance in the fluidised bed reactor are listed in this section. The appropriate operating conditions such as air-fuel ratio, process temperatures, and amount of feedstock are essentially dependent on the chemical and physical properties of the feedstock.

4.2.1 Proximate analysis

The moisture content, ash, fixed carbon, and volatile matter give an indication of the properties of a particular fuel. They are illustrated in Tables 4-1 and 4-2 for as received olive kernels, as received torrefied olive kernels, and palm stones. These properties are significant in approximating characteristics of a certain fuel during thermo-chemical conversion. To ensure a representative sample, the bulk sample of biomass in the sack was tumbled prior to sampling. The method and approach that can be used to determine individual properties are described as follows:

4.2.1.1 Moisture content

The high moisture content of solid fuels fed into a gasifier inhibits the gasification process due to the lowering of temperature, since, in addition to devolatilization, the

chemical reaction of steam with char is endothermic. Fluidised and entrained bed gasifiers have a lower tolerance of moisture content, so the feedstock requirements are such that moisture should be reduced to 5 - 10% [75].

The moisture content in the olive kernels and palm stones were determined according to ISO DIS 18134 (14774-3). The analysis was repeated three times to monitor the repeatability of test samples. In order to test a single sample, three empty ceramic dishes with lids were dried inside an oven at 105℃ until constant mass, and then cooled to room temperature in a desiccator. After cooling, the weight of the dishes with lids was taken to the nearest 0.1 mg. Then one gram of sample, weighed to the nearest 0.1mg, was spread evenly over each dish. The dishes were placed in the oven with the lids next to them (not on them) and dried in an oven at 105℃ for 2 hours. Directly after heating the lids were replaced on the dishes, and transferred to the desiccator for cooling to room temperature. The purpose of the lids was to prevent the biomass from absorbing moisture, since biomass is hygroscopic. The samples were weighed swiftly for the same reason. The expression of the moisture content (M_{ad}) was calculated per equation (4.1).

Where:

$$M_{ad} = \left(\frac{m_2 - m_3}{m_2 - m_1}\right) x100 \qquad (4.1)$$

m_1 is the mass of the empty crucible and lid;

m_2 is the mass of the crucible, lid and biomass before heating;

m_3 is the mass of the crucible, lid and residue after heating.

4.2.1.2 Ash content

According to BS EN 14775:2009 the ash content is defined as the mass of inorganic material left after ignition of fuel under specified conditions. It is expressed as a percentage of the mass of the dry matter in the fuel. To observe the repeatability the test was carried out on three samples. Firstly, three empty porcelain dishes were put in the furnace at a temperature of (550±10) ℃ for 60 minutes as a minimum to remove any volatile material. The dishes were removed, allowed to cool slightly for 5 to 10min, transferred to a desiccator, and then allowed to cool to ambient temperature. When the dishes were cool, the weight was taken to the nearest 0.1 mg and the mass

recorded. One gram to the nearest 0.1 mg of biomass sample was spread over each dish and placed into a cold furnace. The furnace temperature was raised to 250℃ over a period of 30-50 min, (hence, a heating rate of 4.5-7.5℃/min), and then the temperature was maintained for one hour to remove the volatiles before ignition. Subsequently, the furnace temperature was raised to 550℃ over a 30-minute period (a heating rate of 10°C/min). The temperature was maintained at this level for at least 120 minutes to ensure complete combustion. The dishes were removed from the furnace and allowed to cool on a heat resistant plate for 10 minutes then transferred to a desiccator to prevent absorption of moisture from the atmosphere. When the temperature of the dishes reached ambient conditions, the mass was recorded. The following equation was used to calculate the ash content (A_d).

$$A_d = \frac{(m_3 - m_1)}{(m_2 - m_1)} x100 \qquad (4.2)$$

Where:

m_1 is the mass of the empty dish;

m_2 is the mass of the dish and the test sample;

m_3 is the mass of the dish and ash.

4.2.1.3 Volatile matter content

The volatile matter content was determined according to BS EN ISO 15148:2009. The analysis took place in triplicate to monitor the repeatability between test samples. For the purposes of cleaning, three empty fused silica crucibles, with lids to the side, were placed into a furnace at 900℃ for 7 minutes, removed from the furnace, allowed to cool to ambient temperature, then, stored in desiccator. A purpose made rack was used to hold the crucibles when in the furnace. This rack a allowed each crucible to be heated for the same amount of time, because they would all go into and come out of the furnace at once. The weight of the empty crucibles and lids were taken to the nearest 0.1 mg. One gram (to the nearest 0.1mg) of biomass sample was put into each crucible and the corresponding lid replaced. Once all three crucibles were loaded with sample, the rack was transferred into the furnace at 900°C for 7 minutes. After this period, the crucibles were removed, allowed to cool, and weighed. The determination of the content of volatile matter (dry basis) was based on equation.

$$V_d = [\frac{100(m_2 - m_3)}{m_2 - m_1}] \quad (4.3)$$

Where

m_1 is the mass of crucible and lid (empty);

m_2 is the mass of the crucible, lid and biomass (before heating);

m_3 is the mass of the crucible, lid and residue (after heating).

4.2.1.4 Fixed carbon content

By subtracting the percentage of moisture, volatile matter, and ash from a biomass sample, the fixed carbon is determined by using Equation (4.4).

$$FC\ \% = 100 - [M_{ad} - V_d - A_d] \quad (4.4)$$

Where

M_{ad} = moisture content of the biomass;

V_d = volatile matter content of the biomass;

A_d = ash content of the biomass.

Table 4-1 Proximate analysis and high heating values of AROK and ARTOK.

Proximate analysis (wt. %, wet basis)			
AROK		ARTOK	
Fixed carbon	18	Fixed carbon	26.8
Volatile matter	76	Volatile matter	68.93
Ash	0.71	Ash	2. 05
Moisture	5.29	Moisture	2.22
HHV($MJkg^{-1}$)	19.20	HHV($MJkg^{-1}$)	20.8

Table 4-2 Proximate analysis and high heating value of palm stone.

Palm stone (wt. %, wet basis)	
Fixed carbon	6.73
Volatile matter	82.27
Ash	1.45
Moisture	9.55
HHV($MJkg^{-1}$)	20.4

4.2.2 Calorific value

Calorific value (or heating value) is the amount of heat released by a unit weight or unit volume of a substance during complete combustion with oxygen and is usually expressed in joules per kilogram for a given mass of a fuel. Heating value of combustion is expressed in two ways: as high heating value HHV (gross heating value), or low heating value LHV (lower calorific value). The HHV is the value that is usually measured in the laboratory and would be obtained during combustion if energy from condensation of water is included. In this study, the work was done using a bomb calorimeter, model number 6100, from Parr Instrument Company as shown in Figure 4-1. The heat from the combustion of a biofuel sample burned under an oxygen rich environment in a closed pressure vessel (bomb) is measured under controlled conditions. Heat released from the combustion of a sample flows from the bomb through a stainless-steel wall to a water jacket surrounding the bomb. After that, the temperature of the surrounding water jacket is raised and this temperature change is recorded. The test is carried out according BS EN 14918 [198]. Before testing, the calibration of the bomb calorimeter was performed using three benzoic acid pellets. After that, one gram of biomass was added to the bomb; the bomb was sealed and pressurised with oxygen. The cylindrical bomb was submerged in a known volume of distilled water (2000 ml) before the charge was electrically ignited. Energy released from combustion was recorded as the HHV of the sample. After the HHV had been measured, the excess pressure in the bomb was released. To ensure the repeatability between biomass samples, at least two duplicates were used for all the samples and an average value was calculated.

Figure 4-1 Parr 6100 Bomb Calorimeter.

The main difference between HHV and LHV is that the LHV does not include the latent heat contained in the water vapour. LHV can be determine from the following equation [75]:

$$\mathrm{LHV} = \mathrm{HHV} - h_g \left(\frac{9H}{100} + \frac{M}{100}\right) \tag{4.5}$$

Where, HHV, LHV, H, and M are high heating value, low heating value, hydrogen percentage, and moisture percentage, respectively. The value of h_g is 2.260 MJ/kg (the same units as HHV) and represents the latent heat of steam.

4.2.3 Ultimate analysis

Ultimate analysis gives the elemental composition of a fuel. CHNSO represents the carbon, hydrogen, nitrogen, sulphur and oxygen (by difference) measured in a particular fuel through complete combustion. These measured elements are important in determining an appropriate ER for gasification or combustion. In this study, the ultimate analysis of biomass was determined in a CHNSO-IR LECO spectrometric analyser. The results of ultimate analyses of as received olive kernels, as received torrefied olive kernels, and date palm stone are presented in Table 4-3 and Table 4-4.

Table 4-3 Ultimate analysis of AROK and ARTOK.

Ultimate analysis (wt.%, dry basis)			
as received olive kernel		as received torrefied olive kernel	
C	50.93	C	56.93
H	6.16	H	6.32
N	0.01	N	0.14
S	0.02	S	0.02
O	42.11	O	35.66
ASH	0.77	ASH	0.93

Table 4-4 Ultimate analysis of Palm stone

Ultimate analysis (wt.%, dry basis)	
Palm stone	
C	48.68
H	6.6
N	0.77
S	0.075
O	42.3
ASH	1.58

4.2.4 Biomass size reduction

In order to study the effects of particle size reduction in pyrolysis and gasification performance, olive kernels were supplied with a particle size of less than 5mm; this was called as received olive kernel (AROK). For this study, four different particle sizes of olive kernel were chosen (300-500) µm, (500-710) µm, (710-1180) µm, and (1180-1400) µm. The particle size of AROK was reduced by using Labtech-Essa LM1 ring mill machine, as illustrated in Figure 4-2 (a). After the grinding process, the selected sizes were obtained by sieving according to BS 1377-9 1990.

Date palm stones were obtained from Iraq. The dimensions of a stone are about 20-25 mm long and 6-8 mm thick. This large size makes it not only difficult to fluidise but also difficult to control the feeding rate. Therefore, after drying, the date palm stone particle size was reduced by using a Retsch model BB20 crushing machine, see Fig. 4-2 (b), to particle size (2-4mm) in readiness for pyrolysis and gasification testing. This crusher was designed for medium-hard, hard, and tough feed material.

Figure 4-2 Biomass grinding machine a) Labtech-Essa; b) Retsch.

4.3 Sand bulk density

The bulk density is defined as the mass of a batch of particles divided by the total volume therefore this includes particle volume plus void volume between the particles. According to BS 1337-9:1990, the bulk density was measured. The bulk density instrument consists mainly of two parts, pouring cylinder (long cylinder with a cone at the base) and calibrating container (flanged dish) as illustrated in Figure 4-3. A valve separates the conical portion from the cylindrical portion. The bulk density of bed material was measured as follows: (1) the volume in m^3 and weight in kg (m_1) of the empty calibrating cylinder was measured; (2) the weight of bed material that only filled the conical portion of the long cylinder was measured (m_2); (3) after the long cylinder was filled with sand, it was directly placed and fitted on the flanged calibrating container, and the valve was opened to allow the sand to run out and fill the calibrating cylinder and the cone space(m_3); (4) the mass of the sand inside the calibrating container (m_4) is given in following equation.

$$m_4 = m_3 - m_2 - m_1 \quad (4.6)$$

Bulk Density = m_4/volume.

The purpose of weighing including a hump of material (the material that forms in the cone) is to ensure that there is no human intervention to create a flat sample in the calibrating container. For instance, sweeping the sand away by hand or with a straight edge might change the bulk density in the container.

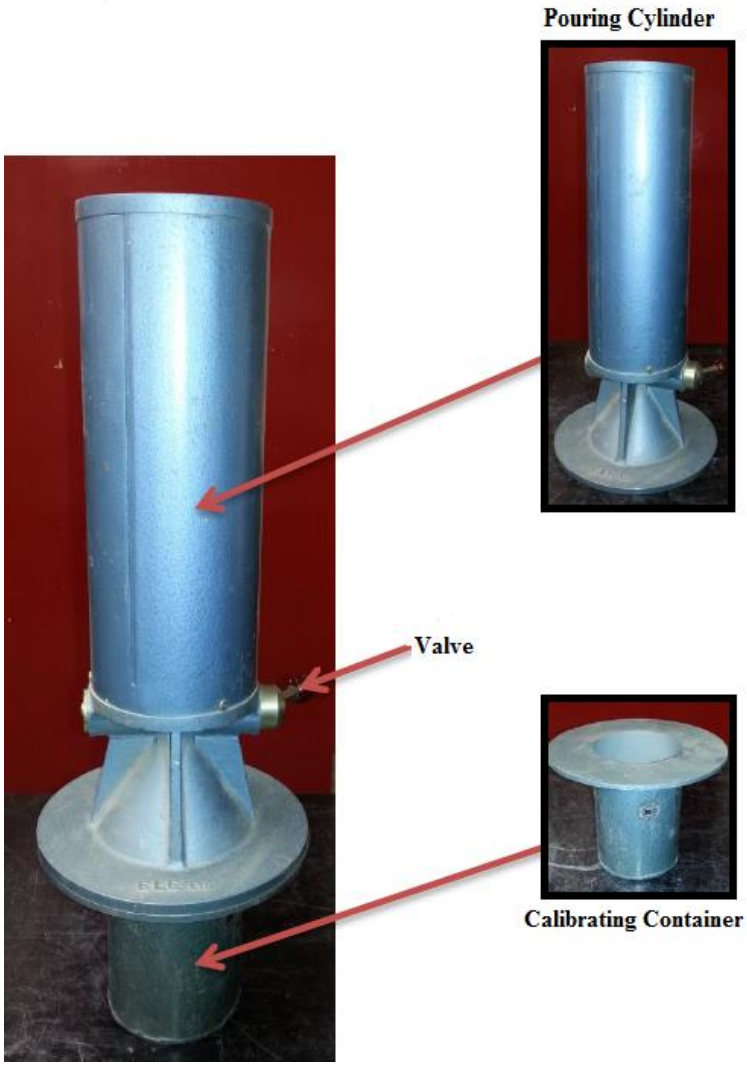

Figure 4-3 Sand bulk density apparatus; pouring cylinder and calibrating container.

4.4 Fluidization regime

The design and operation of fluidised bed reactors are highly dependent on the minimum fluidization velocity U_{mf}. It not only represents the value of drag force which is required to achieve solid suspension in the gas phase of the fluidised bed, but also constitutes a reference for the growth of intensity of the fluidization regime at higher velocity levels [199]. In addition, from the point of view of practical operation, the determination of U_{mf} is significant because it represents the onset of fluidization. There are essentially two methods to determine the U_{mf} : numerical methods and experimental methods (pressure measurement). Many empirical correlations are modified to predict the U_{mf}, but it is dependent on the design and physical parameters of the reactor and the bed material [200]. However, these empirical equations were determined based on reactors with their own inherent geometry and design, for instance the design of the diffuser plate and reactor diameter. Therefore, the equations cannot be universally applied to any new design, but they can be used to give an indication of values for U_{mf}.

A method to determine U_{mf} experimentally is by pressure drop measurements which rely on the fact that pressure drop across the bed is directly proportional to increasing air flow rate, which means that U is less than U_{mf}. When the value of U reaches a critical value; this equals the value of U_{mf}, where the pressure drop attains a maximum value. A slight further increase in the gas velocity, causes the particles to rearrange, and the voidage to change from ε_m to ε_{mf}, where the pressure drop declines slightly as illustrated in Figure 4-4. In this case, pressure drop remains approximately constant despite an increase in the velocity. The pressure drop through the bed is then equal to the bed weight divided by the cross sectional area of the bed, $\Delta p=W/A$ [201]. Where ε_{mf} is bed voidage at U_{mf} and ε_m is the corresponding voidage of the expanded bed. An experimental method was used in this study to obtain accurate results and avoid errors arising from differences in the physical parameters and geometry of this reactor from those of empirical correlations.

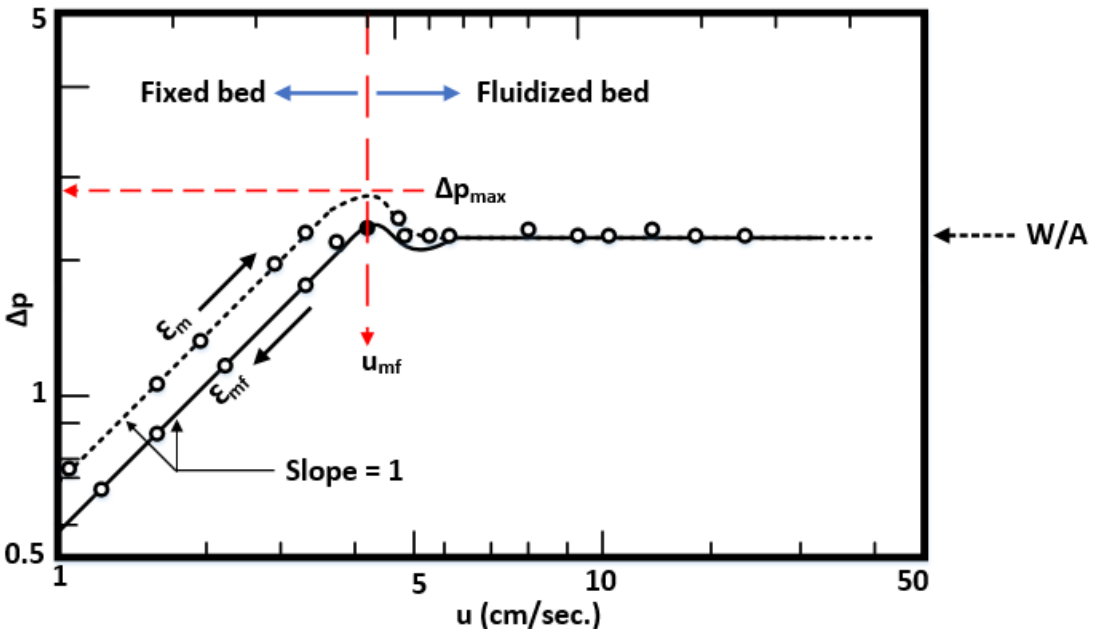

Figure 4-4 Pressure Drop Across a Fluidised Bed as Function of Fluid Velocity.

The fluidised bed gasifier performance predictions working at medium and high temperature normally rely on fluid dynamic models elaborated from experimental measurements obtained under typical room temperature conditions. The elutriation and attrition rates are strongly influenced by increasing U/U_{mf} ratio in a fluidised bed gasifier [202], where U is the superficial velocity. The physical properties of the fluidisation medium are affected by increasing temperature. Therefore, the hydrodynamic phenomena represented by U_{mf} inside the bed are also affected. Pattipati stated that the U_{mf} for small particles (<2mm) decreased when the temperature increased, while U_{mf} increased for large particle size (>2mm) with increasing temperature [203]. From the perspective of practical operation, the detection of minimum fluidization velocity is investigated at elevated temperature.

It should be considered that the properties of the bed material have an important effect on the hydrodynamics of fluidization. Geldart (1973) classified bed material according to behaviour when fluidised by gas into four groups. As shown in Table 4-5, only group B material is appropriate for bubbling fluidised bed gasification according to this classification.

Table 4-5 Geldard's classification of bed material.

Group A	The bubbles form and appear at velocities larger than the minimum fluidisation velocity (dense phase expansion before the beginning of bubbling).
Group B	Gas bubbles appear at the minimum fluidisation velocity. Sometimes these are called sand like or bubbly particles.
Group C	Fine and cohesive particles and difficult to fluidise.
Group D	Coarse particles. Sometimes known as a spoutable group.

4.4.1 Experimental measurement of minimum fluidization velocity.

Sand is the most popular bed material, and performs very well mechanically, as evidenced by its wide industrial use in circulating fluidised bed and bubble fluidised bed combustion implementations [204]. In this study, a known mass of size fractioned (500-600µm) silica sand was added to the top of the fluidised bed column, as shown in Figure 4-5. The details of the fluidised bed column and diffuser design can be found in Chapter 5, Section 1.3.1. The height of the static beds examined were (H_s/D=0.5) and (H_s/D=1). Where H_s and D are the static bed height and reactor diameter. The rig and preheater were set to the temperatures under consideration and the apparatus was allowed to reach thermal equilibrium. The airflow was then increased until the onset of bed fluidisation was detected. After that, the gas velocity was decreased gently until the fluidisation of the bed ceased, i.e. when fixed bed conditions had re-established. At any particular superficial air velocity, sufficient time is given for the exit air to attain the desired temperature. The pressure drop across the distributor plate and the bed were taken by differential pressure measurement manometers; two measuring points were drilled in the plenum and freeboard respectively. Upon measuring the pressure drop with increasing and decreasing superficial velocity, it was plotted against the superficial velocity as illustrated in Figures 4-6 and 4-7 at H_s=0.5D and H_s=D, respectively. The minimum fluidization velocity is commonly measured with decreasing fluidization velocity to avoid reliance on the incipient loading.

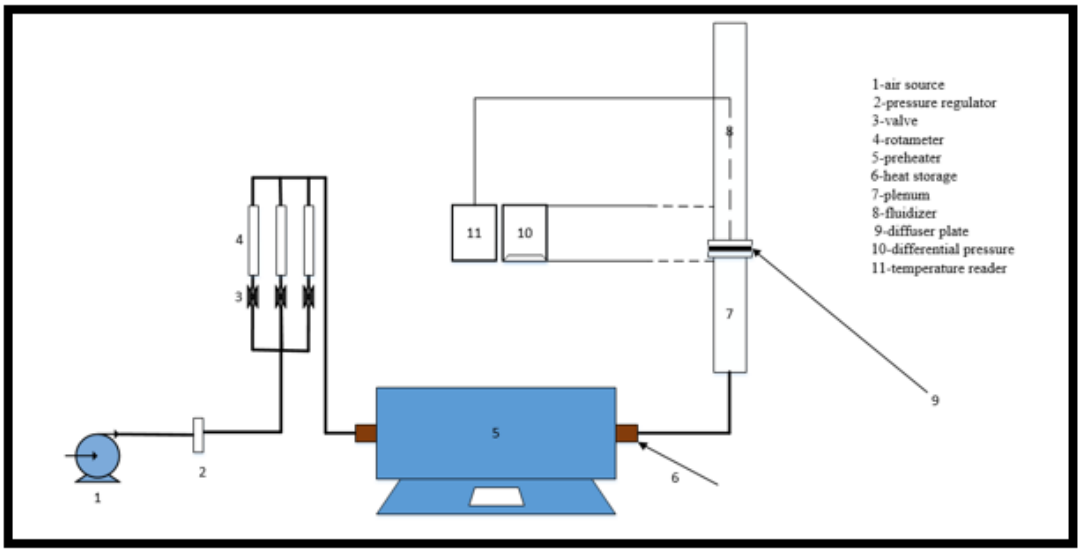

Figure 4-5 Bubble fluidised bed

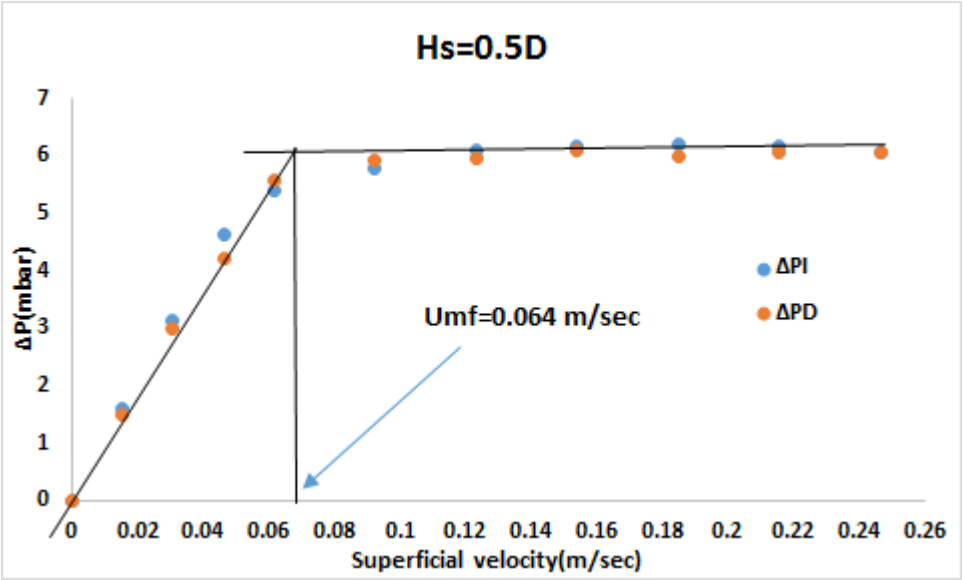

Figure 4-6 The plot of pressure drop against gas velocity at T=300°C, Hs=0.5D of silica sand (500-600 µm), fluidization and de-fluidization curves.

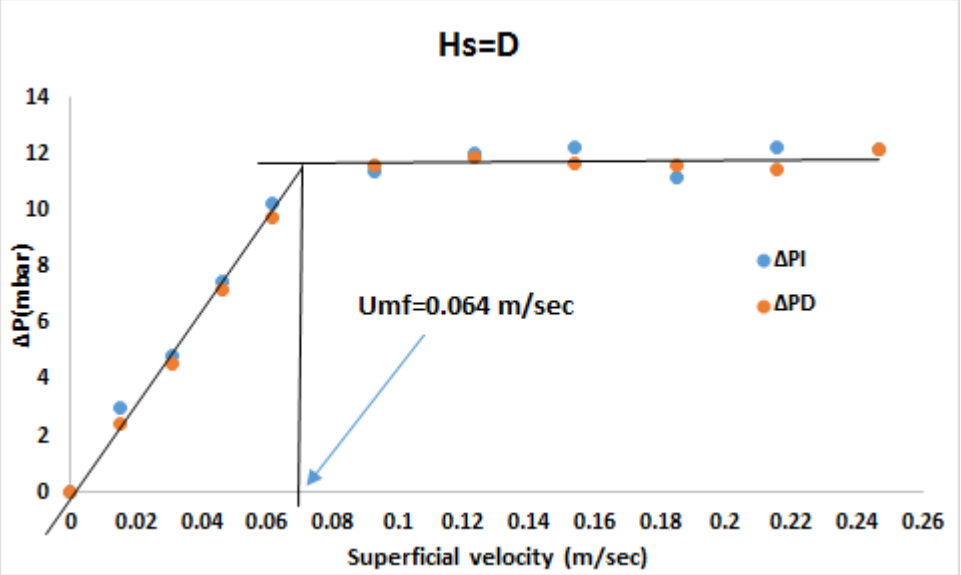

Figure 4-7 The plot of pressure drop against gas velocity at T=300°C, Hs=D of silica sand (500-600µm), fluidization and de-fluidization curves.

The intersection of the diagonal and horizontal lines was defined as the minimum fluidization velocity. The Umf at 300°C was found to equal 0.064 m/sec at Hs=0.5D and Hs=D. The static bed height of the fluidised bed does not affect Umf but only leads to an increase the pressure drop in the bed [205].

According to Choi et al [206], particles which have superficial gas velocity larger than the terminal velocity are usually found in the cyclone product of gas fluidised bed reactors. Therefore, one of the objects of this study was to keep the superficial velocity lower than the terminal velocity to avoid elutriation loss of bed material during experimental work.

Kunni and Levenspiel [207] presented the following equations to determine the terminal velocity.

$$d_p^* = d_p\left[\frac{\rho_g(\rho_s - \rho_g)g}{\mu^2}\right]^{1/3} \quad (4.7)$$

For spherical particles:

$$u^* = \left[\frac{18}{(d_p^*)^2} + \frac{0.591}{(d_p^*)^{0.5}}\right]^{-1} \quad (4.8)$$

Where $\mathbf{d_p^*}$ and **u*** are a dimensionless particle size and a dimensionless gas velocity, respectively.

$$u_t = u^*[\frac{\mu(\rho_s - \rho_g)g}{\rho_g^2}]^{1/3} \quad (4.9)$$

where d_p is the mean particle size in metres; g=9.8 m/s^2; μ is viscosity of gas in kg/m.s; ρ_s is the density of solid particles in kg/m^3; and u_t is the terminal velocity in m/s.

Silica sand with a density of 2650 kg/m^3 was used as a bed material in this experiment. Silica sand was sieved in BS sieves to obtain 500-600μm particle size and the mean particle size was determined using the following equation:

$$d_p = 1/\sum_{i=1}^{n}(\frac{x_i}{d_i}) \quad (4.10)$$

Where x_i is the volume fraction of the particles having d_i as average diameter. The measurements were obtained from a Malvern Mastersizer 3000 (see Figure 4-8), in which the data was determined by a laser diffraction particle size analyser. Figure 4-9 shows the particle size distribution of the sand. It can be seen from the figure that the particle size distribution is narrow and this reduces the probability of the smaller particles slipping into the void spaces of the larger particles. The mean particle size was 540μm.

Figure 4-8 Malvern Mastersizer 3000.

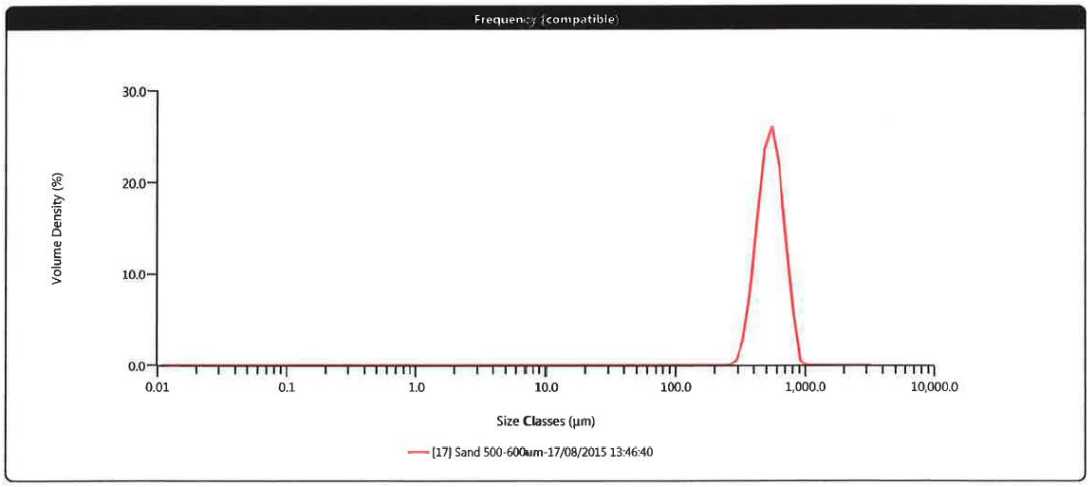

Figure 4-9 Particle size distribution of sand (500-600µm)

For calculation: Air: $\rho_g=1.2\times10^{-3}$ g/cm^3; $\mu=1.8\times10^{-4}$ g/cm.s

Sand: $d_p=540\mu m$; $\rho_s=2.65$ g/cm^3.

The u_t was calculated by using equations (4.7), (4.8), and (4.9). The terminal velocity was found to be 0.89 m/sec higher than the superficial velocity of the upward gas flow.

Olive kernels have a high density compared to other biomass, with a density of about 650 kg/m^3 [51]. The density of palm stones was found to be about 560 kg/m^3 [25]. The biomass was fed from the top of the reactor through a pipe that reached directly into the bed. The top end of this pipe was attached to a closed top hopper to reduce any stream of flow from the reactor. These steps were taken to avoid elutriation of sample which was critical given the measurement accuracy required of mass changes in the reactor.

4.5 Batch pyrolysis experimental procedure

The fast pyrolysis of olive kernels of different particle sizes (300-500, 500-710, 710-1180 µm, and as received) was carried out in a fluidised bed reactor, Figure 5-1, see Chapter 5, shows a schematic diagram of a thermogravimetric fluidised bed reactor (TGFBR). The experimental work was started by heating the reactor to the required temperature whilst keeping the silica sand particles fluidised at a constant rate. After that, the air stream was stopped and the nitrogen stream flowed at twice the value of minimum fluidization velocity (u_{mf}) until steady state temperature conditions inside the reactor were obtained. A flow velocity of ($2u_{mf}$) was chosen because this is the minimum gas velocity required to limit external diffusion (see Section 6.2.1, Chapter 6). Olive kernel biomass was fed from the top of the reactor through a pipe into the hot fluidised bed. The amount of biomass used in each test was 40 g which represented 10% wt. of the total weight of bed material. The weight variation in the TGFBR during pyrolysis was recorded at 1 second time intervals. The same procedure was used for palm stones, however, only 2-4mm particle size was used. In addition, a gas analyser was used during the pyrolysis test to study the influence of bed temperature on product gas.

4.6 Torrefaction experiments

A lab-scale Carbolite furnace and nitrogen supply was used to torrefy the olive kernel samples. A batch of 50g of AROK sample was loaded onto a steel tray, and inserted into the furnace at a pre-set temperature of 280°C for a 30-minute residence time. The nitrogen flow is used to keep the system inert by eliminating the presence of oxygen and sweeping volatile products from the atmosphere of furnace. Once complete, the sample was taken out and cooled for 5-10 minutes and the weight was taken. The torrefaction residence time of 30 minutes was considered to be optimal from

preliminary studies [208]. Moreover, for industrial applications a reduction in residence time will reduce the reactor size, which lowers the investment cost. Figure 4-10 illustrates a schematic view of the experimental setup.

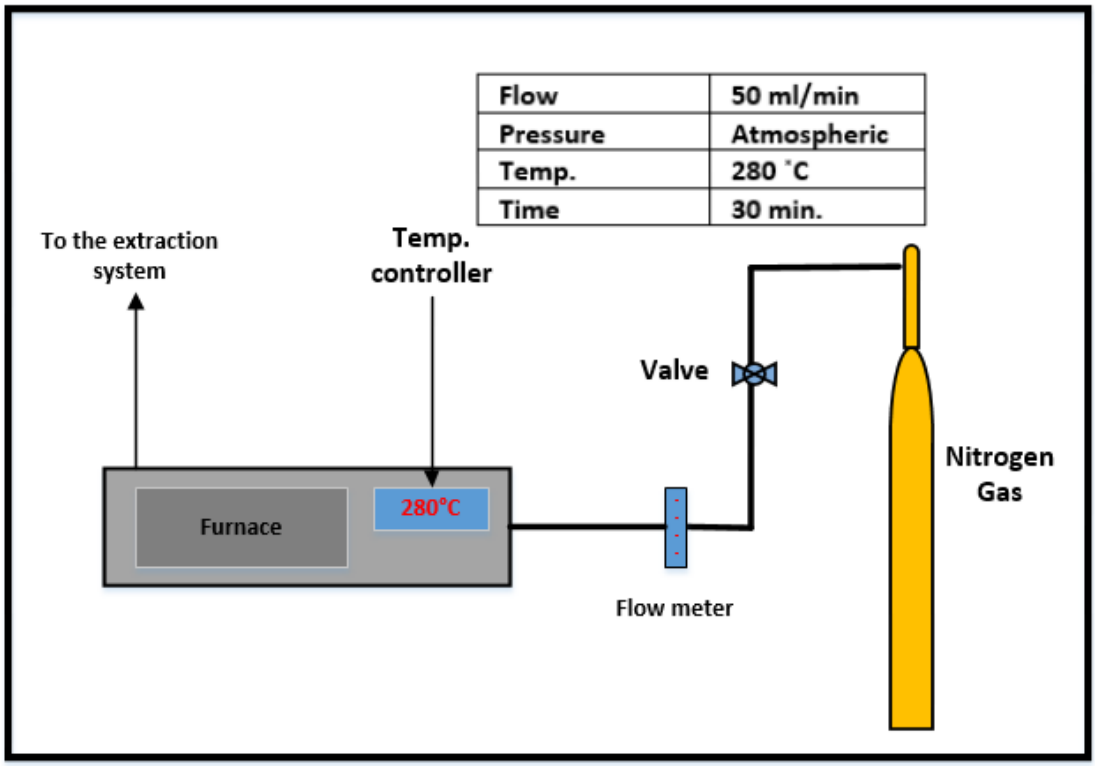

Figure 4-10 Schematic setup of the bench torrefaction unit

Two of the most important parameters in evaluating torrefaction are the mass and energy yield of the process. Where mass yield represents the ratio of actual mass retained after the torrefaction to the initial mass of biomass. The mass and energy yields of the biomass were calculated, based on equations (4.11) and (4.12) cited by Poudel et al [209].

$$\text{Mass yield } (Y_{mass}) = \left(\frac{\text{Mass after torrefaction}}{\text{Mass of raw sample}}\right) \times 100\ \% \tag{4.11}$$

$$\text{Energy yield}\left(Y_{energy}\right) = Y_{mass}\left(\frac{HHV_{\text{torrefied sample}}}{HHV_{\text{raw sample}}}\right) \times 100\ \% \tag{4.12}$$

4.7 Char yield of pyrolytic biomass.

Char yield, Y_{ch}, refers to the char remaining after devolatilization of biomass. Bio-char can be obtained from biomass pyrolysis [210]. The char obtained from the gravimetric method is closely analogous to the actual conditions in a fluidised bed gasifier, because no cooling occurs between the devolatilization stage and gasification [211]. Therefore, this procedure was used to investigate the char yield of biomass under inert conditions (nitrogen gas) by using a similar superficial velocity to that of a full-scale industrial system. It is necessary to calculate char yield during pyrolysis conditions to calculate kinetics later in the gasification experiments.

Both AROK and ARTOK were tested under 40 l/min N_2 at a temperature of 525°C and 550°C, under the assumption that the char yield remains approximately the same, and to maintain consistency of calculations. Prior to pyrolysis testing, the reactor was heated up to the required temperature with $2U_{mf}$ air flow rate. Once heated, the air stream was replaced with the same flow rate of nitrogen until steady state temperature was obtained. In two separate tests, 40 grams of AROK and 40 grams of ARTOK was fed into the reactor. The initial mass fed and the char left inside the reactor were recorded by the weighing scale.

Zabaniotou et al. [19] reported that the olive kernel char yield decreased with increasing temperature during pyrolysis up to 500°C after which the yields tend to be constant. According to Blasi, the final char yield is less affected when the temperature is increased above 650-750K (377-477°C) for all particle sizes. Consequently, (although for different reasons) for both pyrolysis regimes, the char yield value tends to a constant value as the temperature is increased [112].

4.8 Thermogravimetric analysis (TGA).

Thermal decomposition behaviour of various particle sizes of olive kernel biomass under inert conditions was investigated using a thermogravimetric analyser (TGA) and thermogravimetric fluidised bed reactor (TGFBR) as detailed in section 4.5. However, palm stone biomass was only investigated in the TGFBR for one particle size only.
Thermogravimetric analysis (TGA) is a technique in which the mass of material is monitored as a function of time or temperature when the sample is exposed to a controlled temperature program and in a controlled atmosphere. In many processes

such as pyrolysis, gasification, and combustion, TGA is commonly used to study the thermal behaviour by determining the mass loss characteristics of biomass at a wide range of heating rates (0-60°C/min) and temperatures (up to 1300°C), and under pressurised conditions. The most significant application of this technique is to investigate and study the degradation mechanisms and reaction kinetics of biomass in thermochemical conversion processes.

The data obtained from TGA is usually utilised to construct a thermogravimetric (TG) curve. From this curve, the dynamic mass losses against temperature or time can be analysed. By differentiating the TG data, the differential thermogravimetric data (DTG) can be obtained which represents the conversion rate of biomass during the thermal process.

Pyrolysis analysis of olive kernels was carried out in a Mettler Toledo TGA (see Figure 4-11). Approximately, 10 mg of the biomass sample was loaded into an alumina crucible. The crucible was tapped gently on a hard and clean surface to distribute the biomass sample. Then, tweezers were used to carefully place the crucible onto the TGA carousel. After the sample was automatically loaded into the furnace, a program with a heating rate of 20°C/min in an inert atmosphere was started. An inert atmosphere for pyrolysis was achieved using nitrogen with a flow rate of 50ml/min. The nitrogen flow served to carry away gaseous and condensable products in order to reduce any secondary vapour-phase interactions. Mass losses that correspond to temperature change were continuously recorded with data acquisition working in coordination with the furnace. After the programme was finished, the data was exported for analysis. The sieved size classification of the olive kernel sample tested under pyrolysis conditions was 300-500µm, 500-710µm, 710-1180µm and 1180-1400µm.

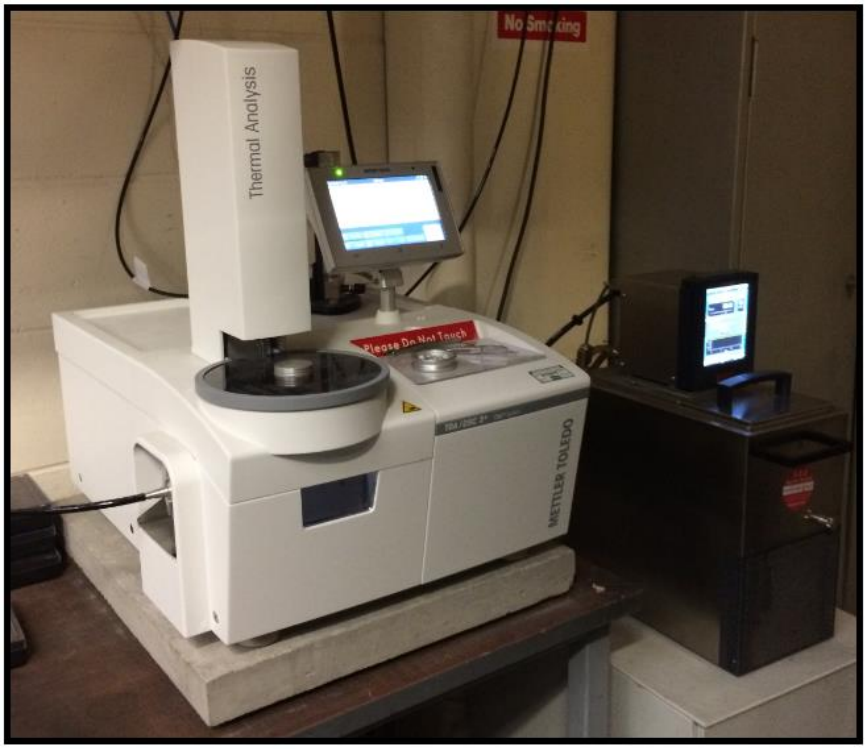

Figure 4-11 TGA-DTA system.

4.9 Summary

The materials and methods used in characterising the sand as a bed material were described in this chapter. Two types of solid biofuel, olive kernels and date palm stones, were also discussed. These materials were characterised according to various standard methods. In order to calculate the mean particle size of the sand, a Malvern Mastersizer 3000 analyser was used. In addition, the sand's bulk density was measured. Grinding machines were used for biomass size reduction.

Proximate and ultimate analyses were used to characterise the biomass fuels. Proximate analysis was utilised to determine biomass characteristics. By using the ultimate analysis, the combustion elements were quantified which was necessary to determine the chosen equivalence ratios. Thermogravimetric analysis was used to investigate the thermal behaviour of different particle sizes of olive kernels under pyrolysis conditions.

The methods used to determine the minimum fluidised bed velocity experimentally using a ΔP-U curve were described. The calculation of terminal velocity from theoretical equations was presented, which is important regarding elutriation loss of bed material in a fluidised bed reactor.

Chapter 5:

Gasifier equipment, experimental procedure and kinetic model

5.1 Gasifier methodology

5.1.1 Introduction

In this chapter, the details of the experimental rig setup, gasification procedure, operating conditions, gasification performance equations, gas analysis method, and kinetic approaches are presented and described.

A small pilot scale thermogravimetric fluidised bed reactor (TGFBR), designed and fabricated in the School of Engineering at Cardiff University was used in this study. A schematic diagram of the TGFBR is illustrated in Figure 5-1 and Figure 5-2. The system consists of seven sections: biomass feeding system, gasifier (which is consists of an air box section and perforated distributor plate), air delivery system, heating system, downstream gas cleaning, and product gas analysis.

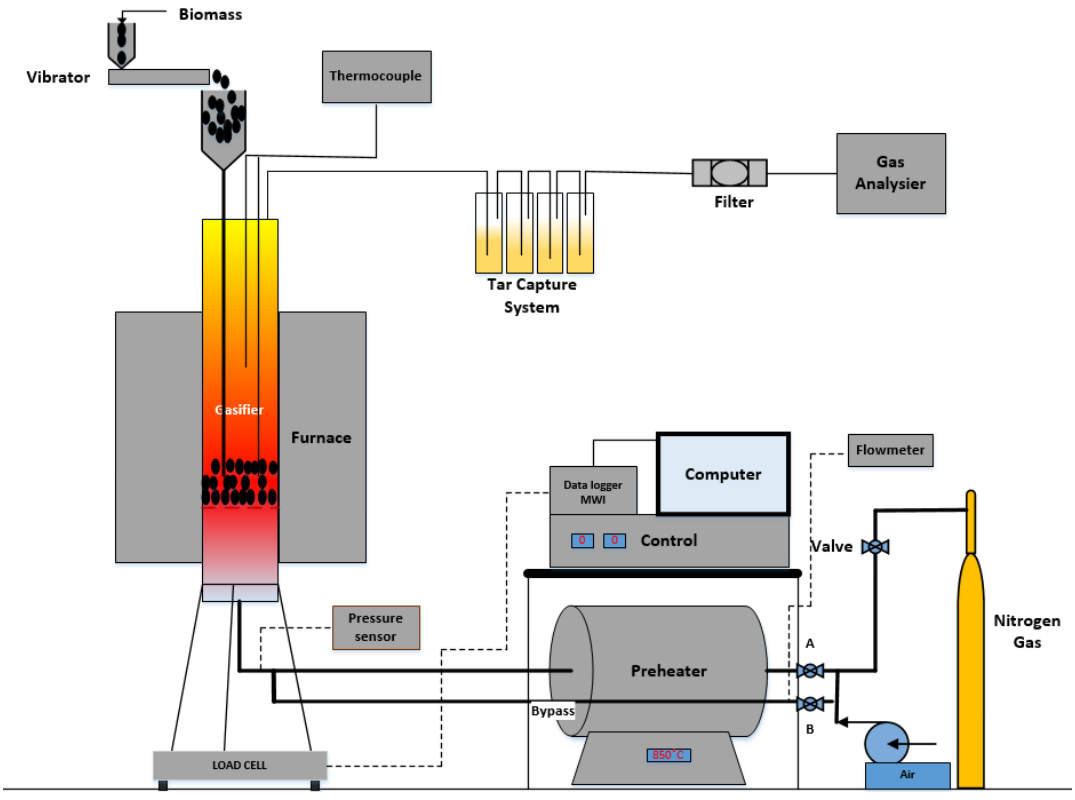

Figure 5-1. Thermogravimetric fluidised bed gasifier (Schematic diagram).

Figure 5-2. Thermogravimetric fluidised bed gasifier.

5.1.2 Biomass Feeding System.

The feeding system for gasification fuels is usually based on screw feeders, but such devices do not give accurate feed rates especially if different particle sizes are used. To avoid this, biomass particles of a pre-determined size were fed into reactor through Fritch vibrating feeder connected at the top of the gasifier (over bed system). The operating principle of the instrument is as follows; a channel made of stainless steel is set in vibration by an electromagnet. A funnel made of stainless steel, which is fastened to a height-adjustable pillar, dips into this channel as showed in Figure 5-3. The biomass to be conveyed is filled into the funnel. The electrical control system determines the oscillation amplitude of the vibrating channel and hence the amount and flow rate of the material conveyed.

Figure 5-3 The fuel feeder (Fritch vibrating feeder).

The feeder drops the biomass inside a closed hopper to prevent any counter current stream of flow coming from reactor as illustrated in Figure 5-4. The biomass is then transferred from the hopper to reaction zone through a 1-inch diameter pipe. The feed systems over the bed are usually less troublesome because there is not direct contact between the feeder and the hot bed material. However, this type of feeding system is limited to higher density of feed material [107]. The mass flow rate was checked and calibrated mass of the biomass over a specific time.

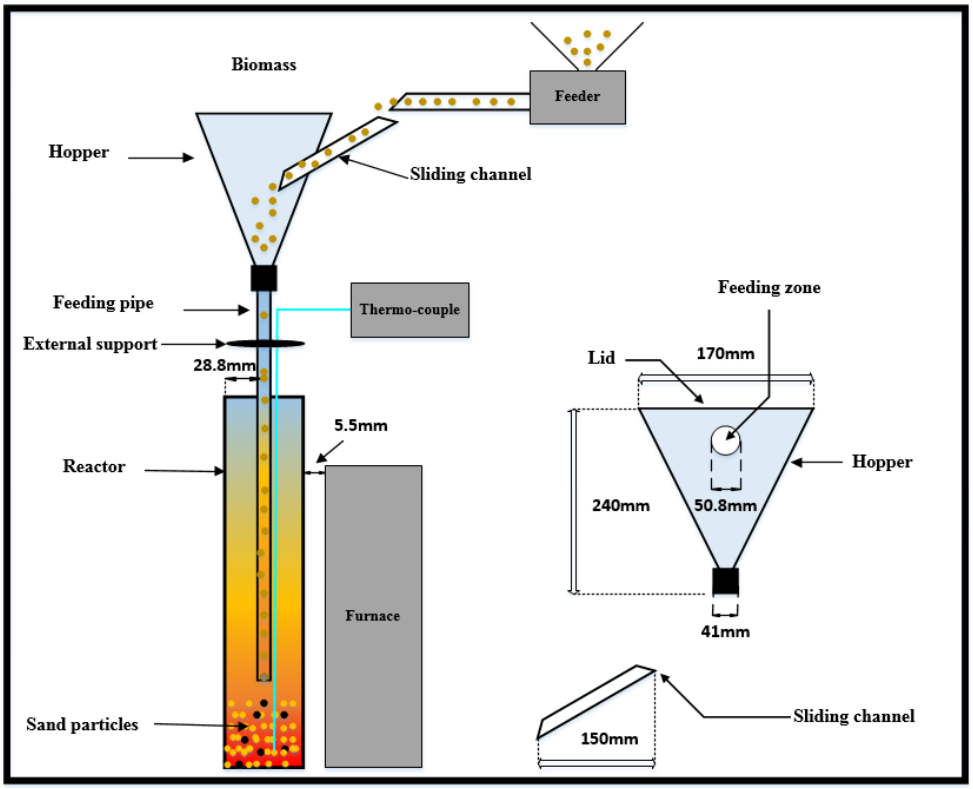

Figure 5-4 Schematic diagram design of hopper and top feeding system unit.

5.1.3 Gasifier

The gasifier is the main part in the gasification process in which the gas solid reaction takes place between the biomass and gasification agent which consists of the following components.

5.1.3.1 Fluidised bed reactor and freeboard.

The fluidised bed reactor was made from cylindrical 316L stainless-steel tube, 1250mm high and inner diameter 83mm. The static bed height used during gasification testing was Hs=0.5D, with the remainder of the height being the freeboard, which is a defined as the distance between the top surface of bed material and the end of the cylindrical tube. In order to reduce the carryover from fluidization, the freeboard should be at least the height of Transport Disengaging Height (TDH), which is an important parameter for the fluidised bed column. Based on the Equation (5.a), the TDH was determined [201].

$$TDH = 0.85U^{1.2}(7.33 - 1.2logU) \quad (5.a)$$

Where, U is superficial velocity, m/sec and TDH in meters.

5.1.3.2 Plenum (Air box).

The plenum is the space located in the lowest part of the gasifier underneath the perforated diffuser plate. The main purpose of the plenum is to distribute the incoming air to help maintain the same air flow rate from each perforation. In addition, the air can be preheated prior to reaching the fluidised bed if the plenum is surrounded by the heater. In literature, there is no design calculation regarding the plenum, only brief design configurations shown by Yang [201]. The plenum was made from the same material as the reactor pipe section. The dimensions of the stainless-steel pipe used to make the plenum were 89mm outside diameter, 83 mm inside diameter, and 500mm height. A flat plate with a 1" diameter hole in the centre was welded to the bottom end of this pipe. Through this 1" diameter hole, a stainless-steel pipe was welded so that the distance from its end to the top of the plenum was 100mm. To this open plenum top end, a larger diameter tube of length 50mm to act as a flange was welded, to hold the diffuser plate. Figure 5-5 illustrates the plenum dimensions.

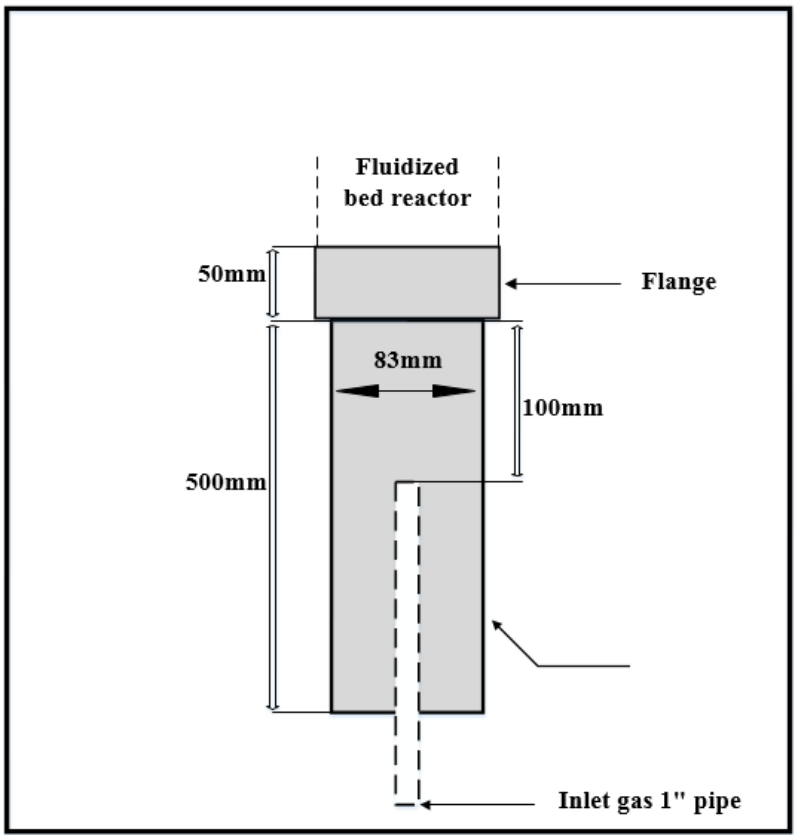

Figure 5-5 Schematic diagram of plenum (Air box).

5.1.3.3 Diffuser Plate.

A perforated diffuser plate was made from 5mm thick stainless steel with 151 uniformly drilled holes of 1 mm diameter arranged in a triangular pitch; this plate was used to retain the bed fluidization material and to supply the bed material with homogeneous air distribution. A perforated plate was used in this study because it improved the mixing significantly (less segregation tendency) compared to a porous plate [212]. Depending on the number of the orifices, the density of orifices (ND) was determined and from that the orifices pitch (P_{pitch}) was calculated, as illustrated in the following Equations ((5.b) and (5.c)) and Figure 5-6.

$$ND = \frac{no.of\ holes}{AREA\ (cm^2)} \quad (5.b)$$

For equidistant, triangular layout:

$$P_{pitch} = \frac{1}{\sqrt{ND * sin60^{\circ}}} \quad (5.c)$$

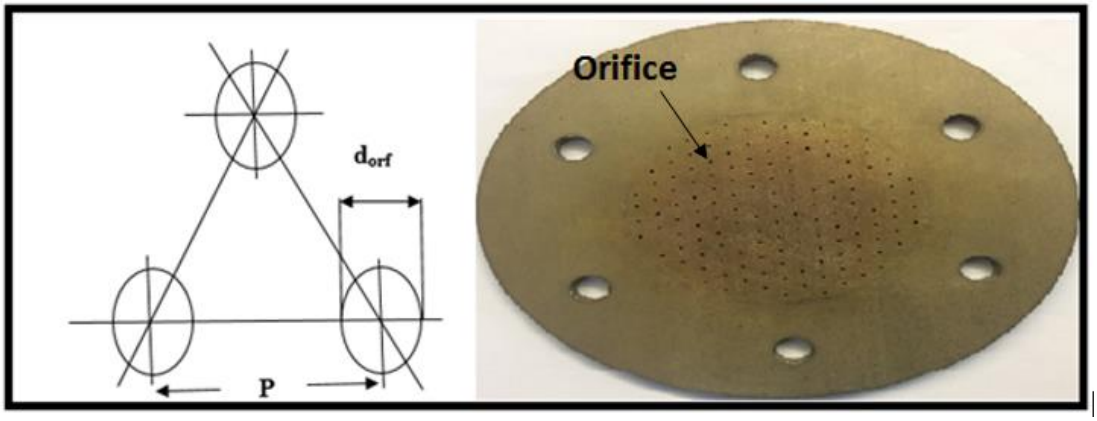

Figure 5-6 Triangular Pitch layout and diffuser plate.

5.1.4 Air delivery system

The air was supplied from a 7-bar air compressor and then controlled to with a regulator valve upstream of the rotameters. Three Platon-type rotameters were used to meter the air flow rate with different capacities of 12 l/min, 50 l/min and 150 l/ min working at ambient conditions. These were manufacturer calibrated to within ±1.25% of reading (as standard). The purpose of using three rotameters was to measure a wide range and give an accurate gas flow rate for hydrodynamic measurements. The fluidization gas entered the plenum through a flexible stainless-steel pipe.

5.1.5 Heating system.

Heating the gasifier was achieved via a vertical split tube furnace that was supplied by LTF, model number PSC 12/100/900 and designed to achieve an extended uniform temperature zone by the use of three control zones, with a maximum set point temperature of 1200ºC. The split tube design enabled the electrical furnace to float around the gasifier and provide heat without contributing to the mass reading on the load cell. This enabled the gasification mass change to be measured without additional components causing errors in the mass readings. In addition, the biomass feeding system, thermocouples, and gasifier outlet pipe to the gas analyser, were independent of the gasifier and did not make physical contact (see Figure 5-4). The only external

physical contact with the gasifier was a flexible stainless-steel supply gas inlet (attached to the base of the plenum). All of the above had to be carefully considered when designing the TGFBR.

In order to avoid temperature decline in the gasifier with increasing flow rate, the fluidising gas was preheated prior to reaching the plenum. This was achieved by passing the supply of fluidising nitrogen/air through a 50mm i.d. 670 mm long tube filled with beads of Impervious Alumina Porcelain (IAP). This tube was surrounded by an electrical horizontal tube furnace, supplied by LTF, model number 12/100/940. The purpose of the IAP beads was to improve heat transfer between the heater and the gas, and to provide thermal mass thus ensuring a steady supply temperature to the gasifier. It was important maintain a constant temperature in the gasifier for the purposes of isothermal measurement. Fig. 5-7 shows a diagram of the preheating arrangement. The rated power output of the split furnace and preheater were the same (4.5 KW).

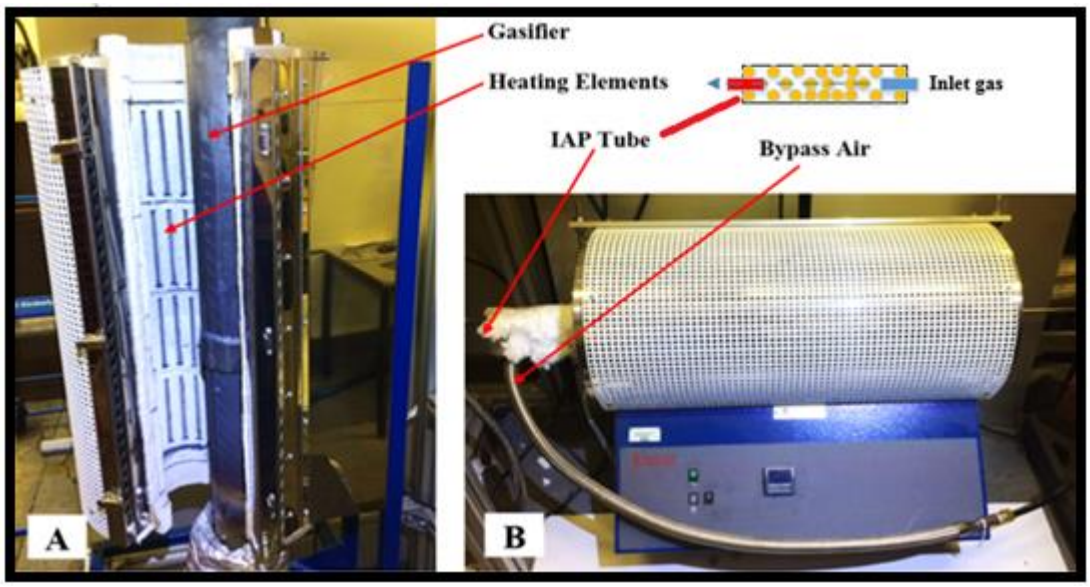

Figure 5-7 Heating system; a-Split furnace, b-Preheater tubular furnace.

5.1.6 Mass and temperature measurement.

The gasifier described in Section 5.1.3 sits on a bespoke platform load cell designed and made for this purpose by Coventry Scale Company. It has a tolerance of +/- 0.5g and a weighing range up to 25 kg. The load cell was connected to a computer via a

multifunction weight indicator, model DFW06XP. The computer used bespoke logging software which enabled the mass change to be recorded at 1 second intervals, during experimentation. Figure 5-8 shows a photograph of the load cell and the multifunction weight indicator.

Pressure transducers are normally used to detect the pressure drop across two different points in the reactor in order to check that the bed is fluidizing correctly, and has not agglomerated. However, the design requirement of this TGFBR was to study the kinetics, so a pressure transducer in the fluidised bed would have added error to the mass measurements, because it would have been an extra accessory attached to the gasifier, when the purpose was to ensure that it floats inside the split furnace with minimal interference. Pressure gauges are needed in the interests of safety. Therefore, a gauge was fitted to the inlet of the plenum, but not inside the gasifier as well. In addition, the real time dynamic mass measurement proved whether the test occurred with or without agglomeration through a sharp increase in the mass recorded, indicating that fluidization had reduced and mass was accumulating in the furnace. This happens because as the bed agglomerates, the inlet air starts to form channels between the agglomerates instead of fluidising the bed. This phenomenon prevents heat transfer and gas diffusion to the biomass which causes poor gasification.

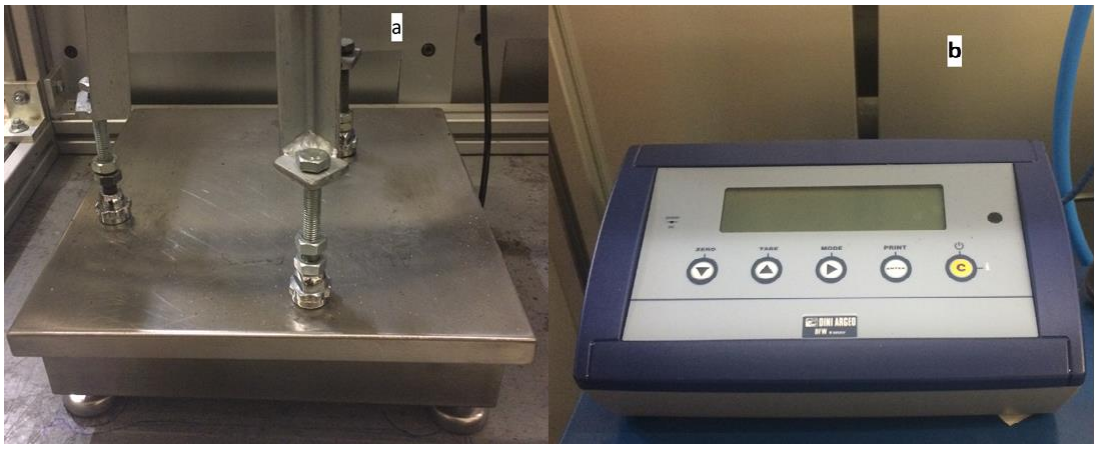

Figure 5-8 a-A bespoke platform load cell, b- A multifunction weight indicator model DFW06XP.

In order to monitor the temperature of the reactor, two Type-K thermocouples were positioned in the reactor at the location marked in Figure 5-1. One of the thermocouples was installed in the bed zone (30 mm above the distributor plate) and

the other was located in the freeboard. Data acquisition hardware (from Omega) was connected to the computer to continuously record the temperatures in the bed and freeboard. DAQ central data logging software was installed in the host computer. A high-speed USB cable transferred the data from the Multiple Channel Data Acquisition Module, model number (OM-DAQ-USB-2401) to the computer. When data acquisition was complete, the data was exported to Excel for analysis.

5.1.7 Downstream cleaning system and gas analyser

In order to obtain a clean product gas, the outlet gas was sent to a downstream cleaning section consisting of a tar capture unit composed of four dreschel bottles, MF 29/3/250, inside a freezer (BEKO, ZA630W) set to -10°C. The bottles contained 99.8% isopropanol. There were two holes on the top side of the freezer, one for the gas inlet from the gasifier and the other for the outlet which led to a fibre filter trap and then into two silica gel bottles before entering the gas analyser. The cleaning system is illustrated in Figure 5-9. A membrane pump was installed after the tar capture unit to overcome the pressure drop resulting from the pipe and tar capture unit and to provide smooth gas flow.

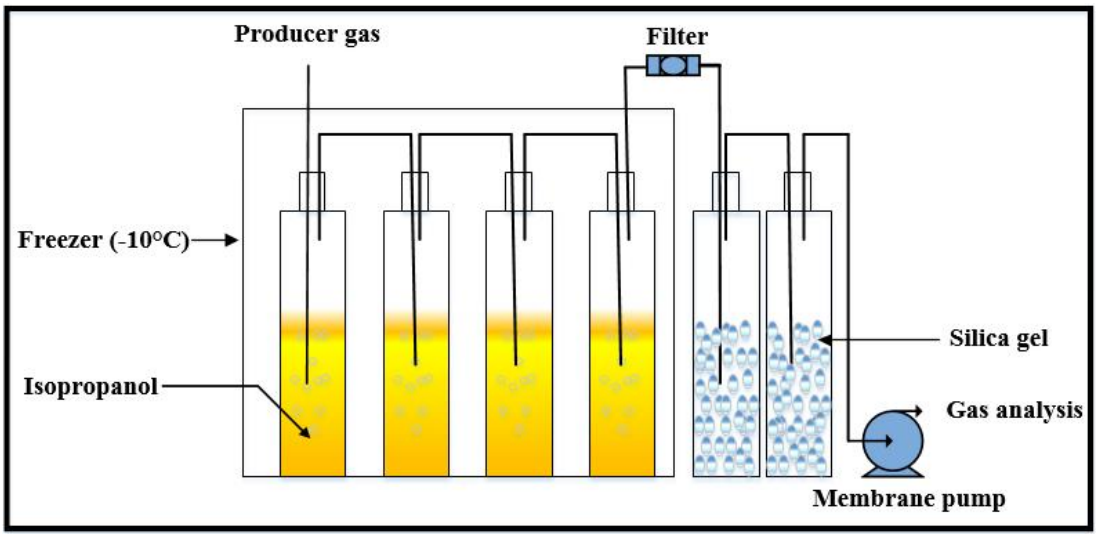

Figure 5-9 Downstream cleaning system.

In this study, the product gas was analysed using an Emersion X-Stream gas analyser, model number XEA04303555317 (see Figure 5-10). In order to control the product gas flow rate to be within the flow rate limitations of the gas analyser, a small-scale rotameter, not exceeding 1 l/min, was used. The chosen gas analyser can measure up

to five different gases based on any combination of the following analysing mechanisms; UV (ultraviolet analysis), IR (non-dispersive infrared analysis), eO2 and pO2 (electrochemical and paramagnetic oxygen analysis), TC= thermal conductivity analysis. This gas analyser was able of detecting CO, CO_2, CH_4, H_2, and O_2. The data obtained from gas analyser was as a volume percentage for each individual gas measured against time.

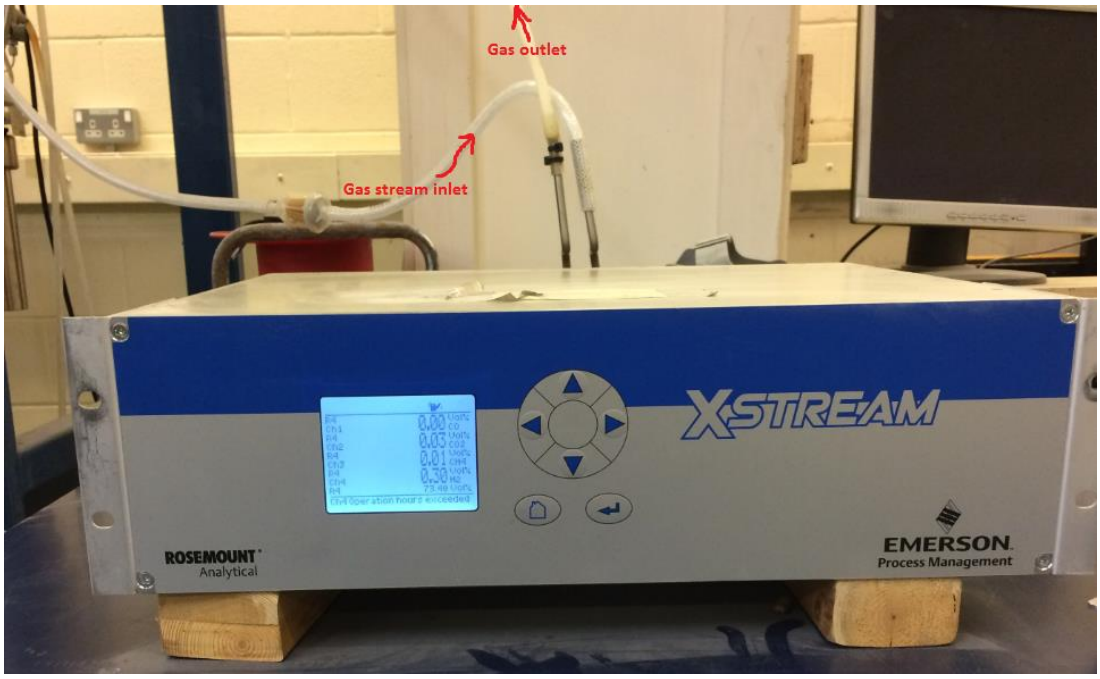

Figure 5-10 gas analyser type X-Stream model XEA04303555317.

5.2 Safety considerations.

The operation of the gasifier comprises certain hazards which are given as follows:

- Elevated temperatures Max. 1000°C (skin burns).
- Extremely toxic and moderately combustible gases (H_2, CO).
- Tar as a carcinogenic substance.
- Hazards associated with gases under pressure (N_2, air).
- Electrical hazard (high voltage).

In order to reduce the above hazards and their consequences, several safety measures were undertaken:

- The gasifier was set up in an isolated area of the combustion lab. The combustible gases produced from the gasifier were removed by a powerful extraction system located directly above the gasification system.
- Two toxic gases detectors were used. One was worn on the person and the other was left beside the gasifier plus lab gas monitoring system.
- The control system, i.e. biomass feeder, air supply, nitrogen source, and data acquisition equipment were placed at a distance from the gasifier in order to have control over the system from outside the risk area.

5.3 Gasification procedure.

The overall experimental preparation procedures undertaken for the operation of the fluidised bed gasifier were as follows:

1. The day before gasification testing the freezer was switched on and 100ml of isopropanol was poured into each of the 250ml dreschel bottles in the tar capture unit located inside the freezer. The freezer was set to -10°C and this was verified with a thermocouple.
2. Prior to testing, the gas analyser was zero calibrated on N_2 and then with span gas mixture supplied by Air Products. The standard gas mixture used for gas analyser calibration was composed of CO, CO_2, H_2, and CH_4 with concentrations of 15%, 15%, 15%, and 5% respectively. The balance was N_2.
3. Depending on the (H_s/D) ratio, a required amount of silica sand with a density of 2650 kg/m^3 was used and added as bed material to the gasifier; its particle size was 500-600µm.
4. The preheater, split furnace and air blower were activated and the temperatures monitored using a data logger. The superficial velocity was constant at 40l/min, twice the value of U_{mf}.
5. The computer was switched on and the data logger and multifunction weight indicator were activated.

6. The vibrating feeder was then calibrated gravimetrically for each mass flow rate depending on ER by direct weighing of the biomass for 5 minutes. The biomass was fed at 80mm above the distributor, through a tube made of stainless steel with 1" i.d. from a hopper by a vibration feeder. The mass flow rate of biomass was varied based on the selected ER and the other condition (air flow rate) was held constant. It should be mentioned that the feeding rate to obtain a desired ER was not the same for torrefied biomass due to the stoichiometry being different. This procedure was repeated three times to ensure repeatability was achieved. The hopper was filled with biomass ready for the gasification test.

5.3.1 Experimental test run.

After the desired temperature and steady state conditions were obtained inside the gasifier, the lab extraction system was switched on. To direct some of the product gases to the gas analyser, the suction pump was activated. The feeder was activated to deliver a consistent flow of biomass at a certain ER into the gasifier and directly the split furnace was switched off. Valve B was opened and valve A closed to provide ambient air to quench the heat generated inside the gasifier during gasification. The load cell started recording the dynamic mass inside the gasifier every second and this information was logged by the computer. After cleaning of the product gas in the tar capture unit, the suction pump discharged the gas to the gas analyser. The gas analyser recorded, in real time, the volume concentration of gases from the reaction as a function of time.

After the gasifier was shutdown, it was allowed to cool to room temperature over a period 5 hr and then the sand was replaced for the next test. The gas analyser was purged with N_2 and re-calibrated. Due to the high tar content in the gasification process and to prevent any blockages, the PVC pipelines which transfer the product gas from the gasifier to the analyser were replaced by a new pipe after each run, whereas the stainless-steel pipes were cleaned.

5.4 Feed rate settings.

Air-fuel ratio is one of the most defining parameters governing the gasification system as discussed previously in Chapter 2. The definition of ER is the ratio of actual air per unit mass of biofuels fed into the gasifier to its corresponding stoichiometric air. The connection between ER and stoichiometric and actual air-fuel ratios was defined using equation (5.1)

$$ER = (air/biomass)_a/(air/biomass)_s \quad (5.1)$$

Where a is actual air biomass ratio and s is stochiometric ratio.

The principle of gasification is based on the partial oxidation of biofuel. To achieve this, the oxygen supply for the actual biomass amount must always be less than its stoichiometric quantity. From the full combustion of C, H and S (from ultimate analysis), the stoichiometric air flow rate was determined. The N is excluded in the combustion calculation because the typical gasification temperature is not high enough to convert N to NO_X.

According to the chemical reactions of combustion from reaction 1 to 3 with the respective combustible species in the fuel (C, H, O, and S), the stoichiometric oxygen amount was determined.

$C+O_2 \rightarrow CO_2$	**Reaction 1**
$H_2+0.5O_2 \rightarrow H_2O$	**Reaction 2**
$S+O_2 \rightarrow SO_2$	**Reaction 3**

The total amount of stoichiometric oxygen was obtained by adding the oxygen required for reactions 1, 2 and 3, and then subtracting the inherent oxygen in the fuel. This enabled the total amount of stoichiometric air to be determined. The air-fuel ratio (AFR) stoichiometry was calculated by dividing the mass of required air by the mass of fuel as illustrated in Table 5.1 and Table 5.2 for raw and torrefied biomass. At a given ER, the actual air fuel ratio was determined for raw and torrefied olive kernels as follows:

$$[\mathrm{AFR}]_a = \mathrm{ER} \times [\mathrm{AFR}]_S \quad (5.2)$$

Where $[\mathrm{AFR}]_a$ is actual air fuel ratio, $[\mathrm{AFR}]_s$ is stoichiometric air fuel ratio.

The actual air ratio is determined by the mass rate of air required $\dot{m}_{air}$ to the mass rate of fuel $\dot{m}_f$. Therefore, the required biomass flow rate can be determined by using Equation (5.3);

$$\dot{m}_f = \dot{m}_{air}/[\mathrm{AFR}]_a \quad (5.3)$$

The air mass flow rate is calculated depending on Equation (5.4);

$$\dot{m}_{air} = \text{volumetric flow rate} * \text{density of air} \quad (5.4)$$

The density of air at ambient temperature is 1.2 kg/m^3. The weight fraction of oxygen and nitrogen used in this calculation were 0.232 and 0.754 respectively.

Olive kernel biomass, a widely available agro-industrial residue of Mediterranean origin, were received as coarse particles with an approximate size of less than 5mm. The initial moisture content of the olive kernels was measured as 13.3%. The samples were dried to 5.29% moisture content and stored in resealable plastic bags. Table 5-3 and Table 5-4, shows the mass flow rate required at different ER for as received and torrefied olive kernel.

Table 5-1 Air-Fuel ratio stoichiometry for gasification of raw olive kernels.

Combustion equation	**Fuel composition**			**Stoichiometric O_2 (g)**
		(%wt)	Mass (g)	
$C+O_2 = CO_2$	C	50.93	0.5093	1.358
$H_2+0.5O_2=H_2O$	H	6.16	0.0616	0.492
	O	42.11	0.4211	-0.4211
	N		0	
$S+O_2=SO_2$	S	0.02	0.0002	0.0002
Total		99.22	0.9922	
Total O_2 required				1.430
Total Air required				6.137
Air-Fuel Ratio (by mass)				6.185

Table 5-2 Air-Fuel ratio stoichiometry for gasification of torrefied olive kernels.

Combustion equation	Fuel composition			Stoichiometric O_2 (g)
		(%wt)	Mass (g)	
$C+O_{2=} CO_2$	C	56.93	0.5693	1.518
$H_2+0.5O_{2=}H_2O$	H	6.32	0.0632	0.5056
	O	35.66	0.3566	-0.3566
	N		0	
$S+O_{2=}SO_2$	S	0.02	0.0002	0.0002
Total		98.93	0.9893	
Total O_2 required				1.667
Total Air required				7.155
Air-Fuel Ratio (by mass)				7.233

Table 5-3 Air-Fuel ratio actual for gasification of raw biomass at different ER.

ER	0.15	0.2	0.25	0.3	0.35
$(AFR)_{actual}$	0.927	1.237	1.546	1.855	2.165
(kg biomass/hr) with moisture	3.24	2.46	1.98	1.62	1.38

Table 5-4 Air-Fuel ratio actual for gasification of torrefied biomass at different ER.

ER	0.15	0.2	0.25	0.3	0.35
$(AFR)_{actual}$	1.085	1.446	1.808	2.17	2.531
(kg biomass/hr) with moisture	2.7	2.04	1.62	1.38	1.14

In order to keep the residence time of air relatively constant, a fixed air rate of 0.12 cm/sec (40 l/min) was used in this study. The biomass mass flow rate was altered by changing the vibrator speed. The same procedure described above was used to calculate the feed rate of palm date stones as shown in Tables 5-5 and 5-6 on a dry basis.

Table 5-5 Air-ratio stoichiometry for gasification of date palm stones.

Combustion equation	Fuel composition			Stoichiometric O_2 (g)
		(%wt)	Mass (g)	
$C+O_{2=}\ CO_2$	C	48.68	0.4868	1.298
$H_2+0.5O_{2=}H_2O$	H	6.6	0.066	0.528
	O	42.3	0.423	-0.423
	N		0	
$S+O_{2=}SO_2$	S	0.075	0.00075	0.00075
Total		97.65	0.97655	
Total O_2 required				1.403
Total Air required				6.025
Air-Fuel Ratio (by mass)				6.169

Table 5-6 Air - Fuel actual for gasification of date palm stones.

ER	0.15	0.2	0.25	0.3	0.35
$(AFR)_{actual}$	0.925	1.233	1.542	1.85	2.159
(kg biomass/hr)	3.11	2.33	1.86	1.55	1.33

5.5 Gasification effectiveness

The effectiveness of the gasification process was evaluated in terms of higher heating value of dry gas (HHV), carbon conversion (η c) and cold gas efficiency (η). The dry gas HHV can be estimated from the gas composition by:

$$\mathrm{HHV} = (12.75[\mathrm{H_2}] + 12.63[\mathrm{CO}] + 39.82[\mathrm{CH_4}] + \cdots)/100 \qquad (5.5)$$

where the species contents are given in mole%, and their heats of combustion, in MJ/Nm^3 [143]. The concentrations of higher hydrocarbons are neglected because they are often too low to be detected.

Olive kernels contain only 0.01% nitrogen, so it was considered reasonable to use the material balance of just the nitrogen content of air to calculate the dry gas yield [213].

$$Y = \frac{Q_a \times 79\%}{\dot{m}_f N_2\%} \quad (5.6)$$

Where Q_a is the volume flow rate of air (Nm^3/h), $\dot{m}_f$ is the biomass mass flow rate (kg/h), and $N_2\%$ is the volumetric percentage of N_2 in the dry fuel gas.

The carbon conversion to product gas was determined on the basis of the gas analysis (volumetric percentage of the fuel gas composition of CO, CO_2, and CH_4) as follows:

Where C% is the mass percentage of carbon in the ultimate analysis of biomass.

$$\mu_c = \frac{Y(CO\% + CO_2\% + CH_4\%) \times 12}{22.4 \times C\%} \times 100\% \quad (5.7)$$

The cold gas efficiency is a crucial index to account for the performance of biomass gasification. It is defined as the ratio of chemical energy in the gas to that in the fuel [214]. This definition excludes the heating value of the condensable substance such as tars, therefore cold gas efficiency is the percentage of the fuel heating value converted into the heating value of the products gas.

The cold gas efficiency was given by:

$$\eta = \frac{HHV \times Y}{HHV_f} \times 100\ \% \quad (5.8)$$

Where HHV is the higher heating value of the product gas in MJ/Nm^3, HHV_f denotes the gross calorific value of the fuel in MJ/kg.

5.6 Kinetic approach in gasification

5.6.1 Introduction

During biomass gasification, the biomass is heated to a high temperature, which causes a series of chemical and physical changes that result in the evolution of volatile products as a first step, and carbonaceous solid residues as a second step. It is basically known that the char gasification of biomass is the rate limiting step in the gasification process, because the devolatilization step is comparatively fast [107]. According to Reschmeier et al. [215], the final step to conversion of the char by heterogeneous solid-gas phase reaction is much slower than the pyrolysis reactions. As the second stage is

slower than the first, it has a significant impact on reactor sizing, and reaction rate control [34].

The chemical reaction rate may be affected by many variables. The temperature, pressure, and composition are the main variables that effect homogeneous systems. In heterogeneous systems, the problem becomes more complex. Because the gasification rate is not only influenced by a number of process variables, such as temperature and composition of reactant material, but also by the physical effects such as reactant diffusion and heat transfer, this can result in an erroneous rate expression if they are not accurately accounted for [216]. According to Latif, the gasification rate of char is the most critical information required for optimum reactor design [217].

The study of kinetic parameters represented by activation energy and rate constant are important in reactor design, modelling and optimization of the process during biomass gasification [218] [217, 219]. Using models such as ASPEN or CFD to describe the gasifier needs knowledge of some controlling phenomena including reaction rates. According to Fernando [80] the information required for the combustion model system is 90% known, whereas only 20% is known for gasifiers, and one of the areas requiring further research is heterogeneous reaction kinetics. Due to there being difficulty in knowing the real rate constant and activation energy of char during continuous feeding of biomass in the gasification unit, the kinetic parameters are not always available in the literature. In this approach, depending on batch experiments that are described in section 4.7, and steady state conditions when there is no further accumulation of char in the gasifier, the real kinetic parameters for AROK and ARTOK were determined by using the approach that is explained in the following section. It is important to study the gasification of biomass with air in continuous feeding, since this is the case for real gasifiers.

5.6.2 Mass balance method to evaluate the kinetic parameters.

A mass balance model is derived and evaluated as a transient model, and utilised by Timmer [220] to predict the mass of the carbon in the reactor at any time ‘t’. However, the rate constant of this model was estimated by assumption that the steady state condition was achieved, and the amount of carbon accumulated is also estimated by stopping the biomass feed and observing the rate of combustion in the reactor, since

the system will subsequently become air rich and hence the remaining carbon can be quantified via mass balance of the produced CO_2. In this study, the same mass balance method was used, but for a char, to determine the rate constant of biomass reaction in a continuous gasification process depending on real steady state conditions inside the gasifier and online track of a char build up inside the reactor until steady state is obtained.

The pyrolytic biomass char enters the reaction zone as a solid particle. During gasification, the char can leave the gasifier via one of two ways: by being converted to volatile gases or by being transported out of the reactor through elutriation. However, based on calculation and observation, the elutriation from the bed was eliminated. According to Scala [221], who suggests that under oxidizing conditions the rate of fines that oxidise in the bed is much larger than the fines elutriation rate. Furthermore, during this study the superficial velocity was kept much lower than the terminal velocity (0.89 m/s) and accordingly no significant losses of bed material were noticed. The reactor is 1250 mm long to ensure most of the particles remained inside the gasifier.

This method is relying on a mass balance of the char as it enters and reacts in the gasifier. In the present work, the drying and the devolatilization of biomass are assumed to be instantaneous and completed at the feeding position. According to Bates et al., Equation (5.9) was used describe char conversion under fluidised bed gasification [211].

$$\mathrm{F} = m_f^o Y_{ch} \tag{5.9}$$

Where, F is char feed rate g/s, Y_{ch} is the char yield after devolatilization (gram of char per gram of biomass), where it is determined experimentally under pyrolysis condition, m_f^o is biomass feed rate (g/s).

Under these circumstances, the differential change in the mass of char solid particles (dm) in the gasifier during differential time (dt) is as follow:

$$\mathrm{dm} = \mathrm{Fdt} - \mathrm{R_r dt} \tag{5.10}$$

Where R_r is chemical reaction rate of char in g/s.

For a first-order reaction of biomass [222], [223], [224], [225], [226].

$$R_r = km \tag{5.11}$$

Where k is the rate constant with unit s^{-1} and m is mass of char solid particles in the reactor (g). By substituting equation (5.11) into (5.10):

$$\frac{dm}{dt} = F - km \tag{5.12}$$

Separation of variables yields:

$$\frac{dm}{F - km} = dt \tag{5.13}$$

Given the initial condition, m(t=0) =0, Equation (5.13) is integrated and Equation (5.14) is obtained.

$$m(t) = \frac{F}{k}[1 - \exp(-kt)] \tag{5.14}$$

Where m(t) is the mass of char at any time t.

According to Timmer, given sufficient time at consistent gasification conditions the mass of solid in the reactor approaches steady state, Equation (5.14) reduces to:

$$m_{ss} = \frac{F}{k} \tag{5.15}$$

Equation (5.15) allows calculation of k if F and m_{ss} are known. In this study, a steady state m_{ss} is measured experimentally and the rate constant is evaluated at five different temperatures. The value of k is substituted into (5.14) to evaluate theoretically the amount of the char with time during the gasification.

The theoretical and experimental work were compared. To evaluate the goodness-of-fit of the predicted values versus the experimental values, this study uses statistical indices such as the R-Squared (i.e., R^2) is simply defined, as follows:

$$R^2 = 1 - \frac{\sum_{i=1}^{n}(Y_i - \hat{Y}_i)^2}{\sum_{i=1}^{n}(Y_i - \overline{Y}_i)^2} \tag{5.16}$$

Where Y represents the measured char in the reactor (gram), $\widehat{\boldsymbol{Y}}$ is the corresponding value of the char predicated by the model(gram), n is the total number of data, and $\overline{\boldsymbol{Y}}$ is the mean of the measured char inside the reactor during the gasification run (gram).

Summary

In this chapter, the details of the rig design and its equipment include the feeder, diffuser plate, plenum, a bespoke platform load cell and heating systems unit are presented. The downstream cleaning system and gas analyser unit are shown. In addition, the calibration procedure of the gas analyser is discussed.

The equations used to calculate the feeding rate at a certain ER for each biomass are described in detail. The equations used to evaluate the gasifier performance such as carbon conversion efficiency and cold gas efficiency are shown.

Finally, the kinetic approach of gasification of char (heterogeneous reaction) was explained in detail in this chapter. In order to compare the experimental work with the theoretical equation, the statical indices such as the $R^{Squared}$ was used.

Chapter 6:

Experimental results

A comparison of the pyrolysis of olive kernel biomass in fluidised and fixed bed conditions.

This work compares the effects of particle size and temperature on pyrolysis kinetics under fixed bed conditions using a conventional bench scale TGA and under fluidisation bed conditions using a novel thermogravimetric fluidisation system (TGFBR) equipped with built-in load cells for the dynamic measurement of biomass conversion. The aim of this work was to investigate the influence of heating rates and heat/mass transfer effects on the kinetic analyses of the results obtained in these different systems, to describe and understand the importance of the bed conditions on the effect of biomass pyrolysis.

6.1 Fixed bed Thermogravimetric analysis (TGA).

The pyrolysis results obtained from thermogravimetric experiments are identified as a function of the conversion x, expressed in Equation (3.7). The degree of conversion against temperature at a heating rate of 20 ºC/min for four particles size classifications of olive kernel were obtained as illustrated in Figure 6-1. Below 250ºC the mass change due to moisture loss occurred during the early heating period. The thermal decomposition of the olive kernel started at 250ºC, but the major decomposition region (active pyrolysis) happened between 260 and 356ºC. The majority of volatile decomposition, up to 80% of the overall mass conversion, occurred during this temperature range. Therefore, for conversion greater than 80%, most of the remaining material is char. Considering only the TGA results, all particle size classifications exhibited the same trend. The effect of particle size on pyrolysis was investigated for four particle sizes as shown in Figure 6-1 and demonstrated that particle size does not have an important influence on the TGA profile of the olive kernel. A similar effect for Codium fragile (a marine biomass) has been reported by Daneshvar et al. [227] for particle sizes from 75 to 1400 µm.

Biomass is composed of cellulose, hemicellulose, and lignin. Due to essential differences in the structure of these constituents, they can be identified and distinguished using thermogravimetric analysis [228]. According to Yang et al. [40] hemi-cellulose decomposes mainly at 220-315 ºC, cellulose at 315-400 ºC, while lignin decomposes over a wide temperature range from 160 to 900 ºC. The differential thermogravimetric analysis (DTG) at heating rate 20ºC/min gives the differential rate of conversion, dm/dt, for particle sizes 300-500, 500-710, 710-1180 and 1180-1400µm as illustrated in Figure 6-2. This figure shows the DTG distribution curves for olive kernel, the first peak below 100 ºC corresponds to the moisture content of the sample. The second peak between 200 and 300°C, suggests the thermal decomposition of hemicellulose. The final peak between 300 and 380°C, may correspond to cellulose decomposition. The slow rate of mass loss at higher temperatures >380°C is consistent with lignin decomposition. Approximately the same trend of DTG has been reported by E Kastanaki et al during the pyrolysis of olive kernel [229] and Jae et al. through pyrolysis of maple wood [230].

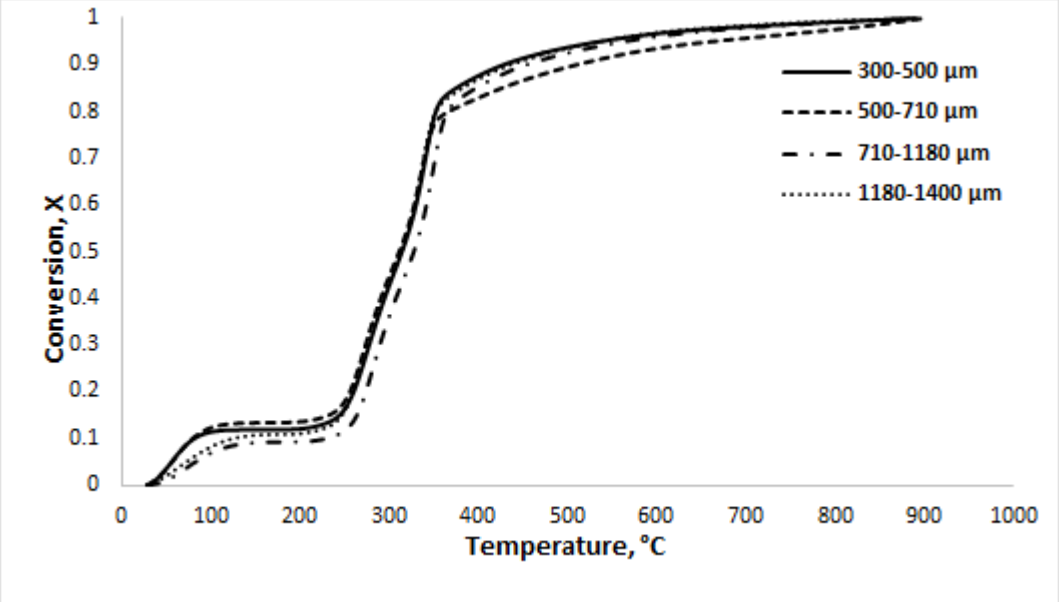

Figure 6-1 Relationship between mass conversion and temperature for olive kernels of different particle sizes. Heating rate 20°C/min, sample wt. ~10mg (TGA), nitrogen flow rate 100 ml/min.

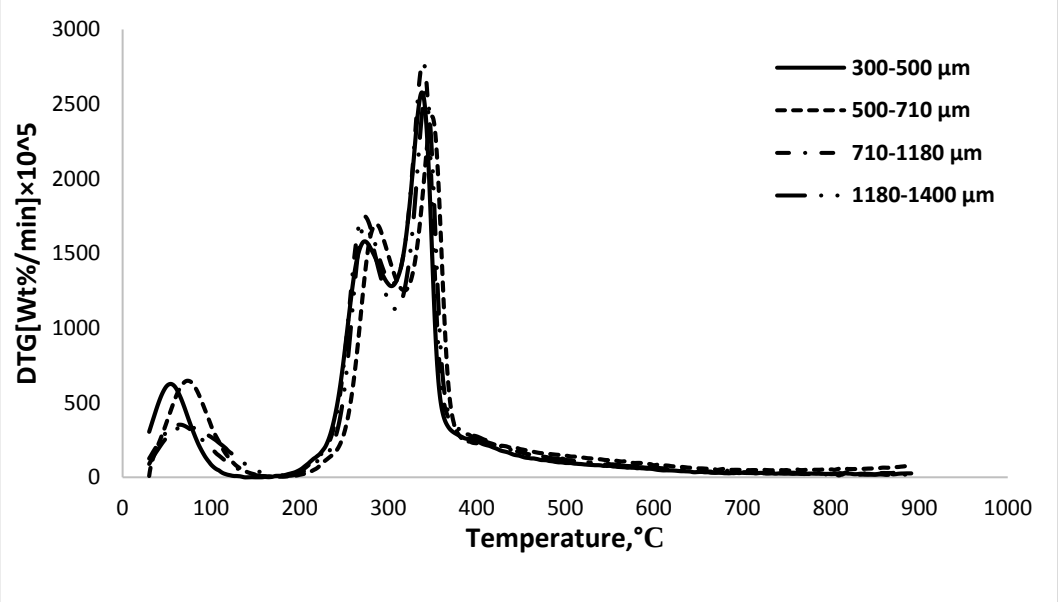

Figure 6-2 Variation of the instantaneous rate of reaction with temperature at 20°C/min heating rate for pyrolysis of olive kernel.

6.2 Fluidised bed reactor thermogravimetric analysis

The experimental measurements using the TGFBR were achieved under preset steady-state temperatures between 300-660ºC, covering the chemically controlled regime area of thermal decomposition as illustrated in Figure 6-2 and silica sand with diameter of 500-600 µm as fluidised bed inert material. The experimental work was started with heating the reactor to the required temperature by keeping the silica sand particles fluidised at constant rate. After that, the air stream was stopped and the nitrogen stream flowed at the minimum fluidization velocity (U_{mf}) until steady state temperature conditions inside the reactor were obtained. Olive kernel biomass was fed from the top of the reactor through a pipe into the hot fluidised bed as shown in Figure 5-1. The amount of biomass used in each test was 40 g representing 10% wt. of total weight of bed material. The weight variation in TGFBR during pyrolysis process was recorded online with the weighing indicators at 1 second time intervals.

6.2.1 Influence of nitrogen flow rate on pyrolysis conversion rate.

A fundamental issue in pyrolysis is the interaction of evolving nascent, hot pyrolysis vapours with the surrounding decomposing solid. The residence time of the vapour

phase of pyrolysis products is affected by the nitrogen flow rate, which alters the extent of secondary reactions such as cracking and char formation [231] and improves the heat transfer from fluid gas to the particle.

Olive kernel was pyrolyzed under different conditions. Figures 6-3 and 6-4 shows the variation of the conversion with reaction time of particle size 1180-1400 µm at temperature 300°C and 500°C respectively using different fluidizing gas flow rates that were below the terminal velocity condition for the silica sand used. The trend of biomass conversion at 300°C for different flow rates of N_2 are the same, which suggests the inhibition of internal and external diffusion effects at this temperature, but there was no effect of increasing the flow rate velocity beyond 0.09 m/s (30 l/min) although a small deviation occurs with the 0.06 m/s (20 l/min) result which is thought to be due to limited silica sand fluidization observed at the beginning of biomass addition.

At the higher temperature of 500 °C, the rate of reaction determined from the slope of the conversion line showed a wide variation up to a velocity of 0.12 m/s (40l/min), after which a much smaller variation occurred. This critical gas flow velocity represents the flow required to minimise the external diffusion inhibition on reaction rate [232]. By operating the gas-solid reaction system at sufficiently high gas flow velocity, the mass transfer effects could be minimized so that any further increase in the gas flow rate did not produce an increase in the overall reaction rate [68]. Therefore, a flow velocity of 0.12 m/s (40 l/min) was chosen as the basis for all experimental work, representing the minimum gas velocity required to limit external diffusion.

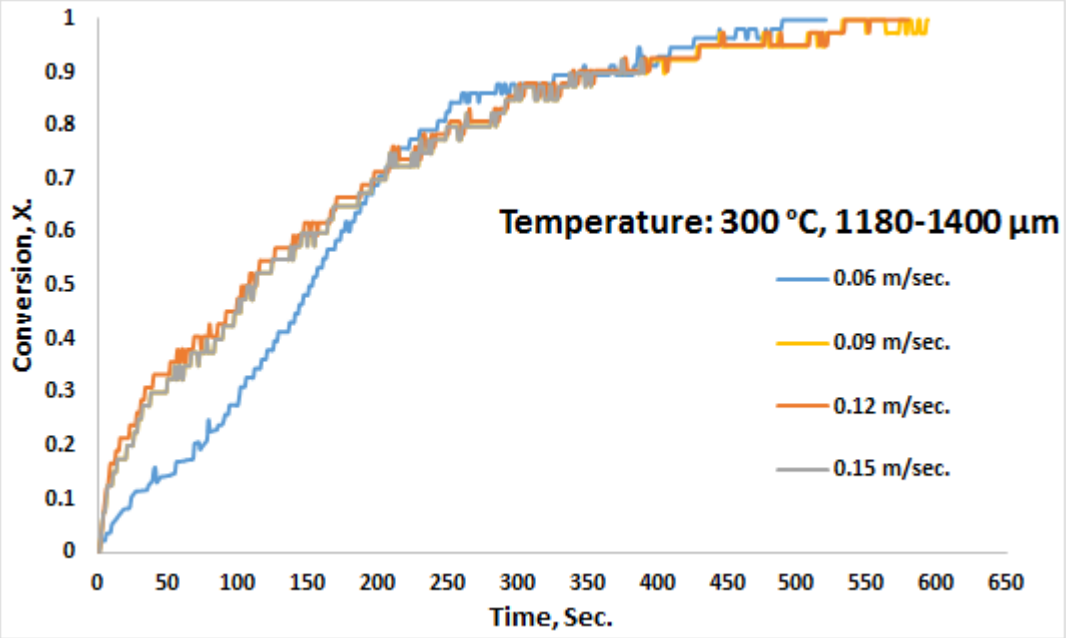

Figure 6-3 Total weight conversion against reaction time in TGFBR at different flowrates, T=300 °C.

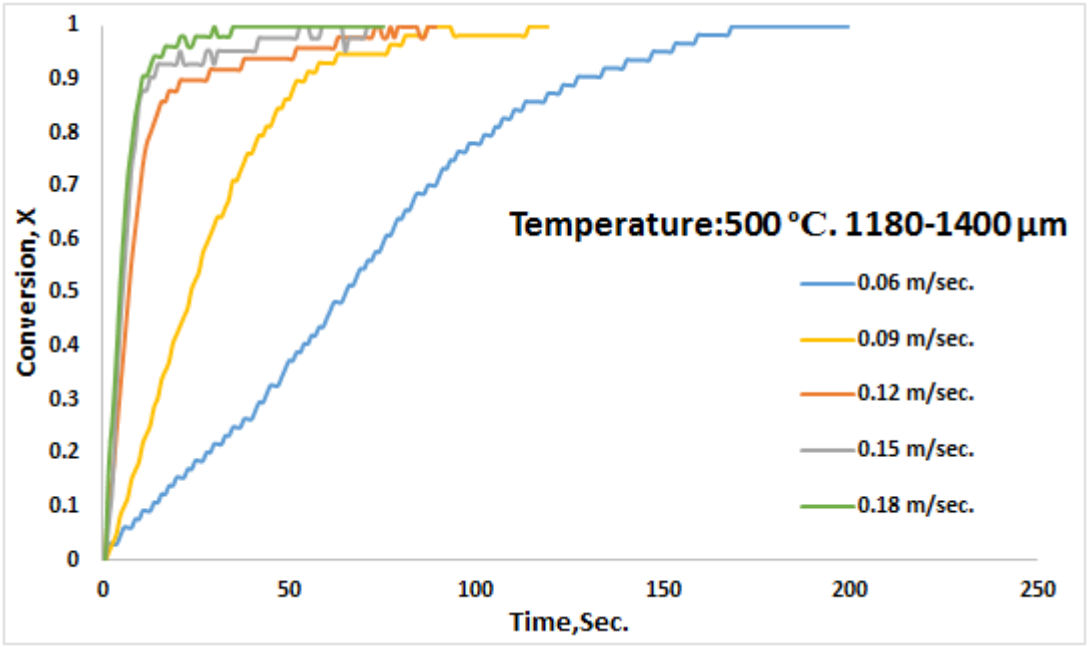

Figure 6-4 Total weight conversion against reaction time in TGFBR at different flowrates, T=500°C.

6.2.2 Effect of particle size

In laboratory scale pyrolysis, particle size can have a significant effect on the reaction rate. When the particle size increases, the temperature gradients inside the particle also increase, so that at any given time, the surface temperature is higher than that of the core, which can increase the solid yields with a corresponding decrease in liquid and gas yield [233]. In this study, Figure 6-5 illustrates the influence of olive kernel particle size on conversion at temperatures of 300°C, 350°C, 400°C and 451°C. At this range of temperature, it was observed that the conversion profile exhibited minimal differences for particle sizes tested. Assuming the temperature and concentration of the produced gases were uniform, it was concluded that the rate of de-volatilisation occurred homogeneously throughout the particle and the rate did not depend on the size of particle. Szekely et al. [68] reported the same explanation for gas solid reactions at low temperature. However, at higher temperatures between 500-660°C as shown in Figure 6-6, the influence of particle size is more obvious. When the particle size decreases the reaction time also decreases. One may therefore assume that at higher temperatures the effect of external diffusion is greater, therefore the effect of temperature gradient is greater leading to heat transfer limitations. The comparatively low thermal conductivity of biomass gives a low heating rate through larger particles which leads to increased char formation [53]. These results are also in agreement with findings reported in the literature that at low temperatures the limitation of the reaction rate is mainly due to chemical kinetics (up to about 400°C), while mass transport phenomena limit the reactions at higher temperatures [196].

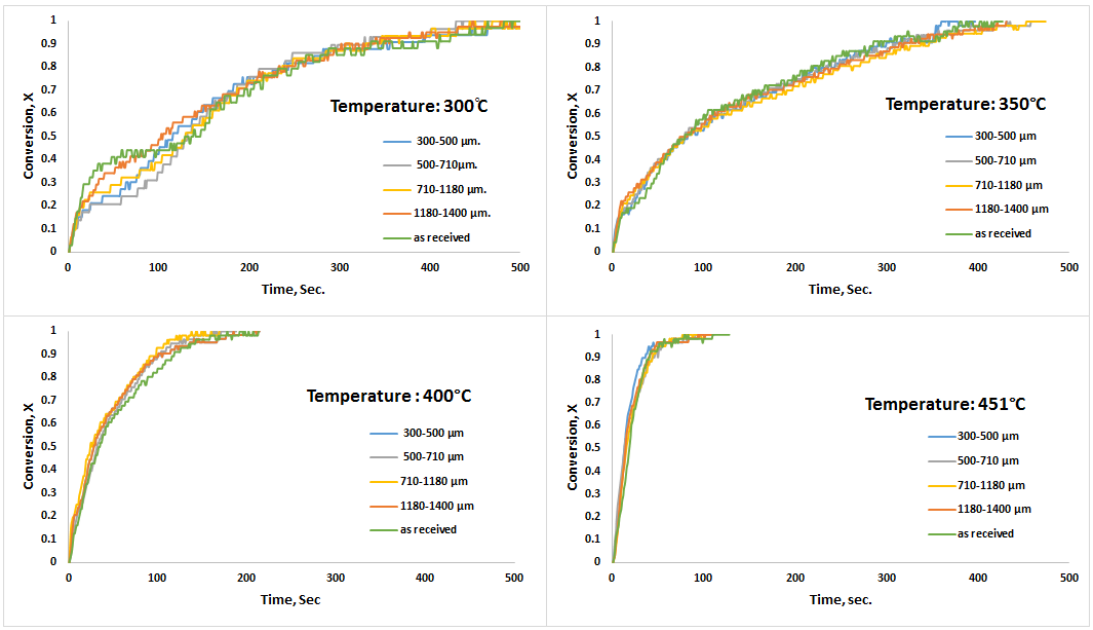

Figure 6-5 Progress of conversion fractions against reaction time at temperatures (300, 350, 400 and 451°C).

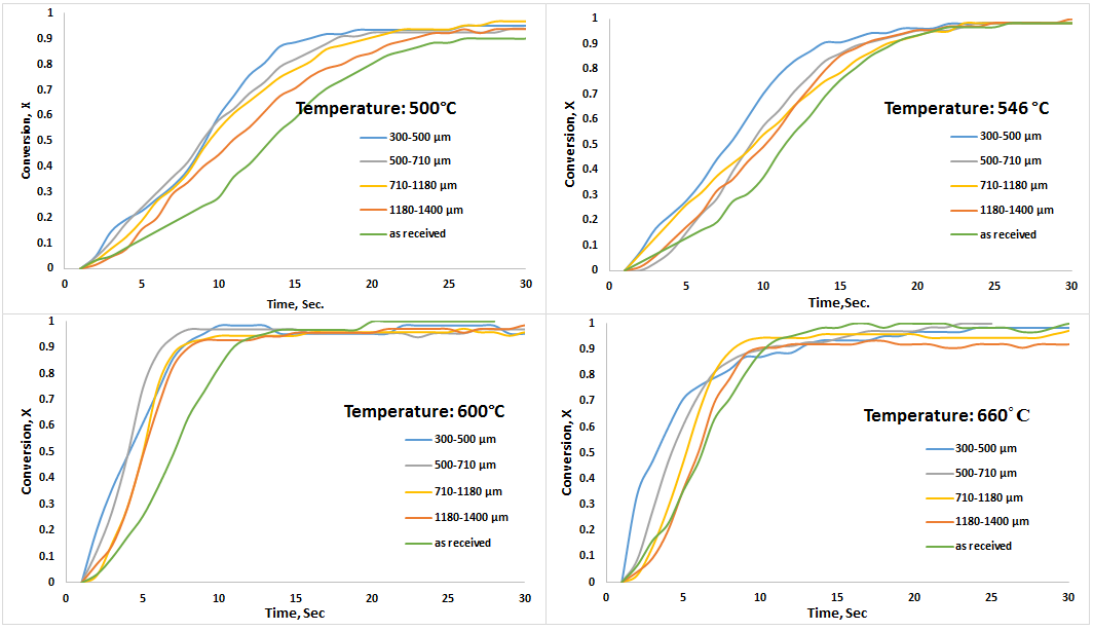

Figure 6-6 Progress of conversion fractions against reaction time at temperatures (500, 546, 600 and 660°C).

6.2.3 Effect of temperature

Figure 6-7 shows the effect of temperature on char yield as a percentage of the original olive kernel mass. For the particle size classifications (300-500, 500-710, 710-1180, 1180-1400 µm and the as received biomass) the char mass percent decreased from between 55 and 60 wt% at 300°C to 9-12 wt% at 660°C. A sudden decrease in the char yield occurred between 300-350°C ranging from 28 % for the largest particle size (as received) to 37 wt% for the smallest size classification 300-500µm. According to A.A Zabaniotou et al. [19] they reported that, the olive kernel char yield decreases with increasing temperature during pyrolysis to a minimum value of 33 wt% of sample and the yield tends to be stabilized above 500°C.

There are two types of reaction through which the thermal degradation occurs: a comparatively slow decomposition and charring on heating at lower temperatures <300°C and a rapid devolatilization accompanied by the formation of levoglucosan from pyrolysis at higher temperatures. At temperatures >300°C, cellulose and hemi-cellulose depolymerizes producing volatile products [210] as shown in Fig. 6-2. For this reason, the significant weight percent change occurring between 300-350°C is likely to be due to the increased devolatilization rate of hemicellulose and cellulose. The char formation decreases with increasing temperature due to further decomposition of biomass and there was little difference observed for the different size classifications.

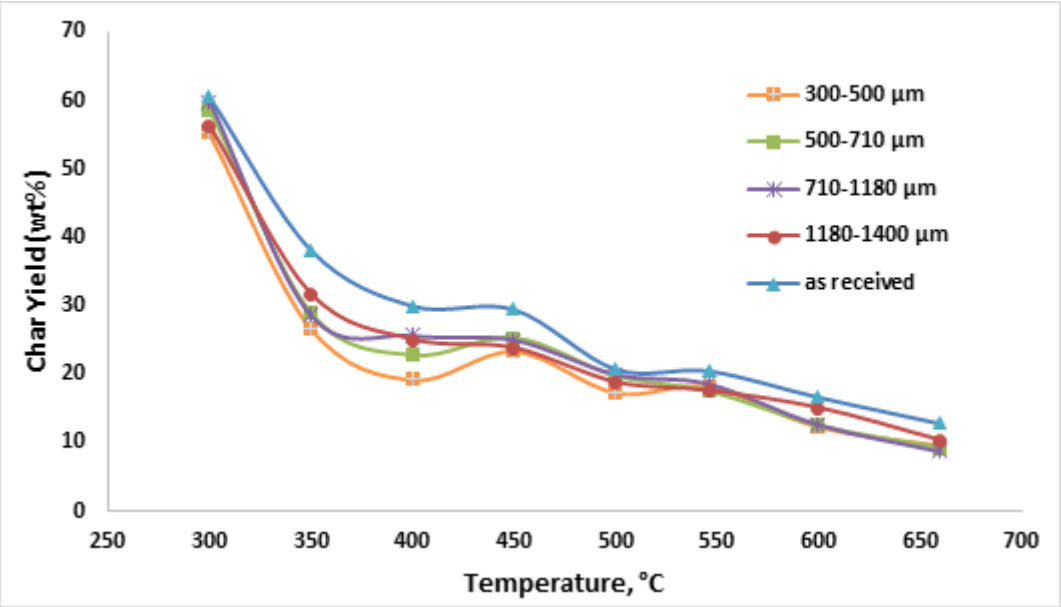

Figure 6-7 Char yield as a function of temperature (TGFBR).

Figure 6-8 illustrates the influence of temperature on conversion, for all particle sizes of olive kernel (300-500, 500-710, 710-1180, 1180-1400 µm and as received). As expected, the completion time of pyrolysis reduced with increasing temperature for all particle sizes. At 300°C, the reaction time was 450 seconds reducing to less than 10 seconds for temperatures above 500°C; this suggests that the increase in temperature leads to a decreased yield of solid and an increased yield of gas product. The moderate temperature, high heat transfer to the biomass particles and short residence time of hot vapour in the reaction zone are the most significant characteristics of fast pyrolysis [234]. Fast pyrolysis is used to describe processes with reaction times of only a few seconds or less [235] and as shown in Figure 6-8, the pyrolysis of olive kernel in the TGFBR occurred under fast pyrolysis conditions.

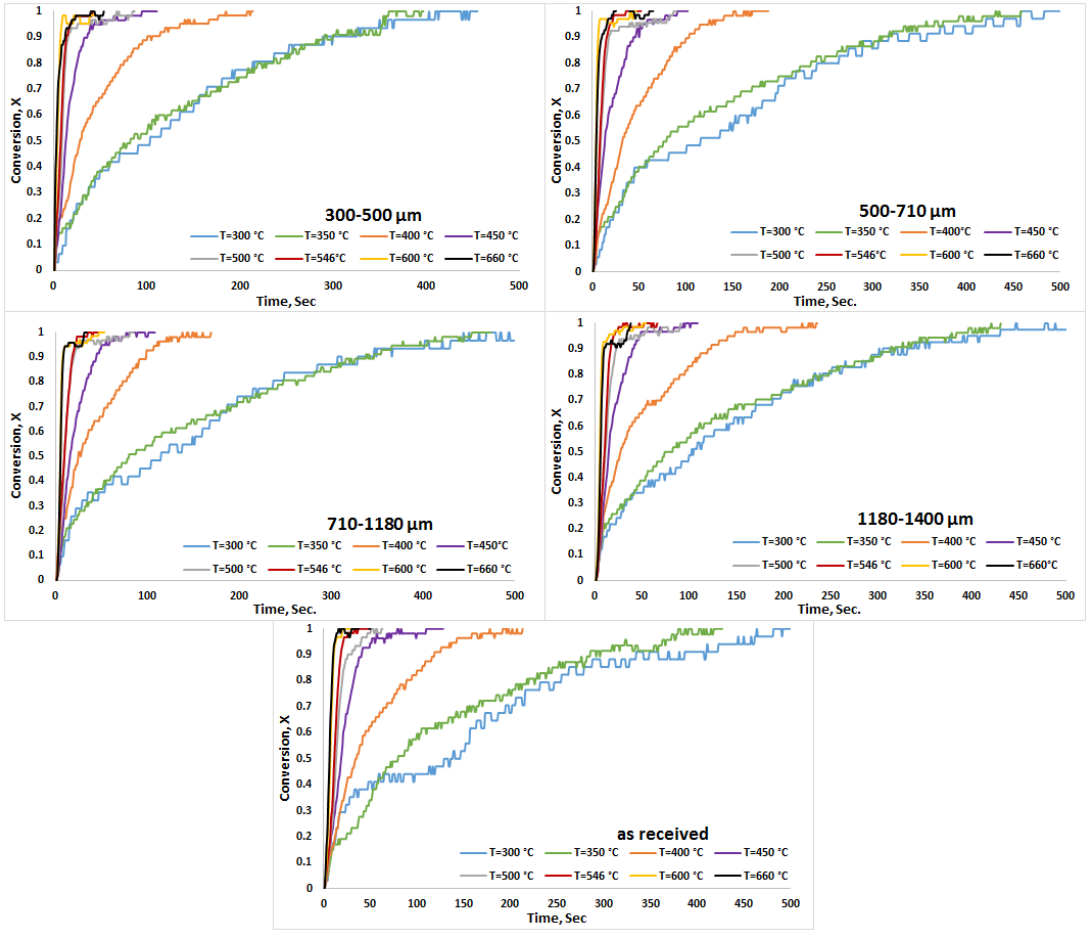

Figure 6-8 Olive kernel conversion versus reaction time in TGFBR

6.2.4 Kinetic analysis of pyrolysis of olive kernel.

Non-isothermal testing of olive kernel was done in the TGA instrument with a 20°C/min heating rate. Several solid-state mechanisms (Table 3-1) were tested for a suitable fit by the Coats-Redfern method in order to determine the mechanisms responsible for the decomposition of biomass of particle size 1180-1400 µm at conversion between x=0.2-0.8, because the main conversion occurs in this study range. Equation 3-19 was applied separately to each model, the form of G(x) which gives a straight line with the highest correlation coefficient was considered to be the model function that best represents the kinetic mass loss reaction. Table 6-2 shows different reaction model and correlation coefficient fits obtained from the plots of

$\ln(G(x)/T^2)$ verses 1/T as illustrated in Figure 6-9. From the slope of each line, the values of activation energies were obtained.

Table 6-1 revealed that the two-dimensional diffusion model (G2) was the best fit. The indication of the high coefficient value demonstrates that the corresponding reaction model fitted the experimental work. The high coefficient value (0.986) demonstrated a good fit the activation energy of olive kernel (1180-1400 µm) measured 74.4 kJ/mole.

Table 6-1 Reaction model for olive kernel decomposition during fixed bed non-isothermal pyrolysis.

NON-ISOTHERMAL (TGA), X=0.2-0.8									
G(X)	**G2**	**G3**	**G6**	**G7**	**G8**	**G9**	**G11**	**G15**	**G17**
R^2	0.9866	0.862	0.9843	0.9809	0.9809	0.9809	0.9763	0.961	0.9763
EA(KJ/MOLE)	74.4	-	97	43.7	43.7	43.7	27.9	64.3	27.9

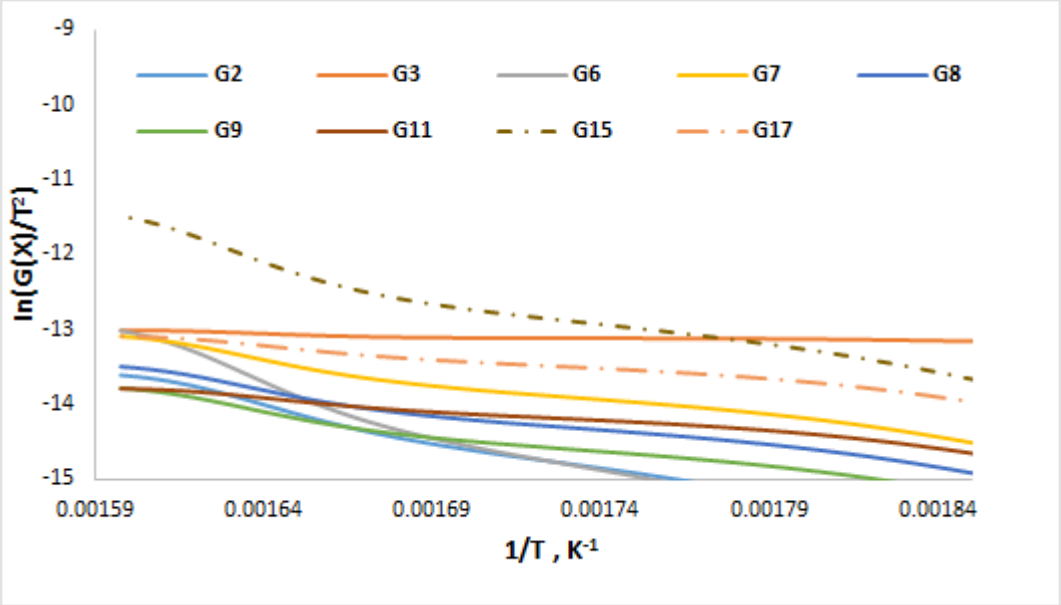

Figure 6-9 Correlation of ln(G(x)/T) versus 1/T for 1180-1400 µm particle size for non-isothermal TGA.

For the isothermal condition, Figure 6-10 (low temperature <500°C) and Figure 6-11 (high temperature ≥500 °C) illustrate the correlation of G(x) against time at different

reaction temperatures for 1180-1400 µm olive kernel in the TGFBR. Based on the fitting accuracy, the most probable reaction models (Table 6-2) were selected from nineteen reaction models shown in Table 3-1. The two-dimensional diffusion (G2) and three-dimensional (G3) model were had the highest fitting accuracy for temperatures between 320-451°C and 500-660°C respectively. The data contained in Table 6-2 verifies the speculation that the decomposition of olive kernel proceeds with different consecutive mechanisms. The mechanism of two-dimensional diffusion could describe the thermal decomposition at low temperature while three-dimensional diffusion described it at high temperatures. G2 is the function for a two-dimensional diffusion controlled process, while G3 is Jander's equation for diffusion-controlled solid state reaction kinetics [16].

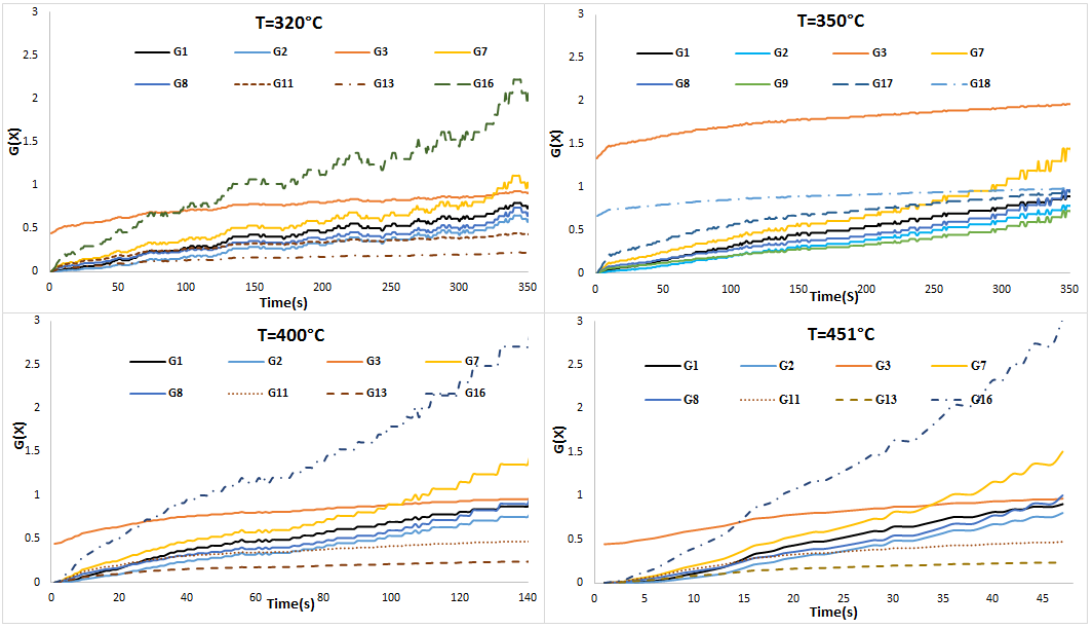

Figure 6-10 Correlation of G(x) versus time at different reaction temperatures for 1180-1400 µm particle size (low temperatures) for TGFBR.

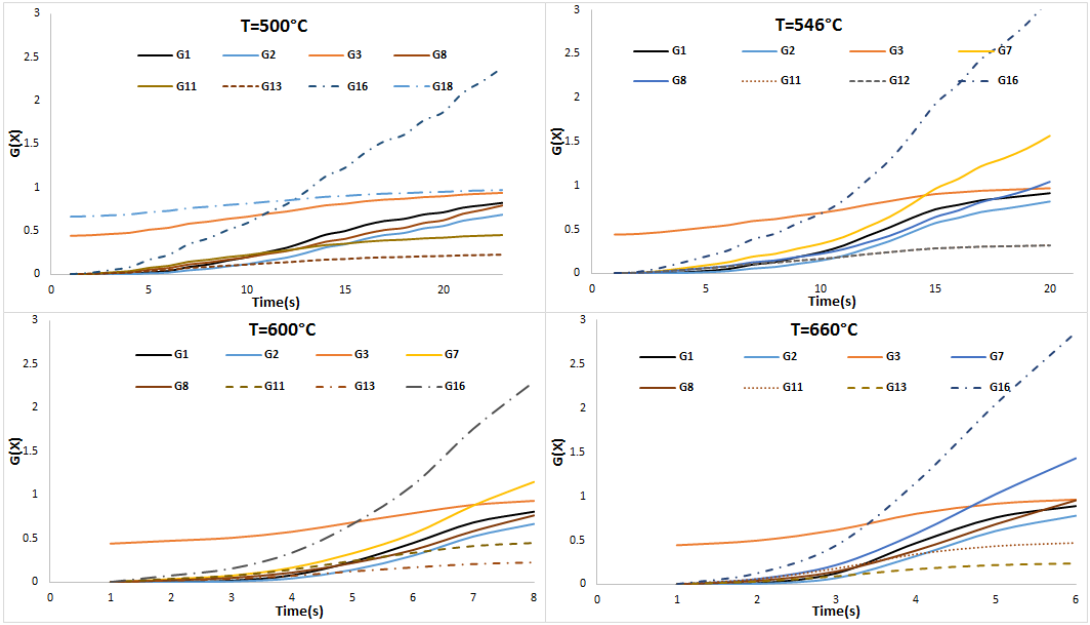

Figure 6-11 Correlation of G(x) versus time at different reaction temperatures for 1180-1400 µm particle size (high temperatures) for TGFBR.

Generally, if a plot is made of G(x) against time and a straight line is obtained, the slope of that line will enable a calculation of k(T) to be made. From straight line plots of the experimental data at different temperatures, the values of k relating to the Arrhenius function with temperature (see Fig. 6-12 and 6-13) are shown. From the lnk versus 1/T plot, the slope (- $\frac{E_a}{R}$) was used to obtain the values of activation energy for the experiments between 320-451°C and 500-660°C for the olive kernel pyrolysis, giving activation energies of 67.4 and 60.8 kJ/mole respectively. Table 6-2 shows the correlation coefficients, conversion range and the normal logarithm of rate constant obtained from the plot of G(x) against t.

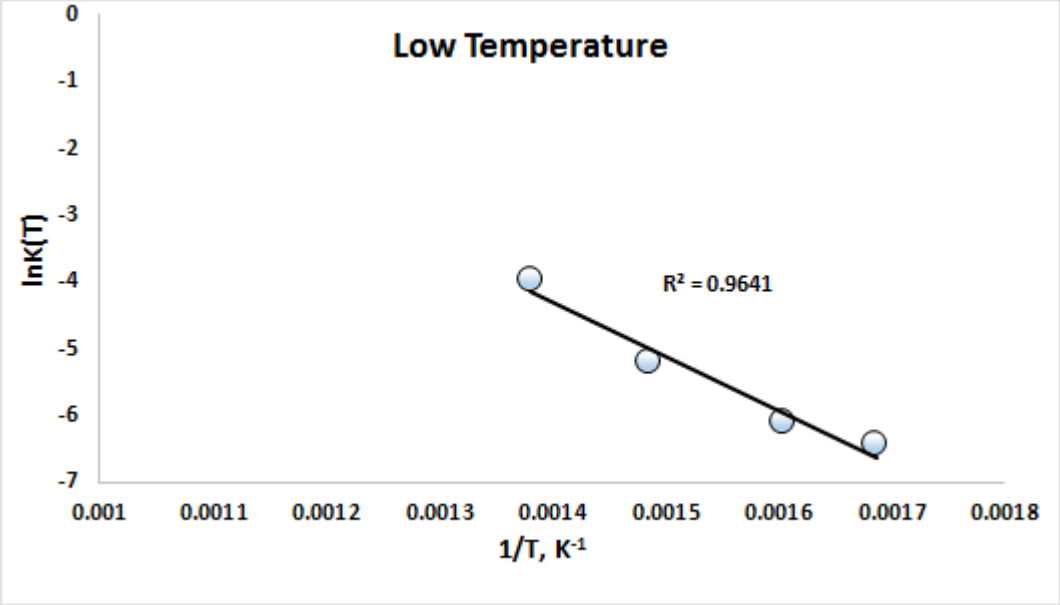

Figure 6-12 Arrhenius plot for olive kernel pyrolysis (low temperature).

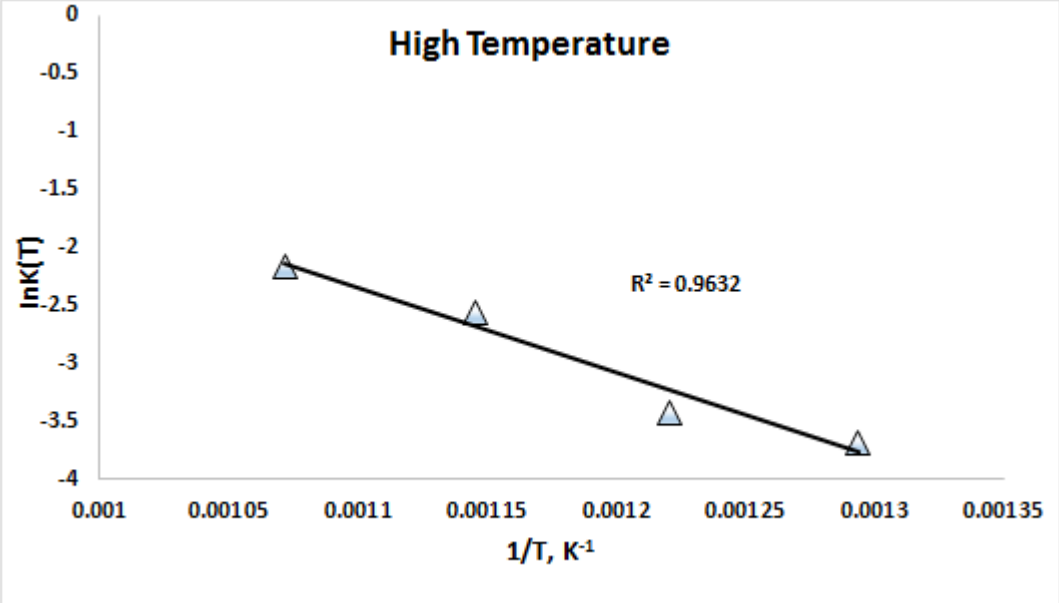

Figure 6-13 Arrhenius plot for olive kernel pyrolysis (high temperature).

Table 6-2 Reaction model for olive kernel decomposition during fluidised bed isothermal pyrolysis

G(X)	**G1**	**G2**	**G7**	**G16**	**G1**	**G2**	**G7**	**G1**	**G2**	**G7**
TEMP	320°C	320°C	320°C	320°C	350°C	350°C	350°C	400°C	400°C	400°C
R^2	0.972	0.974	0.962	0.962	0.99	0.993	0.97	0.978	0.993	0.975
LnK(T)	-6.214	-6.437	-5.991	-5.29	-6.032	-6.119	-5.654	-5.099	-5.203	-4.688
X	0-0.90	0-0.90	0-0.90	0-0.9	0-0.95	0-0.95	0-0.95	0-0.95	0-0.95	0-0.95
G(X)	G1	G2	G7	G16	G1	G3	G8	G3	G11	G13
TEMP	451°C	451°C	451°C	451°C	500°C	500°C	500°C	546°C	546°C	546°C
R^2	0.983	0.99	0.98	0.98	0.972	0.983	0.976	0.983	0.981	0.981
LnK(T)	-3.825	-3.973	-3.467	-2.77	-3.135	-3.68	-3.28	-3.422	-3.952	-4.24
X	0-0.95	0-0.95	0-0.95	0-0.95	0-0.90	0-0.90	0-0.90	0-0.95	0-0.95	0-0.95
G(X)	G3	G11	G13	G16	G3	G11	G13			
TEMP	600°C	600°C	600°C	600°C	660°C	660°C	660°C			
R^2	0.970	0.80	0.970	0.89	0.971	0.970	0.970			
LnK(T)	-2.56	-3.31	-3.343	-1.106	-2.161	-2.258	-2.95			
X	0-0.90	0-0.90	0-0.90	0-0.90	0-0.95	0-0.95	0-0.95			

Comparing the result obtained from fixed bed TGA (non-isothermal condition) to the fluidised bed (isothermal condition) in the TGFBR, both exhibits the same mechanism at <451°C, and three-dimensional diffusion control at ≥500°C. However, the activation energy obtained from TGA was higher and may be due to the effect of external gas diffusion in the TGA at low heating rates [236]. The behaviour of three-dimensional diffusion may be associated with the greater degradation of hemicellulose and cellulose content at high heating rates leading to higher volatility of the main biomass components. In addition, the pore lattice defects are considered a significant factor because these defects promote reactivity and diffusion of material [166]. The phenomena of two and three dimensional diffusion has been noticed by Li [237]; where during the study the kinetic mechanism of the reduction reactions of Ferrum niobate were quantified. In addition, the pyrolytic reactions of oil-palm shell at the low and high temperature regimes were found to be based on two mechanisms according to Guo et al. [238]. In comparison to the thermogravimetric pyrolysis methods other researchers have also reported that different mechanisms and sequences

involved in the formation of gas species, for example three dimensional diffusion found responsible for production of hydrogen and methane during pyrolysis process [185, 194].

Summary

In this chapter, the reaction kinetics of olive kernel biomass were measured using a thermogravimetric fluidised bed reactor (TGFBR), which was developed to enable real time measurement of the dynamic mass during reaction under a high heating rate. The range of the pyrolysis test was between 300°C and 660°C; the results were compared with a TGA as a fixed bed technique. Under non-isothermal and isothermal conditions, the mechanism of reaction was identified. It was shown that a two-dimensional diffusion model was controlling the reaction in the TGA as well as the TGFBR at temperatures less than 451°C. However, at higher temperatures, the results show that a three-dimensional diffusion model controls the reaction in the TGFBR.

The effect of low and high heating rate on particle size using TGA and TGFBR are presented in detail. The results shown no measurable effect on the reaction rate of different particle sizes at low heating rate, whereas a clear dependence of reaction rate on biomass particle size was demonstrated at high heating rate.

The influence of different gas velocities on reaction rate is presented. It was shown that the reaction time decreased when the gas velocity increased up to (0.12) 40 l/min, after which no significant different was noticed.

Chapter 7:

Gasification of AROK and ARTOK

7.1 Introduction

In this section of work, an experimental system was designed, in which the user can track the build-up of char inside the gasifier until steady-state conditions are reached, as well gain insight into the effect of temperature on gasification rate. In addition, this enables the user to minimise the effect of external diffusion by using different gas velocities whilst monitoring the mass variation rate. This is important to explain what is actually happening inside the gasifier apparatus.

7.1.1 Fuel characterization

Data from the proximate analysis and ultimate analysis of AROK and ARTOK are given in Table 4-1 and Table 4-3 respectively. Torrefaction is a way to increase the energy density of the biomass by removing oxygen and moisture. From the ultimate analysis reported in Table 4-3, it can be seen that the oxygen content decreased from 42.11% for the parent biomass down to 35.66% for the torrefied biomass, which represents a decrease of 15.3 % after torrefaction. In terms of the O/C ratio, the value decreased from 0.82 to 0.62 upon torrefaction; which is in agreement with literature [239] and the mass and energy yield were 86 % and 93 % respectively (where energy yield represents the ratio of actual energy conserved after the torrefaction process, compared to the initial energy content of biomass). A typical mass and energy yield of woody biomass torrefaction would be 70% of the original mass, containing 90% of the initial energy content [29]. The ash content increases, which is related to the loss of mass of organic matter during torrefaction [35, 240]. The fixed carbon content of torrefied biomass is greater than the parent material and this can increase its energy density. Similar observations were also found in the study of torrefied biomass [41, 208]. Prins et al. state that compared to the parent biomass, the heating value of torrefied biomass can increase by 5-25%, and that the volatiles can decrease from around 80% to around 60-75% [35]. In this study, the heating value of olive kernel biomass increased after torrefaction by 8.3%. Compared to AROK, the ARTOK fuel

property moves along the coalification series towards the composition of peat, according to the Van Krevelen diagram (see Figure 1-5).

7.1.2 Gasifier operation

Figures 7-1 and 7-2 show the recorded temperatures during the gasification experiments at reactor preset temperatures of 550, 600, 650, 700, and 750°C for AROK and ARTOK. As each result shows, the process initially undergoes a heating phase, where the thermochemistry within the reactor is approaching equilibrium, generally considered to be endothermic. When the heat generation rate matches or exceeds the rate of heat loss, the process becomes self-sustaining [75]. The middle portion of the figure represents the gasification reaction phase, and it is clear that the initially unstable process has reached thermal equilibrium. This resultant temperature is used in the calculation of the reaction kinetics. Comparing the biomass samples, the ARTOK generally reached steady-state conditions at higher temperatures than the AROK at identical preset temperatures. This is in agreement with other work [241], where the same difference was noticed between the gasification of raw and torrefied biomass. According to Bridgeman et al [239], there is possible explanation for this phenomenon, as follows. During gasification, the initial volatiles released from AROK are low in calorific value being principally composed of water and carbon dioxide, and that any combustible gases are not particularly energetic. Therefore, the energy required to release the water and carbon dioxide is compensated by the energy produced from combustion of the low energy volatiles, leading to marginal, if any, energy gain. When the biomass has been torrefied, the energy intensive water and carbon dioxide has been lost, as have any low energy volatiles. Therefore, when ARTOK is gasified, higher temperatures are achieved, as in Figures 7-1 and 7-2, because it contains high energy volatiles and char which react directly to produce higher temperatures.

Biomass feeding was halted when the mass variation in the experiment was less than 1g per second, with the air flow maintained constant. The data in Figure 7-1 and Figure 7-2 show that the response to the stop in feeding was a rapid temperature increase (commencing within 5 seconds after the feeder stopped). This is attributed to the

reactor stoichiometry shifting into the combustion regime, thus providing more exothermic conditions as the remaining mass of biomass in the bed is oxidised under excess air.

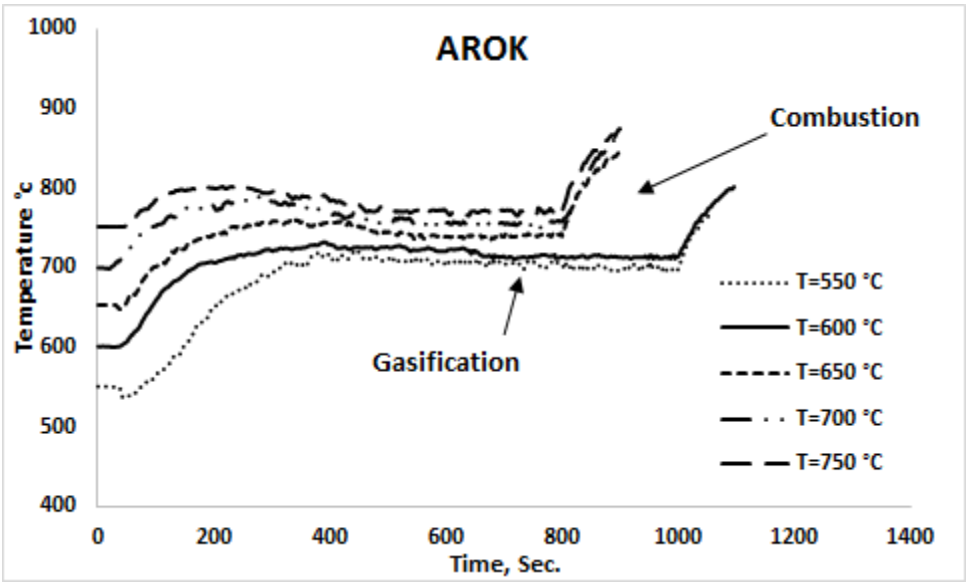

Figure 7-1 Stable temperature zone in the gasifier for gasification of AROK

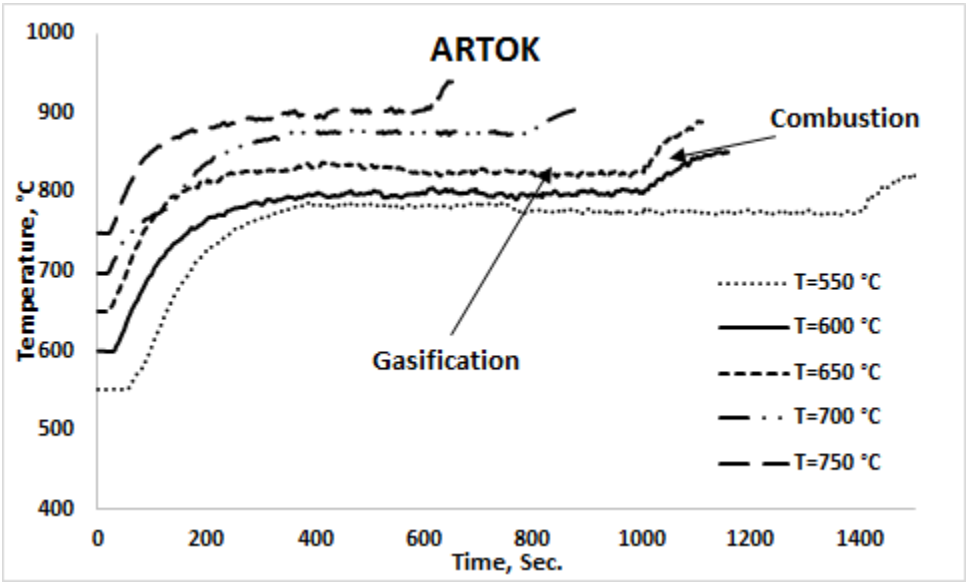

Figure 7-2 Stable temperature zone in the gasifier for gasification of ARTOK

7.1.3 Effect of bed reactor temperature on the gas yield.

The product gas composition in the gasifier was the result of the combination of a series of complex and competing reactions, as given in reactions (R1) - (R10). Bed temperature is one of the most significant parameters affecting all the chemical reactions in the combustion and gasification process. In order to simplify the gasification mechanism, the proposed reaction scheme was used to explain biomass gasification in the fluidised bed as follows [242, 243]:

$$\text{Pyrolysis biomass} \rightarrow \text{char} + \text{tar} + \text{gases } (H_2, CO, CO_2, CH_4, C_nH_m) \quad \text{R1}$$

$$\text{Tar} \rightarrow CO_2 + CO + H_2 + CH_4 + \text{light H/C} \quad \text{R2}$$

Water-gas

$$C + H_2O \rightarrow CO + H_2 \qquad +131\ \text{kJ/mol} \quad \text{R3}$$

Boudouard

$$C + CO_2 \rightarrow 2CO \qquad +172\ \text{kJ/mol} \quad \text{R4}$$

Oxidation reaction

$$C + 0.5\ O_2 \rightarrow CO \qquad -111\ \text{kJ/mol} \quad \text{R5}$$

$$C + O2 \rightarrow CO2 \qquad -394\ \text{kJ/mol} \quad \text{R6}$$

Water-gas shift reaction

$$CO + H_2O \leftrightarrow CO_2 + H_2 \qquad -41.98\ \text{kJ/mol} \quad \text{R7}$$

Dry reforming

$$CH_4 + CO_2 \leftrightarrow 2CO + 2H_2 \qquad +247\ \text{kJ/mol} \quad \text{R8}$$

Methanation reaction

$$C + 2H_2 \rightarrow CH_4 \qquad -75\ \text{kJ/mol} \quad \text{R9}$$

$$C_nH_m(\text{tar}) + nCO_2 \rightarrow (m/2)H_2 + 2nCO \quad \text{Endothermic} \quad \text{R10}$$

The temperature for the overall biomass gasification process is crucial. In this study, gasification tests were achieved by varying the bed temperature between 550°C and 750°C in 50°C increments and keeping the ER constant at 0.15 and 0.2 for AROK and ARTOK. The experimental results are presented in Figures 7-3 and 7-4 respectively.

Figure 7-3 and 7-4 show the product gas composition (CO, CO_2) and (H_2, CH_4) as a function of the gasifier temperature of AROK and ARTOK at ER=0.15 and ER=0.2. For AROK, H_2 content increased from 2.41% to 6.76% at ER=0.15 and 5.52% to 6.57% at ER=0.2 when the gasifier temperature was increased from 550°C to 750°C. CO in the fuel gas increased from 13.22% to 18.28% at ER=0.15 and 12.79% to 16.44% at ER=0.2 with the same gasifier temperature increase, meanwhile CO_2 fell from 19.58% to 16.12% at ER=0.15 and 16.30% to 14.95% at ER=0.2.

The major gasification reactions R3 and R4, as well as R2, are intensive endothermic processes. Higher temperature favours the products in an endothermic reaction. It is known that the water-gas and Boudouard reactions (R3 and R4) are favoured at higher temperatures [75]. Water vapour and CO_2 promote H_2 production in the biomass gasification process, through reaction R3 by water vapour and through the combination of reaction R4 by CO_2 and reaction R7 by water vapor [244]. The influence of bed temperature on these reactions likely explains the findings where, as bed temperature was increased, the concentration of CO and H_2 increased while the concentration of CO_2 decreased.

Finally, over the same temperature range methane from AROK was produced at comparatively low concentrations (<6% vol) under all test conditions. At atmospheric pressure, CH_4 from the syngas is normally the product of biomass pyrolysis, i.e. from reaction R1 [243]. At higher temperatures, the gas generated from biomass in the pyrolysis zone could undergo further reactions (secondary reactions) such as tar cracking, as described by reaction R2, which leads to an increase in CH_4 concentration with bed temperature. Skoulou et al [20] demonstrated that methane was generally produced at low concentration (CH_4<5%vv) under all test conditions from olive kernels in a fluidised bed reactor and they explained that methane was reforming at higher temperatures due to reaction R2. The same result was obtained by Mohammed

et al. [245] and Lucas et al. [118] who demonstrated that as the gasifier temperature increases, the H_2, CO, and CH_4 increases, whilst CO_2 content decreases.

For ARTOK as illustrated in Figures 7-3 and 7-4, at ER=0.15 and ER=0.2, it can be seen that as the temperature increases from 550°C to 750°C, the concentration of H_2 increased from 5.09% to 7.65% at ER=0.15 and 5.62% to 7.64% at ER=0.2. The content of CO rose from 16.36% to 18.44% at ER=0.15 and 15.53% to 19.41% at ER=0.2. This is likely due to the improved Boudouard reaction (R4), but could also be due to enhancement of the carbon partial oxidation reaction (R5). This trend is in agreement with the results published by another researcher [242].

It is notable that the air gasification process produces high CO_2 content [246]. The results also revealed high CO_2 content at low temperature, which then decreased when the temperature was increased. CO_2 is produced through reaction R6. However, the generated CO_2 was consumed through tar cracking R10 and Boudouard reaction R4 and methane dry reforming R8 to yield more CO and H_2. The CO_2 composition decreased with an increase in temperature, from 17.64% to 15.11% at ER=0.15 and from 16.88% to 14.73% at ER=0.2 across the temperature range. The trends of CH_4 did not show obvious variation with temperature; this could be due to thermal cracking at high temperature as the char methanation reaction rate for reaction R9 is relatively slow compared with other reactions [95], or the generated CH_4 can be consumed through methane dry reforming R8. Thus, it seems that there was a balance between CH_4 generated and consumption rate that kept the methane level approximately constant even at high temperature. The trend of methane not showing obvious variation is in agreement with results published by Xue et al. [247] when torrefied Miscanthus X giganteus was gasified in an air-blown bubbling fluidised bed gasifier. The same author reported a similar trend observing a decrease of CO_2 concentration with temperature. This is potentially because the CO_2 was consumed by reactions R4 and R10.

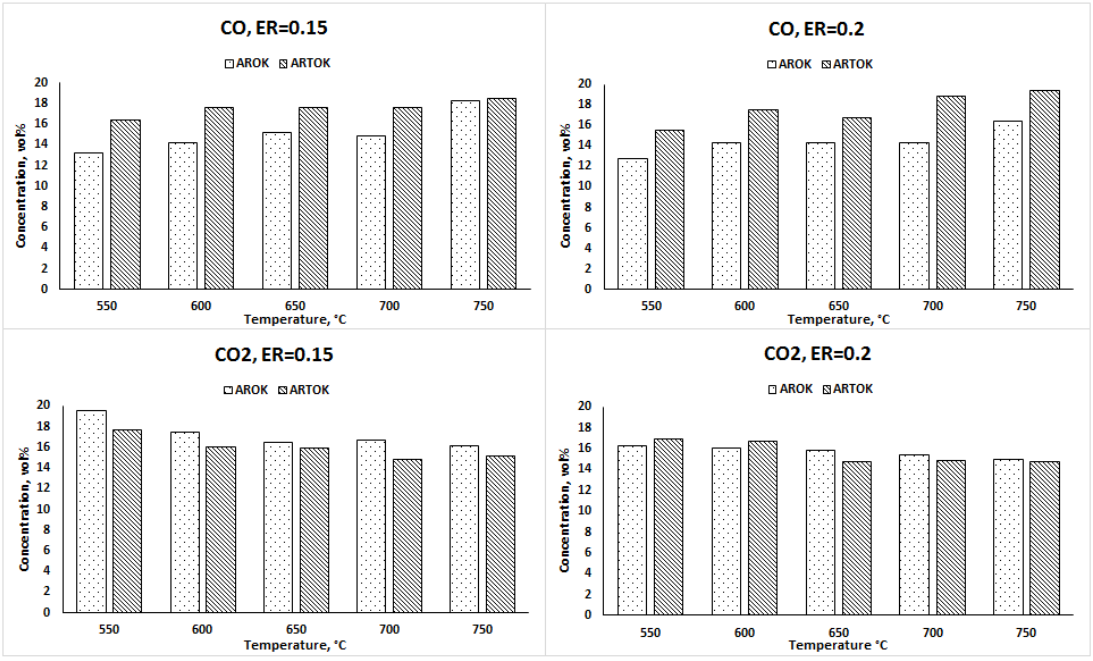

Figure 7-3 Comparison of CO and CO_2 gas in AROK and ARTOK at ER=0.15 and 0.2 at different bed temperatures.

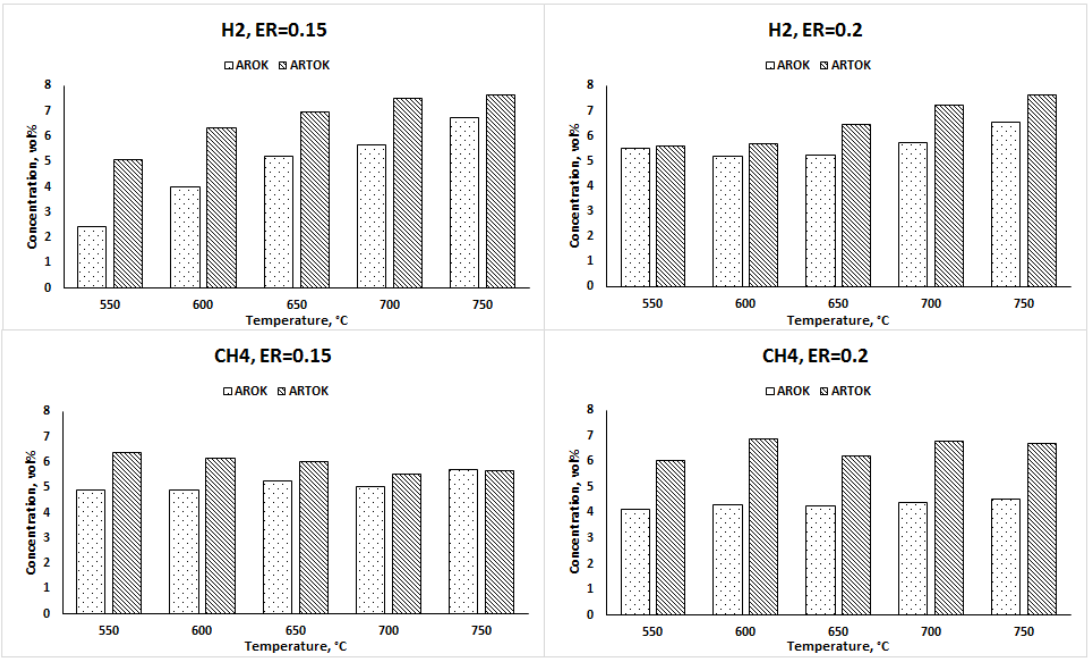

Figure 7-4 Comparison of H_2 and CH_4 gas in AROK and ARTOK at ER=0.15 and ER=0.2 at different bed temperatures.

The analysis indicates that the gasification of the ARTOK produced more CO and less CO_2 than the parent AROK with the exception of temperatures below 650°C at ER=0.2. The oxygen content of ARTOK was lower than that of AROK and the fixed carbon content was higher, which enhanced the Boudouard reaction (R4). According to Kuo et al. [248] the gasification of raw biomass gives lower CO concentration than torrefied biomass, which is stemming from the lower carbon content of raw biomass. The marginal behaviour of CO_2 concentration below 650°C at ER=0.2 is likely due to the water-gas shift reaction (R7) being more dominant at this conditions [249].

The gasification of AROK and ARTOK at different temperatures indicated that the ARTOK produced more H_2 as shown in Figure7-4, which implies that the hydrogen-producing reactions are being favoured at the higher temperatures provided by the ARTOK reactions. This was expected because the gasification of torrefied biomass produced more CH_4 gas compared to AROK thus promoting R8. The hydrogen conversion into dry gas was higher for torrefied biomass since the gasification of this feedstock results in higher yield of CH_4 and C_2H_6 [250]. From the same figure, the results revealed that the CH_4 content in ARTOK was more than the parent AROK in all conditions. This is in an agreement with Taba et al., who stated that the biomass having low contents of volatile matter is more suitable for significant H_2 production [251].

7.1.4 Effect of equivalence ratio (ER).

In addition to temperature, the equivalence ratio also plays a vital role as it affects the gasification process, including syngas composition. The effects of ER were evaluated for product gases of AROK and ARTOK through a set of experiments, performed isothermally at T=750°C, and varying ER between 0.15 to 0.35 in 0.05 increments. Different ERs were obtained by varying the biomass feeding rate and keeping the air flow rate constant at 40l/min.

In the AROK gasification tests, the ER had a significant effect on the concentration of CO, CO_2, H_2, HHV and carbon conversion, as illustrated in Figure 7-5. As the ER was increased in Figure 7-5, the CO and H_2 concentration decreased due to increasing char oxidation as well as partial oxidation. However, the CO_2 value at ER=0.15 is higher,

hence most of the CO_2 comes from reaction R1. This can be attributed to the reactor approaching pyrolysis conditions at this lower ER. According to Zabaniotou et al. [19] the major gaseous products from the pyrolysis of olive residues (cuttings and kernels) are CO and CO_2. The reduction in H_2 and CO can be explained by further oxidation to H_2O and CO_2 by oxidation reactions of H_2 and CO illustrated as reaction R11 and R12 respectively, owing to the increase in available oxygen at the higher equivalence ratios [95].

The following reactions show oxidation of hydrogen and carbon monoxide:

$$H_2 + 0.5O_2 \rightarrow H_2O \qquad \text{R11}$$

$$CO + 0.5O_2 \rightarrow CO_2 \qquad \text{R12}$$

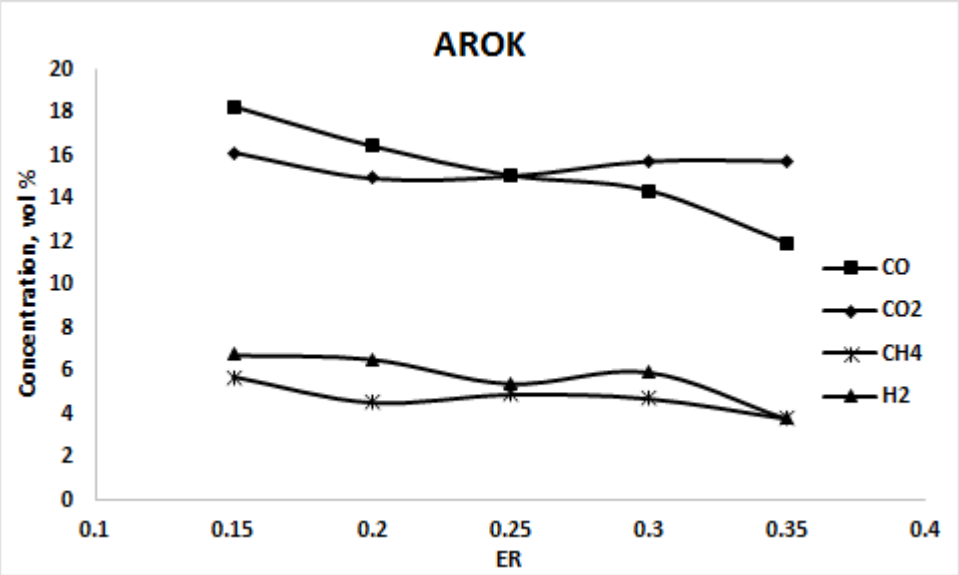

Figure 7-5 Effect of ER at 750°C on concentration of product gas.

The profile of product gases is comparable to other published results for fluidised bed gasifiers. According to Gil [96] , the H_2 and CO content decreases and the CO_2 content increases with increasing ER during gasification of pine wood in a bubbling fluidised bed . In figure 7-5, the CH_4 decreases from 5.71% to 3.81% as the ER increases from 0.15 to 0.35. According to Loha et al. [141], at higher ER, more oxygen is available which favours the oxidation reactions and as a result more CO_2 is produced, whilst H_2, CO and CH_4 are consumed.

As shown in Figure 7-6, at high ER (ER=0.35), the lowest HHV (3.5MJ/m^3) of the product gas was obtained due to a reduction in the concentration of combustible (energetic) species. The carbon conversion efficiency increases from 48.22% to 74.67% and this can be explained by more oxygen being supplied for biomass reactions which have a trend towards fuel combustion when ER increases. As a result, the increasing trend of carbon dioxide increases the carbon conversion efficiency of up to ER=0.3, after which it starts to decline. The results obtained agree with an earlier study where biomass was gasified in a bubbling fluidised bed; Narvaez noticed that when the ER was increased from 0.2 to 0.45, there was an increase in gas yield, and a decrease in the lower heating value of the gas, and a reduction in H_2, CO, CH_4 and tar content [88].

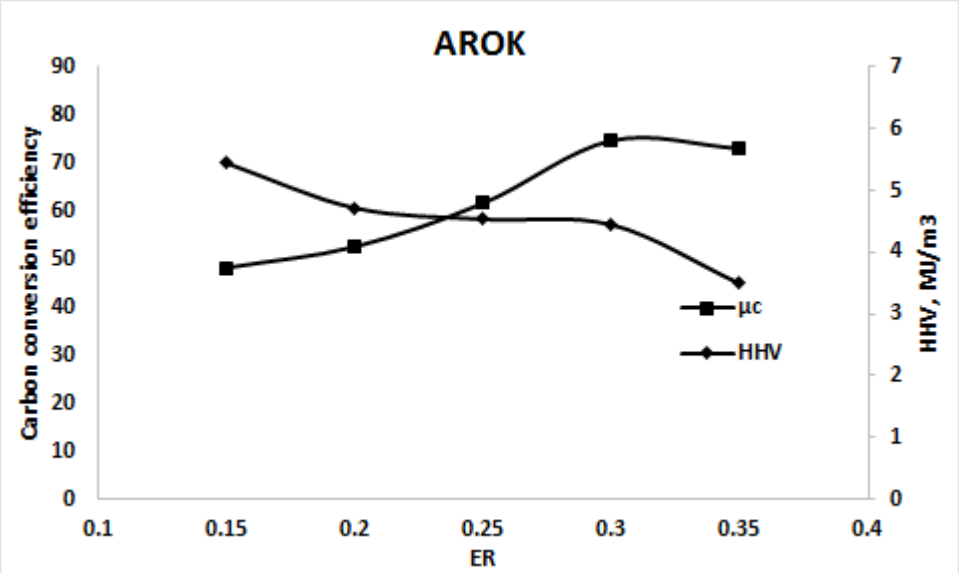

Figure 7-6 Effect of ER at 750°C of AROK on carbon conversion efficiency and high heating value.

For ARTOK gasification tests, the effect of ER on concentration of CO, CO_2, H_2, and HHV and carbon conversion is shown in Figures 7-7 and 7-8.

CO and H_2 are at their highest concentrations at low ER (ER=0.15 and 0.2), after which point they steadily decrease until the highest ER=0.35, as illustrated in Figure 7-7. The main reason for the decrease of CO and H_2 is the increased stoichiometric O_2 supply which gives rise to oxidation reactions R11 and R12. This was verified by the

increased concentration of CO_2 in product gas which increased from 15.11% to 15.85%. Similar results were reported by other authors [247, 252]. An ER of 0.2 was the optimum value for gas production in the investigated range, where the volume concentrations of CO, H_2, CH_4 and CO_2 were 19.4%, 7.6%, 6.7% and 14.7%, respectively.

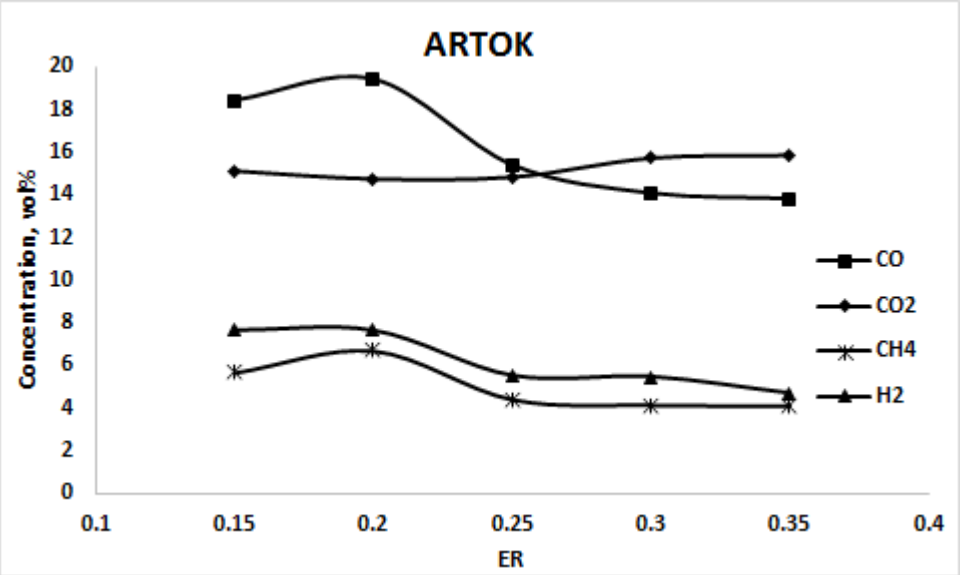

Figure 7-7 Effect of ER at 750°C of ARTOK on concentration of product gas.

Figure 7-8 shows the high heating value and carbon conversion efficiency; the HHV reached a maximum value (6.09 MJ/m^3) at ER=0.2. Evidently, it is influenced by the concentration of combustible gas species in the product gas as previously discussed. Beyond ER=0.2, the HHV decreased with increasing ER. A similar result was reported by another researcher [253]. Changing the ER has two effects: to promote the degradation due to more oxidation reactions; and to accelerate the gasification rate improving the product quality to a certain extent [116].

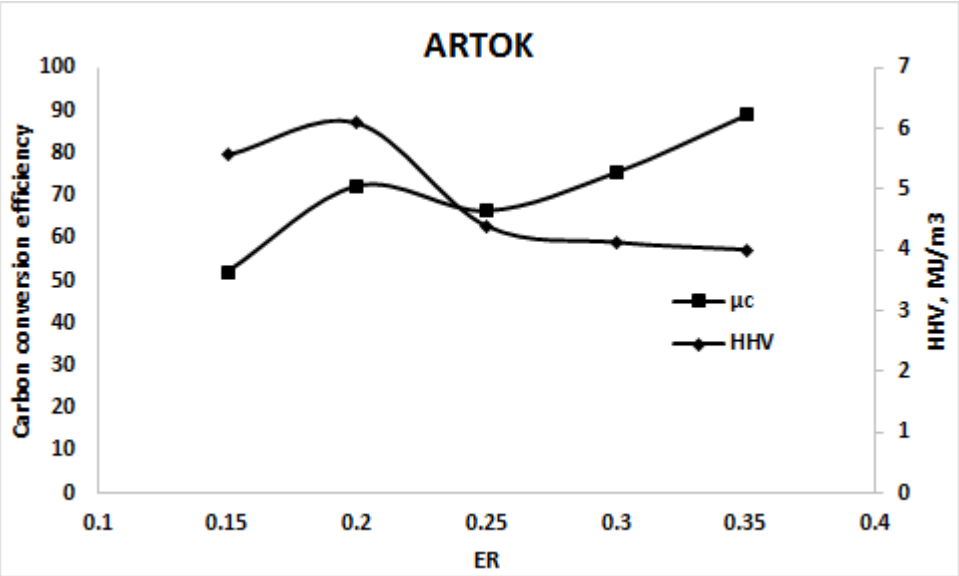

Figure 7-8 Effect of ER at 750°C on carbon conversion efficiency and high heating value.

Gas yield is the volume of dry fuel gas generated in Nm^3 per kg of fuel and is a significant parameter for evaluating the performance of the gasifier. As shown in Figure 7-9, the gas yield increased with increasing ER for both AROK and ARTOK. The highest gas yield was observed for the highest ER, but this is coupled with a decrease in HHV, specifically, a decrease of 25 % for AROK and 34 % for ARTOK compared to that of ER=0.2. This is logical since the higher concentration of oxygen results in more complete combustion. The results attained agree with another researcher where high carbon wood biomass was gasified in a bubbling fluidised bed [254]. However, ARTOK exhibited more gas yield compared to AROK for all ERs tested. The increased ARTOK gas yield can be accounted for by improved endothermic char gasification reactions [247]. When the gasifier temperatures increases, the carbon conversion increases hence gas yield also increases [251].

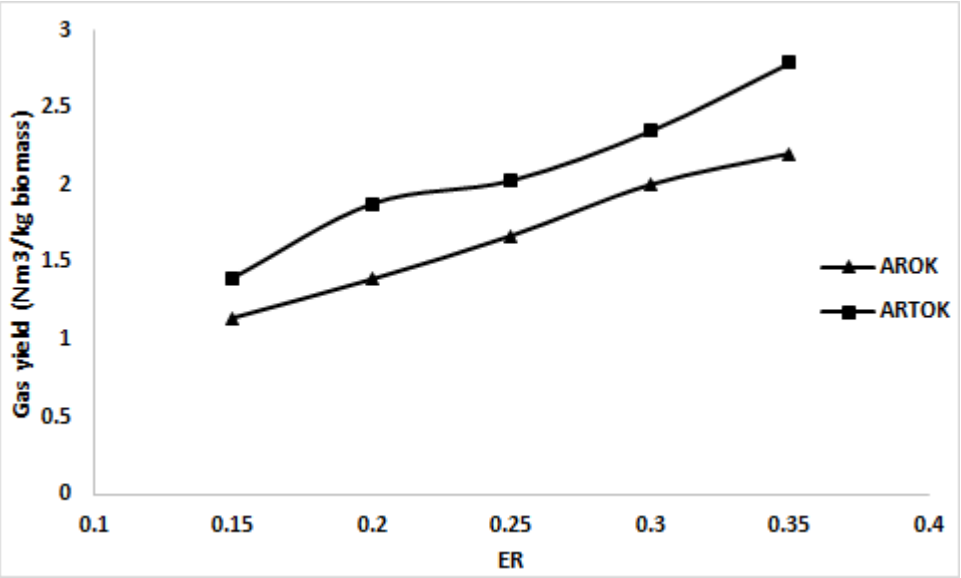

Figure 7-9 Influence of ER on gas yield of AROK and ARTOK.

7.1.5 Effect of bed temperature on HHV and cold gas efficiency of AROK and ARTOK

The effectiveness of the gasification process was evaluated in terms of HHV of dry gas, and cold gas efficiency. Figures 7-10 and 7-11 show the HHV and η respectively for AROK and ARTOK across a range of bed temperatures, 550°C to 750°C in 50°C increments, using an ER of 0.2.

Figure 7-10 illustrates the effect of bed temperature on HHV of the product gas for AROK and ARTOK. An increase of bed temperature from 550°C to 750°C improved the gas HHV from 3.96 to 4.72 MJ/Nm^3 for AROK and from 5.08 to 6.09 MJ/Nm^3 for ARTOK. As explained earlier, higher temperatures enhanced the evolution of combustible gases, especially H_2 and CO, which in turn results in an increase in HHV of the product gas.

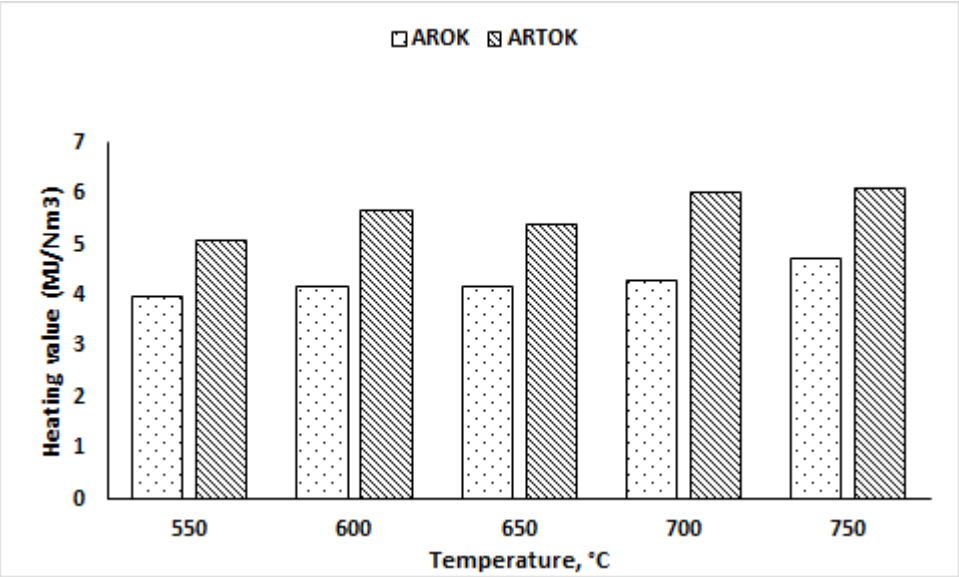

Figure 7-10 Effect of bed temperature on gasification HHV for AROK and ARTOK.

The variation of cold gas efficiency with temperature is given in Figure 7-11. The highest η values are to be found at T=750°C and were 34.23% and 55.03%, respectively, for AROK and ARTOK. Lahijani and Zainal [242] reported higher gasification efficiency, product gas yield, and carbon conversion efficiency, with increasing temperature. Sadaka reported that during gasification of raw and torrefied cotton gin wastes (CGW), the torrefied biomass showed higher values of cold gas efficiency and HHV as compared to raw biomass. This is due to the higher concentration of combustible gases produced during gasification of torrefied CGW. The values of η found were between 30.1% and 43% at temperatures from 750°C to 950°C, and the HHV of raw CGW and torrefied CGW were 4.8 $MJm^{-3}$and 5.4 MJm^{-3} respectively [255]. The cold gasification efficiency for raw bamboo was found to be lower than torrefied bamboo in an entrained flow reactor, mainly due to the relatively low caloric value of the raw bamboo [241].

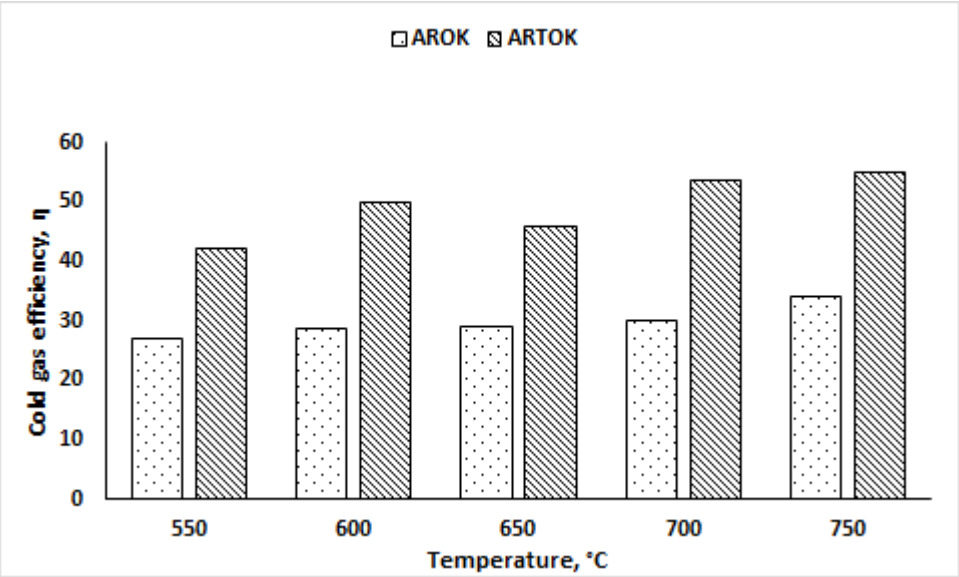

Figure 7-11 Effect of bed temperature on gasification cold gas efficiency of AROK and ARTOK.

External mass transfer resistance is responsible for restricting the flow of volatiles generated in a biomass particle from travelling outward from its surface [256]. From the proximate analysis of the two samples (Table 4-1) it can be inferred that the external resistance of ARTOK will be less than the AROK. Hence, the volatile matter generated from the AROK will form a comparatively large vapour field around the particles, which displaces oxygen and results in a diffusion-controlled zone around the particle, limiting oxidation reactions with the char. In the case of the ARTOK, the smaller quantity of volatile matter implies that this vapour field is smaller and therefore greater contact with oxygen is permitted, hence a higher reaction rate can be achieved. This is in agreement with Chen et al [257] who stated that torrefaction improves the physical and chemical characteristics of biomass, hence the syngas quality and cold gas efficiency are improved; this gives good application prospects for gasification processes.

7.1.6 Gas production from AROK ground to a particle size of 1180-1400µm.

The effects of reducing the particle size on gas composition were investigated at ER=0.2 and different bed temperatures of 550, 600, 650, 700, and 750°C. Smaller particles contributed to a large surface area and faster heating rate; high heating rate means more light gases [112]. Figure 7-12 illustrated the effect of temperature on gas

production of AROK of particle size 1180-1400µm. As can be seen in the Figure, the CO increased from 14.17% to 18.72% from 550°C to 750°C which could be due to the improved Boudourd reaction R4 and oxidation reaction R5. The particle size of 1180-1400µm yields more CO in comparison to AROK (12.79% to 16.44%) at the same temperature range. On the other hand, the CO_2 decrease from 17.49% to 14.46%. A suggested reason is that the CO_2 is consumed by reaction R4. It was observed that the concentration of CH_4 increased from 4.44% to 6.06 % from 550°C to 700°C which may be the result of improved reaction R2. However, subsequently the CH_4 reduced at 750°C. Fidalgo et al, reported that the 700-800°C range was the most suitable temperature for dry reforming of methane [258]. The results suggest that R8 was more active at this temperature. It is worthy of note that the particle size of 1180-1400µm produced more CH_4 than AROK (a percentage increase of between 7.8% to 38.4%). Finally, the H_2 production increased with temperature, it was 2.92% at T=550°C and became 6.54% at T=750°C. It may be the overall result of the promotion of the water-gas reaction R3 as well as R8. However, the concentration of H_2 was less than AROK for all temperatures tested.

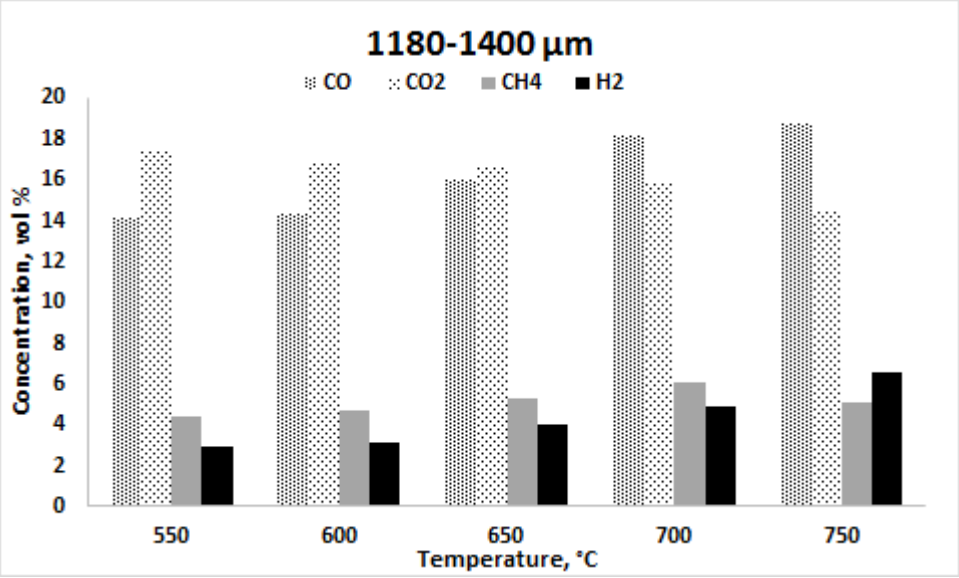

Figure 7-12 Effect of bed temperatures on gas production for AROK of particle size (1180-1400).

7.1.7 Influence of superficial gas velocity on gasification.

Whilst maintaining a constant equivalence ratio between the biomass and air, the superficial gas velocity was altered through the reactor. Increasing the superficial gas velocity will lead to an increase in the degree of agitation and gas-to-particle heat transfer. In a gas-solid reaction, the mass transfer of the gas first takes place from the main stream of fluid to the external surface of the particle [259]. As a result, the overall reaction is influenced by external diffusion.

A series of five tests were performed at temperature 750°C and ER=0.2 to investigate the effect of external diffusion on the gasification of AROK. The results are shown in Figure 7-13. This gives the calculated mass of instantaneous char remaining inside the gasifier during continuous gasification. The data shows that the rate of reaction was affected by changing the superficial velocity up to $2U_{mf}$, whereafter the effect seemed to saturate. In this gas-solid reaction system, the mass transfer effects could be minimized when the system is operated at sufficiently high gas velocity, so that the overall reaction rate does not increase with further increase in gas velocity [260]. Therefore, a superficial velocity of $2U_{mf}$ was selected as the basis for all tests, representing the minimum air velocity required to reduce external diffusion. At high gas velocity, the boundary layer thickness around the particle becomes sufficiently small that it no longer offers any resistance to the diffusion of gas, eliminating external diffusion from the reaction rate [176].

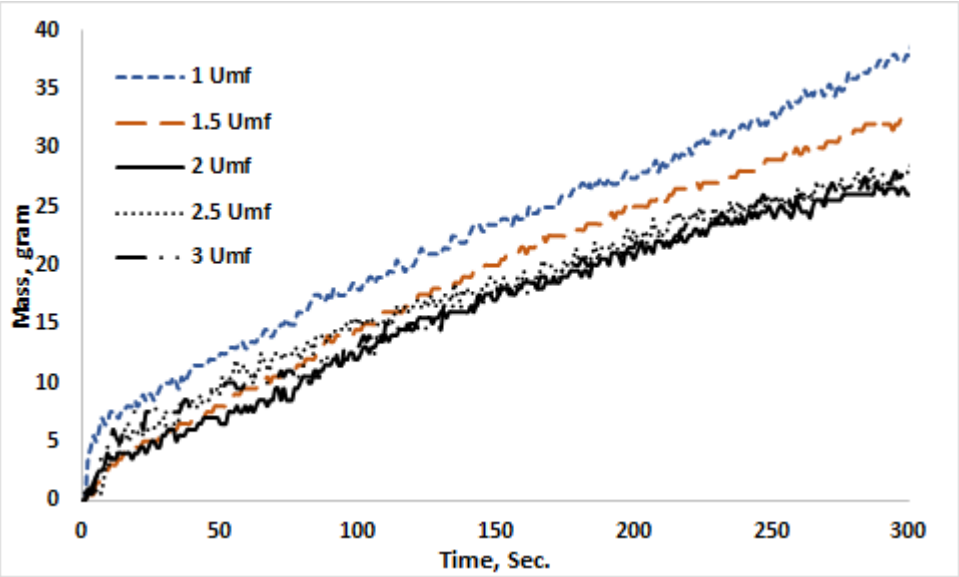

Figure 7-13 Mass of char build up in the gasifier at different superficial velocity.

7.1.8 Kinetic parameters

The controlling kinetic parameters were examined by investigating the mass-time behaviour of the reactor. This was undertaken at five preset temperatures (550, 600, 650, 700, and 750°C), 2 U_{mf} and one equivalence ratio (0.2) for AROK and ARTOK. All experiments were undertaken at isothermal conditions for a sufficient time until steady state conditions were obtained for each case.

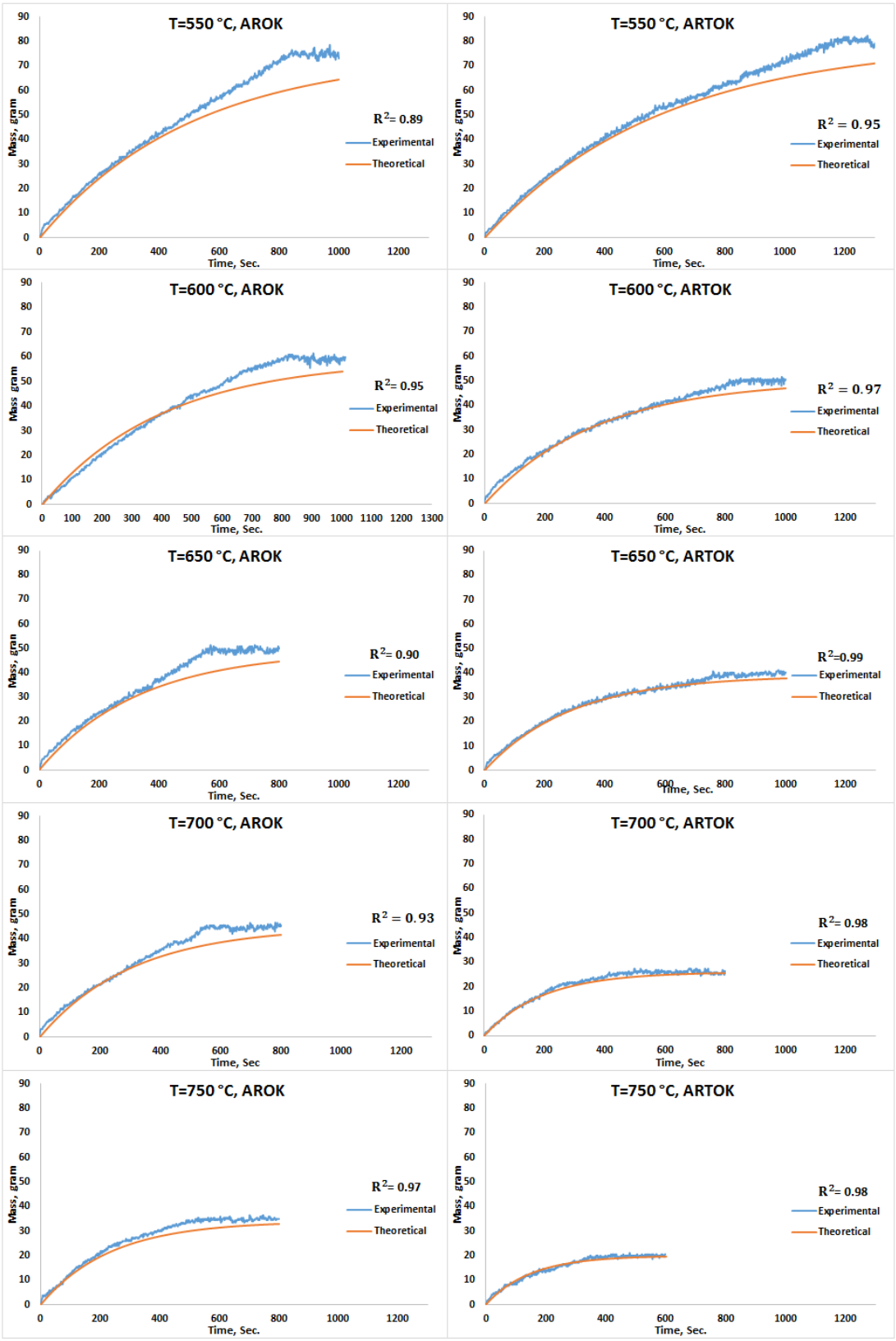

Figure 7-14 Calculated mass of the char in the gasifiers as measured by experimental work and predicated by the mass balance model at different preset temperatures for (a) AROK and (b) ARTOK.

Figure 7-14 illustrates the instantaneous mass of char in the bed, from initial fuel feeding to steady-state conditions, where there is no further increase in the measured mass of char inside the reactor. The behaviour is shown for both AROK and ARTOK samples, on identical axes scales to aid in comparison. As the system approaches equilibrium during continuous feeding of biomass, the amount of char builds up in the reactor while the rate of devolatilization remains constant. After sufficient time under consistent gasification conditions, steady state char conversion is achieved. As can be seen from the figure, the final equilibrium mass and time are found to be dependent on temperature. The reaction rate is shown to be faster at higher temperatures for both biomass samples [261]. Note that above 550°C the equilibrium condition mass of ARTOK was always lower than the AROK, since the oxidation of carbon in the char takes place parallel to thermal decomposition and release of volatile matter [262]. Therefore, the amount of char left at steady state is less for ARTOK except at T=550°C, where it may be that torrefied biomass was less reactive at this temperature. Furthermore, the hydrocarbon gases such as CO and CH_4 were found to be higher with ARTOK (see Figure 7-3 and 7-4). In addition, the ARTOK reached the highest temperature during gasification reactions (See Figures 7-1 and 7-2). This in agreement with Hu et al. who stated that torrefied biomass had a more steady-state burning process and a higher combustion efficiency [263].

To give a more conceptual picture about the difference between AROK and ARTOK Figures 7-15, 7-16, and 7-17 illustrate the instantaneous mass of char in the gasifier for 5-minute runs for AROK, AROK of particle size of 1180-1400 µm, and ARTOK, respectively, at ER=0.2 and preset temperatures (550, 600, 650, 700, and 750°C).

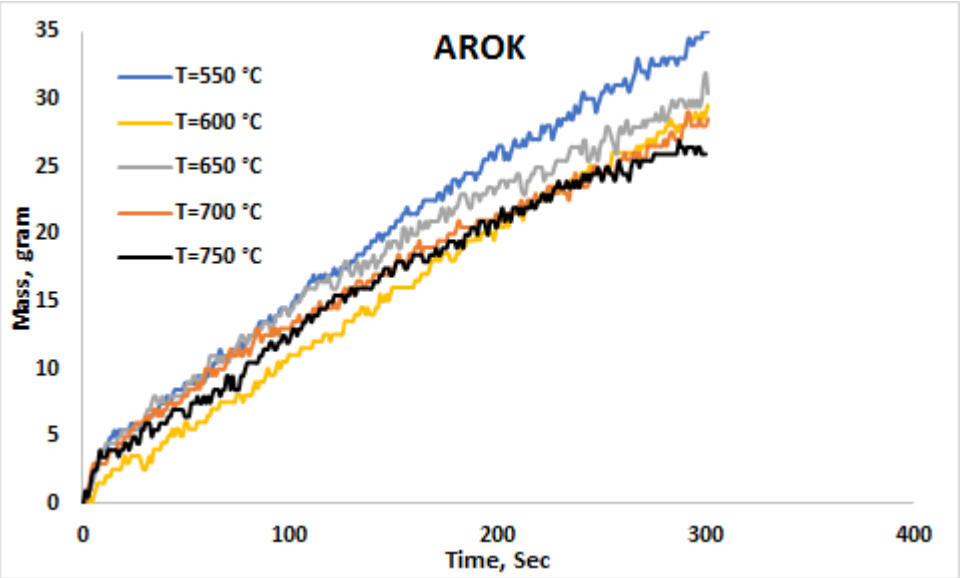

Figure 7-15 Mass accumulation rate of char during 5-minute run of AROK at different preset temperatures.

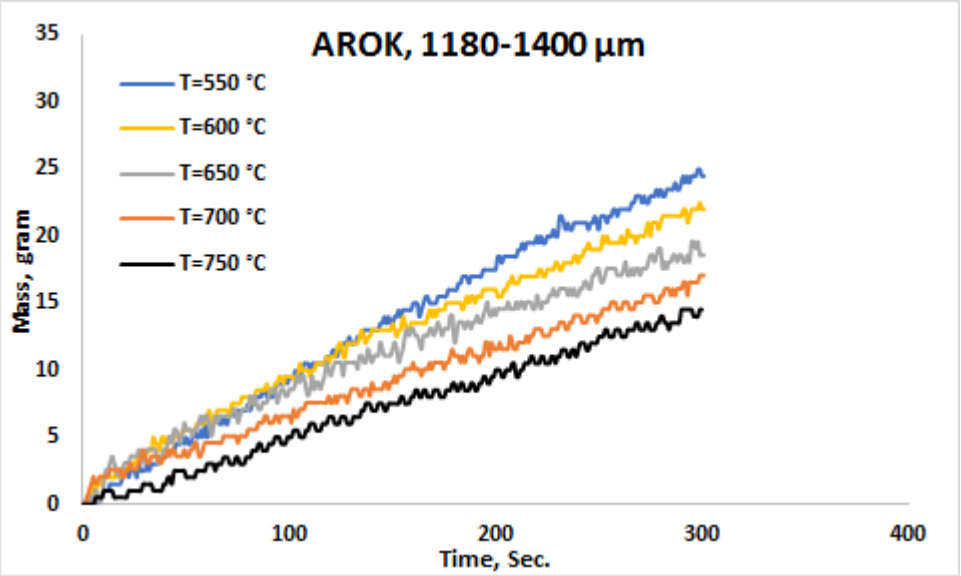

Figure 7-16 Mass accumulation rate of char during 5-minute run of AROK of particle size 1180-1400µm at different preset temperatures.

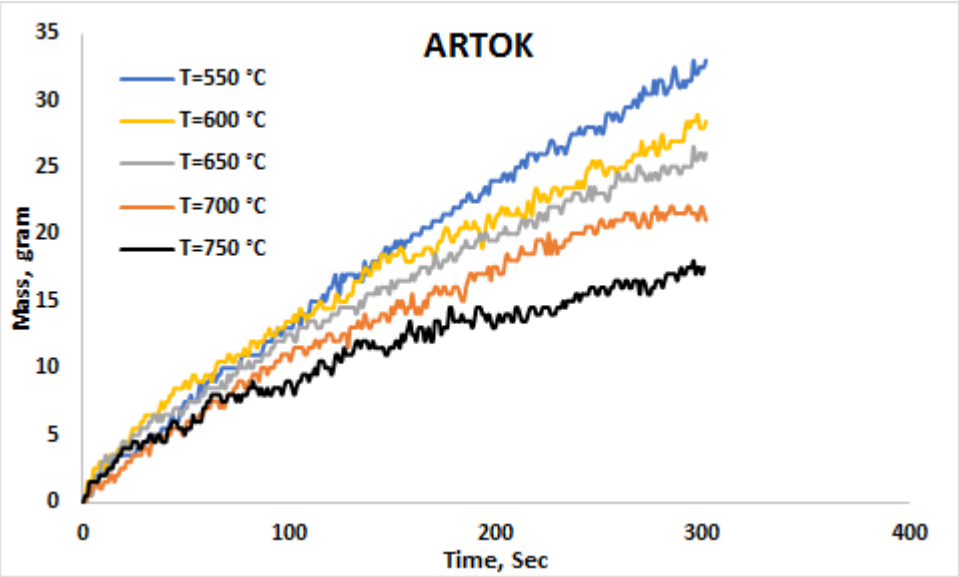

Figure 7-17 Mass accumulation rate of char during 5-minute run of ARTOK at different preset temperature.

It was observed for AROK (particle size <5mm) that there was little difference in the variation of the mass profile for the different temperatures (see Figure 7-15). According to Sami et al. [264], the volatiles may burn in jets or as a flame envelope. An enveloping flame acts like a shroud, preventing oxygen from reaching the particle surface and therefore preventing heterogeneous oxidation of char. Another explanation is that pore diffusion cannot be the only reason for the lower reaction rate of the larger particles (3.15-4.5mm); the enrichment of product gases inside the larger particles caused by low diffusion coefficients or high flow resistances is responsible for the inhibition of the reaction rates [265]. The influence of the ejected volatile matter on gasification likely explains the findings where no significant variation in mass build-up of char was observed at different temperatures due to inhibition of the reaction rate and heat transfer limitations in AROK. The temperature dependence is high when chemical reaction is the rate-controlling step and low if the mass transfer is rate-controlling [217].

The rate at which biomass combusts depends largely on two predominant factors: the rate of the heat transfer, and the kinetic rate of the reaction [266]. Particle size dominates the influence of heat transfer, i.e. small particles will heat more rapidly

(thermally thin). Biomass gasification consists of two partially overlapping processes: very fast pyrolysis also known as volatilization or charring followed by the slower reaction of the solid residue (char) with the air stream. The difference between AROK and the AROK of 1180-1400 μm (see Fig. 7-16) was that the volatile material released through pyrolysis of the smaller particles occurred faster than AROK, leading to oxidation dominating (heterogeneous reaction) at an earlier stage, which explains why the small particles of AROK produce more CO and CH_4 in comparison with AROK. Chemical reaction rate, therefore, was the controlling factor in the case of the smaller particles, whereas mass transport phenomena was the controlling factor for the reactions of the larger particles [267]. Finer biomass particles offer less resistance to the escape of condensable gases, which therefore escape relatively easily to the surroundings before undergoing secondary reactions [75].

The reduction of the oxygen to carbon ratio in fuels correlates with an increase in resistance to thermal degradation (see the ultimate analysis of AROK and ARTOK), which is one of the objectives of torrefaction and carbonization, justifying the results observed on Figure 7-18. It was observed that ARTOK has a lower mass loss rate than AROK due to a higher resistance to thermal degradation. Fuels with higher contents of fixed carbon and low volatile matter tend to decompose slowly and offer higher resistance to thermal degradation [268]. This is in agreement with Ren et al. [269] who noticed that the raw biomass lost mass faster than torrefied biomass during the pyrolysis of woody biomass. As shown in Figure 7-18, the AROK released volatiles faster during pyrolysis than ARTOK, the time difference being about 2-3 sec. Hence, ARTOK has a lower volatile loss rate than AROK, so there is less flow resistance to outward gas diffusion during gasification (see proximate analysis), which gave the ARTOK priority to react with oxygen. Figure 7-17 shows the mass change of ARTOK, under the temperatures described at ER=0.2. This is explained by the findings where the mass accumulation of ARTOK char reduced as the temperature increased, likewise for the small particle size (1180-1400μm) fuel, owing to the fact that both samples offered less resistance to oxygen reaching the surface of the particle thus promoting char reaction as the temperature was increased. On the contrary, AROK biomass did not exhibit significant variation because there was a higher resistance to oxygen

reaching the particle surface for char oxidation, even as the temperature was increased, owing to the larger particle size.

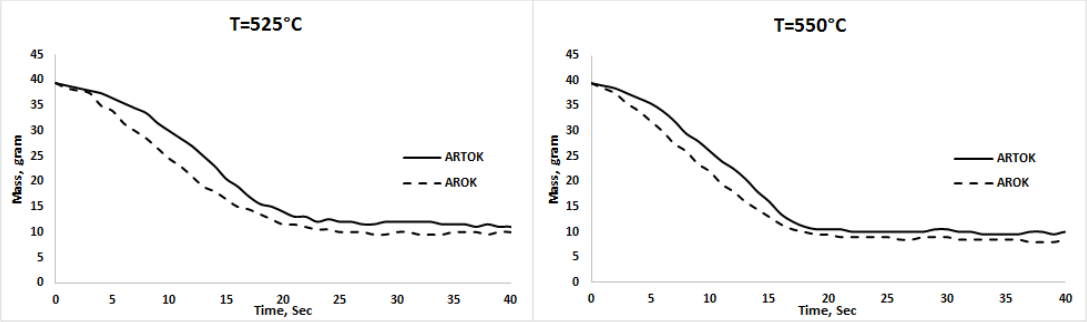

Figure 7-18 Mass loss with time of AROK and ARTOK under pyrolysis conditions at temperature 525°C and 550°C.

According to the weighing scale recorded values during the batch pyrolysis experiment at T=550°C (see Figure 7-18), the char yield was found to be 21.5% for AROK and 24% for ARTOK. The torrefied biomass formed more biochar in pyrolysis [269]. Using Equation (5.9), a mass feed rate of 41g/min for AROK and 34g/min for ARTOK (see Table 5-3 and Table 5-4), gave a char feed rate (F) of 0.147g/sec and 0.136g/sec for AROK and ARTOK respectively.

The values of steady state mass and critical point time (the time when the mass becomes steady state) for AROK and ARTOK were obtained with a MATLAB program using linear change point models based on Equation (7.1) [270]. This equation shows the relationship between mass and time.

$$Y = \beta_1 + \beta_2 (X - \beta_3)^+ \qquad (7.1)$$

Where β_1 is steady state mass, β_2 is the slope, β_3 is critical point time, X is the input time, $(^+)$ means that only positive differences between X and β_3 are taken into account, and Y is the output mass.

Figure 7-19 illustrates the model predicted value using MATLAB and experimental work value of AROK and ARTOK as two examples, the other temperatures can be found in the Appendix B.1&B.2.

From the values of m_{ss}, the rate constant k was evaluated experimentally at steady state char loading in the reactor using Equation (5.15). The calculated value of k for different steady state reaction temperatures (see Figures 7-1 and 7-2) using the results of Figure 7-19 are included in Table 7-1. m_{ss} denotes the steady state condition mass of char in the reactor.

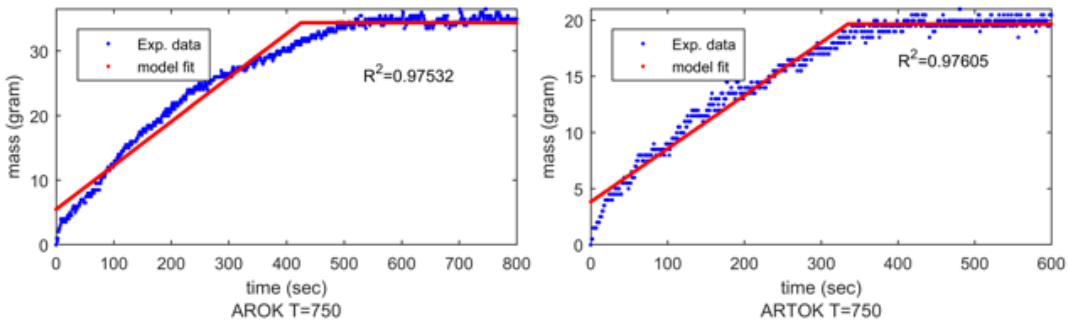

Figure 7-19 Experimental work and predicted values using MATLAB for AROK and ARTOK at a temperature of 750°C.

Table 7-1 Rate constant (k), steady state temperatures and mass load of AROK and ARTOK at the range of steady reaction temperatures examined.

AROK, ER=0.2			**ARTOK, ER=0.2**		
Reaction steady temperature, K	m_{ss} (gram)	k, s^{-1} $x10^3$	Reaction steady temperature, K	m_{ss} (gram)	k, s^{-1} $x10^3$
973	75	1.96	1048	79	1.7
986	59	2.49	1073	49	2.7
1011	49	3	1097	38	3.5
1028	45	3.26	1148	26	5.2
1043	34	4.3	1173	20	6.8

The values of F and k are substituted into Equation (5.14) yielding the mass balance model for the char load in the reactor in grams. The predicted behaviour of AROK and ARTOK is shown in Figure 7-14 together with the corresponding experimental data at different temperatures. It can be seen that this model is also a good fit to the

experimental data. ARTOK exhibits higher regression than AROK between 95 and 99%, which means ARTOK obeys the first order reaction more than AROK.

From the results presented in Table 7-1 the Arrhenius equation can be plotted for K in terms of reciprocal temperature. Linear regression of the data in Figure 7-20 and 7-21 for AROK and ARTOK respectively, yields the lines of best fit. From the ln(k) versus 1/T plot, the slope (E_a/R) was used to obtain the values of activation energies for the AROK and ARTOK, giving activation energies of 84 and 106 kJ/mole respectively. This means that a lower amount of energy is necessary for the raw olive kernel to start reacting than for torrefied biomass [271].

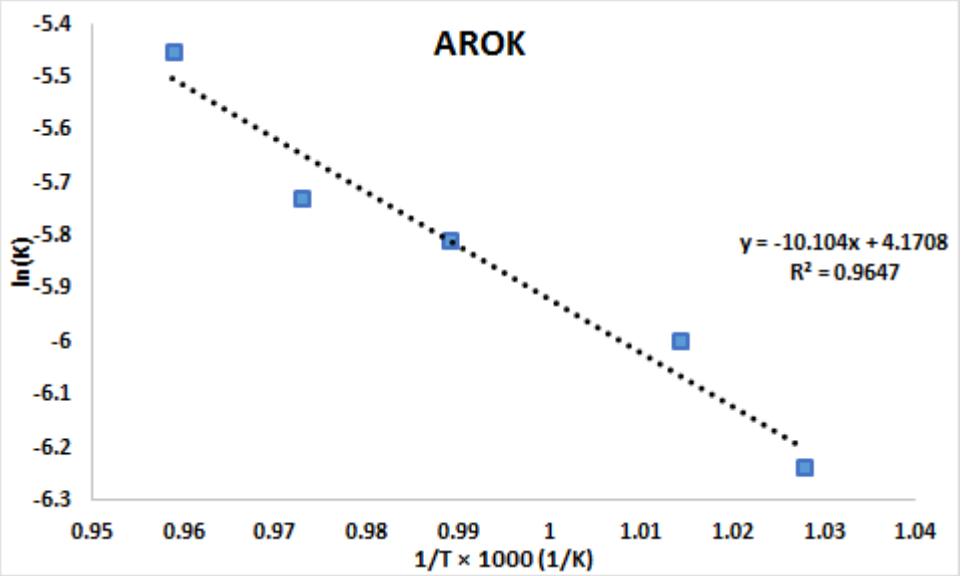

Figure 7-20 Arrhenius plot for AROK

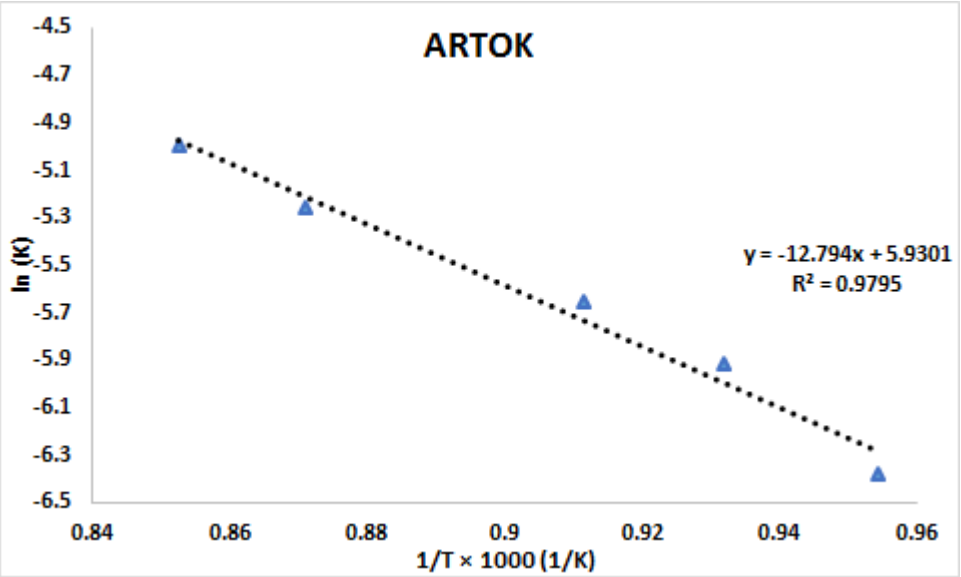

Figure 7-21 Arrhenius plot for ARTOK.

At present, there is limited information available in the literature that focuses on the gasification kinetics of raw and torrefied biomass. However, the activation energy of seed corn biomass was found to be 78 kJ/mole during gasification in a bubbling fluidised bed during continuous gasification by using a transient model, and it was suggested that the reactions are limited by pore diffusion, therefore this value represented the apparent activation energy [220]. In many gas-solid systems with fast reactions, the overall rate is found to be controlled by mass transport between the reaction surface and the bulk fluid [260]. According to the same author, in the experimental determination of kinetic parameters, it is very important to ensure that the measurements are carried out under conditions such that the overall rate is indeed controlled by chemical kinetics, where pore diffusion and gas phase mass transfer do not play an appreciable role. The calculated activation energy of ARTOK suggests that the reactions are chemically controlled when compared with AROK which is diffusion controlled. However, the activation energy of raw olive kernels under inert conditions (pyrolysis) was investigated in previous work and found to be 60.8 kJ/mole [272], which agrees well with the results of [25, 189] , who found that the activation energy in air was higher than in a nitrogen atmosphere.

The values of m_{ss} were found by inserting the critical time point (the time at which the mass becomes steady state) into Equation (5.14). The critical time point was found from the MATLAB model fit method as illustrated graphically in Figure 7-19, and plotted tabularly in Table 7-2 and Table 7-3 at a given feeding rate and rate constant for AROK and ARTOK. Table 7-2 and 7-3 show the percentage error of the steady state mass (MATLAB) and the steady state mass obtained from Equation (5.14). It can be seen that the percentage error of ARTOK is less than AROK for the whole temperature range.

Table 7-2 Percentage error between mass obtained from MATLAB model and mass obtained from Equation (5.14) of AROK.

AROK			
Temp. °C	t_{ss} (sec)	m_{ss} (predicated), gm	Error %
550	808	60	20
600	705	49	16.9
650	554	40	18.3
700	535	37	17.7
750	425	29	14.7

Table 7-3 Percentage error between mass obtained from model using MATLAB and mass obtained from Equation (5.14) of ARTOK.

ARTOK			
Temp. °C	t_{ss} (sec)	m_{ss} (predicated), gm	Error %
550	1038	66	16.4
600	724	43	12.2
650	573	34	10.5
700	345	22	15.3
750	335	18	10

7.1.9 Repeatability

The kinetic gasification tests were repeated under the same conditions as described in (7.1.8) to investigate the repeatability of the results. The experiments should be repeated for all samples for an accurate representation but due to the limitation of time and materials, repeats were only performed for ARTOK and AROK at T=700 °C and T=750 °C. As shown in Table 7-4, the error of the two experiments ranges between 1.9-7.5%. This is expected due to the difficulty of maintaining a consistent feed rate of biomass during the gasification period. The results can be found in Appendix C.

Table 7-4 Experimental conditions for the repeated tests

Case	Temperature °C	m_{ss} (gram)	Air flow rate (l/min)	Error%
AROK	700	43.5	40	3.3
AROK	750	36.5	40	7.3
ARTOK	700	26.5	40	1.9
ARTOK	750	21.5	40	7.5

7.2 Effect of biomass particle size

The gasification behaviour of four sizes of olive kernels, ranging from fine to coarse, was compared. The effects of particle size on gas composition, char yield, and gasification performance from gasification of olive kernels were investigated at reactor temperature T=750°C and ER=0.2 for five-minute runs, and the test results are illustrated in Table 7-5 and Figure 7-22.

It is normally accepted that the composition and gas yield are related to the heating rate of biomass particles: high heating rate means more light gases as well as less char and condensate [112]. Smaller particles result in a larger surface area and faster particle heating rate, therefore, it can be predicted that the gas composition, char yield and gasification performance will be affected by particle size [267].

Table 7-5 Experimental results of different olive kernels particle size.

Biomass particle size (mm)	0.5-0.71	0.71-1.18	1.18-1.4	<5
Average size (mm)	0.6	0.94	1.29	3
Gas HHV (MJ/Nm^3)	5.8	5.6	5.24	4.72
Gas yield (Nm^3/kg biomass)	1.56	1.51	1.45	1.39
Carbon conversion efficiency (%)	69.19	65.24	58.4	52.6
Cold gas efficiency (%)	47	43.96	40	34.23
Char (%)	6.09	6.34	7.07	12.68

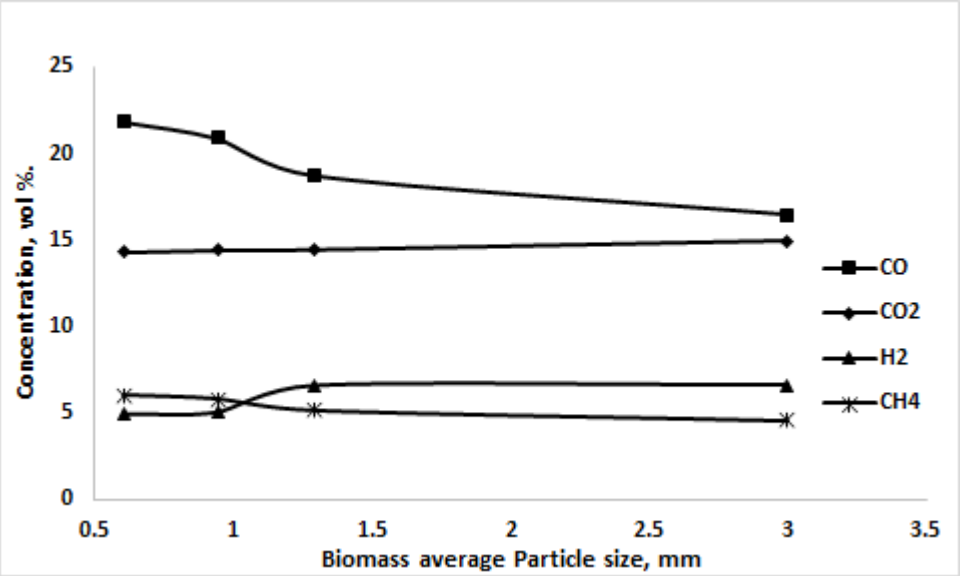

Figure 7-22 Influence of olive kernels particle size on gas composition at ER=0.2; T=750°C

As can be seen in Figure 7-22 and Table 7-5, the greatest variation in gas composition occurs below a particle size of 1.5 mm. Increasing particle size above this has a marginal effect, with the exception of CO gas which exhibits a downward trend.

With decreasing the particle size, the concentration of CO and CH_4 produced is greater, while the CO_2 and H_2 are shown to be less. It can be noticed that the CO and CH_4 increased from 16.44% to 21.85% and from 4.54% to 6.02%, respectively when the particle size decreased from <5mm to 0.5-0.71mm. Meanwhile CO_2 and H_2 decrease from 14.95% to 14.31% and from 6.57% to 4.96% respectively.

It is known that the water-gas shift reaction ($CO+H_2O \leftrightarrow CO_2 + H_2$ -41.2 KJ/mole) is one of the reactions responsible for H_2 and CO_2 gas production. These results are also related to the fact that the molar fractions of H_2, CO, and CO_2 are linked together by the equilibrium of the water-gas shift reaction, which is an important exothermic gas-phase reaction [273]. Yu et al. [274] reported that the CO content decreased with increased particle size because of some CO reacting with H_2O. Furthermore, the temperature in the oxidation zone of small particles was found to be much higher than that of large particle size [275]. Le Chatelier's principle states that higher temperatures favour the reactants in exothermic reactions and favour the products in the endothermic reaction. Therefore, the endothermic reactions were strengthened with the increase in temperature.

This outcome suggests that more CO was converted to CO_2 when the particle size increased due to a decrease in the temperature of the oxidation zone. Decreasing the temperature of a system in dynamic equilibrium favours the exothermic reaction. With respect to CH_4 content, the concentration of gas is produced by the reactions R1 and R2. In addition, the percentage of char remaining after the gasification process decreased with decreasing particle size. According to Wei et al. [276], the volatiles can undergo secondary reactions (e.g. cracking, condensation and polymerization) inside biomass particles. Polymerization of some of the volatile material may result in the deposition of large molecules on the walls of the pores, leading to an increase in char yield and a decrease in volatile evolution; this is more likely for larger biomass particle sizes, as illustrated in Table 7-5. The gas composition results are consistent with those obtained in literature except for H_2 gas which showed the opposite [86, 115]. But Lv et al. [267] reported a similar trend observing an increase of H_2 gas content with particle size for the gasification of pine sawdust.

An explanation is tentatively suggested that when the particle size is decreased, the pyrolysis process mainly happens very fast, which leads to a sufficient contact area between biomass and gasifying agent and the gasification processes under kinetic control. While in large particle sizes, the product gas generatead inside the particle is more difficult to diffuse out, hence, the process is mainly controlled by gas diffusion. This was the reason why the gas yield, HHV, carbon conversion efficiency and cold

gas efficiency were improved when the particle size of biomass was decreased which is similar to the results of Guo et al. [277].

7.3 Effect of Static Bed Height

In order to study the influence of static bed height on gasification performance, four static bed height (H_s) were used. Static bed height to bed diameter ratios (H_s/D) of 0.5, 0.75, 1, and 1.25 were chosen, where D is the bed diameter equal to 8.3cm. This gave static bed heights of 4.15cm, 6.225cm, 8.3cm, and 10.375cm, respectively. The gasification test occurred at T=750°C, ER=0.2, and an air velocity of $2U_{mf}$. Figure 7-23 and Table 7-6 show the effect of static bed height on the gas composition, μc, η, and HHV. At a given reactor temperature and a fixed fluidizing velocity, increasing bed height gives an opportunity for the gas produced to stay longer in the high-temperature dense bed and allows for increased heat transfer. The high temperature will promote secondary reactions of heavy hydrocarbons, tars and char gasification reactions, which will cause an increase in the gas yield [278].

As shown in Figure, the CO content increased from 16.44 to 17.03 % up to bed height of 1D and then decreased, but the H_2 decreased from 6.57 to 5.01 % from bed height 0.5-1.25D. However, the CO_2 gas increased from 14.95 % at 0.5D to 17.07 % at 1.25D, while CH_4 slightly increased up to 1D and then decreased. The decrease in H_2 may be attributed to methanation reaction R9, which resulted in CH_4 increasing slightly up to 1D, then decreasing at 1.25D.

Comparing our findings with literature, palm kernel shells (PKS) were gasified in a fluidised bed gasifier, and the results show that CO and CO_2 increased with bed height while H_2 decreased with increased the static bed height. In addition, the CH_4 increased slightly as the bed height was increased [106]. These findings are the same as found in olive kernels. It should be mentioned, however, that the coconut shells investigated in the literature showed the same findings for CO and H_2 production as for PKS and olive kernels, but not for CO_2 and CH_4 production. This could be due to the different physical and chemical properties of different biomass.

Referring to Table 7-6, the gas yield, μc, η, HHV increased from 1.39, 52.6, 34.23 and 4.72 to 1.5, 61.2, 37.3 and 4.8 up to 1D of static bed height and then started to decrease beyond this height. The increases in gas yield, μc, η, and HHV for the first three bed heights could possibly be explained by the changing concentrations of CO, CO_2, H_2 and CH_4 in the product gas. The CO, CO_2 and CH_4 used to described the carbon conversion (μc) in product gas, while the CO, CH_4, and H_2 used to calculate the HHV and η. However, when the gasification performance decreased beyond 1D; it may be that 1D is an optimal bed height for a particular ER, at which the maximum gas yield and carbon conversion efficiency were obtained. Poorer performance beyond a bed height of 1D can be explained by fluidization dynamics such as a slugging flow, which reduces the bed temperature thereby lowering the conversion of char to gases. Slugging not only causes poor mass transfer and heat transfer but it might lead to mechanical failure of the reactor supporting structure [104].

It is important to keep the weight measurement away from the vibration effect of fluidization. Therefore, for kinetic purpose study, Hs=0.5D was used in all experiments, because it gave a negligible vibration effect on measurements.

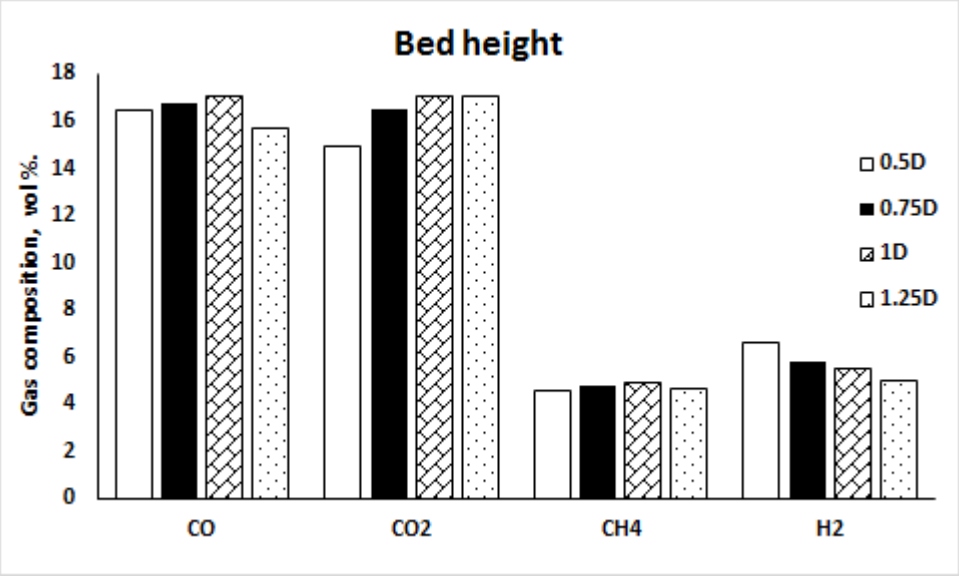

Figure 7-23 Influence of static bed height on gas compositions of olive kernels

Table 7-6 effects of static bed height on gasification performance.

Bed Height mm	**0.5D**	**0.75D**	**1D**	**1.25D**
Gas yield (Nm^3/ kg biomass)	1.39	1.49	1.5	1.39
μc %	52.6	59.84	61.2	54.83
HHV (MJ/Nm^3)	4.72	4.75	4.8	4.48
Cold gas efficiency % (η)	34.23	37	37.3	32.5

Summary

This chapter shows the results of gasification of AROK and ARTOK in a bubbling fluidised bed gasifier. The fuel characterization of AROK and ARTOK are described. The autothermal operation of the gasifier, steady state gasification temperature, and combustion profile temperature are presented.

The influence of operating conditions on gasification performance is explained. The results show that temperature increased combustible gas production in both biomasses, however, more combustible gases were formed with ARTOK. Also, the results of the effect of ER in gasification performance are discussed. Particle size and bed height were investigated. It was found that for the smaller particle size, the greater production of gas. Furthermore, the procedure to reduce the effect of external diffusion is shown.

By using a mass balance model and a gravimetric method to track the formation of char until steady state conditions are reached inside the gasifier, the activation energy of AROK and ARTOK can be measured. The results suggest that gas diffusion controls the reaction of AROK, whereas chemical reaction controls gasification of ARTOK.

Chapter 8

Results and Discussion of Palm Stone Pyrolysis and Gasification

8.1 Introduction

This chapter investigates the influence of 1) superficial velocity on the conversion rate during pyrolysis of palm stone, 2) the effect of temperature on total conversion and gas evolved, finally 3) evaluates the kinetic parameters and mechanism of the thermal decomposition of biomass. Fast pyrolysis experiments have been performed in the fluidised bed reactor. The pyrolysis procedure was described in section 4.5.

The influence of operating conditions (temperature and equivalence ratio) on gasification performance is investigated in the bubbling fluidised bed. The overall mass balance and carbon mass balance is described in this chapter. The gasification procedure was described in section 8.3.1 and 8.3.2, while the values of ERs used in gasification can be found in Table 5-6 chapter 5.

8.2 Pyrolysis Results

8.2.1 Influence of superficial velocity on total mass conversion rate.

Figure 8-1shows the total mass conversion versus reaction time at different superficial gas velocities below the terminal velocity of silica sand. With flow rates increasing, the complete reaction time decreased, and was 63 seconds as flow rate reached up to 0.123m/sec, while it was 278 seconds at 0.061 m/sec at temperature of 450°C. The rate of reaction can be expressed in terms of the slope of the curve, as can be seen in the figure, the slope change in the curve beyond this point is unnoticeable even with increase in flow rate. Consequently, this flow rate represents the gas velocity that accelerates the reaction rate and largely reduces the limitation of external diffusion [236]. To avoid external diffusion limitations, most authors conduct preliminary thermogravimetric tests at increasing gas flow rate until no influence on the measured rate is found [279]. Therefore, the superficial velocity of 0.123 m/sec was selected as the basis for all experimental work, representing the gas velocity required to minimize external diffusion.

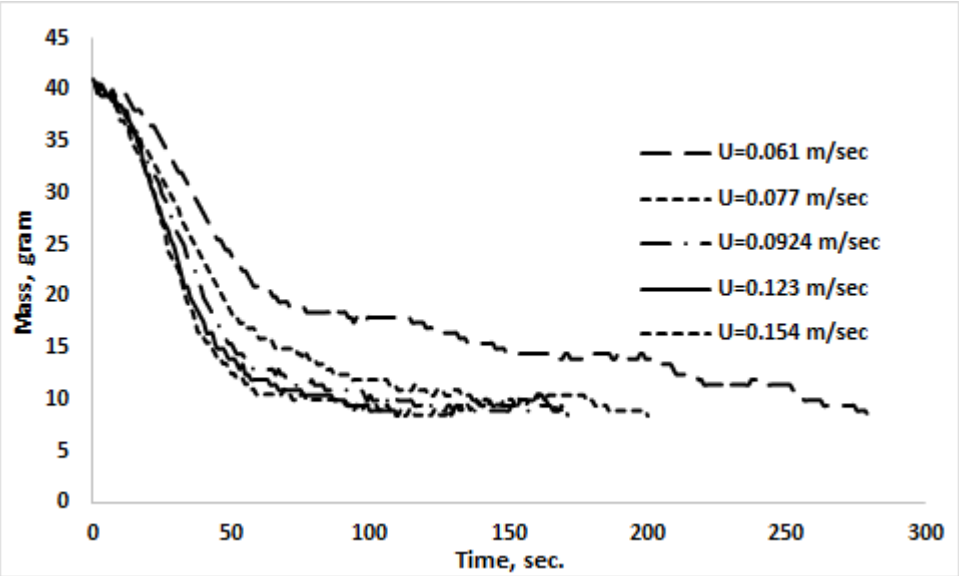

Figure 8-1 Total mass conversion versus reaction time in fluidised bed reactor at different flow rates.

8.2.2 Gas evolved varying with fluidised bed temperature.

It is basically known that pyrolysis is a step of primary importance in the gasification of biomass in a fluidised bed reactor. Therefore, pyrolysis results could be used to obtain useful information in the development of lab and pilot scale fluidised bed gasification process. A set of experiments on palm stones was performed at a temperature range of 350°C to 750°C at 50°C increments. Palm stone pyrolysis in a fluidised bed reactor yields the gas products CO, CO_2, CH_4 and H_2 for various reaction temperatures and $2U_{mf}$ velocity.

The effect of reaction temperature on product gas concentration is illustrated in Figure 8-2. Below 500°C, CH_4 and H_2 was not produced. However, above this temperature the volume percentage of methane and hydrogen started to increase and reached a peak amount at about 750°C. The formation of CH_4 is generated from the cracking of tar at high temperatures [185]. Nonetheless, the decomposition of CH_4 also increases with temperature especially when the bed temperature exceeds 700°C. The increase, at elevated temperatures, in the individual yields of the major gaseous species products is thought to be predominantly due to secondary cracking of the pyrolysis vapours [52, 280]. The production of CO increased steadily for each subsequent reaction

temperature with the highest value being 14.93% by volume at 750°C. The production of CO_2 also increased with temperature, but only up to 500°C, after which, there is a slight decrease at 550°C. At 550°C and onwards, the CO_2 concentration remains similar. Below 550°C the production of CO is less than CO_2, and at 550°C onwards, the production of CO exceeds that of CO_2.

This result indicates that CO is produced more rapidly with increasing temperature. Higher temperatures promote the cracking reaction leading to an increase in CO production. Comparing with literature, biomass was pyrolyzed in a micro fluidised bed and the results showed that the CO_2 started to be released at low temperatures. The initial low temperature formation of CO_2 exceeding CO, implying that the carboxyl reaction might occur more easily than other reaction. However, in the temperature range of 600-900°C the CO_2 varies little and remains at a low value, suggesting that the carboxyl or ester functional group can completely decompose at temperatures above 600°C [40, 170]. Similar observations have been made in the current study where all the gas components exhibited certain differences in the release sequence and time span of release at two different temperatures, 350°C and 600°C, see Figure 8-3. One can identify that at 350°C, more CO_2 than CO was released at the beginning of the time span. The situation changed at 600°C, where CO release exceeded that of CO_2. In other work, it has been reported that the thermal decomposition of hydrocarbons in the gaseous products is favoured at high pyrolysis temperatures, which leads to an increase in the yield of hydrogen and CO content and a reduction in the CO_2 content [281]. The results from the pyrolysis, in this section, suggest that at higher pyrolysis temperatures, CO was the major component of the pyrolysis gas mixture from palm stones. Therefore, in subsequent work, 600°C and above will be used in the gasification tests of palm stones to study the effect of temperature on gasification performance.

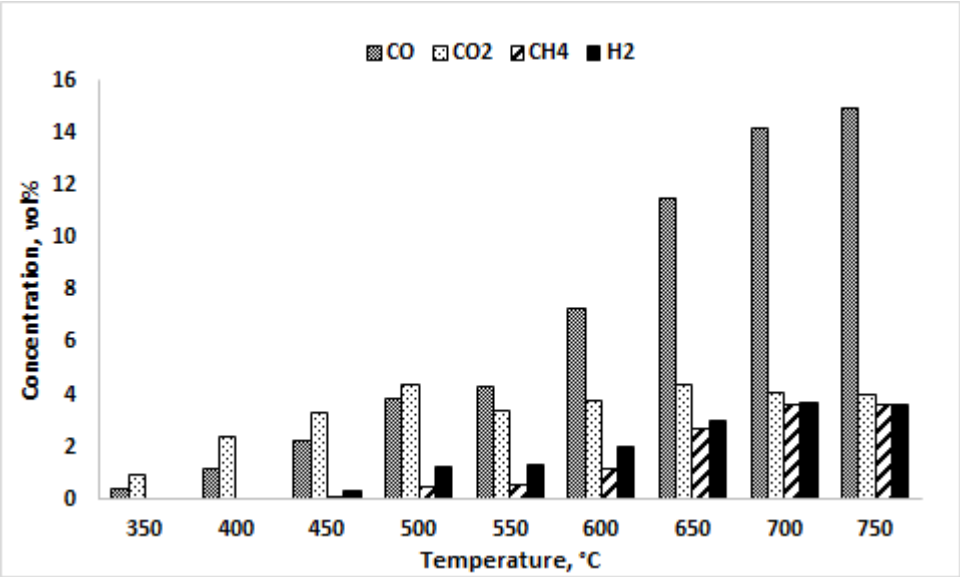

Figure 8-2 Effect of temperature on gas product from pyrolysis of palm stones.

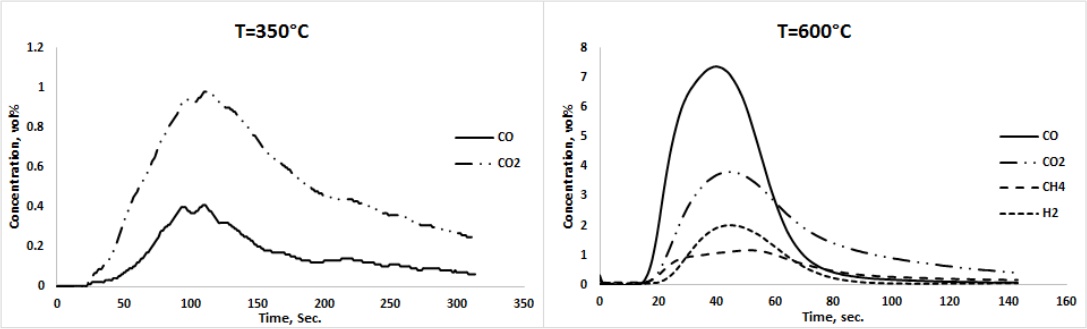

Figure 8-3 Evolved major gas species of palm stones and their release sequences during pyrolysis

8.2.3 Influence of bed temperature on total conversion rate.

Figure 8-4, shows the total conversion of palm stone vs. temperature. This constitutes the major conversion reaction mainly due to decomposition of the organic constitutes into volatiles and char. The progress of reactions in pyrolysis process is markedly affected by the temperature change that accompanies the reaction. Fluidised bed pyrolysis utilises the effective good solids mixing to transfer approximately 90% of the heat to the biomass by solid-solid heat transfer with a small contribution from gas solid convective heat transfer of up 10% [282]. Fast pyrolysis is a process in which

very high heat flux is imposed to biomass particles, leading to high heating rate. Research has shown that maximum liquids yields are obtained with high heating rates, at reaction temperatures around 500°C [283]. The experimental results showed high conversion levels, measured in terms mass loss at T=500°C and above. The pyrolysis reached an approximate value in conversion (about 90% at less than 45 sec), and a further increase in temperature did not significantly improve conversion, suggesting that the pyrolysis of palm stones occurred under fast pyrolysis conditions. In addition, the rapid decomposition rates of palm stones at high temperature as seen from the conversion figure was due to the high volatile content and low ash content in the biomass (see proximate analysis Table 4-2), which was in agreement with Munir et al. [189]. On the other hand, above 500°C, there was enrichment of combustible gases during pyrolysis obtained from the thermal decomposition of heavy hydrocarbons (tar) with increasing temperature (see Figure 8-2). Tar could be effectively decomposed into lighter gases by thermal cracking and reaction temperature was a key factor affecting the generation of major gas components [284]. This is in agreement with Yu et al. [171] who noticed that high temperature pyrolysis produces more non-condensable gases and less tar. Encinar et al. [285] observed that the increase of reactor temperature leads to a decrease in the liquid yield and an increase in the gas yield during pyrolysis of olive bagasse, which suggests that the increase observed in gas yield is partially due to strong cracking of liquid at high temperature. Therefore, the temperature between 350 to 600°C was selected to investigate the kinetic data of palm stones.

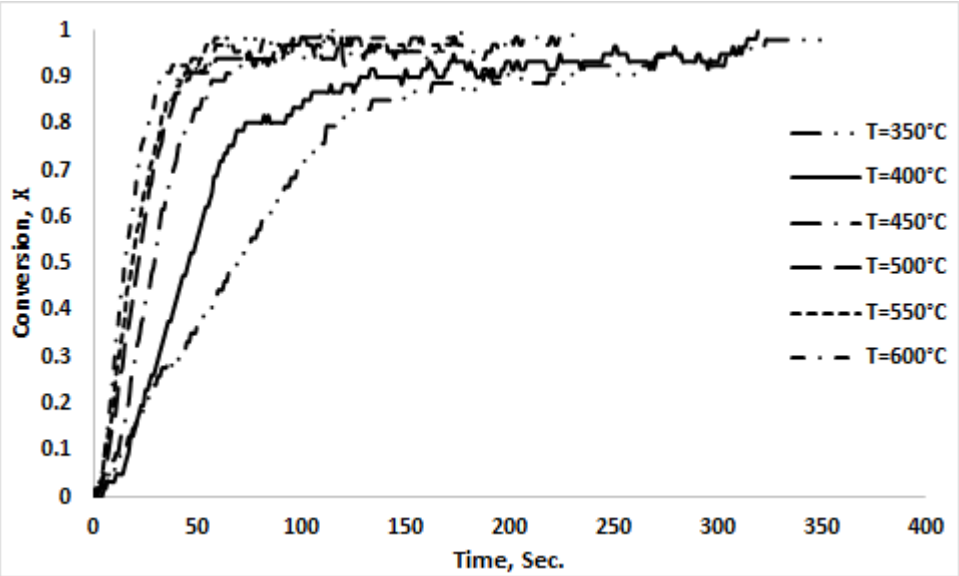

Figure 8-4 Conversion vs reaction time in fluidised bed reactor at different temperatures.

8.2.4 Kinetic Parameters

Based on the continuous measurements of the weight of the palm stones during pyrolysis, the conversion of biomass as a function of reaction time at six reaction temperatures ranging from 350°C to 600°C were obtained. Pyrolysis of palm stone in a fluidised bed reactor is a typical heterogeneous reaction under isothermal conditions, which can be analysed with a universal integral method to determine the most probable reaction mechanisms for palm stone pyrolysis in a fluidised bed reactor.

Based on Equation (3.11), the correlation of G(x) versus t at a given reaction temperature can be fitted to a straight line, and the slope equal to k(t). Several solid-state mechanism models (Table 3-1) were tested for a suitable fit. Five probable reaction models were adopted according to the quality of fitting correlation coefficient (R^2), which were shown in Figures 8-5 and 8-6.

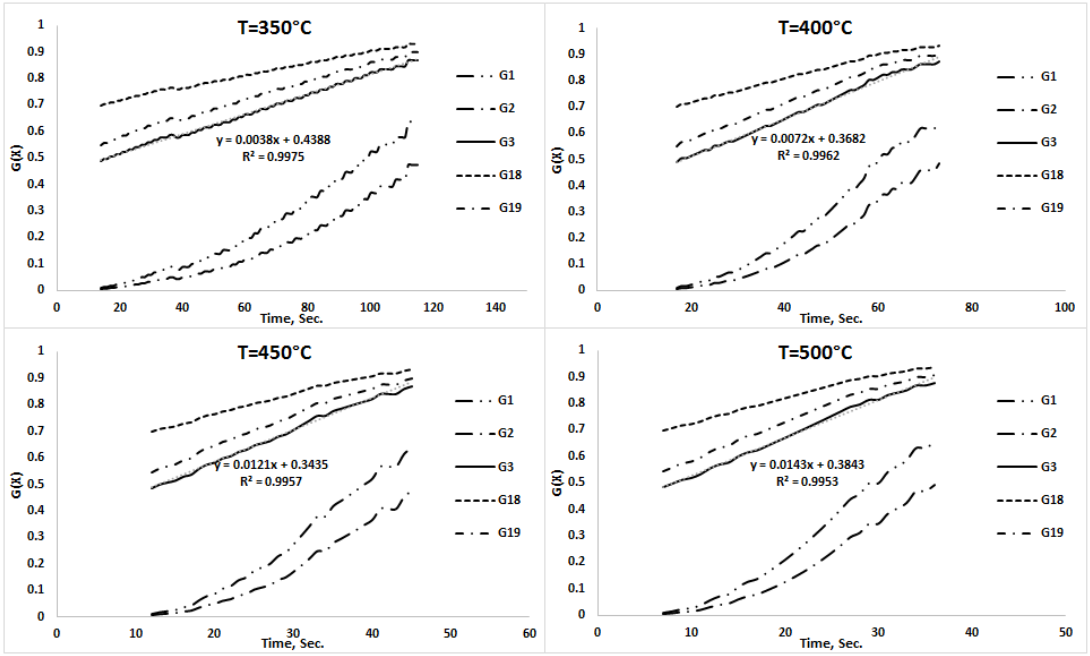

Figure 8-5 Correlation of G(X) versus time at temperatures 350, 400, 450, and 500°C for palm stones.

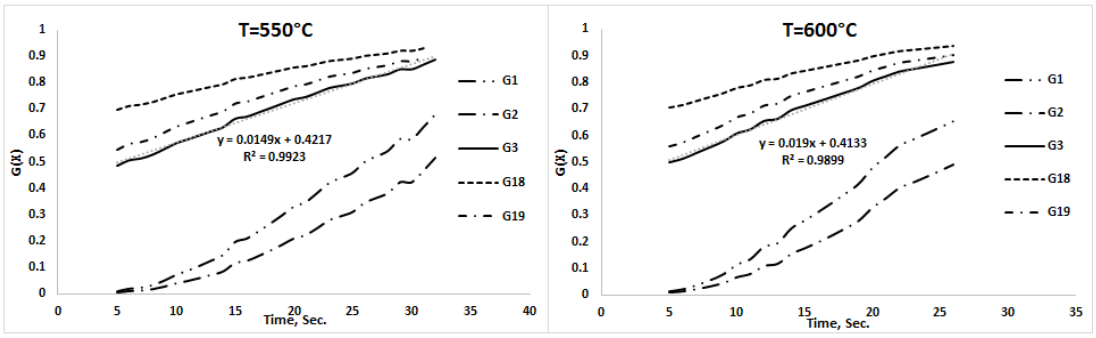

Figure 8-6 Correlation of G(X) versus time at temperatures 350, 400, 450, and 500°C.

Table 8-1, illustrates the kinetics parameters for major five models and fitting correlations coefficients (R^2). Three-dimensional diffusion was the most probable reaction mechanism that could have described the thermal decomposition of palm stones in the fluidised bed reactor. The behaviour of three-dimensional diffusion could be associated with greater degradation of hemicellulose and cellulose content that can be lead to a higher volatility of the main biomass components at this range of

temperature. The same mechanisms for biomass were observed by Poletto et al [286]. and Wang et al [287].

Table 8-1 Reaction model for palm stone decomposition during fluidised bed isothermal pyrolysis.

G(x)	G1	G2	G3	G18	G19
Temp (°C)	350	350	350	350	350
R^2 (%)	96.84	94.07	99.75	99.72	99.72
ln k(T)	-5.051	-5.381	-5.572	-6.074	-5.683
Temp (°C)	400	400	400	400	400
R^2 (%)	97.54	95.40	99.62	99.43	99.43
ln k(T)	-4.390	-4.699	-4.933	-5.426	-5.035
Temp (°C)	450	450	450	450	450
R^2 (%)	98.05	96.10	99.57	99.18	99.18
ln k(T)	-3.892	-4.213	-4.414	-4.919	-4.509
Temp (°C)	500	500	500	500	500
R^2 (%)	97.94	95.98	99.53	99.16	99.16
ln k(T)	-3.709	-4.011	-4.247	-4.744	-4.342
Temp (°C)	550	550	550	550	550
R^2 (%)	98.96	97.21	99.23	98.52	98.52
ln k(T)	-3.661	-3.963	-4.206	-4.688	-4.290
Temp (°C)	600	600	600	600	600
R^2 (%)	98.91	97.64	98.99	98.27	98.27
ln k(T)	-3.411	-3.684	-3.963	-4.474	-4.068

From straight line plots of the experimental data at various reaction temperatures, the values of k relating to the Arrhenius function with temperature (see Fig.8-7) are shown. From the lnk versus 1/T plots, the slope of ($-E_a/R$) was used to obtain the value of activation energy for the experiment between 350 – 600°C for the palm stones pyrolysis, giving an activation energy of 27.67 kJ/mole. In comparison with in TGA, the activation energy of palm stones pyrolysis was determined for non-isothermal conditions by using TGA, the value of E_a found equal to 30.7 kJ/mole [25]. The higher E_a for the TGA should be related to its lower heating rate (than for the fluidised bed) and the TGA itself which is inhibited by gas diffusion when compared to fluidised bed reactor, which was in agreement with Yu et al [232]. The results of the kinetic studies of palm stone pyrolysis coupled with description of transport phenomena could supply useful information for the design and optimization of thermo-chemical process.

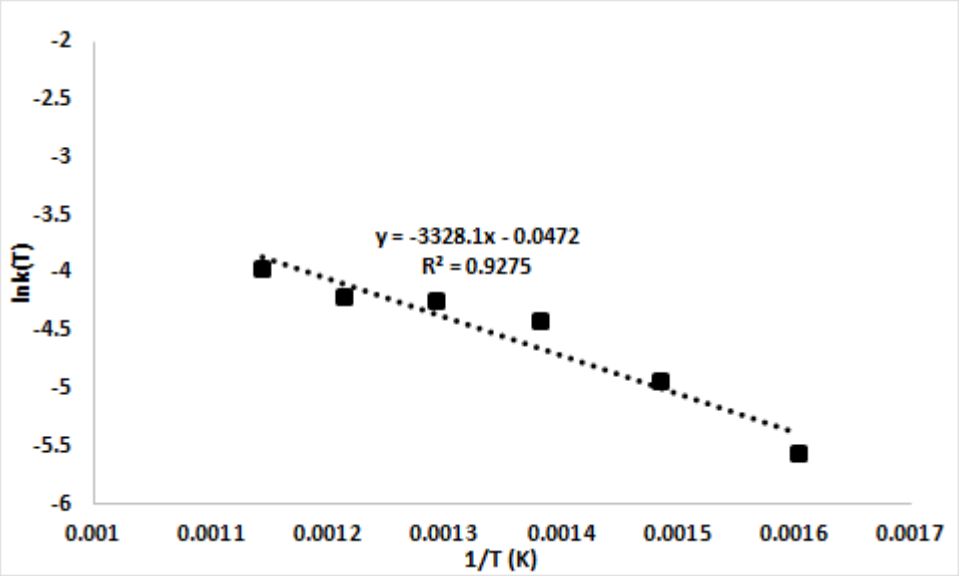

Figure 8-7 Kinetic plots for palm stone pyrolysis.

8.3 Gasification results

Two parameters (bed temperature and ER) are used to investigate the gasification performance of palm stones in a bubble fluidised bed.

8.3.1 Effect of Different bed temperatures.

Temperature is a crucial factor for the overall biomass gasification process. In the present study, bed temperature was changed from 600 to 750°C in 50°C increments at ER=0.2. The experimental results are presented in Figure 8-8 and Table 8-2.

The results show that CO, H_2 and CH_4 exhibit an increasing trend with rise in temperature, ranging from 11.97 to 17.54 vol% for CO, 3.11 to 5.5 vol% for H_2 and 3.22 to 5.01 vol% for CH_4. Le Chatelier's principle states that, higher temperatures favour the reactants in exothermic reactions and favour the products in the endothermic reaction. Therefore, the endothermic reactions were strengthened with the increase in temperature. The formation of H_2 gas was favored by increasing the gasifier bed temperature, which is assumed to be due to an increase in the cracking of tar in the initial stage R2 [288] as well as promotion of the water-gas reaction R3. The water-gas reaction can happen in any gasifier, not only due to the existence of water in the biomass but also due to water vapor in the air supplied to the gasifier. According to Cao et al. [244], water vapor and CO_2 promote H_2 production in the gasification of biomass. The content of CO increases with temperature, which can be attributed to R1 (see Fig. 8-2), R4, and R10. It can be clearly seen that CO_2 content showed a decreasing rate as the temperature increased, while CO content exhibited the opposite trend. The heat required to sustain the reaction occurs mainly through the oxidation reaction; the CO_2 released was probably consumed through tar cracking and Boudouard reactions, therefore the CO_2 concentration is reduced at the higher temperature tested [289]. The CO_2 was found to decrease from 15.03% at T=600°C to 13.18% at T=750°C. Methane evolution can occur at elevated temperature due to the cracking of tar to CH_4, H_2, and CO [242]. This is corroborated by Esfahani who stated that an increase of gas concentration with temperature could be due to different reasons, such as (i) at higher temperatures, the gas production is faster during the initial pyrolysis stage, (ii) At higher temperatures, the endothermic char gasification reactions are favourable, which leads to further production of gases, and (iii) As a result of cracking of heavier hydrocarbons and tars, the gas yield increases with temperature [86].

Variation of the parameters of cold gas efficiency, carbon conversion efficiency, gas yield, and HHV are illustrated in Table 8-2. The carbon conversion and cold gas

efficiency of this process reached its maximum of 56.3% and 34.47%, respectively, at 750°C. The carbon conversion efficiency of the system increased rapidly with increase in temperature due to the increase of the oxidation reaction and that led to an increase in the production of combustible gases, hence increased cold gas efficiency.

As anticipated, an increase in bed temperature led to higher gas yields, which could be due to further thermal decomposition of liquids and boosted char reaction with the gasification agent. The overall gas yield was found to increase from 1.25 m^3/kg at T=600°C to 1.43 m^3/kg at T=750°C. The higher temperatures contributed to lower concentration of char and heavy tars and led to higher gas yield due to release of more volatiles [290]. Finally, the HHV was found at T=750°C and equal to 4.91 MJ/m^3, which is due to presence of combustible gases of CO, H_2, and CH_4.

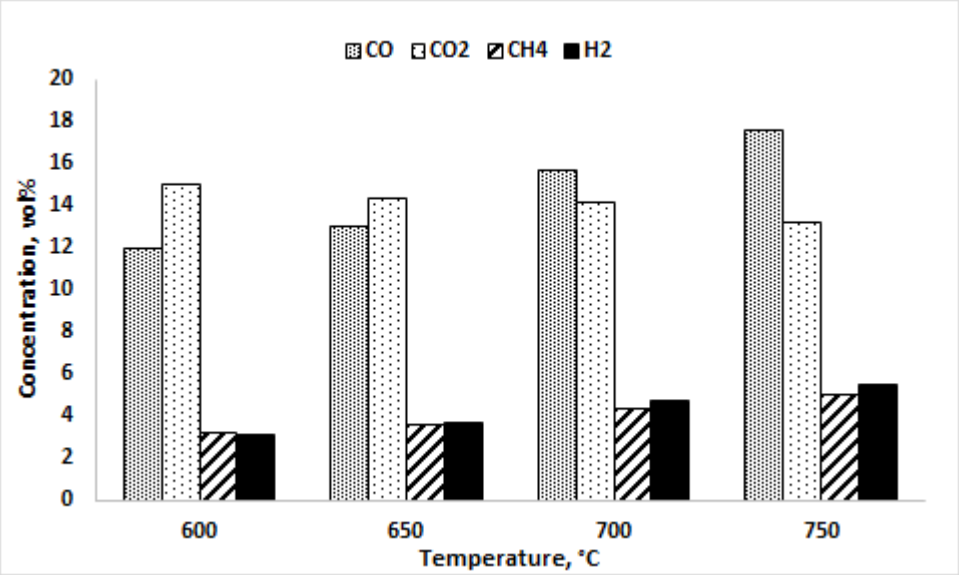

Figure 8-8 Effect of temperature on gas composition of palm stones at ER=0.2.

Table 8-2 Summary of results for application of different gasification temperatures of palm stones.

Temperature °C	600	650	700	750
Gas yield (m^3/kg)	1.25	1.28	1.37	1.43
Carbon conversion efficiency (%)	41.83	43.67	51.7	56.3
Cold gas efficiency (%)	19.67	22.19	29.1	34.47
HHV (MJ/Nm^3)	3.19	3.53	4.31	4.91

8.3.2 Effect of Equivalence ratio (ER).

To study the effect of ER on gasification performance, ER was varied from 0.15 to 0.35 through changing the mass flow rate and holding the air flow rate at a constant value, to have a small effect on gas residence time while the bed temperature was 750°C. According to the ERs, the biomass feed rate was changed between 3.11 kg/hr to 1.33 kg/hr as shown in Table 8-3. The tests results of the effect of ER on product gas composition are shown in Figure 8-9. As can be seen in this Fig., the CO, CO_2, H_2, and CH_4 formation slightly increases with increase in ER from 0.15 to 0.2 and then further increase of ER to 0.35 where the formation of CO_2 is continuously improved while the productions of CO, CH_4, and H_2 decreased. When the ER increased, the air flow rate supplied compared with biomass was increased and that led to a higher degree of combustion, which improves the char oxidation reaction to produce CO_2 at the expense of combustible gases represented by CO, CH_4, and H_2. More precisely, at low ER, reaction R5 was more likely to occur than the reaction $C+O_2 \rightarrow CO_2$ because of the lack of oxygen and that led to improve CO gas formation in addition to CH_4 and H_2, which are produced from the thermal decomposition of carbonaceous material at low ER. However, beyond ER=0.2 reaction R11 and R12 dominated, where the CO, CH_4 and H_2 contents dropped from 17.54%, 5.01, and 5.5 at ER=0.2 to 9.03%, 2.4%, and 2.75% respectively at ER=0.35, while CO_2 increased from 13.18% to 15.45% at ER=0.35. This agreed with Skoulou [21] , who stated, changing the ER in a gasification process may lead to one of the two extreme operating conditions: one corresponding to complete gasification towards CO and another to complete combustion towards CO_2.

Table 8-3, shows the influence of HHV, gas yield, cold gas efficiency, and energy as a function of ER. The calculation of energy yield (MJ/kg $_{biomass}$) of these five tests are based on gas yield (Nm^3/kg $_{biomass}$) and HHV (MJ/m^3). As shown in this table, the gas yield increased with increase in ER from 1.07 Nm^3/kg at ER=0.15 to 2.09 Nm^3/kg at ER=0.35. The increase in the gas yield can be linked to increase in the concentration of N_2 in gas yield, which made the quantity of gas produced highest at ER=0.35 but its HHV was the lowest value and equal to 2.44 MJ/m^3 because of the strengthened

oxidation reactions of combustible product gases [116]. The carbon conversion efficiency increased with ER and the maximum value was found at ER=0.3.

The result suggested that the ER had a positive effect at ER=0.15 and 0.2, so the HHV and cold gas efficiency increased from 4.78 to 4.9 MJ/m^3 and from 25.09% to 34.47% respectively, which corresponds to the increased content of combustible gases.

The results of palm stones gasification were compared to the findings of other research on biomass gasification. The cold gas efficiency and HHV were found equal to 40% and 4.53 MJ/m^3 during gasification of palm empty fruit bunches using an air blown fluidised bed at T=770°C [242]. Kim et al. [291] gasified the wood pellet in an air blown fluidised bed reactor; the biomass was fed at the top of the gasifier. The result showed the concentration of syngas tended to increase as ER went from 0.27 to 0.19 and the maximum calorific value of product gas was found equal to 4.7 MJ/Nm^3.

Through the analysis on the experimental data of different values of ER, it can be understood that is unfeasible to apply too small or too large ER in biomass gasification. Lower reaction temperature (tar increase) is the result of too small an ER, which is not favourable for palm stone gasification. More combustible gases will be consumed through oxidation reactions when too large ER is used. So, in the present study, the optimal value of ER was found as 0.2 under the conditions listed in Table 8-3, where the energy yield of product gas found equal to 7 (MJ/kg $_{biomass}$).

Table 8-3 Summary of results for the application of different ER in palm stone gasification.

ER	**0.15**	**0.2**	**0.25**	**0.3**	**0.35**
Biomass flow rate dry basis (kg/hr)	3.11	2.33	1.86	1.55	1.33
Air flow rate (Ndm^3/min)	40	40	40	40	40
Temperature, °C	750	750	750	750	750
HHV (MJ/m^3)	4.78	4.9	3.77	3.15	2.44
Gas yield (Nm^3/kg)	1.07	1.43	1.64	1.88	2.09
Cold gas efficiency (η)	25.09	34.47	30.52	29.12	25.14
Carbon conversion μ_c	41.44	56.3	57.46	62.15	62.0
Energy yield (MJ/kg)	5.11	7.0	6.18	5.92	5.09

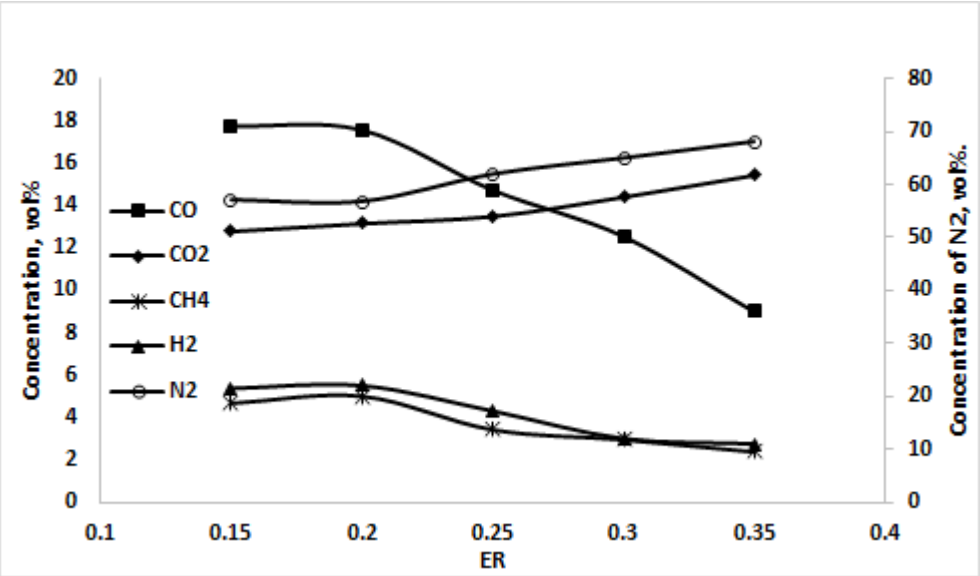

Figure 8-9 Influence of ER on gas composition for palm stone gasification at 750°C.

8.4 Material balance

Material balance, as well as carbon species mass balance in the gasification process, were implemented to monitor the conversion of palm stones into product gas and residues as illustrated in Figure 8-10. A material balance will allow the inputs to be compared with the outputs. This is useful because it gives an indication of how well the gasifier is performing, and it may enable problems to be noticed, such as material loss.

When the palm stones and air were fed into the gasifier and the reaction was carried out, the products obtained could be classified into volatiles and char. The volatiles evolved from the gasifier can be classified into two groups, namely, tar and product gases. The product gases can be further divided into carbonaceous (CO, CO_2, CH_4) and non-carbonaceous (H_2, O_2, N_2) gases. The compositions of these gases were measured in volume percent, while the N_2 was determined by difference. On the other side, char represented the unburnt carbon at the end of the process.

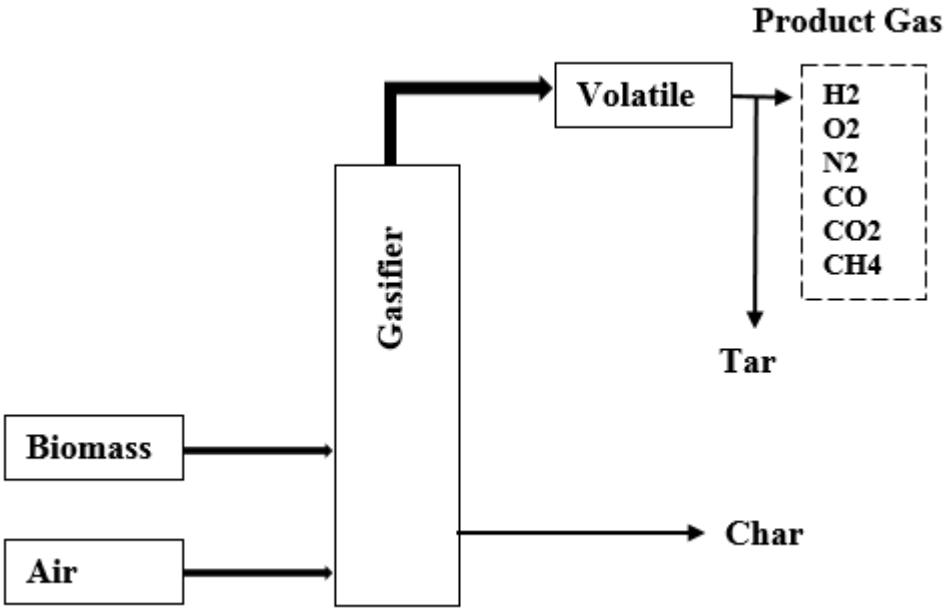

Figure 8-10 Material flow distribution of inputs and outputs in the gasification process.

Collecting tar from the downstream equipment would have been difficult to achieve, owing to build up of tar in all of the pipework, in addition the tar that was filtered and accumulated in the isopropanol flasks. As such, this study only considered the product gas and the char, to determine the overall and carbon mass balances of the gasification process.

Based on Equation (8-1), the overall material balance in the gasification process was determined. The palm stones fed into the gasifier were weighed using a laboratory scale, and the subsequent char produced was found from the load cell attached to the gasifier. Therefore, the value for the mass of char represents the real mass of char inside the reactor. According to the equations (8.2) and (8.6) the mass rate of air and product gas were determined. The mass flow rate unit of all the input and output streams were taken in g/min and 1 min was taken as basis of the calculations. Each gasification test lasted for 5 min.

$$[\dot{m}_{air} + \dot{m}_{fuel}]_{input} = [\dot{m}_{gas} + \dot{m}_{char}]_{Output} \quad (8.1)$$

$$\dot{m}_{air} = Q_{air} \times \rho_{air} \quad (8.2)$$

Where $\boldsymbol{Q_{air}}$ and $\boldsymbol{\rho_{air}}$ are the air flow rate (l/min) and density of air at ambient temperature (1.2 kg/m^3) respectively.

The mass rate of product gas can be determined as follows:

The product gas yield was determined using Equation (5.6) in chapter 5, While the gas yield of individual gas produced was determined using Equation (8.3).

$$y_i = Y \times x_i \tag{8.3}$$

Where $\boldsymbol{Y}$, $\boldsymbol{y_i}$, $\boldsymbol{x_i}$ are the total yield of product gas in (Nm^3/kg biomass feed), the gas yield of each gas produced in (Nm^3/kg biomass feed) and individual gas mole fraction. Using Equation (8.4), the unit of (the mass of individual gas /mass of biomass feed) can be obtained through converting the individual gas yield to $\boldsymbol{Z_i}$, hence, for ideal gas each 1 kmol of the gas occupied 22.4 Nm^3.

$$\mathrm{Z_i} = \mathrm{y_i} \times \mathrm{Mwt_i}/22.4 \tag{8.4}$$

Therefore,

$$\dot{m}_i = Z_i * \dot{m}_{fuel} \tag{8.5}$$

The mass rate of product gas is obtained from the following equation;

$$\dot{m}_{gas} = \Sigma \dot{m}_i \tag{8.6}$$

Where $\boldsymbol{Mwt_i}$ and $\boldsymbol{\dot{m}_{gas}}$ are the molecular weight of each individual gas in the product and the mass flow rate of each gas in g/min.

In order to monitor the conversion of biomass in terms of carbon to product, the carbon mass balance was calculated. The output represented by product gases and char were considered only as the main source of carbon. In the input stream, the air was not considered because it has negligible carbon content, hence only the biomass fuel was considered as the main source of carbon. Using Equation (8.7), the mass balance was determined.

$$\dot{\mathrm{c}}_{\mathrm{fuel}} = \dot{\mathrm{c}}_{\mathrm{gas}} + \dot{\mathrm{c}}_{\mathrm{char}} \tag{8.7}$$

Where $\dot{c}_{fuel}$, $\dot{c}_{gas}$, and $\dot{c}_{char}$ are the carbon mass rate in inlet biomass stream, product gas and char, respectively. The unit of carbon mass rate is g/min. By using Equations ((8.8), (8.10), and (8.11)), the carbon mass rates of inlet and outlet streams were determined.

$$\dot{c}_{fuel} = cc_{fuel} \times \dot{m}_{fuel} \tag{8.8}$$

Using the ultimate analysis table, the value of CC_{fuel} obtained, which represented the carbon content in biomass.

$$\dot{c}_i = c_i \times \dot{m}_{fuel} = (y_i \times \frac{12}{22.4}) \times \dot{m}_{fuel} \tag{8.9}$$

Where c_i and $\dot{c}_i$ are carbon mass and carbon mass rate of the carbonaceous gas (i), respectively. The carbon mass rate of product gas could be obtained from the following equation;

$$\dot{c}_{gas} = \Sigma \dot{c}_i \tag{8.10}$$

Char balance is as follows;

$$\dot{c}_{char} = cc_{char} \times m_{char}/t \tag{8.11}$$

Where cc_{char} and m_{char} are the weight percent of carbon in the char and mass of char remaining, respectively. Due to low ash content, the char is considered as carbon. This simplification was made because it would have been difficult to separate the char from the sand. However, ideally, this separation would have been done and subsequently taken for LECO carbon analysis.

The comparison of material balance as well as carbon mass balance between input and output streams were achieved using the following equation;

$$\%\ \text{error} = \frac{\text{input} - \text{output}}{\text{input}} \times 100 \tag{8.12}$$

The effect of operating conditions of temperature and equivalence ratio on gasification of palm stones were discussed in chapter 8 section 8.3. The overall and carbon mass

balances for each experiment were measured and calculated. The results from each experiment are shown in Tables 8-4 and 8-5.

Table 8-4 shows percentage error outlined against temperature for overall mass balance and carbon mass balance at different gasification temperatures test at ER=0.2. It can be seen that as the temperature is increased, the percentage error decreases. Tar is produced during the gasification process, but at the higher temperatures of 700°C and 750°C, it can be seen that there is around half the percentage error. The percentage error is positive when the output mass is lower than the input mass, and negative when the outputs exceed the inputs, see Equation (8.12). It would be possible to obtain negative error if the biomass feeder supplied more biomass than was actually stipulated in the calculations, because this would lead to more product gas. It is assumed in this piece of work that the feeder is reliable, and not providing more than it should. When determining the overall mass balance and carbon mass balance, the tar was neglected, hence less output mass, and therefore a positive error. At the higher temperatures, the thermal decomposition of heavy hydrocarbons, such as tar, into product gases increased. This led to a higher volume percent of gases being measured, which in turn lowered the percentage error. As illustrated in Figure 8-11, the carbon yield increased from 41% at temperature 600 °C to 56 % at a temperature of 750 °C. In addition, the gas analyser was not capable of measuring anything heavier than CH_4, which is why heavy hydrocarbons were not accounted for.

Table 8-4 Overall mass and carbon balance % error with temperature. ER=0.2.

Temperature, °C	Total mass balance, g/min			Carbon mass balance, g/min		
	In	out	% error	In	out	% error
600	86.9	70.9	18.4	18.93	15.25	19.44
650	86.9	71.43	17.79	18.93	15.24	19.49
700	86.9	75.05	13.63	18.93	16.73	11.62
750	86.9	76.41	12.07	18.93	17.13	9.47

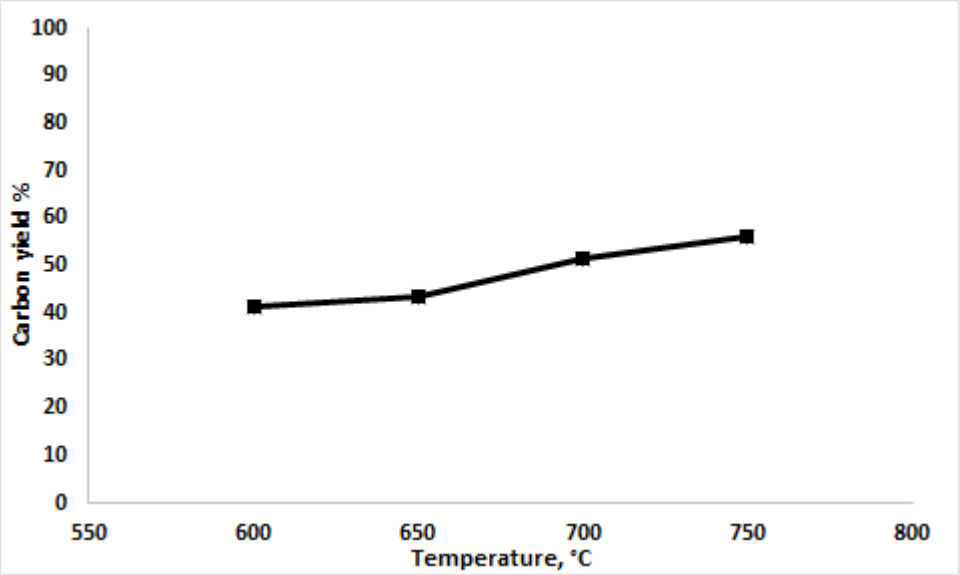

Figure 8-11 Carbon yield in product gas with different temperature of palm stone under gasification conditions.

Table 8-5 outlines percentage error of overall mass and carbon mass balance against equivalence ratio, based on experimental data. The feed rate of biomass at the first data point is at its greatest, and this was done to lower the equivalence ratio, making the oxygen to be in short supply. It can be seen that the percentage error is at its greatest when at the lowest equivalence ratio so there is more tar being produced. This data point (ER=0.15) is near to pyrolysis conditions. In these conditions, high yield of liquid products is obtained; these liquids include water, and light and heavy hydrocarbons. Since these hydrocarbons contain carbon, neglecting these compounds is the main reason behind the deviation of the mass carbon balance. However, the error beyond ER=0.15 is seen to reduce because of an increase in the amounts of converted volatiles to gas. The error was found to range from 7.6-12.07 % for overall mass balance and from 5.05- 9.86 % for carbon mass balance. Hence, when the experiment exceeds ER=0.15, it can be seen that the percentage error is consistent at around 10% for all of the other equivalence ratios.

Table 8-5 Overall material balance and carbon mass balance % error with ER.

Equivalence ratio (ER), T=750°C	Total mass balance, g/min			Carbon mass balance, g/min		
	In	out	% error	In	out	% error
0.15	99.86	78.91	20.97	25.24	19.56	22.52
0.2	86.9	76.41	12.07	18.93	17.13	9.47
0.25	79	70.38	10.9	15.14	13.65	9.86
0.3	73.9	67.55	8.59	12.62	11.71	7.23
0.35	70.22	64.86	7.6	10.81	10.27	5.05

The overall mass and carbon balance of all gasification tests and their detailed stream are shown in the Appendix D.1&D.2.

Summary

In this chapter, the influence of gas velocity on reaction time is shown. It was noticed that the mass loss variation became negligible beyond $2U_{mf}$. The effect of pyrolysis temperature on gas evolved and total conversion rate are presented. At higher pyrolysis temperatures, CO was the major component of the gas mixture.

Based on the model fitting method, the kinetic parameters of palm stone pyrolysis in TGFBR under isothermal conditions are presented. Three-dimensional diffusion was the mechanism controlling the reaction.

The results of the possibility of gasification of date palm stones in the bubbling fluidised bed gasifier are shown in this chapter. The effect of operation conditions represented by temperature and ER has been presented and discussed in detail. Temperature has shown a positive effect on product gas, whereas ER exhibited two contrary extremes.

Conclusions and future work

9.1 Conclusions

I. Related to the pyrolysis of olive kernels:

It was shown that above 500°C, the time taken to fully react a 40 g sample in a bed of sand is less than 10 s. Furthermore, the fast pyrolysis exhibited in the TGFBR provided a uniform temperature inside the reactor and supressed the external diffusion effects, which is confirmed by little variation in the reaction time above 40 l/ min flow rate of the fluidising gas.

In the TGA apparatus particle size had no measurable effect on the reaction rate, whereas a clear dependence of reaction rate on biomass particle size was demonstrated in the TGFBR. In both apparatus, at low heating rates (< 451°C) the reaction time was unaffected by the biomass particle size over the ranges tested. However, for the TGFBR there was a dependence of reaction rate on particle size above 500°C when it was observed that the reaction time increased with larger particle sizes.

The pyrolysis reaction kinetics were studied under non-isothermal conditions in the TGA and isothermal conditions in the TGFBR. A two-dimensional diffusion model was the controlling mechanism identified with the best fit for the fixed bed TGA with an activation energy of 74.46kJ/mole. In comparison, 2-dimensional and 3-dimensional reaction mechanisms gave the best fits to describe the reaction kinetics of the biomass particles over 2 temperature ranges in the TGFBR which could be divided into two stages: the two-dimensional diffusion reaction mechanism from 320 to 451°C with an activation energy of 67.36 kJ/mole; and the three-dimensional diffusion reaction mechanism from 500 to 660°C with an activation energy of 60.8 kJ/mole.

Bench top TGA analysis of pyrolysis is a rapid and valuable method for comparing the behaviour of biomass reactivity, but the small sample sizes tested and low heating rates places limits on the relevance of results. In comparison, the larger scale TGFBR

fitted with load cells allows detailed measurements at conditions likely to be more representative of those encountered on large scale systems where heat distribution, heat transfer and mass diffusion effects play a major role in the reactivity of biomass.

II. Related to the gasification of AROK and ARTOK

Raw and torrefied olive kernels were gasified in a thermogravimetric bubbling fluidised bed gasifier to investigate the influence of temperature and ER on the gasification performance. Such experimental results gave considerable information about performance and scale-up in order to explore the potential of ARTOK compared to that of AROK. The usage of torrefaction can be expanded if the product gas quality as well as cold gas efficiency are improved through gasification of pre-treatment of biomass. On the basis of the data obtained for the gasification in the studied range of operating process parameters the following conclusions are made:

- The raw and torrefied biomass showed different characteristics, thus making them exhibited different in gas composition and heating value. Torrefied biomass showed consistently higher product gas heating value and cold gas efficiency, which was attributed to higher production rates of CO, H_2 and light hydrocarbons.
- The reaction characteristics of raw and torrefied biomass in oxidative atmospheres at various temperatures have been investigated and qualitative agreement between model prediction and experimental data was achieved. From the kinetic analysis carried out, the results suggest that the reaction is controlled by mass transfer in the parent sample, while char oxidation was the controlling factor in the torrefied sample.
- From gasification experiments performed across a range of preset temperatures (550-750°C) it can be stated that kinetics of gasification of torrefied biomass are comparable to that of the parent biomass. However, the activation energy from torrefied biomass is higher than the parent biomass.

- The bubbling fluidised bed reactor was used to obtain activation energies of the olive kernel samples giving values of 84 kJ/mole in the parent and 106 kJ/mole in the torrefied material.
- By comparing experimental results, thermal pre-treatment of biomass before gasification is a promising concept for the operation of full-scale processes.
- Regarding parent biomass, this study investigated also the effect of particle size on product gas and performance. The results show that the production rates of CO and CH_4, and HHV and gas cold efficiency increases with reduction in the particle size.
- The effect of bed height on gasification performance and product gas of parent biomass was investigated. Increasing the bed height improved the product gas and gasification performance. However, the gasification performance decreased beyond 1D; it may be that 1D is an optimal bed height for a particular ER, at which the maximum gas yield and carbon conversion efficiency were obtained.
- The kinetics of biomass gasification has been and still is a subject of intensive investigation. Despite this, the results of such investigations, to date, have flowed into the design procedures for commercial gasification reactors to only a limited extent. The suppressed external diffusion limitations and higher heating rate prevailing in the TGFBR were responsible for all these kinetic parameters. They demonstrate the capability and superiority of the TGFBR for analysing biomass gasification, and it is believed that this data e.g. activation energy (Ea) and rate constant (k), supports a deep insight into the gasification mechanism, and gasifier design, which could help with future commercial reactors.

III. Related to the pyrolysis and gasification of palm stone

Palm stones are an interesting biomass because they are an agricultural residue and in abundance. The fast pyrolysis process has been undertaken by using a bubbling fluidised bed reactor. Depending on different superficial velocity used during

pyrolysis, the superficial velocity of $2U_{mf}$ was found as a minimum velocity that can minimize the external diffusion.

The pyrolysis bed temperature had a significant influence on product gas and total conversion of biomass. It was found that CH_4 and H_2 were not produced below 500°C. After this temperature, the formation of these gases increased with temperature due to an increase the thermal decomposition of heavy hydrocarbons. The CO_2 formation increased with temperature, however, at 550°C and onwards, became insensitive to the temperature. The CO concentration increased with the temperature and reached a maximum value at T=750°C. The experimental results showed high conversion levels, measured in terms mass loss at T=500°C and above.

Based on the model-fitting method, the kinetic parameters of thermal decomposition of palm stone under pyrolysis conditions was evaluated. The activation energy was found equal to 27.67 kJ/mole and the mechanism of the reaction was three-dimensional diffusion.

Regarding the gasification of palm stones in the bubbling fluidised bed gasifier temperature and equivalence ratio had a significant effect on gas distribution. The increase of temperature showed a positive effect on the production of combustible gases while negative effect on CO_2 formation. Also, the carbon conversion and cold gas efficiency improved with temperature. The parameter of ER was investigated and it was preferable to work at low ER. The optimum conditions were found at T=750°C and ER=0.2 for palm stones at the range of the temperatures used in this study with maximum HHV of 4.9 (MJ/m^3), which is suitable for internal combustion engines.

Finally, the overall and carbon mass balance in the gasification of biomass in fluidised bed has been investigated to monitor the balancing of inlet and outlet streams. Due to the elimination of tar from calculations, it seems the increasing temperature had a significant effect to reduce the error between inlet and outlet streams.

9.2 Future work

- In addition to the overall rate constant of thermal degradation of biomass as a one stage reaction model, the rate constant of individual species such as tar would need to be evaluated. Knowing the overall rate constant and tar rate constant, the rate constant of gas can then be determined. These values are of importance to simulation studies. Optical measurements could be used to track tar formation during pyrolysis.
- The influence of adding catalysts on the activation energy of pyrolysis, and gasification performance, need to be investigated for biomasses. The catalysts could be added as a percentage with sand or used alone, depending on the physical properties and the availability of the catalyst. It may be possible to replace the sand with a catalyst if it is cost effective enough to be used as a direct replacement.
- To increase the biomass gasification performance, further research work is needed to investigate the influence of increasing the residence time of volatile material on product gas composition. This can be achieved by using baffles inside the freeboard or by providing a wider freeboard section.
- To enhance the production of combustible gases, further experimental work under high bed temperatures could be carried out. This would require using different bed materials and anti-agglomeration materials such as limestone or dolomite.
- Under the same conditions as used in this study, different gasification agents such as CO_2 and steam could be used to investigate their influence on gasification performance. This is could be achieved by using this agent as a percentage of main air stream.
- Based on the activation energies values and rate constant of AROK and ARTOK obtained from this study, the ASPEN PLUS simulator can be used to compare the experimental result with predictable.

References:

[1] M. Van der Hoeven, "CO2 emissions from fuel combustion–highlights," *IEA Statistics*, 2014.

[2] A. Schmittner, A. Oschlies, H. D. Matthews, and E. D. Galbraith, "Future changes in climate, ocean circulation, ecosystems, and biogeochemical cycling simulated for a business-as-usual CO2 emission scenario until year 4000 AD," *Global Biogeochemical Cycles*, vol. 22, 2008.

[3] R. W. Bentley, "Global oil & gas depletion: an overview," *Energy policy*, vol. 30, pp. 189-205, 2002.

[4] S. Shafiee and E. Topal, "When will fossil fuel reserves be diminished?," *Energy Policy*, vol. 37, pp. 181-189, 1// 2009.

[5] J. Thomas B, etal., "Renewable energy: Sources for fuels and electricity," *Island press*, p. 3, 1993.

[6] S. Kane and J. F. Shogren, "Linking adaptation and mitigation in climate change policy," *Climatic Change*, vol. 45, pp. 75-102, 2000.

[7] R. E. Sims, H.-H. Rogner, and K. Gregory, "Carbon emission and mitigation cost comparisons between fossil fuel, nuclear and renewable energy resources for electricity generation," *Energy policy*, vol. 31, pp. 1315-1326, 2003.

[8] W. E. Council, "World Energy Trilemma Index | 2016.," London, UK2016.

[9] M. B. Nikoo and N. Mahinpey, "Simulation of biomass gasification in fluidized bed reactor using ASPEN PLUS," *Biomass and Bioenergy*, vol. 32, pp. 1245-1254, 12// 2008.

[10] G. Zanchi, N. Pena, and N. Bird, "Is woody bioenergy carbon neutral? A comparative assessment of emissions from consumption of woody bioenergy and fossil fuel," *GCB Bioenergy*, vol. 4, pp. 761-772, 2012.

[11] A. Demirbas, "Combustion of biomass," *Energy sources, Part A: Recovery, utilization, and environmental effects*, vol. 29, pp. 549-561, 2007.

[12] A. Demirbaş, "Biomass resource facilities and biomass conversion processing for fuels and chemicals," *Energy Conversion and Management*, vol. 42, pp. 1357-1378, 7// 2001.

[13] A. Robinson, J. Rhodes, and D. Keith, "Assessment of potential carbon dioxide reductions due to biomass-coal cofiring in the United States," *Environmental science & technology*, vol. 37, pp. 5081-5089, 2003.

[14] "The Michigan Biomass Energy Program, www.michigan bioenergy. org."

[15] "Energy resources for north Carolina teachers," *Avilable: https://alternativeenergyatunc.wordpress.com/*, March 2013.

[16] M. V. Gil, D. Casal, C. Pevida, J. J. Pis, and F. Rubiera, "Thermal behaviour and kinetics of coal/biomass blends during co-combustion," *Bioresource Technology*, vol. 101, pp. 5601-5608, 7// 2010.

[17] A. Demirbas, "Progress and recent trends in biofuels," *Progress in Energy and Combustion Science*, vol. 33, pp. 1-18, 2// 2007.

[18] A. Abuadala and I. Dincer, "A review on biomass-based hydrogen production and potential applications," *International Journal of Energy Research*, vol. 36, pp. 415-455, 2012.

[19] A. A. Zabaniotou, G. Kalogiannis, E. Kappas, and A. J. Karabelas, "Olive residues (cuttings and kernels) rapid pyrolysis product yields and kinetics," *Biomass and Bioenergy*, vol. 18, pp. 411-420, 5// 2000.

[20] V. Skoulou, G. Koufodimos, Z. Samaras, and A. Zabaniotou, "Low temperature gasification of olive kernels in a 5-kW fluidized bed reactor for H2-rich producer gas," *International Journal of Hydrogen Energy*, vol. 33, pp. 6515-6524, 11// 2008.

[21] V. Skoulou, A. Zabaniotou, G. Stavropoulos, and G. Sakelaropoulos, "Syngas production from olive tree cuttings and olive kernels in a downdraft fixed-bed gasifier," *International journal of hydrogen energy,* vol. 33, pp. 1185-1194, 2008.
[22] J. M. R. H. S. Ahmed and H. A. Mossa, "Analysis of Troposphere Carbon Dioxide in IRAQ from Atmosphere Infrared Sounder (AIRS) data: 2010-2011."
[23] L. I. El-Juhany, "Degradation of date palm trees and date production in Arab countries: causes and potential rehabilitation," *Australian Journal of Basic and Applied Sciences,* vol. 4, pp. 3998-4010, 2010.
[24] W. Erskine, A. T. Moustafa, A. E. Osman, Z. Lashine, A. Nejatian, T. Badawi, *et al.*, "Date palm in the GCC countries of the Arabian Peninsula," in *Proc. Regional Workshop on Date Palm Development in the Arabian Peninsula, Abu Dhabi, UAE,* 2004.
[25] H. H. Sait, A. Hussain, A. A. Salema, and F. N. Ani, "Pyrolysis and combustion kinetics of date palm biomass using thermogravimetric analysis," *Bioresource Technology,* vol. 118, pp. 382-389, 8// 2012.
[26] Q.-V. Bach, K.-Q. Tran, R. A. Khalil, and Ø. Skreiberg, "Wet Torrefaction of Forest Residues," *Energy Procedia,* vol. 61, pp. 1196-1199, 2014/01/01 2014.
[27] D. Maski, M. J. Darr, and R. P. Anex, "Torrefaction of Cellulosic Biomass Upgrading—Energy and Cost Model," 2010.
[28] J. S. Tumuluru, S. Sokhansanj, C. T. Wright, and R. D. Boardman, "Biomass torrefaction process review and moving bed torrefaction system model development," Idaho National Laboratory (INL)2010.
[29] M. J. C. van der Stelt, H. Gerhauser, J. H. A. Kiel, and K. J. Ptasinski, "Biomass upgrading by torrefaction for the production of biofuels: A review," *Biomass and Bioenergy,* vol. 35, pp. 3748-3762, 10// 2011.
[30] P.-C. Kuo, W. Wu, and W.-H. Chen, "Gasification performances of raw and torrefied biomass in a downdraft fixed bed gasifier using thermodynamic analysis," *Fuel,* vol. 117, Part B, pp. 1231-1241, 1/30/ 2014.
[31] D. Tapasvi, R. S. Kempegowda, K.-Q. Tran, Ø. Skreiberg, and M. Grønli, "A simulation study on the torrefied biomass gasification," *Energy Conversion and Management,* vol. 90, pp. 446-457, 1/15/ 2015.
[32] B. Arias, C. Pevida, J. Fermoso, M. G. Plaza, F. Rubiera, and J. J. Pis, "Influence of torrefaction on the grindability and reactivity of woody biomass," *Fuel Processing Technology,* vol. 89, pp. 169-175, 2// 2008.
[33] W.-H. Chen, C.-J. Chen, C.-I. Hung, C.-H. Shen, and H.-W. Hsu, "A comparison of gasification phenomena among raw biomass, torrefied biomass and coal in an entrained-flow reactor," *Applied Energy,* vol. 112, pp. 421-430, 12// 2013.
[34] E. M. Fisher, C. Dupont, L. I. Darvell, J. M. Commandré, A. Saddawi, J. M. Jones, *et al.*, "Combustion and gasification characteristics of chars from raw and torrefied biomass," *Bioresource Technology,* vol. 119, pp. 157-165, 9// 2012.
[35] M. J. Prins, K. J. Ptasinski, and F. J. J. G. Janssen, "More efficient biomass gasification via torrefaction," *Energy,* vol. 31, pp. 3458-3470, 12// 2006.
[36] M. J. Prins, K. J. Ptasinski, and F. J. Janssen, "From coal to biomass gasification: Comparison of thermodynamic efficiency," *Energy,* vol. 32, pp. 1248-1259, 2007.
[37] P. Basu, "biomass gasification and pyrolysis: Practica," *Elsevier,* p. 2.
[38] M. Barrio, *Experimental investigation of small-scale gasification ofwoody biomass*: Fakultet for ingeniørvitenskap og teknologi, 2002.
[39] H. Yang, R. Yan, H. Chen, C. Zheng, D. H. Lee, and D. T. Liang, "In-depth investigation of biomass pyrolysis based on three major components: hemicellulose, cellulose and lignin," *Energy & Fuels,* vol. 20, pp. 388-393, 2006.
[40] H. Yang, R. Yan, H. Chen, D. H. Lee, and C. Zheng, "Characteristics of hemicellulose, cellulose and lignin pyrolysis," *Fuel,* vol. 86, pp. 1781-1788, 8// 2007.

[41] G. Xue, M. Kwapinska, W. Kwapinski, K. M. Czajka, J. Kennedy, and J. J. Leahy, "Impact of torrefaction on properties of Miscanthus× giganteus relevant to gasification," *Fuel*, vol. 121, pp. 189-197, 2014.
[42] W.-H. Chen and P.-C. Kuo, "Torrefaction and co-torrefaction characterization of hemicellulose, cellulose and lignin as well as torrefaction of some basic constituents in biomass," *Energy*, vol. 36, pp. 803-811, 2// 2011.
[43] P. Rousset, C. Aguiar, N. Labbé, and J.-M. Commandré, "Enhancing the combustible properties of bamboo by torrefaction," *Bioresource Technology*, vol. 102, pp. 8225-8231, 9// 2011.
[44] J. Peng, H. Bi, S. Sokhansanj, and J. Lim, "A study of particle size effect on biomass torrefaction and densification," *Energy & Fuels*, vol. 26, pp. 3826-3839, 2012.
[45] J. Wannapeera, B. Fungtammasan, and N. Worasuwannarak, "Effects of temperature and holding time during torrefaction on the pyrolysis behaviors of woody biomass," *Journal of Analytical and Applied Pyrolysis*, vol. 92, pp. 99-105, 9// 2011.
[46] M. Strandberg, I. Olofsson, L. Pommer, S. Wiklund-Lindström, K. Åberg, and A. Nordin, "Effects of temperature and residence time on continuous torrefaction of spruce wood," *Fuel Processing Technology*, vol. 134, pp. 387-398, 2015/06/01/ 2015.
[47] J. Li, G. Bonvicini, E. Biagini, W. Yang, and L. Tognotti, "Characterization of high-temperature rapid char oxidation of raw and torrefied biomass fuels," *Fuel*, vol. 143, pp. 492-498, 3/1/ 2015.
[48] P. C. Bergman, A. R. Boersma, J. H. Kiel, M. J. Prins, K. J. Ptasinski, and F. Janssen, "Torrefaction for entrained-flow gasification of biomass," ed, 2005.
[49] Z. A. B. Z. Alauddin, P. Lahijani, M. Mohammadi, and A. R. Mohamed, "Gasification of lignocellulosic biomass in fluidized beds for renewable energy development: A review," *Renewable and Sustainable Energy Reviews*, vol. 14, pp. 2852-2862, 2010.
[50] P. M. N.Mahinpey, T. Mani, and R. Raian, "Analysis of bio-oil, bio-gas and bio-char from pressurized pyrolysis of wheat straw using a tubular reactor," *Energy Fuels*, vol. 23, p. 5, 2009.
[51] A. Zabaniotou and T. Damartzis, "Modelling the intra-particle transport phenomena and chemical reactions of olive kernel fast pyrolysis," *Journal of Analytical and Applied Pyrolysis*, vol. 80, pp. 187-194, 8// 2007.
[52] D. Xianwen, W. Chuangzhi, L. Haibin, and C. Yong, "The fast pyrolysis of biomass in CFB reactor," *Energy & Fuels*, vol. 14, pp. 552-557, 2000.
[53] A. Bridgwater, D. Meier, and D. Radlein, "An overview of fast pyrolysis of biomass," *Organic Geochemistry*, vol. 30, pp. 1479-1493, 1999.
[54] R. H. Venderbosch and W. Prins, "Fast Pyrolysis," in *Thermochemical Processing of Biomass*, ed: John Wiley & Sons, Ltd, 2011, pp. 124-156.
[55] A. V. Bridgwater and G. V. C. Peacocke, "Fast pyrolysis processes for biomass," *Renewable and Sustainable Energy Reviews*, vol. 4, pp. 1-73, 3// 2000.
[56] F. Karaosmanoğlu, E. Tetik, and E. Göllü, "Biofuel production using slow pyrolysis of the straw and stalk of the rapeseed plant," *Fuel Processing Technology*, vol. 59, pp. 1-12, 4// 1999.
[57] D. S. Scott, P. Majerski, J. Piskorz, and D. Radlein, "A second look at fast pyrolysis of biomass—the RTI process," *Journal of Analytical and Applied Pyrolysis*, vol. 51, pp. 23-37, 7// 1999.
[58] B. M. Jenkins, L. L. Baxter, and J. Koppejan, "Biomass Combustion," in *Thermochemical Processing of Biomass*, ed: John Wiley & Sons, Ltd, 2011, pp. 13-46.
[59] A. Demirbas, "Potential applications of renewable energy sources, biomass combustion problems in boiler power systems and combustion related environmental issues," *Progress in Energy and Combustion Science*, vol. 31, pp. 171-192, // 2005.

[60] P. McKendry, "Energy production from biomass (part 2): conversion technologies," *Bioresource Technology,* vol. 83, pp. 47-54, 5// 2002.
[61] W. J. Filho, "BIOMASS FOR POWER GENERATION AND COMBINED HEAT & POWER (CHP)

" *http://www.crusus.org/home_htm_files/WilsonJordaoBiomassforheat.pdf,* 2010.
[62] K. R. G. Hein and J. M. Bemtgen, "EU clean coal technology—co-combustion of coal and biomass," *Fuel Processing Technology,* vol. 54, pp. 159-169, 3// 1998.
[63] T. Nussbaumer, "Combustion and co-combustion of biomass: fundamentals, technologies, and primary measures for emission reduction," *Energy & fuels,* vol. 17, pp. 1510-1521, 2003.
[64] M. Gil, D. Casal, C. Pevida, J. Pis, and F. Rubiera, "Thermal behaviour and kinetics of coal/biomass blends during co-combustion," *Bioresource Technology,* vol. 101, pp. 5601-5608, 2010.
[65] G. J. Stiegel and R. C. Maxwell, "Gasification technologies: the path to clean, affordable energy in the 21st century," *Fuel Processing Technology,* vol. 71, pp. 79-97, 6// 2001.
[66] P. Quaak, H. Knoef, and H. E. Stassen, *Energy from biomass: a review of combustion and gasification technologies* vol. 23: World Bank Publications, 1999.
[67] A. V. Bridgwater, "The technical and economic feasibility of biomass gasification for power generation," *Fuel,* vol. 74, pp. 631-653, 5// 1995.
[68] e. a. Julian Szekely, "Gas Solid Reactions " *ACADEMIC PRESS.INC,* pp. 65-112, 1976.
[69] P. Lv, J. Chang, T. Wang, C. Wu, and N. Tsubaki, "A kinetic study on biomass fast catalytic pyrolysis," *Energy & Fuels,* vol. 18, pp. 1865-1869, 2004.
[70] A. Demirbaş, "Gaseous products from biomass by pyrolysis and gasification: effects of catalyst on hydrogen yield," *Energy Conversion and Management,* vol. 43, pp. 897-909, 5// 2002.
[71] C. Di Blasi, "Combustion and gasification rates of lignocellulosic chars," *Progress in Energy and Combustion Science,* vol. 35, pp. 121-140, 4// 2009.
[72] D. Baruah and D. C. Baruah, "Modeling of biomass gasification: A review," *Renewable and Sustainable Energy Reviews,* vol. 39, pp. 806-815, 11// 2014.
[73] M. Baláš, M. Lisý, and O. Štelcl, "The effect of temperature on the gasification process," *Acta Polytechnica,* vol. 52, 2012.
[74] S. Baumlin, F. Broust, M. Ferrer, N. Meunier, E. Marty, and J. Lédé, "The continuous self stirred tank reactor: measurement of the cracking kinetics of biomass pyrolysis vapours," *Chemical Engineering Science,* vol. 60, pp. 41-55, 1// 2005.
[75] P. Basu, *Biomass gasification and pyrolysis: practical design and theory*: Academic press, 2010.
[76] J. Hunt, A. Ferrari, A. Lita, M. Crosswhite, B. Ashley, and A. Stiegman, "Microwave-specific enhancement of the carbon–carbon dioxide (Boudouard) reaction," *The Journal of Physical Chemistry C,* vol. 117, pp. 26871-26880, 2013.
[77] P. Nanou, *Biomass gasification for the production of methane*: Universiteit Twente, 2013.
[78] J. M. Lee, Y. J. Kim, W. J. Lee, and S. D. Kim, "Coal-gasification kinetics derived from pyrolysis in a fluidized-bed reactor," *Energy,* vol. 23, pp. 475-488, 6// 1998.
[79] M. v. d. B. CHristopher Higman, "Gasification," *Elsevier Science,* p. 2, 2003.
[80] R. Fernando, "Developments in modelling and simulation of coal gasification," 2014.
[81] P. McKendry, "Energy production from biomass (part 3): gasification technologies," *Bioresource Technology,* vol. 83, pp. 55-63, 5// 2002.

[82] L. Devi, K. J. Ptasinski, and F. J. J. G. Janssen, "A review of the primary measures for tar elimination in biomass gasification processes," *Biomass and Bioenergy,* vol. 24, pp. 125-140, 2// 2003.
[83] R. R. H. Boerrigter, "Review of applications of gases from biomass gasification," 2006.
[84] P. V. Aravind and W. de Jong, "Evaluation of high temperature gas cleaning options for biomass gasification product gas for Solid Oxide Fuel Cells," *Progress in Energy and Combustion Science,* vol. 38, pp. 737-764, 12// 2012.
[85] A. Van der Drift and H. Boerrigter, *Synthesis gas from biomass for fuels and chemicals*: ECN Biomass, Coal and Environmental Research, 2006.
[86] R. M. Esfahani, W. A. Wan Ab Karim Ghani, M. A. Mohd Salleh, and S. Ali, "Hydrogen-rich gas production from palm kernel shell by applying air gasification in fluidized bed reactor," *Energy & Fuels,* vol. 26, pp. 1185-1191, 2012.
[87] V. Kirsanovs, A. Žandeckis, D. Blumberga, and I. Veidenbergs, "The influence of process temperature, equivalence ratio and fuel moisture content on gasification process: A review," *publication. editionName,* pp. 15-30, 2014.
[88] I. Narvaez, A. Orio, M. P. Aznar, and J. Corella, "Biomass gasification with air in an atmospheric bubbling fluidized bed. Effect of six operational variables on the quality of the produced raw gas," *Industrial & Engineering Chemistry Research,* vol. 35, pp. 2110-2120, 1996.
[89] M. R. Mahishi and D. Goswami, "Thermodynamic optimization of biomass gasifier for hydrogen production," *International Journal of Hydrogen Energy,* vol. 32, pp. 3831-3840, 2007.
[90] N. Couto, A. Rouboa, V. Silva, E. Monteiro, and K. Bouziane, "Influence of the Biomass Gasification Processes on the Final Composition of Syngas," *Energy Procedia,* vol. 36, pp. 596-606, // 2013.
[91] L. Wilson, G. R. John, C. F. Mhilu, W. Yang, and W. Blasiak, "Coffee husks gasification using high temperature air/steam agent," *Fuel processing technology,* vol. 91, pp. 1330-1337, 2010.
[92] W. Ngamchompoo and K. Triratanasirichai, "Experimental investigation of high temperature air and steam biomass gasification in a fixed-bed downdraft gasifier," *Energy Sources, Part A: Recovery, Utilization, and Environmental Effects,* vol. 39, pp. 733-740, 2017.
[93] E. Salaices, B. Serrano, and H. de Lasa, "Biomass catalytic steam gasification thermodynamics analysis and reaction experiments in a CREC riser simulator," *Industrial & engineering chemistry research,* vol. 49, pp. 6834-6844, 2010.
[94] P. Lv, Z. Yuan, L. Ma, C. Wu, Y. Chen, and J. Zhu, "Hydrogen-rich gas production from biomass air and oxygen/steam gasification in a downdraft gasifier," *Renewable Energy,* vol. 32, pp. 2173-2185, 10// 2007.
[95] N. Abdoulmoumine, A. Kulkarni, and S. Adhikari, "Effects of Temperature and Equivalence Ratio on Pine Syngas Primary Gases and Contaminants in a Bench-Scale Fluidized Bed Gasifier," *Industrial & Engineering Chemistry Research,* vol. 53, pp. 5767-5777, 2014.
[96] J. Gil, J. Corella, M. a. P. Aznar, and M. A. Caballero, "Biomass gasification in atmospheric and bubbling fluidized bed: effect of the type of gasifying agent on the product distribution," *Biomass and Bioenergy,* vol. 17, pp. 389-403, 1999.
[97] V. Skoulou, G. Koufodimos, Z. Samaras, and A. Zabaniotou, "Low temperature gasification of olive kernels in a 5-kW fluidized bed reactor for H 2-rich producer gas," *International Journal of Hydrogen Energy,* vol. 33, pp. 6515-6524, 2008.
[98] P. Basu, *Combustion and gasification in fluidized beds*. Taylar and Francis: CRC press, 2006.
[99] V. Belgiorno, G. De Feo, C. Della Rocca, and R. M. A. Napoli, "Energy from gasification of solid wastes," *Waste Management,* vol. 23, pp. 1-15, // 2003.

[100] A. Mustafa, R. K. Calay, and M. Y. Mustafa, "A Techno-economic Study of a Biomass Gasification Plant for the Production of Transport Biofuel for Small Communities," *Energy Procedia*, vol. 112, pp. 529-536, 2017.
[101] J. Corella, J. Herguido, and F. Alday, "Pyrolysis and steam gasification of biomass in fluidized beds. Influence of the type and location of the biomass feeding point on the product distribution," in *Research in thermochemical biomass conversion*, ed: Springer, 1988, pp. 384-398.
[102] R. Radmanesh, J. Chaouki, and C. Guy, "Biomass gasification in a bubbling fluidized bed reactor: Experiments and modeling," *AIChE Journal*, vol. 52, pp. 4258-4272, 2006.
[103] P. Vriesman, E. Heginuz, and K. Sjöström, "Biomass gasification in a laboratory-scale AFBG: influence of the location of the feeding point on the fuel-N conversion," *Fuel*, vol. 79, pp. 1371-1378, 9// 2000.
[104] P. J. van den Enden and E. S. Lora, "Design approach for a biomass fed fluidized bed gasifier using the simulation software CSFB," *Biomass and Bioenergy*, vol. 26, pp. 281-287, 3// 2004.
[105] E. Natarajan, A. Nordin, and A. N. Rao, "Overview of combustion and gasification of rice husk in fluidized bed reactors," *Biomass and Bioenergy*, vol. 14, pp. 533-546, 5// 1998.
[106] W. Wan Ab Karim Ghani, R. A. Moghadam, M. Salleh, and A. Alias, "Air gasification of agricultural waste in a fluidized bed gasifier: hydrogen production performance," *Energies*, vol. 2, pp. 258-268, 2009.
[107] P. Samy Sadaka and P. Eng, "1. Gasification."
[108] T. Lou, Z.-x. Zhang, J.-j. Fan, H.-q. An, Z.-h. Zhou, and P.-j. Yue, "Experiment Research on Gasification Character of Pulve-rized Coal at Medium Temperature," *Energy and Power Engineering*, vol. 5, p. 315, 2013.
[109] J. J. Hernández, G. Aranda-Almansa, and A. Bula, "Gasification of biomass wastes in an entrained flow gasifier: Effect of the particle size and the residence time," *Fuel Processing Technology*, vol. 91, pp. 681-692, 6// 2010.
[110] R. Font, A. Marcilla, J. Devesa, and E. Verdu, "Gaseous hydrocarbons from flash pyrolysis of almond shells," *Industrial & engineering chemistry research*, vol. 27, pp. 1143-1149, 1988.
[111] R. Warnecke, "Gasification of biomass: comparison of fixed bed and fluidized bed gasifier," *Biomass and Bioenergy*, vol. 18, pp. 489-497, 6/1/ 2000.
[112] C. Di Blasi, "Kinetic and heat transfer control in the slow and flash pyrolysis of solids," *Industrial & Engineering Chemistry Research*, vol. 35, pp. 37-46, 1996.
[113] S. Luo, B. Xiao, Z. Hu, S. Liu, Y. Guan, and L. Cai, "Influence of particle size on pyrolysis and gasification performance of municipal solid waste in a fixed bed reactor," *Bioresource Technology*, vol. 101, pp. 6517-6520, 8// 2010.
[114] P. S. Maa and R. C. Bailie, "Influence of Particle Sizes and Environmental Conditions on High Temperature Pyrolysis of Cellulosic Material—I (Theoretical)," *Combustion Science and Technology*, vol. 7, pp. 257-269, 1973.
[115] R. Yin, R. Liu, J. Wu, X. Wu, C. Sun, and C. Wu, "Influence of particle size on performance of a pilot-scale fixed-bed gasification system," *Bioresource Technology*, vol. 119, pp. 15-21, 9// 2012.
[116] P. Lv, Z. Xiong, J. Chang, C. Wu, Y. Chen, and J. Zhu, "An experimental study on biomass air–steam gasification in a fluidized bed," *Bioresource technology*, vol. 95, pp. 95-101, 2004.
[117] N. Jand and P. U. Foscolo, "Decomposition of wood particles in fluidized beds," *Industrial & engineering chemistry research*, vol. 44, pp. 5079-5089, 2005.
[118] C. Lucas, D. Szewczyk, W. Blasiak, and S. Mochida, "High-temperature air and steam gasification of densified biofuels," *Biomass and Bioenergy*, vol. 27, pp. 563-575, 12// 2004.
[119] T. Reed and A. Das, *Handbook of biomass downdraft gasifier engine systems*: Biomass Energy Foundation, 1988.

[120] S. Chopra and A. K. Jain, "A review of fixed bed gasification systems for biomass," *Agricultural Engineering International: CIGR Journal*, 2007.
[121] C. Mandl, I. Obernberger, and F. Biedermann, "Modelling of an updraft fixed-bed gasifier operated with softwood pellets," *Fuel*, vol. 89, pp. 3795-3806, 2010.
[122] M. Dogru, A. Midilli, and C. R. Howarth, "Gasification of sewage sludge using a throated downdraft gasifier and uncertainty analysis," *Fuel Processing Technology*, vol. 75, pp. 55-82, 2002.
[123] C. Di Blasi, G. Signorelli, and G. Portoricco, "Countercurrent fixed-bed gasification of biomass at laboratory scale," *Industrial & engineering chemistry research*, vol. 38, pp. 2571-2581, 1999.
[124] D. L. Giltrap, R. McKibbin, and G. R. G. Barnes, "A steady state model of gas-char reactions in a downdraft biomass gasifier," *Solar Energy*, vol. 74, pp. 85-91, 1// 2003.
[125] S. Mahapatra, "Experiments and Analysis on Wood Gasification in an Open Top Downdraft Gasifier," Indian Institute of Science Bangalore, India, 2016.
[126] Z. Fang, *Pretreatment techniques for biofuels and biorefineries*: Springer, 2013.
[127] I. Janajreh and I. Adeyemi, "Effect of Process Parameters on Gasification: Review."
[128] S. B. Sethupathy and E. Natarajan, "Hydrodynamic study on gasification of biomass in a fluidized bed gasifier," *International Journal of Engineering and Technology*, vol. 4, pp. 316-323, 2012.
[129] M. Öhman, L. Pommer, and A. Nordin, "Bed agglomeration characteristics and mechanisms during gasification and combustion of biomass fuels," *Energy & fuels*, vol. 19, pp. 1742-1748, 2005.
[130] S. Jarungthammachote and A. Dutta, "Equilibrium modeling of gasification: Gibbs free energy minimization approach and its application to spouted bed and spout-fluid bed gasifiers," *Energy Conversion and Management*, vol. 49, pp. 1345-1356, 6// 2008.
[131] N. Epstein and J. R. Grace, "Spouting of particulate solids," in *Handbook of powder science & technology*, ed: Springer, 1997, pp. 532-567.
[132] P. Abdul Salam and S. C. Bhattacharya, "A comparative study of charcoal gasification in two types of spouted bed reactors," *Energy*, vol. 31, pp. 228-243, 2// 2006.
[133] R. Xiao, M. Zhang, B. Jin, Y. Xiaong, H. Zhou, Y. Duan, *et al.*, "Air blown partial gasification of coal in a pilot plant pressurized spout-fluid bed reactor," *Fuel*, vol. 86, pp. 1631-1640, 7// 2007.
[134] W. Zhong and M. Zhang, "Pressure fluctuation frequency characteristics in a spout-fluid bed by modern ARM power spectrum analysis," *Powder Technology*, vol. 152, pp. 52-61, 4/29/ 2005.
[135] C. K. Gupta and D. Sathiyamoorthy, *Fluid bed technology in materials processing*: CRC Press, 1998.
[136] M. Olazar, M. J. San Jose, A. T. Aguayo, J. M. Arandes, and J. Bilbao, "Design factors of conical spouted beds and jet spouted beds," *Industrial & engineering chemistry research*, vol. 32, pp. 1245-1250, 1993.
[137] J. P. Ciferno and J. J. Marano, "Benchmarking biomass gasification technologies for fuels, chemicals and hydrogen production," *US Department of Energy. National Energy Technology Laboratory*, 2002.
[138] J. W. Bohlig and D. R. Casella, "System and method for integrated waste storage," ed: Google Patents, 2009.
[139] M. Siedlecki, W. De Jong, and A. H. Verkooijen, "Fluidized bed gasification as a mature and reliable technology for the production of bio-syngas and applied in the production of liquid transportation fuels—a review," *Energies*, vol. 4, pp. 389-434, 2011.
[140] J. A. P. Peña, "Bubbling Fluidized Bed (BFB), When to use this technology?," *Industrial Fluidization South Africa*, pp. 1-12, 2011.

[141] C. Loha, H. Chattopadhyay, and P. K. Chatterjee, "Three dimensional kinetic modeling of fluidized bed biomass gasification," *Chemical Engineering Science*, vol. 109, pp. 53-64, 2014.
[142] M. Rüdisüli, T. J. Schildhauer, S. M. A. Biollaz, and J. R. van Ommen, "Scale-up of bubbling fluidized bed reactors — A review," *Powder Technology*, vol. 217, pp. 21-38, 2// 2012.
[143] X. T. Li, J. R. Grace, C. J. Lim, A. P. Watkinson, H. P. Chen, and J. R. Kim, "Biomass gasification in a circulating fluidized bed," *Biomass and Bioenergy*, vol. 26, pp. 171-193, 2// 2004.
[144] X. Li, J. Grace, C. Lim, A. Watkinson, H. Chen, and J. Kim, "Biomass gasification in a circulating fluidized bed," *Biomass and bioenergy*, vol. 26, pp. 171-193, 2004.
[145] Y. Fang, J. Huang, Y. Wang, and B. Zhang, "Experiment and mathematical modeling of a bench-scale circulating fluidized bed gasifier," *Fuel Processing Technology*, vol. 69, pp. 29-44, 1// 2001.
[146] A. van der Drift, J. van Doorn, and J. W. Vermeulen, "Ten residual biomass fuels for circulating fluidized-bed gasification," *Biomass and Bioenergy*, vol. 20, pp. 45-56, 1// 2001.
[147] J. W. Brown, "Biomass gasification: fast internal circulating fluidised bed gasifier characterisation and comparison," 2006.
[148] O. Morin, "Technical and Environmental Comparison of Circulating Fluidized Bed (CFB) and Moving Grate Reactors," Columbia University, 2014.
[149] J. R. Grace, T. Knowlton, and A. Avidan, *Circulating fluidized beds*: Springer Science & Business Media, 2012.
[150] A. V. Bridgwater and G. Evans, *An assessment of thermochemical conversion systems for processing biomass and refuse*: Energy Technology Support Unit Harwell, 1993.
[151] V. V. Ranade, *Computational flow modeling for chemical reactor engineering* vol. 5: Academic press, 2001.
[152] M. Mortimer, Taylor, P G, Smart, Lesley E *Molecular World, Volume 6 : Chemical Kinetics and Mechanism*. Cambridge, GBR: Royal Society of Chemistry, 2007.
[153] D. Baruah and D. Baruah, "Modeling of biomass gasification: a review," *Renewable and Sustainable Energy Reviews*, vol. 39, pp. 806-815, 2014.
[154] M. M. Prins, "Thermodynamic analysis of biomass gasification and torrefaction," 2005.
[155] A. K. Coker, *Modeling of chemical kinetics and reactor design* vol. 1: Gulf Professional Publishing, 2001.
[156] M. V. Kök and M. R. Pamir, "Comparative pyrolysis and combustion kinetics of oil shales," *Journal of Analytical and Applied Pyrolysis*, vol. 55, pp. 185-194, 7// 2000.
[157] M. Mortimer, P. G. Taylor, and L. E. Smart, *Molecular World, Volume 6 : Chemical Kinetics and Mechanism*. Cambridge, GBR: Royal Society of Chemistry, 2007.
[158] A. K. Galwey and M. E. Brown, "Kinetic background to thermal analysis and calorimetry," 1998.
[159] O. Levenspiel, "Chemical reaction engineering," *John Wiley & Sons, Inc.*, p. 2, 1999.
[160] S. Nanda and M. Pharm, "Reactors and fundamentals of reactors design for chemical reaction," *Doctoral Report. Dept of pharmaceutical sciences. MD University Rohtak, Haryana*, 2008.
[161] K. A. Coonnors, "Chemical Kinetics - The study of reaction rates in solution," pp. 17-23, 1990.
[162] H. S. Fogler, "Elements of chemical reaction engineering," 1999.
[163] A. Gómez-Barea and P. Ollero, "An approximate method for solving gas–solid non-catalytic reactions," *Chemical Engineering Science*, vol. 61, pp. 3725-3735, 6// 2006.
[164] C. Wen, "Noncatalytic heterogeneous solid-fluid reaction models," *Industrial & Engineering Chemistry*, vol. 60, pp. 34-54, 1968.

[165] J. E. White, W. J. Catallo, and B. L. Legendre, "Biomass pyrolysis kinetics: A comparative critical review with relevant agricultural residue case studies," *Journal of Analytical and Applied Pyrolysis,* vol. 91, pp. 1-33, 5// 2011.
[166] J. E. House, "Principles of chemical kinetics-Second addition," 2007.
[167] J. H. Flynn and L. A. Wall, "A quick, direct method for the determination of activation energy from thermogravimetric data," *Journal of Polymer Science Part B: Polymer Letters,* vol. 4, pp. 323-328, 1966.
[168] N. Phusunti, "Pryolytic and kinetic study of Chlorella Vulgaris under isothermal and non-isothermal conditions," Aston University, 2013.
[169] S. Vyazovkin, K. Chrissafis, M. L. Di Lorenzo, N. Koga, M. Pijolat, B. Roduit, *et al.*, "ICTAC Kinetics Committee recommendations for collecting experimental thermal analysis data for kinetic computations," *Thermochimica Acta,* vol. 590, pp. 1-23, 8/20/ 2014.
[170] J. Yu, J.-h. Zhu, F. Guo, Z.-k. Duan, Y.-y. Liu, and G.-w. Xu, "Reaction kinetics and mechanism of biomass pylolysis in a micro-fluidized bed reactor," *Journal of Fuel Chemistry and Technology,* vol. 38, pp. 666-672, 12// 2010.
[171] J. Yu, J. Yue, Z. Liu, L. Dong, G. Xu, J. Zhu, *et al.*, "Kinetics and mechanism of solid reactions in a micro fluidized bed reactor," *AICHE journal,* vol. 56, pp. 2905-2912, 2010.
[172] O. Ebrahimpour, J. Chaouki, and C. Dubois, "Diffusional effects for the oxidation of SiC powders in thermogravimetric analysis experiments," *Journal of Materials Science,* vol. 48, pp. 4396-4407, 2013.
[173] R. K. Agrawal, "Analysis of non-isothermal reaction kinetics: Part 1. Simple reactions," *Thermochimica Acta,* vol. 203, pp. 93-110, 1992.
[174] F. Yao, Q. Wu, Y. Lei, W. Guo, and Y. Xu, "Thermal decomposition kinetics of natural fibers: Activation energy with dynamic thermogravimetric analysis," *Polymer Degradation and Stability,* vol. 93, pp. 90-98, 1// 2008.
[175] M. A. A. Mohammed, A. Salmiaton, W. A. K. G. Wan Azlina, and M. S. Mohamad Amran, "Gasification of oil palm empty fruit bunches: A characterization and kinetic study," *Bioresource Technology,* vol. 110, pp. 628-636, 4// 2012.
[176] H. S. Fogler, "Elements of chemical reaction engineering," p. 1, 2014.
[177] J. Flynn, "Temperature dependence of the rate of reaction in thermal analysis," *Journal of thermal analysis,* vol. 36, pp. 1579-1593, 1990.
[178] C. Di Blasi, "Modeling chemical and physical processes of wood and biomass pyrolysis," *Progress in Energy and Combustion Science,* vol. 34, pp. 47-90, 2008.
[179] T. R. Nunn, J. B. Howard, J. P. Longwell, and W. A. Peters, "Product compositions and kinetics in the rapid pyrolysis of sweet gum hardwood," *Ind. Eng. Chem. Process Des. Dev.;(United States),* vol. 24, 1985.
[180] T. Cordero, F. Garcia, and J. Rodriguez, "A kinetic study of holm oak wood pyrolysis from dynamic and isothermal TG experiments," *Thermochimica acta,* vol. 149, pp. 225-237, 1989.
[181] J. Fermoso, B. Arias, C. Pevida, M. Plaza, F. Rubiera, and J. Pis, "Kinetic models comparison for steam gasification of different nature fuel chars," *Journal of Thermal Analysis and Calorimetry,* vol. 91, pp. 779-786, 2008.
[182] C. Gai, Y. Dong, Z. Lv, Z. Zhang, J. Liang, and Y. Liu, "Pyrolysis behavior and kinetic study of phenol as tar model compound in micro fluidized bed reactor," *International Journal of Hydrogen Energy,* 2015.
[183] K. O. Oluoti, T. Richards, T. Doddapaneni, and D. Kanagasabapathi, "Evaluation of the Pyrolysis and Gasification Kinetics of Tropical Wood Biomass," *BioResources,* vol. 9, pp. 2179-2190, 2014.
[184] K. Slopiecka, P. Bartocci, and F. Fantozzi, "Thermogravimetric analysis and kinetic study of poplar wood pyrolysis," *Applied Energy,* vol. 97, pp. 491-497, 2012.
[185] C. Gai, Y. Dong, Z. Lv, Z. Zhang, J. Liang, and Y. Liu, "Pyrolysis behavior and kinetic study of phenol as tar model compound in micro fluidized bed reactor," *International Journal of Hydrogen Energy,* vol. 40, pp. 7956-7964, 2015.

[186] M. R. B. Guerrero, M. Marques da Silva Paula, M. M. Zaragoza, J. S. Gutiérrez, V. G. Velderrain, A. L. Ortiz, *et al.*, "Thermogravimetric study on the pyrolysis kinetics of apple pomace as waste biomass," *International Journal of Hydrogen Energy*, vol. 39, pp. 16619-16627, 10/2/ 2014.
[187] P. J. Haines, "Principles of thermal analysis and calorimetry-Royal society of chemistry," pp. 42-47, 2002.
[188] J. Yu, X. Zeng, J. Zhang, M. Zhong, G. Zhang, Y. Wang, *et al.*, "Isothermal differential characteristics of gas–solid reaction in micro-fluidized bed reactor," *Fuel*, vol. 103, pp. 29-36, 2013.
[189] S. Munir, S. S. Daood, W. Nimmo, A. M. Cunliffe, and B. M. Gibbs, "Thermal analysis and devolatilization kinetics of cotton stalk, sugar cane bagasse and shea meal under nitrogen and air atmospheres," *Bioresource Technology*, vol. 100, pp. 1413-1418, 2// 2009.
[190] K. G. Mansaray and A. E. Ghaly, "Determination of kinetic parameters of rice husks in oxygen using thermogravimetric analysis," *Biomass and Bioenergy*, vol. 17, pp. 19-31, 7// 1999.
[191] Y. El may, M. Jeguirim, S. Dorge, G. Trouvé, and R. Said, "Study on the thermal behavior of different date palm residues: Characterization and devolatilization kinetics under inert and oxidative atmospheres," *Energy*, vol. 44, pp. 702-709, 8// 2012.
[192] M. Grønli, M. J. Antal, and G. Várhegyi, "A round-robin study of cellulose pyrolysis kinetics by thermogravimetry," *Industrial & Engineering Chemistry Research*, vol. 38, pp. 2238-2244, 1999.
[193] D. K. Seo, S. S. Park, J. Hwang, and T.-U. Yu, "Study of the pyrolysis of biomass using thermo-gravimetric analysis (TGA) and concentration measurements of the evolved species," *Journal of Analytical and Applied Pyrolysis*, vol. 89, pp. 66-73, 9// 2010.
[194] Y. Jian, J.-h. ZHU, G. Feng, Z.-k. DUAN, Y.-y. LIU, and G.-w. XU, "Reaction kinetics and mechanism of biomass pylolysis in a micro-fluidized bed reactor," *Journal of fuel chemistry and technology*, vol. 38, pp. 666-672, 2010.
[195] E. Grieco and G. Baldi, "Analysis and modelling of wood pyrolysis," *Chemical Engineering Science*, vol. 66, pp. 650-660, 2011.
[196] R. Reschmeier, D. Roveda, D. Müller, and J. Karl, "Pyrolysis kinetics of wood pellets in fluidized beds," *Journal of Analytical and Applied Pyrolysis*, vol. 108, pp. 117-129, 2014.
[197] X. Zeng, F. Wang, Y. Wang, A. Li, J. Yu, and G. Xu, "Characterization of Char Gasification in a Micro Fluidized Bed Reaction Analyzer," *Energy & Fuels*, vol. 28, pp. 1838-1845, 2014.
[198] B. S. Institute, "Solid biofuels. Determination of calorific value, BSI. London.," 2009b.
[199] W. Zhong, B. Jin, Y. Zhang, X. Wang, and R. Xiao, "Fluidization of biomass particles in a gas− solid fluidized bed," *Energy & Fuels*, vol. 22, pp. 4170-4176, 2008.
[200] C.-L. Lin, M.-Y. Wey, and S.-D. You, "The effect of particle size distribution on minimum fluidization velocity at high temperature," *Powder Technology*, vol. 126, pp. 297-301, 8/12/ 2002.
[201] W.-C. Yang, "Handbook of fluidization and fluid particle systems," *Taylor & Francis Group*, 2003.
[202] F. Miccio, B. Piriou, G. Ruoppolo, and R. Chirone, "Biomass gasification in a catalytic fluidized reactor with beds of different materials," *Chemical Engineering Journal*, vol. 154, pp. 369-374, 11/15/ 2009.
[203] C. Y. W. R.R. Pattipati, "Minimum fluidization velocity at high temperatures," *Ind. Eng. Chem. Proc. Des. Dev.*, vol. 20, 1981.

[204] S. Rapagnà, N. Jand, A. Kiennemann, and P. U. Foscolo, "Steam-gasification of biomass in a fluidised-bed of olivine particles," *Biomass and Bioenergy*, vol. 19, pp. 187-197, 9// 2000.
[205] D. Escudero and T. J. Heindel, "Bed height and material density effects on fluidized bed hydrodynamics," *Chemical Engineering Science*, vol. 66, pp. 3648-3655, 8/15/ 2011.
[206] J.-H. Choi, J.-M. Suh, I.-Y. Chang, D.-W. Shun, C.-K. Yi, J.-E. Son, *et al.*, "The effect of fine particles on elutriation of coarse particles in a gas fluidized bed," *Powder Technology*, vol. 121, pp. 190-194, 11/26/ 2001.
[207] D. Kunii and O. Levenspiel, *Fluidization engineering*: Elsevier, 2013.
[208] M. Phanphanich and S. Mani, "Impact of torrefaction on the grindability and fuel characteristics of forest biomass," *Bioresource Technology*, vol. 102, pp. 1246-1253, 1// 2011.
[209] J. Poudel and S. C. Oh, "Effect of torrefaction on the properties of corn stalk to enhance solid fuel qualities," *Energies*, vol. 7, pp. 5586-5600, 2014.
[210] A. Demirbas, "Effects of temperature and particle size on bio-char yield from pyrolysis of agricultural residues," *Journal of Analytical and Applied Pyrolysis*, vol. 72, pp. 243-248, 11// 2004.
[211] R. B. Bates, C. Altantzis, and A. F. Ghoniem, "Modeling of biomass char gasification, combustion, and attrition kinetics in fluidized beds," *Energy & Fuels*, vol. 30, pp. 360-376, 2016.
[212] D. Gauthier, S. Zerguerras, and G. Flamant, "Influence of the particle size distribution of powders on the velocities of minimum and complete fluidization," *Chemical Engineering Journal*, vol. 74, pp. 181-196, 7/19/ 1999.
[213] R. Xiao, M. Zhang, B. Jin, Y. Huang, and H. Zhou, "High-temperature air/steam-blown gasification of coal in a pressurized spout-fluid bed," *Energy & Fuels*, vol. 20, pp. 715-720, 2006.
[214] E. Natarajan, A. Nordin, and A. Rao, "Overview of combustion and gasification of rice husk in fluidized bed reactors," *Biomass and Bioenergy*, vol. 14, pp. 533-546, 1998.
[215] R. Reschmeier, D. Roveda, D. Müller, and J. Karl, "Pyrolysis kinetics of wood pellets in fluidized beds," *Journal of Analytical and Applied Pyrolysis*, vol. 108, pp. 117-129, 7// 2014.
[216] P. Ollero, A. Serrera, R. Arjona, and S. Alcantarilla, "Diffusional effects in TGA gasification experiments for kinetic determination," *Fuel*, vol. 81, pp. 1989-2000, 10/1/ 2002.
[217] A. Latif, "A study of the design of fluidized bed reactors for biomass gasification," University of London, 1999.
[218] L. Lin, E. Gustafsson, and M. Strand, "High-temperature kinetics of fine biomass char particles in air and CO2," 2010.
[219] P. Basu, *Biomass gasification, pyrolysis and torrefaction: practical design and theory*: Academic press, 2013.
[220] K. J. Timmer, *Carbon conversion during bubbling fluidized bed gasification of biomass*: ProQuest, 2008.
[221] F. Scala, P. Salatino, and R. Chirone, "Fluidized bed combustion of a biomass char (Robinia pseudoacacia)," *Energy & fuels*, vol. 14, pp. 781-790, 2000.
[222] A. C. C. Chang, H.-F. Chang, F.-J. Lin, K.-H. Lin, and C.-H. Chen, "Biomass gasification for hydrogen production," *International Journal of Hydrogen Energy*, vol. 36, pp. 14252-14260, 10// 2011.
[223] J. E. House, *Principles of chemical kinetics*: Academic Press, 2007.
[224] M. Van de Velden, J. Baeyens, A. Brems, B. Janssens, and R. Dewil, "Fundamentals, kinetics and endothermicity of the biomass pyrolysis reaction," *Renewable energy*, vol. 35, pp. 232-242, 2010.
[225] A. Saddawi, J. Jones, A. Williams, and M. Wojtowicz, "Kinetics of the thermal decomposition of biomass," *Energy & Fuels*, vol. 24, pp. 1274-1282, 2009.

[226] J. A. Caballero, R. Font, A. Marcilla, and J. A. Conesa, "New kinetic model for thermal decomposition of heterogeneous materials," *Industrial & engineering chemistry research,* vol. 34, pp. 806-812, 1995.
[227] S. Daneshvar and K. Otsuka, "Pyrolytic behavior of green macro algae and evaluation of its activation energy," *Int J Chem Eng Appl,* vol. 3, pp. 256-263, 2012.
[228] W.-H. Chen and P.-C. Kuo, "A study on torrefaction of various biomass materials and its impact on lignocellulosic structure simulated by a thermogravimetry," *Energy,* vol. 35, pp. 2580-2586, 2010.
[229] E. Kastanaki, D. Vamvuka, P. Grammelis, and E. Kakaras, "Thermogravimetric studies of the behavior of lignite–biomass blends during devolatilization," *Fuel Processing Technology,* vol. 77–78, pp. 159-166, 6/20/ 2002.
[230] J. Jae, G. A. Tompsett, Y.-C. Lin, T. R. Carlson, J. Shen, T. Zhang, *et al.*, "Depolymerization of lignocellulosic biomass to fuel precursors: maximizing carbon efficiency by combining hydrolysis with pyrolysis," *Energy & Environmental Science,* vol. 3, pp. 358-365, 2010.
[231] J. M. Encinar, J. F. González, and J. González, "Fixed-bed pyrolysis of Cynara cardunculus L. Product yields and compositions," *Fuel Processing Technology,* vol. 68, pp. 209-222, 12// 2000.
[232] J. Yu, C. Yao, X. Zeng, S. Geng, L. Dong, Y. Wang, *et al.*, "Biomass pyrolysis in a micro-fluidized bed reactor: Characterization and kinetics," *Chemical Engineering Journal,* vol. 168, pp. 839-847, 4/1/ 2011.
[233] J. Encinar, J. Gonzalez, and J. Gonzalez, "Fixed-bed pyrolysis of Cynara cardunculus L. Product yields and compositions," *Fuel Processing Technology,* vol. 68, pp. 209-222, 2000.
[234] S. Czernik and A. Bridgwater, "Overview of applications of biomass fast pyrolysis oil," *Energy & Fuels,* vol. 18, pp. 590-598, 2004.
[235] D. S. Scott, J. Piskorz, M. A. Bergougnou, R. Graham, and R. P. Overend, "The role of temperature in the fast pyrolysis of cellulose and wood," *Industrial & engineering chemistry research,* vol. 27, pp. 8-15, 1988.
[236] G. Xu, S. Gao, J. Yu, Q. Li, J. Zhu, and Z. Duan, "CHARACTERISTICS AND KINETICS OF BIOMASS PYLOLYSIS IN A MICRO FLUIDIZED BED REACTOR," 2010.
[237] Y. Yang, J. Han, W. Zhao, and B. Zhang, "Kinetic mechanism in the process of carbothermal reduction of ferrum niobate," *Journal of Wuhan University of Technology-Mater. Sci. Ed.,* vol. 30, pp. 918-922, 2015.
[238] J. Guo and A. C. Lua, "Kinetic study on pyrolytic process of oil-palm solid waste using two-step consecutive reaction model," *Biomass and Bioenergy,* vol. 20, pp. 223-233, 3// 2001.
[239] T. G. Bridgeman, J. M. Jones, I. Shield, and P. T. Williams, "Torrefaction of reed canary grass, wheat straw and willow to enhance solid fuel qualities and combustion properties," *Fuel,* vol. 87, pp. 844-856, 5// 2008.
[240] R. H. Ibrahim, L. I. Darvell, J. M. Jones, and A. Williams, "Physicochemical characterisation of torrefied biomass," *Journal of Analytical and Applied Pyrolysis,* vol. 103, pp. 21-30, 2013.
[241] W.-H. Chen, C.-J. Chen, C.-I. Hung, C.-H. Shen, and H.-W. Hsu, "A comparison of gasification phenomena among raw biomass, torrefied biomass and coal in an entrained-flow reactor," *Applied Energy,* vol. 112, pp. 421-430, 12// 2013.
[242] P. Lahijani and Z. A. Zainal, "Gasification of palm empty fruit bunch in a bubbling fluidized bed: a performance and agglomeration study," *Bioresource Technology,* vol. 102, pp. 2068-2076, 2011.
[243] T. Song, J. Wu, L. Shen, and J. Xiao, "Experimental investigation on hydrogen production from biomass gasification in interconnected fluidized beds," *biomass and bioenergy,* vol. 36, pp. 258-267, 2012.

[244] Y. Cao, Y. Wang, J. T. Riley, and W.-P. Pan, "A novel biomass air gasification process for producing tar-free higher heating value fuel gas," *Fuel Processing Technology,* vol. 87, pp. 343-353, 4// 2006.
[245] M. A. A. Mohammed, A. Salmiaton, W. A. K. G. Wan Azlina, M. S. Mohammad Amran, and A. Fakhru'l-Razi, "Air gasification of empty fruit bunch for hydrogen-rich gas production in a fluidized-bed reactor," *Energy Conversion and Management,* vol. 52, pp. 1555-1561, 2// 2011.
[246] F. Pinto, C. Franco, R. N. Andre, C. Tavares, M. Dias, I. Gulyurtlu, *et al.*, "Effect of experimental conditions on co-gasification of coal, biomass and plastics wastes with air/steam mixtures in a fluidized bed system," *Fuel,* vol. 82, pp. 1967-1976, 2003.
[247] G. Xue, M. Kwapinska, A. Horvat, W. Kwapinski, L. Rabou, S. Dooley, *et al.*, "Gasification of torrefied Miscanthus× giganteus in an air-blown bubbling fluidized bed gasifier," *Bioresource technology,* vol. 159, pp. 397-403, 2014.
[248] P.-C. Kuo, W. Wu, and W.-H. Chen, "Gasification performances of raw and torrefied biomass in a downdraft fixed bed gasifier using thermodynamic analysis," *Fuel,* vol. 117, pp. 1231-1241, 2014.
[249] C. Couhert, S. Salvador, and J. M. Commandré, "Impact of torrefaction on syngas production from wood," *Fuel,* vol. 88, pp. 2286-2290, 11// 2009.
[250] M. Kwapinska, G. Xue, A. Horvat, L. P. Rabou, S. Dooley, W. Kwapinski, *et al.*, "Fluidized Bed Gasification of Torrefied and Raw Grassy Biomass (Miscanthus× gigantenus). The Effect of Operating Conditions on Process Performance," *Energy & Fuels,* vol. 29, pp. 7290-7300, 2015.
[251] L. Emami Taba, M. F. Irfan, W. A. M. Wan Daud, and M. H. Chakrabarti, "The effect of temperature on various parameters in coal, biomass and CO-gasification: A review," *Renewable and Sustainable Energy Reviews,* vol. 16, pp. 5584-5596, 10// 2012.
[252] J. J. Manyà, J. L. Sánchez, J. Ábrego, A. Gonzalo, and J. Arauzo, "Influence of gas residence time and air ratio on the air gasification of dried sewage sludge in a bubbling fluidised bed," *Fuel,* vol. 85, pp. 2027-2033, 2006.
[253] G. Xue, M. Kwapinska, A. Horvat, Z. Li, S. Dooley, W. Kwapinski, *et al.*, "Gasification of Miscanthus x giganteus in an air-blown bubbling fluidized bed: a preliminary study of performance and agglomeration," *Energy & Fuels,* vol. 28, pp. 1121-1131, 2014.
[254] A. K. James, S. S. Helle, R. W. Thring, P. M. Rutherford, and M. S. Masnadi, "Investigation of air and air-steam gasification of high carbon wood ash in a fluidized bed reactor," *Energy and Environment Research,* vol. 4, p. 15, 2014.
[255] S. Sadaka, "Gasification of raw and torrefied cotton gin wastes in an auger system," *Applied Engineering in Agriculture,* vol. 29, pp. 405-414, 2013.
[256] A. Dhungana, "Torrefaction of biomass," 2011.
[257] Q. Chen, J. Zhou, B. Liu, Q. Mei, and Z. Luo, "Influence of torrefaction pretreatment on biomass gasification technology," *Chinese Science Bulletin,* vol. 56, pp. 1449-1456, 2011.
[258] B. Fidalgo, A. Domínguez, J. J. Pis, and J. A. Menéndez, "Microwave-assisted dry reforming of methane," *International Journal of Hydrogen Energy,* vol. 33, pp. 4337-4344, 8// 2008.
[259] R. Klaewkla, M. Arend, and W. F. Hoelderich, *A review of mass transfer controlling the reaction rate in heterogeneous catalytic systems* vol. 5: INTECH Open Access Publisher, 2011.
[260] J. W. E. Julain Szekely, Hong Yong Sohn, "Gas-Solid Reactions," *Academic press,* 1976.
[261] F. Wang, X. Zeng, R. Shao, Y. Wang, J. Yu, and G. Xu, "Isothermal Gasification of in Situ/ex Situ Coal Char with CO2 in a Micro Fluidized Bed Reaction Analyzer," *Energy & Fuels,* vol. 29, pp. 4795-4802, 2015.

[262] F. Guo, Y. Dong, Z. Lv, P. Fan, S. Yang, and L. Dong, "Kinetic behavior of biomass under oxidative atmosphere using a micro-fluidized bed reactor," *Energy Conversion and Management*, vol. 108, pp. 210-218, 2016.
[263] W. Hu, X. Yang, B. Mi, F. Liang, T. Zhang, B. Fei, *et al.*, "INVESTIGATING CHEMICAL PROPERTIES AND COMBUSTION CHARACTERISTICS OF TORREFIED MASSON PINE," *Wood and Fiber Science*, vol. 49, pp. 33-42, 2017.
[264] M. Sami, K. Annamalai, and M. Wooldridge, "Co-firing of coal and biomass fuel blends," *Progress in Energy and Combustion Science*, vol. 27, pp. 171-214, // 2001.
[265] L. Lahaye and P. Ehrburger, *Fundamental issues in control of carbon gasification reactivity* vol. 192: Springer Science & Business Media, 2012.
[266] B. M. Jenkins, L. L. Baxter, T. R. Miles Jr, and T. R. Miles, "Combustion properties of biomass," *Fuel Processing Technology*, vol. 54, pp. 17-46, 3// 1998.
[267] P. M. Lv, Z. H. Xiong, J. Chang, C. Z. Wu, Y. Chen, and J. X. Zhu, "An experimental study on biomass air–steam gasification in a fluidized bed," *Bioresource Technology*, vol. 95, pp. 95-101, 10// 2004.
[268] T. d. P. Protásio, I. C. N. A. d. Melo, M. Guimarães Junior, R. F. Mendes, and P. F. Trugilho, "Thermal decomposition of torrefied and carbonized briquettes of residues from coffee grain processing," *Ciência e Agrotecnologia*, vol. 37, pp. 221-228, 2013.
[269] S. Ren, H. Lei, L. Wang, Q. Bu, S. Chen, and J. Wu, "Thermal behaviour and kinetic study for woody biomass torrefaction and torrefied biomass pyrolysis by TGA," *Biosystems engineering*, vol. 116, pp. 420-426, 2013.
[270] Y. Zhang, Z. O'Neill, B. Dong, and G. Augenbroe, "Comparisons of inverse modeling approaches for predicting building energy performance," *Building and Environment*, vol. 86, pp. 177-190, 2015.
[271] A. Uhrig, "Determination of pyrolysis reaction kinetics of raw and torrefied biomass," University of Twente, 2014.
[272] A. Al-Farraji, R. Marsh, and J. Steer, "A Comparison of the Pyrolysis of Olive Kernel Biomass in Fluidised and Fixed Bed Conditions," *Waste and Biomass Valorization*, pp. 1-12.
[273] S. Luo, B. Xiao, X. Guo, Z. Hu, S. Liu, and M. He, "Hydrogen-rich gas from catalytic steam gasification of biomass in a fixed bed reactor: Influence of particle size on gasification performance," *International Journal of Hydrogen Energy*, vol. 34, pp. 1260-1264, 2// 2009.
[274] F. Yu, X. Bo, G. Klaus, C. Gong, and W. Jingbo, "Influence of particle size and temperature on gasification performance in externally heated gasifier," *Smart Grid and Renewable Energy*, vol. 2011, 2011.
[275] V. R. Patel, D. S. Upadhyay, and R. N. Patel, "Gasification of lignite in a fixed bed reactor: Influence of particle size on performance of downdraft gasifier," *Energy*, vol. 78, pp. 323-332, 12/15/ 2014.
[276] L. Wei, S. Xu, L. Zhang, H. Zhang, C. Liu, H. Zhu, *et al.*, "Characteristics of fast pyrolysis of biomass in a free fall reactor," *Fuel Processing Technology*, vol. 87, pp. 863-871, 2006.
[277] X. Guo, B. Xiao, X. Zhang, S. Luo, and M. He, "Experimental study on air-stream gasification of biomass micron fuel (BMF) in a cyclone gasifier," *Bioresource technology*, vol. 100, pp. 1003-1006, 2009.
[278] J. F. González, S. Román, D. Bragado, and M. Calderón, "Investigation on the reactions influencing biomass air and air/steam gasification for hydrogen production," *Fuel Processing Technology*, vol. 89, pp. 764-772, 8// 2008.
[279] A. Gómez-Barea, P. Ollero, and R. Arjona, "Reaction-diffusion model of TGA gasification experiments for estimating diffusional effects," *Fuel*, vol. 84, pp. 1695-1704, 9// 2005.
[280] P. A. Horne and P. T. Williams, "Influence of temperature on the products from the flash pyrolysis of biomass," *Fuel*, vol. 75, pp. 1051-1059, 1996.
[281] R. Z. Vigouroux, "Pyrolysis of biomass," *Royal Institute of Technology*, 2001.

[282] A. V. Bridgwater, "Principles and practice of biomass fast pyrolysis processes for liquids," *Journal of Analytical and Applied Pyrolysis,* vol. 51, pp. 3-22, 7// 1999.
[283] Y. Chhiti and M. Kemiha, "Thermal Conversion of Biomass, Pyrolysis and Gasification," *International Journal of Engineering and Science (IJES),* vol. 2, pp. 75-85, 2013.
[284] C. Gai, Y. Dong, P. Fan, Z. Zhang, J. Liang, and P. Xu, "Kinetic study on thermal decomposition of toluene in a micro fluidized bed reactor," *Energy Conversion and Management,* vol. 106, pp. 721-727, 2015.
[285] J. M. Encinar, F. J. Beltrán, A. Ramiro, and J. F. González, "Pyrolysis/gasification of agricultural residues by carbon dioxide in the presence of different additives: influence of variables," *Fuel Processing Technology,* vol. 55, pp. 219-233, 6// 1998.
[286] M. Poletto, A. J. Zattera, and R. M. Santana, "Thermal decomposition of wood: kinetics and degradation mechanisms," *Bioresource Technology,* vol. 126, pp. 7-12, 2012.
[287] J. Wang, G. Wang, M. Zhang, M. Chen, D. Li, F. Min, *et al.*, "A comparative study of thermolysis characteristics and kinetics of seaweeds and fir wood," *Process Biochemistry,* vol. 41, pp. 1883-1886, 8// 2006.
[288] V. Skoulou, A. Swiderski, W. Yang, and A. Zabaniotou, "Process characteristics and products of olive kernel high temperature steam gasification (HTSG)," *Bioresource technology,* vol. 100, pp. 2444-2451, 2009.
[289] A. Almeida, M. Vieira, M. Neto, I. Pereira, A. Ribeiro, A. Ribeiro, *et al.*, "Effect of temperature on the gasification of olive bagasse particles," in *6th International Congress of Energy and Environment Engineering and Management, Paris*, 2015.
[290] A. A. Ahmad, N. A. Zawawi, F. H. Kasim, A. Inayat, and A. Khasri, "Assessing the gasification performance of biomass: A review on biomass gasification process conditions, optimization and economic evaluation," *Renewable and Sustainable Energy Reviews,* vol. 53, pp. 1333-1347, 2016.
[291] Y. D. Kim, C. W. Yang, B. J. Kim, K. S. Kim, J. W. Lee, J. H. Moon, *et al.*, "Air-blown gasification of woody biomass in a bubbling fluidized bed gasifier," *Applied Energy,* vol. 112, pp. 414-420, 12// 2013.

[292] M. T. Paulus, "Algorithm for explicit solution to the three parameter linear change-point regression model," *Science and Technology for the Built Environment,* vol. 23, pp. 1026-1035, 2017/08/18 2017.

Appendix of Gasification Experiments

A.1 Product Gas Profile of AROK at Different Temperatures.

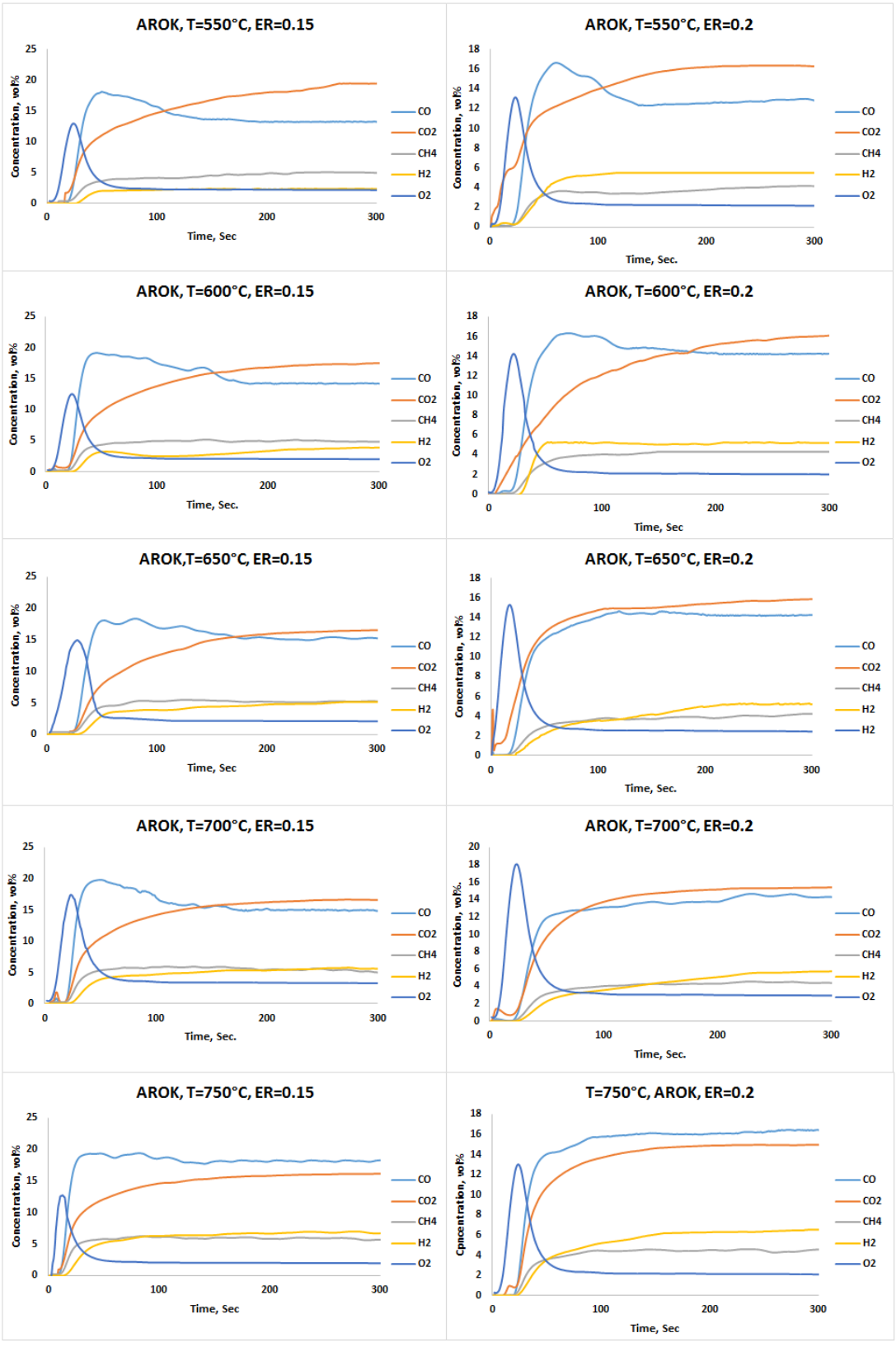

A.2 Product Gas Profile of AROK at Different Temperatures.

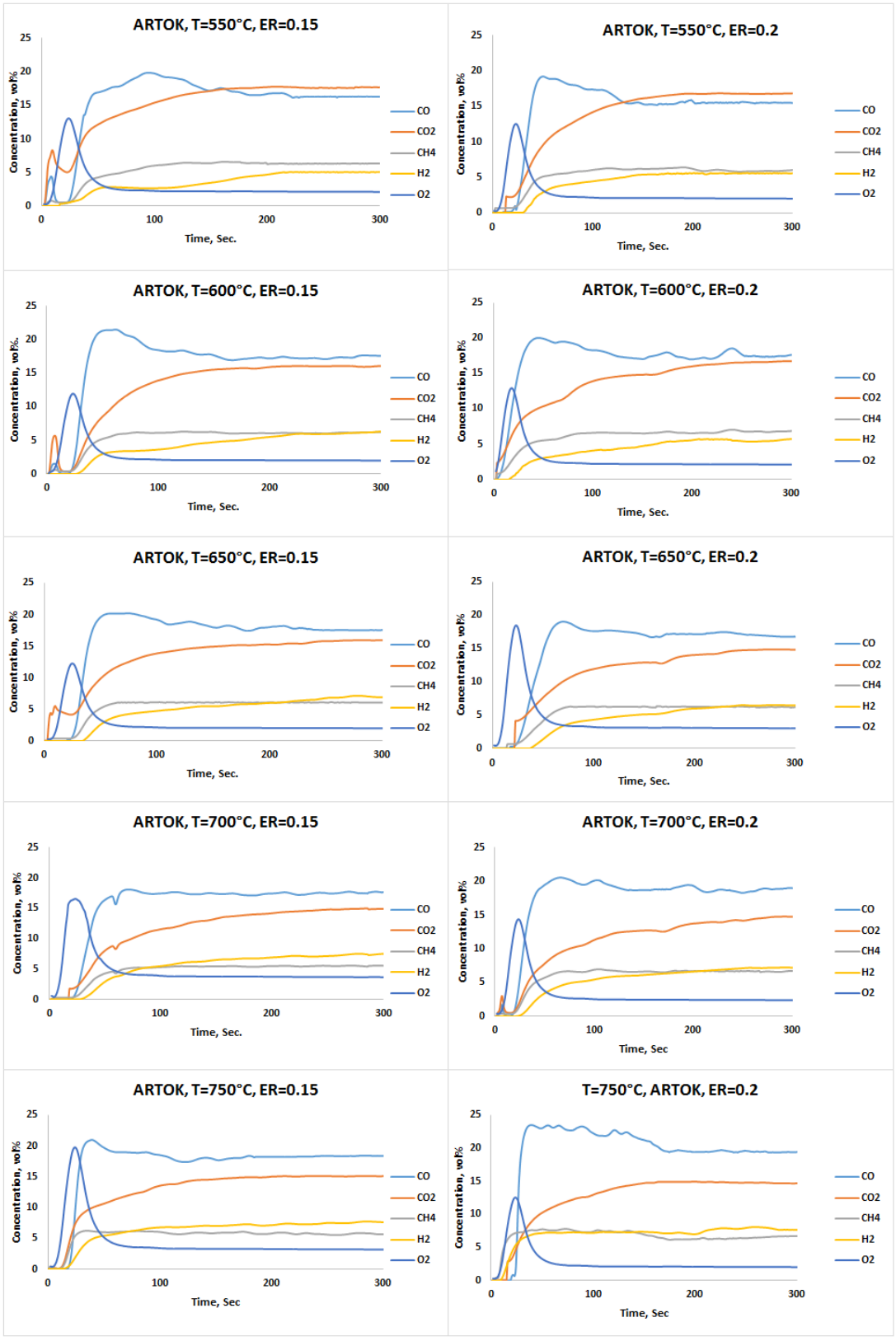

B.1 MATLAB Program for Determine of the Steady State Mass Load

```
% main code for reading the excel data
clc
clear
[data_a, data_b, alldata_received]=xlsread('data.xlsx',1);
[data_a, data_b, alldata_torrefied]=xlsread('data.xlsx',2);
nn=0;
T={'550','600','650','700','750'};
for i=1:2:size(alldata_received,2)
    nn=nn+1;
    x=cell2mat(alldata_received(3:end,i+1));
    y=cell2mat(alldata_received(3:end,i));
    x(isnan(x))=[];
    y(isnan(y))=[];
    [coefficients, minSSE] = threeparameterCP(x,y)
    yfit=coefficients(1) + coefficients(2)*(max(coefficients(3)-
x,0));
    R21=1-sum((y-yfit).^2)/sum((y-mean(y)).^2);
    received_mass_CP(nn,1)=coefficients(1);  %mass
    received_mass_CP(nn,2)=coefficients(3);  %time
    received_mass_CP(nn,3)=-coefficients(2); %slope
    figure
    plot( x,y,'b.');
    hold on
    plot(x,yfit,'r.');
    legend('Exp. data','model fit','Location','northwest');
    ax=gca;
    x_lim=ax.XLim;
    y_lim=ax.YLim;

text(x_lim(2)*2/3,y_lim(2)*2/3,['R^2=',num2str(R21)],'fontsize',8);
    xlabel({'time (sec)',['AROK T=',T{nn}]})
    ylabel('mass (gram)')
    set(gca,'Fontsize',8)
    set(gcf,'Units', 'centimeters');
    set(gcf,'position',[5,5, 9, 9/1.618]);
    set(gca,'LooseInset',get(gca,'TightInset'))
    set(gcf,'paperpositionmode','auto');
    axis tight
    colormap('default');
    print('-dpng', '-r600', ['AROK T=',T{nn}]);
end
nn=0;
for i=1:2:size(alldata_torrefied,2)
    nn=nn+1;
    x=cell2mat(alldata_torrefied(3:end,i+1));
    y=cell2mat(alldata_torrefied(3:end,i));
    x(isnan(x))=[];
    y(isnan(y))=[];
    [coefficients, minSSE] = threeparameterCP(x,y)
    yfit=coefficients(1) + coefficients(2)*(max(coefficients(3)-
x,0));
    R22=1-sum((y-yfit).^2)/sum((y-mean(y)).^2);
    torrefied_mass_CP(nn,1)=coefficients(1); %mass
    torrefied_mass_CP(nn,2)=coefficients(3); %time
    torrefied_mass_CP(nn,3)=-coefficients(2); %slope
    figure
```

```
    plot( x,y,'b.');
    hold on
    plot(x,yfit,'r.');
    legend('Exp. data','model fit','Location','northwest');
    ax=gca;
    x_lim=ax.XLim;
    y_lim=ax.YLim;

text(x_lim(2)*2/3,y_lim(2)*2/3,['R^2=',num2str(R22)],'fontsize',8);
    xlabel({'time (sec)',['ARTOK T=',T{nn}]})
    ylabel('mass (gram)')
    set(gca,'Fontsize',8)
    set(gcf,'Units', 'centimeters');
    set(gcf,'position',[5,5, 9, 9/1.618]);
    set(gca,'LooseInset',get(gca,'TightInset'))
    set(gcf,'paperpositionmode','auto');
    axis tight
    colormap('default');
    print('-dpng', '-r600', ['ARTOK T=',T{nn}]);
end
xlswrite('data.xlsx',[received_mass_CP torrefied_mass_CP],3,'B4')
close all
TT=[550 600 650 700 750]';
```

Subroutine is as following:

```
function [coefficients, minSSE] = threeparameterCP(x,y)
% revised from reference [292]
[xSorted, sortIndex] = sort(x); %Sort the input arrays by increasing
x
ySorted = y(sortIndex);
minSSE = inf; %initially set min SSE to arbitrarily high value
%Calculate variables that are unrelated to location of split
decision
n = length(x);
sumY = sum(y);
xSquared = xSorted.^2;
xy = xSorted.*ySorted;
for m = 3:n
    L = m - 1; %Using capital L because lowercase l looks similar to
1.
    numLess = L; %n_<
    sumYLess = sum(ySorted(1:L));
    sumXLess = sum(xSorted(1:L));
    sumXSquaredLess = sum(xSquared(1:L));
    sumXYLess = sum(xy(1:L));
    %EQ. 27
    b0 = mean(ySorted(m:n));

    %EQ. 28
    b1 = (sumXLess*sumYLess-numLess*sumXYLess)/ ...
        (numLess*sumXSquaredLess-sumXLess*sumXLess);
    %EQ. 30  N_<
    N = n*sumXLess*sumXYLess -numLess*sumXLess*sumXYLess
+numLess*sumXSquaredLess*sumY- ...
        sumY*(sumXLess)^2-...
        n*sumXSquaredLess*sumYLess+sumYLess*(sumXLess)^2;

    %EQ. 31. D_<
```

```
    D =(n-numLess)*(numLess*sumXYLess-sumXLess*sumYLess);
    %EQ. 29
    b2 = N/D;
    residuals = y - b0 - b1*(max(b2-x,0)); %for heating
    sse = sum(residuals.^2);
    if sse < minSSE
        minSSE = sse;
        coefficients(1) = b0;
        coefficients(2) = b1;
        coefficients(3) = b2;
    end
end
```

B.2 MATLAB Figures

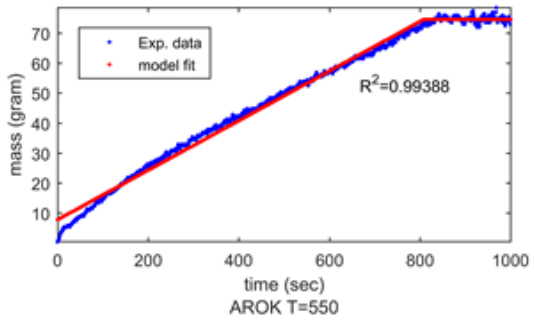

AROK T=550

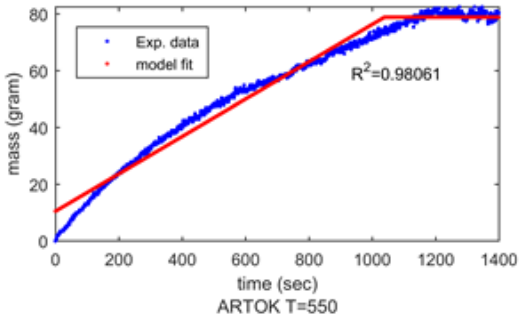

ARTOK T=550

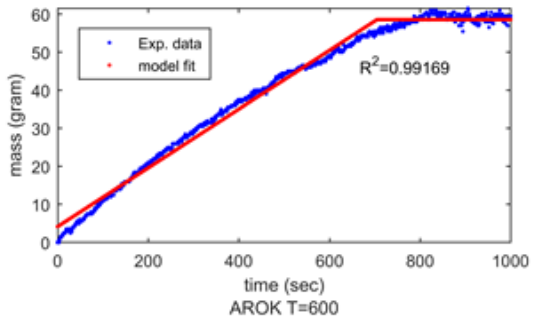

AROK T=600

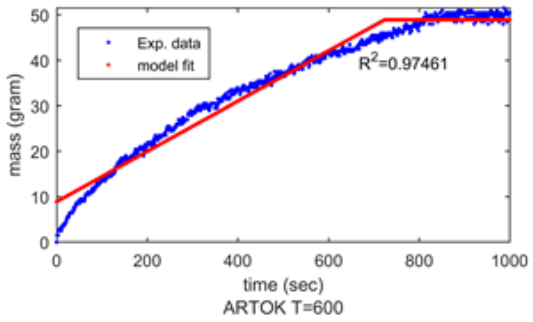

ARTOK T=600

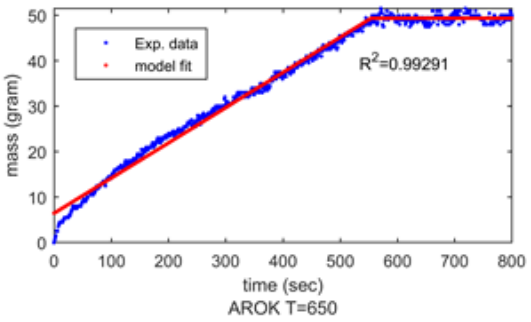

AROK T=650

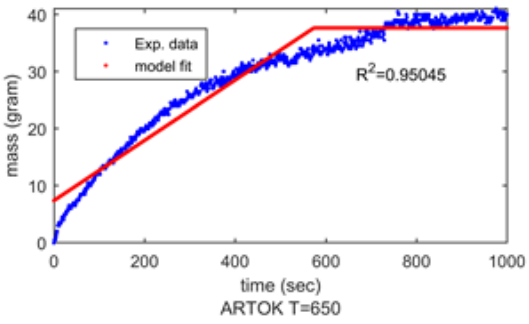

ARTOK T=650

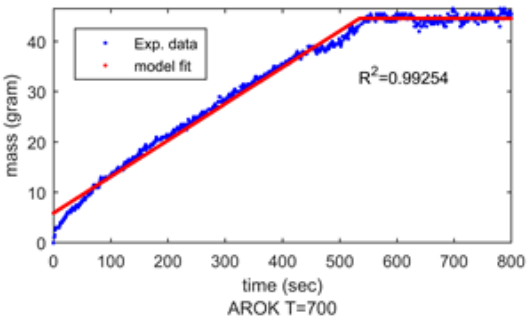

AROK T=700

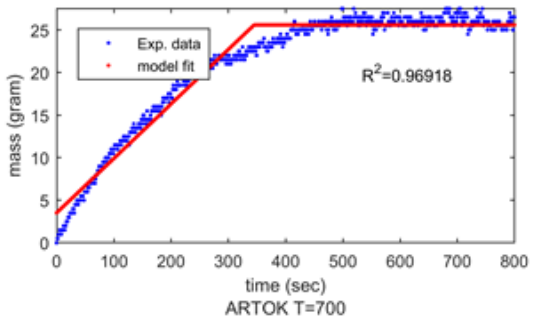

ARTOK T=700

C. Repeatability of Experimental Work

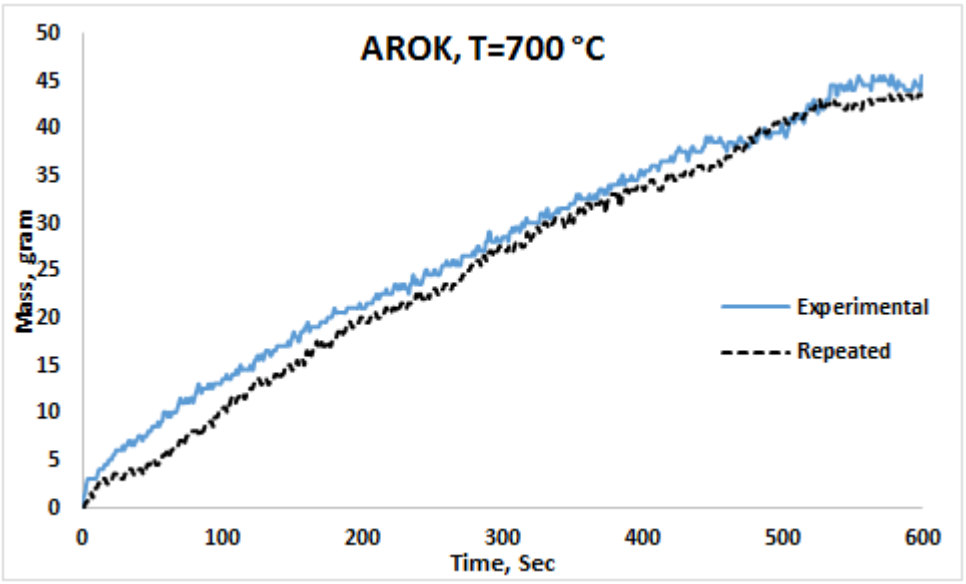

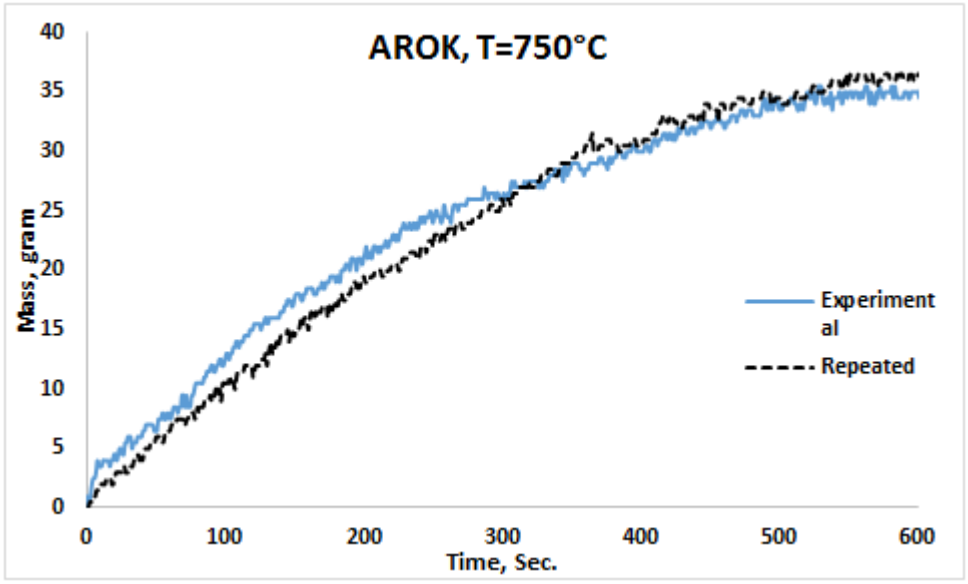

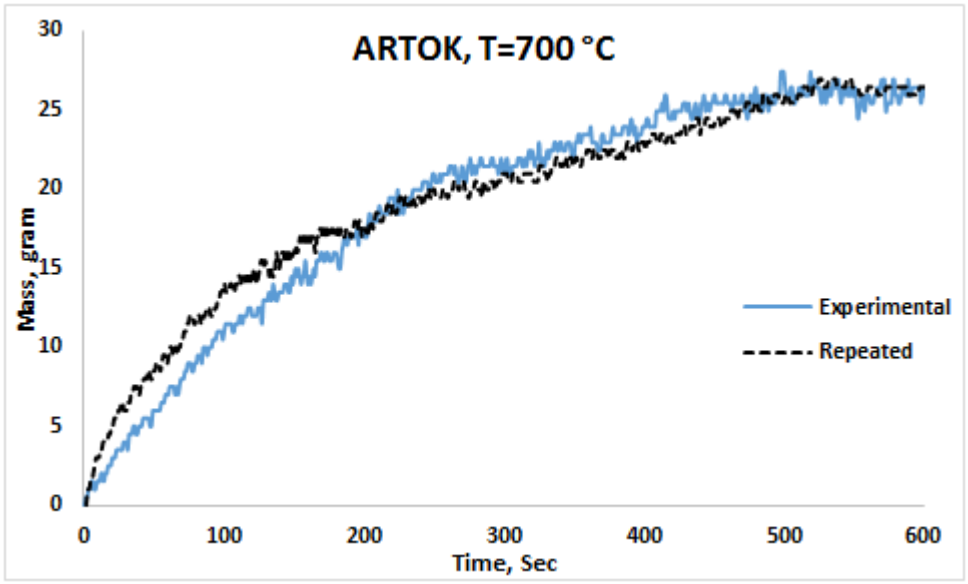
ARTOK, T=700 °C
Mass, gram
Time, Sec
Experimental
Repeated
0
5
10
15
20
25
30
0
100
200
300
400
500
600

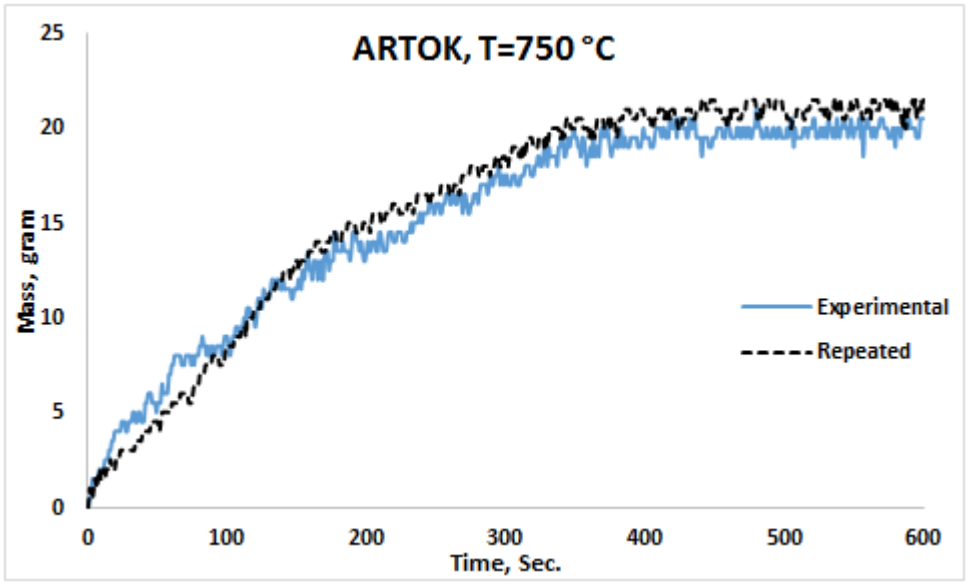
ARTOK, T=750 °C
Mass, gram
Time, Sec.
Experimental
Repeated
0
5
10
15
20
25
0
100
200
300
400
500
600

D.1 Overall mass and carbon balances for palm stone at different temperatures.

Temperature, °C	Stream	Total mass balance, g/min			Carbon mass balance, g/min		
		Input	Output	% Error	Input	Output	% Error
600	Biomass fuel	38.948	-	-	18.93	-	-
	Air	-	-	-	-	-	-
	Product gas	-	63.5	-	-	7.85	-
	Char		7.4	-		7.4	-
	Total	86.9	70.9	18.4	18.93	15.25	19.44
650	Biomass fuel	38.948	-	-	18.93	-	-
	Air	-	-	-	-	-	-
	Product gas	-	64.437	-	-	8.247	-
	Char			-			-
	Total	86.9	71.43	17.79	18.93	15.24	19.49
700	Biomass fuel	38.948	-	-	18.93	-	-
	Air	-	-	-	-	-	-
	Product gas	-	68.057	-	-	9.737	-
	Char			-			-
	Total	86.9	75.05	13.63	18.93	16.73	11.62
750	Biomass fuel	38.948	-	-	18.93	-	-
	Air	-	-	-	-	-	-
	Product gas	-	69.916.5	-	-	10.636.5	-
	Char			-			-
	Total	86.9	76.41	12.07	18.93	17.137	9.47

D.2 Overall mass and carbon balances for palm stones at different ERs.

ER at 750°C	Stream	Total mass balance, g/min			Carbon mass balance, g/min		
		Input	Output	% Error	Input	Output	% Error
0.15	Biomass fuel Air Product gas Char	51.86 48 - -	- - 69.81 9.1	- - - -	25.24 - - -	- - 10.46 9.1	- - - -
	Total	99.86	78.91	20.97	25.24	19.56	22.52
0.2	Biomass fuel Air Product gas Char	38.9 48 - -	- - 69.91 6.5	- - - -	18.93 - - -	- - 10.63 6.5	- - - -
	Total	86.9	78.91	12.07	18.93	17.137	9.47
0.25	Biomass fuel Air Product gas Char	31 48 - -	- - 65.38 5	- - - -	15.14 - - -	- - 8.65 5	- - - -
	Total	79	70.38	10.9	15.14	13.65	9.86
0.3	Biomass fuel Air Product gas Char	25.9 48 - -	- - 63.65 3.9	- - - -	12.62 - - -	- - 7.81 3.9	- - - -
	Total	73.90	67.55	8.59	12.62	11.71	7.23
0.35	Biomass fuel Air Product gas Char	22.22 48 - -	- - 61.26 3.6	- - - -	10.81 - - -	- - 6.67 3.6	- - - -
	Total	70.22	64.86	7.63	10.81	10.27	5.05